

How bees land

Visual guidance and sensorimotor control of landing maneuvers in bees



Pulkit Goyal

Propositions

1. Bumblebees and honeybees land by stepwise modulating their set-point of optical expansion rate.
(this thesis)
2. The average kinematics of multiple landing maneuvers of bees does not capture the underlying control system dynamics.
(this thesis)
3. Analyzing large datasets has the inherent risk of finding significant correlations without any biological or societal relevance.
4. The search for a perfect model undermines the purpose of modelling.
5. Massive Open Online Courses (MOOCs) are a major step towards universal access to education.
6. The limitations of a study should be explicitly discussed in scientific reports.
7. The SARS-CoV-2 pandemic has widened the economic inequality.
8. The burden of changing a system should not lie on the shoulders of people who are oppressed by it.

Propositions belonging to the thesis, entitled

How bees land—Visual guidance and sensorimotor control of landing maneuvers in bees

Pulkit Goyal

Wageningen, 26th of January 2022

How bees land

Visual guidance and sensorimotor control
of landing maneuvers in bees

Pulkit Goyal

Thesis committee

Promotors

Dr F. T. Muijres

Associate professor, Experimental Zoology Group
Wageningen University & Research

Prof. Dr J. L. van Leeuwen

Professor of Experimental Zoology
Wageningen University & Research

Co-promotor

Prof. Dr G. C. H. E. de Croon

Professor of Bio-inspired Micro Air Vehicles
Delft University of Technology

Other members

Prof. Dr J. J. A. van Loon, Wageningen University & Research

Prof. Dr S. Combes, University of California, Davis, United States of America

Dr A. Stöckl, Julius-Maximilians-Universität Würzburg, Germany

Prof. Dr F. Ruffier, Aix-Marseille University, France

This research was conducted under the auspices of the Graduate School
Wageningen Institute of Animal Sciences (WIAS)

How bees land

Visual guidance and sensorimotor control
of landing maneuvers in bees

Pulkit Goyal

Thesis

submitted in fulfilment of the requirements for the degree of doctor
at Wageningen University

by the authority of the Rector Magnificus,

Prof. Dr A. P. J. Mol,

in the presence of the

Thesis Committee appointed by the Academic Board

to be defended in public

on Wednesday 26 January 2022

at 4 p.m. in the Aula.

Pulkit Goyal

How bees land—Visual guidance and sensorimotor control of landing maneuvers in bees
258 pages.

PhD thesis, Wageningen University, Wageningen, the Netherlands (2022)

With references, with summaries in English, Punjabi and Hindi

ISBN 978-94-6447-005-5

DOI 10.18174/555606

For mummy, papa and guddu

Contents

1	General introduction	10
2	Bumblebees land rapidly and robustly using a sophisticated modular flight control strategy	28
3	Bumblebees land rapidly by robustly accelerating towards the surface during visually guided landings	84
4	Bumblebees actively compensate for the adverse effects of steady sidewinds during visually guided landings	126
5	Visual guidance of landing approaches in honeybees	180
6	General discussion	214
	Summaries	
	English	237
	Punjabi	241
	Hindi	245
	Acknowledgements	249
	About the author	253
	List of symbols	255
	Educational and training activities	257



Chapter 1

General introduction

After millions of years of evolution, animals today can achieve sophisticated feats during flight. Natural selection has produced dragonflies that can complete 180° turns in as little as three wing beats (Beckemeyer, 2009), mosquitoes that can carry blood as much as twice their weight while flying (Muijres et al., 2017), and arctic terns that can traverse distance equivalent to three return trips to the Moon in their lifetime (Egevang et al., 2010). Once airborne, flying animals must approach a surface for landing to feed, rest, or reproduce. These landings can result in animals gently touching the surface, grasping it or crashing on it (Roderick et al., 2017). Analyzing how animals approach a landing surface can provide a fundamental understanding of their flight control. In addition, it can aid in providing the bioinspired solutions for a similar control in man-made aerial vehicles (Srinivasan, 2011a,b; Serres and Ruffier, 2017).

The development of a controlled landing is likely a key step in the evolution of animal flight. This is because a failed landing can cause injury or death, or simply prevent the animal from reaching a food source or its home. However, despite its importance in animal flight, we do not yet fully understand how animals execute their landing behavior. In this thesis, I investigate the landing strategy of bees, in particular bumblebees (*Bombus terrestris*) and honeybees (*Apis mellifera ligustica*), and how they use their sensorimotor control system to advance towards the landing surface. This chapter provides the background information of visual guidance and sensorimotor flight control (including landing) in bees, delineates the open questions, and lists the aims and outline of this thesis.

1.1 Bees

Bees are believed to have first appeared approximately 130 million years ago (Goulson, 2010). Today, there are about 25,000 species of bees, spreading over all continents, except Antarctica (Goulson, 2010). Although most bees are solitary, there are a few that are eusocial. A solitary female bee constructs its own nest and raises its offspring. In contrast, eusocial bees live in colonies with labor distributed among them such as a queen lays eggs and workers forage, care for the brood, and defend the colony (Michener, 2007; Goulson, 2010). Irrespective of their sociality, bees have coevolved with flowers as they obtain their food from them (Danforth et al., 2006; Klinkhamer, 2006; Willmer, 2011). Foraging bees collect nectar and pollen from flowers, which provide energy, minerals and proteins necessary for their survival and reproduction (Wilson, 1984; Michener, 2007; Goulson, 2010).

Bees are relentless foragers. They frequently visit flowers, sometimes even more than 1,000 times in an hour (Ribbands, 1949; Heinrich, 1979, 2004; Goodwin et al., 2011; Couvillon et al., 2015). Most bees forage during the day and only a few (approximately 250 species) forage during the night (Michener, 2007; Wcislo and Tierney, 2009). Among the bee species used in this research, both bumblebees and honeybees are eusocial bees with a specialized forager workforce. Their forager bees are diurnal generalist foragers, as they forage during the day and gather food from a vast range of plant species. Depending upon the eco-

logical niche, environmental conditions such as light intensity, wind, temperature, solar radiation can influence the foraging behavior of bees (Benedek, 1976; Burrill and Dietz, 1981; Corbet, 1990; Riley et al., 1999; Peat and Goulson, 2005; Goulson, 2010; Polatto et al., 2014; Reber et al., 2015; Crall et al., 2017; Clarke and Robert, 2018; Hennessy et al., 2020, 2021). Compared to honeybees, bumblebees can forage in lower temperatures (Corbet et al., 1993). Moreover, they can fly in low light intensities, allowing them to forage earlier in the morning and late in the evening (Reber et al., 2016).

To visit flowers, all bees rely on flight as a mode of locomotion (Goulson, 2010). During flight, they use their multimodal sensory system to acquire information very rapidly (every $\sim 20 - 100$ ms) about the environment and themselves (Taylor and Krapp, 2007). They subsequently process this information to regulate wing and body kinematics. By doing so, they produce aerodynamic forces and torques for performing rapid and precise flight maneuvers. This allows them to avoid obstacles, escape predators, navigate complex cluttered environment, and land on the food sources and their hive entrance (Altshuler et al., 2005; Srinivasan, 2011a,b; Sun, 2014; Vance et al., 2014; Shyy et al., 2016; Serres and Ruffier, 2017; Combes et al., 2020).

1.2 The sensory system of bees

All bees, including nocturnal ones, use vision to mediate many of their flight behaviors (Land, 2004; Warrant et al., 2004; Warrant, 2007, 2008; Srinivasan, 2011a,b; Baird et al., 2020). They possess three small eyes called ocelli and a pair of apposition compound eyes as visual sensors (Land and Nilsson, 2013). Both the ocelli and the compound eyes likely play a role in the navigation, flight control, and visual discrimination (Taylor and Krapp, 2007; Taylor et al., 2016; Tichit, 2021). During flight, the motion of a bee relative to its environment causes different features in its visual field to apparently move with respect to the bee. This apparent movement is caused by the shifts in the retinal images of the visual scene and is termed as optic flow (Gibson, 1950, 1955; Horridge, 2009; Rogers, 2021). The role of optic flow in bee flight control is well documented (Serres et al., 2008; Portelli et al., 2010, 2011; Srinivasan, 2011a,b; Baird et al., 2020).

Besides the vision, bees also possess mechanosensors that likely aid in the flight control. A pair of antenna, located on the head of insects, have been identified as a key wind-encoding sensors in various insects such as fruit flies, locusts, honeybees (Gewecke, 1970; Budick et al., 2007; Taylor et al., 2013) and possibly also bumblebees (Jakobi et al., 2018). In addition to antennae, the wind sensing hairs on the head have also been implicated in flight control in insects (Taylor and Krapp, 2007) (for details on other sensors, see Taylor and Krapp, 2007).

While airborne, insects (including bees) likely combine information from multiple sensory modalities synergistically to aid flight control (Taylor et al., 2013; Fuller et al., 2014; Ravi et al., 2016).

1.3 Visual guidance strategy during free-flight

Flight requires precise control to travel fast and avoid collisions with obstacles. For this purpose, bees use translatory optic flow (front-to-back apparent motion of the visual scene) to fly efficiently and safely (Srinivasan, 2011a; Baird et al., 2020; Tichit, 2021). The translatory optic flow T_{OF} provides the bee with a ratio of its flight speed V_F and its distance from the surface D as $T_{OF} = V_F/D$ (Koenderink, 1986).

Bees fly by flexibly measuring the translatory optic flow in their visual field (frontal, lateral, ventral, and dorsal) and are suggested in literature to hold a measure of it constant during their cruising flight (Serres et al., 2008; Portelli et al., 2010, 2011; Srinivasan, 2011a,b; Baird et al., 2020). This constant is referred to as a set-point T_{OF}^* . Following a set-point enables the bees to automatically reduce flight speed when they are closer to a surface and fly faster when they are farther from it (Barron and Srinivasan, 2006; Baird et al., 2010). This visual guidance strategy of holding the translatory optic flow constant enables bees to exhibit a range of behaviors, such as controlling both their height and flight-speed in open spaces, increasing their distance from the oncoming obstacle or observing centering behavior while flying in the narrow corridors (for reviews, see Srinivasan, 2011a,b; Serres and Ruffier, 2017; Baird et al., 2020). The control of flight-speed and distance from the surface using translatory optic flow has also been suggested for flies and may also occur in other insects such as mosquitoes, moths and locusts (Kennedy, 1940, 1951; David, 1982; Kuenen and Baker, 1982; Preiss, 1987; Fry et al., 2009; Rohrseitz and Fry, 2011; Medici and Fry, 2012).

1.4 Visual guidance strategy during landing

Among other flight behaviors, landing is arguably one of the most difficult behaviors, whereby an animal needs to regulate its speed as it reaches closer to the surface. Precisely reducing the flight speed such that the speed is close to zero when reaching the landing surface can avoid damage that can be caused by high-impact collisions. On the other hand, reducing the speed to zero before reaching the target could cause a stall and a crash landing, or might require the animal to abort the landing.

In addition, foraging bees specifically need to perform these landings rapidly. Individual flowers typically contain a minute quantity of nectar (Southwick and Southwick, 1986; Keasar et al., 2008), and therefore foraging bees need to visit hundreds to thousands of flowers to gather a substantial quantity (Ribbands, 1949; Heinrich, 1979, 2004; Goodwin et al., 2011; Couvillon et al., 2015). During these visits, bees are prone to wing damage that may happen due to collisions (Foster and Cartar, 2011; Mountcastle and Combes, 2014; Rajabi et al., 2020). Thus, a landing bee requires precise flight control to accurately regulate its flight speed with distance to the surface, allowing it to land rapidly with minimal risk of damage.

Bees mostly use optical expansion cues to control their approach speed during landings

(Baird et al., 2013; Chang et al., 2016; Shackleton et al., 2019; Tichit et al., 2020b). This mechanism is similar to the use of translatory optic flow suggested in bees for regulating the forward flight speed. When a bee approaches a landing surface, various features in the image appear to move radially outward from the center (Gibson, 1955; Edwards and Ibbotson, 2007). The bees can use these cues to measure the relative-rate-of-expansion (r), which equals the ratio of their approach speed V and their distance from the landing surface y as $r = V/y$ (Wagner, 1982; Baird et al., 2013).

By determining the average landing dynamics of multiple honeybees (*Apis mellifera ligustica*), it was shown that the average honeybee reduces its approach speed linearly with distance to the surface. This suggests that honeybees land by keeping the relative-rate-of-expansion constant at a set-point r^* . Bumblebees (*Bombus impatiens*, Chang et al., 2016) and fruit flies (*Drosophila melanogaster*, Van Breugel and Dickinson, 2012; Baird et al., 2013) have been suggested to use similar strategies. Moreover, it is likely that stingless bees (*Melipona scutellaris*, *Scaptotrigona depilis* and *Partamona helleri*) also use a landing strategy similar to honeybees, at least up until 20 cm from the surface (Shackleton et al., 2019; Baird et al., 2020; Tichit et al., 2020a). At distances smaller than 20 cm, the stingless bees (*P. helleri* and *S. depilis*) start accelerating towards the surface, possibly to defend their nest entrance from the predators or to reduce traffic congestion near it (Shackleton et al., 2019; Tichit et al., 2020a). These studies suggest that many insects approach the landing surfaces by keeping the optical expansion rate constant at a set-point r^* , although there are some deviations in this behavior.

In contrast to insects, pigeons (*Columba livia*), hummingbirds (*Colibri coruscans*), and mallard ducks (*Anas platyrhynchos*), approach a landing surface by using the so-called constant- $\dot{\tau}$ strategy (Lee et al., 1991, 1993; Whitehead, 2020). Here, $\dot{\tau}$ is the time-derivative of time-to-contact τ which is the inverse of relative-rate-of-expansion r as $\tau = 1/r$ (see **Chapter 2** for details) (Lee et al., 1991, 1993; Whitehead, 2020). The landing strategy found in birds results in faster landings than the landing strategy suggested to be used by many insects (Baird et al., 2013).

The vision-based landing strategy described above for insects and birds has been found by quantifying the average landing kinematics of multiple landing maneuvers. Although this type of analysis provides valuable insights into their landing performance, it does not capture the complex sensorimotor control dynamics of individual landing maneuvers (see **Chapters 2** and **5** for details). Therefore, in this thesis, I develop a novel methodology to analyze the landing kinematics of individual landing maneuvers. Using this individual-based analysis method, I studied how individual bumblebees (*Bombus terrestris*) and honeybees (*Apis mellifera ligustica*) use vision to guide their landing approach.

Moreover, in natural conditions, bees perform two possibly distinct types of landing maneuvers: firstly, when moving between nearby flowers in the same flower patch, foraging bees perform multiple landings directly after a take-off; secondly, when landing on the hive entrance at the end of a foraging trip or when travelling between flower patches, bees land

from free-flight conditions. The landings immediately after a take-off are expected to occur more often and with lower approach speeds compared to the landings from a free-flight condition. However, it is currently not known how the vision-based guidance strategy in landings after a take-off is different than the landings from a free-flight. In **Chapters 2 and 4**, I use the aforementioned custom-developed methodology to analyze the individual landing maneuvers and find how these landing maneuvers differ from each other.

1.5 Behind visual guidance: sensorimotor control systems

To follow a certain set-point of optic flow during a forward flight or landing approach (T_{OF}^* or r^* , respectively), bees need to use their sensorimotor control system. This system allows them to continuously parse information from their sensors and produce body accelerations or decelerations by changing the wing and body kinematics. This in turn allows bees to first reach and then maintain the optic flow set-point (Portelli et al., 2010; Srinivasan, 2011a,b). Reaching a set-point is needed, for example, when a bee starts its flight from a take-off or encounters disturbances such as tapering walls, obstacles, or a wind gust (Srinivasan, 2011b; Jakobi et al., 2018; Baird et al., 2020).

Executing sensorimotor control presents enormous processing challenges, which bees seemingly handle easily with their miniature brains (Giurfa, 2015). It employs intricate neuronal sensorimotor control pathways to process the sensory stimuli and produces motor actions needed to perform the required action (for example, reaching an optic flow set-point, escaping a predator, catching prey, or approaching a mate). In control theory, these pathways and their complex physiological mechanisms are abstracted using a system-level approach (for reviews, see Taylor et al., 2008; Cowan et al., 2014; Roth et al., 2014; Dickinson and Muijres, 2016). In this context, the behavior of reaching and maintaining a set-point in an animal is similar to the negative feedback loops in control engineering (Ogata, 2010). Here, the sensory measurement obtained by a flying animal is compared with its set-point to generate an error-input for a controller. The controller acts on this error-input and produces motor actions, such as changes in the wing and body kinematics. These actions result in the production of aerodynamic forces and torques and consequently make the animal rotate and accelerate, which changes the sensory measurement. The resulting continuous sensorimotor feedback loop causes the sensory measurement to converge towards the set-point.

The studies aimed at identifying system-level descriptions can be broadly categorized into two categories — *open-loop* and *closed-loop* studies (Taylor et al., 2008; Cowan et al., 2014; Roth et al., 2014). In open-loop studies, the environment in which an animal is moving is altered in real-time to influence the sensory output of the animal (as in Fry et al., 2009; Rohrseitz and Fry, 2011; Medici and Fry, 2012). These studies are useful to identify the parameters that an animal uses in flight control, and to obtain a functional descrip-

tion of one or multiple subsystems identified in the negative feedback loops (controller, plant, sensory system, or motor system). In contrast, in closed-loop studies, one can study the response of the complete system by exciting it using a known input, such as a step or sinusoidal inputs (Van den Hof, 2012). This provides an understanding of how multiple subsystems together act as one dynamical system for achieving a desired goal (for example, see Stöckl et al., 2017).

Understanding how animals perform sensorimotor control helps in elucidating how animals exhibit their behavior on multiple levels (Taylor et al., 2008; Cowan et al., 2014; Roth et al., 2014). First, it helps in identifying different variables involved in flight control; second, it establishes a causal relationship between the perception (sensory measurements) and the action (motor actions). Together, they form the building blocks that can be used in further studies to understand how animals integrate information from their multiple sensors and act on this information to exhibit a particular behavior (Fuller et al., 2014).

Here, I used the closed-loop research approach to study sensorimotor control of landing maneuvers in bumblebees (*Bombus terrestris*) and honeybees (*Apis mellifera ligustica*). This allowed me to elucidate their visual guidance strategy for landing, and how they use their sensorimotor control to execute these landings. The identified building blocks that represent the landing behavior can be translated as an algorithm onto man-made systems (Franceschini et al., 2007; Srinivasan, 2011a; Karásek et al., 2018).

1.6 The effect of environmental conditions on the visual guidance and the sensorimotor control systems

Depending upon their habitat, bees forage in a wide range of environmental conditions. For example, diurnal bumblebees forage from dawn to dusk while battling wind speeds similar to their own flight speed (Michener, 2007; Goulson, 2010; Crall et al., 2017). While there have been some studies depicting the influence of environmental conditions on the visual guidance in free-flight, understanding their effect on the visual guidance during landing and underlying sensorimotor control has received very little attention (Baird, 2005; Baird et al., 2015; Reber et al., 2015; Baird et al., 2020; Burnett et al., 2020; Baird et al., 2021). Honeybees (*Apis mellifera ligustica*) were shown to exhibit more variation in their landing approaches in the presence of weak expansion cues (Baird et al., 2013) and bumblebees (*Bombus impatiens*) were shown to exhibit high impact landings in the presence of winds (Chang et al., 2016). Despite these useful observations, it still remains unknown how a change in the environment actually affects the guidance strategy of landing bees.

Understanding how visual-guidance strategy and sensorimotor control of landing bees is influenced by the environmental conditions will contribute to our understanding of the biology of bees, and can help reveal their resilience or vulnerability to the rapidly changing abiotic conditions in the ecosystems (Baird et al., 2020; Tichit, 2021). This can guide our efforts for conserving them and their contribution to the pollination of plants. Therefore,

in this thesis, I explored how light intensity (**Chapters 2 and 3**), wind speed (**Chapter 4**) and the strength of expansion cues (**Chapters 2 and 3**) influence the landing strategy and the sensorimotor control system of bumblebees (*Bombus terrestris*).

1.7 Aims and content of this thesis

Foraging bees regularly land on flowers. These seemingly effortless landings are not easy to execute, especially in adverse environmental conditions. It requires enormous processing of sensory feedback and fine motor control. A small miscalculation can cause a collision and damage their rapidly beating wings. Cumulative wing damage can lead to loss of flight ability and death.

To execute a safe landing, bees need to slow down but not too early as flying slowly can negatively impact their energy gain during foraging. In this thesis, we aim to elucidate the mechanism behind the landing behavior of bees. Specifically, we aim to find

1. how bees use their visual sensors to control their approach speed with distance to the landing surface, and
2. how their visual guidance and underlying sensorimotor control system is influenced by three abiotic conditions, namely, wind speed, environmental light intensity and the strength of optic cues on the landing surface.

In **Chapter 2**, I first present a novel methodology to analyze the individual landing maneuvers of bees. This methodology forms the basis of analyses in the subsequent chapters. Using this methodology, I then investigate the vision-based guidance strategy that bumblebees (*Bombus terrestris*) use during landings. Hereby, I separately identify the guidance strategy for bumblebees landing from a free-flight condition and bumblebees landing immediately after a take-off. In this chapter, I also elucidate how bumblebees adjust their visual guidance strategy with (a) light intensities ranging from twilight to sunrise and (b) the strength of optic expansion cues. Finally, I compare the identified landing strategy of bumblebees with the known landing strategies of birds and honeybees.

In **Chapter 3**, I focus on the sensorimotor control system that bumblebees use to execute their landing strategy. Conventionally, to identify and understand a sensorimotor control system, it needs to be excited in some manner. Based on the results from **Chapter 2**, I first explain that the newly found landing strategy of bumblebees offers natural excitation of their sensorimotor control system. I then postulate that bumblebees use the relative rate of expansion as a control variable and modulate their motor output (wing and body kinematics) to reach the desired set-points. I corroborate this hypothesis by using system identification techniques from control theory. Furthermore, I identify (a) how bumblebees use the transient response of this natural excitation to advance towards the landing surface, and (b) how this transient response varies between the tested environmental conditions (light

intensity and the strength of optic expansion cues) and starting conditions (landings from a free-flight or directly after a take-off).

In **Chapter 4**, I use the analyses techniques developed in **Chapters 2** and **3** to explore how wind influences the visual guidance strategy and the sensorimotor control of landing bumblebees. Winds in nature are often characterized as mean wind speeds and the fluctuations around it. In this chapter, I identify the adverse effects of mean wind speeds on the landing dynamics of bumblebees and show how bumblebees compensate for these effects. Furthermore, I take advantage of the natural excitation that bumblebees offer during landing to propose how they integrate information from the wind-encoding mechanoreceptors with their vision-based sensorimotor control system.

In **Chapter 5**, I revise the landing strategy of honeybees previously proposed in literature. Based on the average landing dynamics of multiple landing maneuvers, it has been suggested that honeybees land by holding the relative rate of expansion constant throughout their approach (Baird et al., 2013). I used my novel analysis technique developed in **Chapter 2** to find if individual honeybees also follow this strategy. Moreover, I extend the analysis to elucidate the mechanism that honeybees use to excite their sensorimotor control system during landing.

In **Chapters 2, 4, and 5**, I repeat the above-mentioned analysis based on the average landing dynamics of multiple landing maneuvers and compare the resulting outcomes with the analysis based on the individual landing maneuvers. I then discuss the advantages and shortcomings of both methods.

Finally, in **Chapter 6**, I first summarize the results of this thesis and then compare the landing strategies of bumblebees and honeybees found in this thesis. Furthermore, I put the findings of this research in the broader context of landing and free-flight research in bees specifically, and for insects and birds in general. I also discuss how the knowledge obtained in this research can be used for bioinspired applications. I conclude with an outlook on the future research to deepen the knowledge of landing dynamics in bees as well as other flying animals.

References

- Altshuler, D. L., Dickson, W. B., Vance, J. T., Roberts, S. P. and Dickinson, M. H. (2005). Short-amplitude high-frequency wing strokes determine the aerodynamics of honeybee flight. *Proceedings of the National Academy of Sciences* **102**, 18213–18218.
- Baird, E. (2005). Visual control of flight speed in honeybees. *Journal of Experimental Biology* **208**, 3895–3905.
- Baird, E., Boeddeker, N., Ibbotson, M. R. and Srinivasan, M. V. (2013). A universal strategy for visually guided landing. *Proceedings of the National Academy of Sciences of the United States of America* **110**, 18686–18691.
- Baird, E., Boeddeker, N. and Srinivasan, M. V. (2021). The effect of optic flow cues on

- honeybee flight control in wind. *Proceedings of the Royal Society B: Biological Sciences* **288**, 20203051.
- Baird, E., Fernandez, D. C., Wcislo, W. T. and Warrant, E. J.** (2015). Flight control and landing precision in the nocturnal bee *Megalopta* is robust to large changes in light intensity. *Frontiers in Physiology* **6**, 1–7.
- Baird, E., Kornfeldt, T. and Dacke, M.** (2010). Minimum viewing angle for visually guided ground speed control in bumblebees. *Journal of Experimental Biology* **213**, 1625–1632.
- Baird, E., Tichit, P. and Guiraud, M.** (2020). The neuroecology of bee flight behaviours. *Current Opinion in Insect Science* **42**, 8–13.
- Barron, A. and Srinivasan, M. V.** (2006). Visual regulation of ground speed and head-wind compensation in freely flying honey bees (*Apis mellifera* L.). *Journal of Experimental Biology* **209**, 978–984.
- Beckemeyer, R. J.** (2009). Kinematics of a territorial defense maneuver by the dragonfly *Pachydiplax longipennis* (Odonata: Anisoptera: Libellulidae). *Transactions of the Kansas Academy of Science (1903-)* **112**, 169–180.
- Benedek, P.** (1976). Effect of environmental factors on the foraging rates of honeybees in red clover fields. *Zeitschrift für Angewandte Entomologie* **81**, 14–20.
- Budick, S. A., Reiser, M. B. and Dickinson, M. H.** (2007). The role of visual and mechanosensory cues in structuring forward flight in *Drosophila melanogaster*. *Journal of Experimental Biology* **210**, 4092–4103.
- Burnett, N. P., Badger, M. A. and Combes, S. A.** (2020). Wind and obstacle motion affect honeybee flight strategies in cluttered environments. *Journal of Experimental Biology* **223**.
- Burrill, R. M. and Dietz, A.** (1981). The response of honeybees to variations in solar radiation and temperature. *Apidologie* **12**, 319–328.
- Chang, J. J., Crall, J. D. and Combes, S. A.** (2016). Wind alters landing dynamics in bumblebees. *The Journal of Experimental Biology* **219**, 2819–2822.
- Clarke, D. and Robert, D.** (2018). Predictive modelling of honey bee foraging activity using local weather conditions. *Apidologie* **49**:3 **49**, 386–396.
- Combes, S. A., Gagliardi, S. F., Switzer, C. M. and Dillon, M. E.** (2020). Kinematic flexibility allows bumblebees to increase energetic efficiency when carrying heavy loads. *Science Advances* **6**.
- Corbet, S.** (1990). Pollination and the weather. *Israel J. Bot.* **39**, 13–30.
- Corbet, S. A., Fussel, M., Ake, R., Fraser, A., Gunson, C., Savage, A. and Smith, K.** (1993). Temperature and the pollinating activity of social bees. *Ecological Entomology* **18**, 17–30.

- Couvillon, M. J., Walter, C. M., Blows, E. M., Czaczkes, T. J., Alton, K. L. and Ratnieks, F. L. (2015). Busy Bees: Variation in Insect Flower-Visiting Rates across Multiple Plant Species. *Psyche (London)* 2015.
- Cowan, N. J., Ankarali, M. M., Dyhr, J. P., Madhav, M. S., Roth, E., Sefati, S., Sponberg, S., Stamper, S. A., Fortune, E. S. and Daniel, T. L. (2014). Feedback control as a framework for understanding tradeoffs in biology. *Integrative and Comparative Biology* 54, 223–237.
- Crall, J. D., Chang, J. J., Oppenheimer, R. L. and Combes, S. A. (2017). Foraging in an unsteady world: Bumblebee flight performance in fieldrealistic turbulence. *Interface Focus* 7.
- Danforth, B. N., Sipes, S., Fang, J. and Brady, S. G. (2006). The history of early bee diversification based on five genes plus morphology. *Proceedings of the National Academy of Sciences* 103, 15118–15123.
- David, C. T. (1982). Compensation for height in the control of groundspeed by *Drosophila* in a new, ‘barber’s pole’ wind tunnel. *Journal of comparative physiology* 1982 147:4 147, 485–493.
- Dickinson, M. H. and Mujires, F. T. (2016). The aerodynamics and control of free flight manoeuvres in *Drosophila*. *Philosophical Transactions of the Royal Society B: Biological Sciences* 371, 20150388.
- Edwards, M. and Ibbotson, M. R. (2007). Relative sensitivities to large-field optic-flow patterns varying in direction and speed. *Perception* 36, 113–124.
- Egevang, C., Stenhouse, I. J., Phillips, R. A., Petersen, A., Fox, J. W. and Silk, J. R. D. (2010). Tracking of Arctic terns *Sterna paradisaea* reveals longest animal migration. *Proceedings of the National Academy of Sciences* 107, 2078–2081.
- Foster, D. J. and Cartar, R. V. (2011). What causes wing wear in foraging bumble bees? *Journal of Experimental Biology* 214, 1896–1901.
- Franceschini, N., Ruffier, F. and Serres, J. (2007). A Bio-Inspired Flying Robot Sheds Light on Insect Piloting Abilities. *Current Biology* 17, 329–335.
- Fry, S. N., Rohrseitz, N., Straw, A. D. and Dickinson, M. H. (2009). Visual control of flight speed in *Drosophila melanogaster*. *Journal of Experimental Biology* 212, 1120–1130.
- Fuller, S. B., Straw, A. D., Peek, M. Y., Murray, R. M. and Dickinson, M. H. (2014). Flying *Drosophila* stabilize their vision-based velocity controller by sensing wind with their antennae. *Proceedings of the National Academy of Sciences* 111, E1182–E1191.
- Gewecke, M. (1970). Antennae: Another Wind-sensitive Receptor in Locusts. *Nature* 1970 225:5239 225, 1263–1264.
- Gibson, J. J. (1950). *The perception of the visual world*. Oxford, England: Houghton Mifflin.

- Gibson, J. J. (1955). The optical expansion-pattern in aerial locomotion. *The American journal of psychology* **68**, 480–484.
- Giurfa, M. (2015). The amazing mini-brain: lessons from a honey bee. *Bee World* **84**, 5–18.
- Goodwin, R., Cox, H., Taylor, M., Evans, L. and McBrydie, H. (2011). Number of honey bee visits required to fully pollinate white clover (*Trifolium repens*) seed crops in Canterbury, New Zealand. *New Zealand Journal of Crop and Horticultural Science* **39**, 7–19.
- Goulson, D. (2010). *Bumblebees: Behaviour, Ecology, and Conservation*. Oxford biology. OUP Oxford.
- Heinrich, B. (1979). Resource heterogeneity and patterns of movement in foraging bumblebees. *Oecologia* **40**, 235–245.
- Heinrich, B. (2004). *Bumblebee economics*. Harvard University Press, 245 pp.
- Hennessy, G., Harris, C., Eaton, C., Wright, P., Jackson, E., Goulson, D. and Ratnieks, F. F. (2020). Gone with the wind: effects of wind on honey bee visit rate and foraging behaviour. *Animal Behaviour* **161**, 23–31.
- Hennessy, G., Harris, C., Pirot, L., Lefter, A., Goulson, D. and Ratnieks, F. L. (2021). Wind slows play: increasing wind speed reduces flower visiting rate in honey bees. *Animal Behaviour* **178**, 87–93.
- Horridge, A. (2009). *What does the Honeybee See? And how do we Know?: A critique of scientific reason*. ANU Press.
- Jakobi, T., Kolomenskiy, D., Ikeda, T., Watkins, S., Fisher, A., Liu, H. and Ravi, S. (2018). Bees with attitude: the effects of directed gusts on flight trajectories. *Biology Open* **7**.
- Karásek, M., Muijres, F. T., Wagter, C. D., Remes, B. D. W. and de Croon, G. C. H. E. (2018). A tailless aerial robotic flapper reveals that flies use torque coupling in rapid banked turns. *Science* **361**, 1089–1094.
- Keasar, T., Sadeh, A. and Shmida, A. (2008). Variability in nectar production and standing crop, and their relation to pollinator visits in a Mediterranean shrub. *Arthropod-Plant Interactions* **2008 2:2**, 117–123.
- Kennedy, J. S. (1940). The Visual Responses of Flying Mosquitoes. *Proceedings of the Zoological Society of London* **A109**, 221–242.
- Kennedy, J. S. (1951). The migration of the desert locust (*Schistocerca gregaria* Forsk.). I. The behaviour of swarms. II. A theory of long-range migrations. *Philosophical transactions of the Royal Society of London. Series B, Biological sciences* **235**, 163–290.
- Klinkhamer, P. (2006). Plant-pollinator interactions: from specialization to generalization: Waser NM, Ollerton J. eds. 2006.: Chicago: Chicago: The University of Chicago Press. \$45 (paperback). 488 pp. *Annals of Botany* **98**, 899–900.

- Koenderink, J. J. (1986). Optic flow. *Vision Research* **26**, 161–179.
- Kuonen, L. P. and Baker, T. C. (1982). Optomotor regulation of ground velocity in moths during flight to sex pheromone at different heights. *Physiological Entomology* **7**, 193–202.
- Land, M. F. (2004). Nocturnal vision: Bees in the dark. *Current Biology* **14**, R615–R616.
- Land, M. F. and Nilsson, D.-E. (2013). *Animal Eyes*. Oxford: Oxford University Press.
- Lee, D. N., Davies, M. N. O., Green, P. R. and (Ruud). Van Der Weel, F. R. (1993). Visual control of velocity of approach by pigeons when landing. *Journal of Experimental Biology* **180**, 85–104.
- Lee, D. N., Reddish, P. E. and Rand, D. T. (1991). Aerial docking by hummingbirds. *Naturwissenschaften* **78**, 526–527.
- Medici, V. and Fry, S. N. (2012). Embodied linearity of speed control in *Drosophila melanogaster*. *Journal of The Royal Society Interface* **9**, 3260–3267.
- Michener, C. D. (2007). *The Bees of the World*. Johns Hopkins University Press.
- Mountcastle, A. M. and Combes, S. A. (2014). Biomechanical strategies for mitigating collision damage in insect wings: Structural design versus embedded elastic materials. *Journal of Experimental Biology* **217**, 1108–1115.
- Muijres, F. T., Chang, S. W., van Veen, W. G., Spitzen, J., Biemans, B. T., Koehl, M. A. R. and Dudley, R. (2017). Escaping blood-fed malaria mosquitoes minimize tactile detection without compromising on take-off speed. *Journal of Experimental Biology* **220**, 3751–3762.
- Ogata, K. (2010). *Modern Control Engineering*. Instrumentation and controls series. Prentice Hall.
- Peat, J. and Goulson, D. (2005). Effects of Experience and Weather on Foraging Rate and Pollen versus Nectar Collection in the Bumblebee, *Bombus terrestris*. *Behavioral Ecology and Sociobiology* **58**, 152–156.
- Polatto, L. P., Chaud-Netto, J. and Alves-Junior, V. V. (2014). Influence of Abiotic Factors and Floral Resource Availability on Daily Foraging Activity of Bees. *Journal of Insect Behavior* **27**, 593–612.
- Portelli, G., Ruffier, F. and Franceschini, N. (2010). Honeybees change their height to restore their optic flow. *Journal of Comparative Physiology A* **196**, 307–313.
- Portelli, G., Ruffier, F., Roubieu, F. L. and Franceschini, N. (2011). Honeybees' speed depends on dorsal as well as lateral, ventral and frontal optic flows. *PLoS ONE* **6**.
- Preiss, R. (1987). Motion parallax and figural properties of depth control flight speed in an insect. *Biological Cybernetics* **57**, 1–9.
- Rajabi, H., Dirks, J. H. and Gorb, S. N. (2020). Insect wing damage: Causes, consequences and compensatory mechanisms. *Journal of Experimental Biology* **223**.

- Ravi, S., Kolomenskiy, D., Engels, T., Schneider, K., Wang, C., Sesterhenn, J. and Liu, H. (2016). Bumblebees minimize control challenges by combining active and passive modes in unsteady winds - Supplement material. *Scientific Reports* **6**, 1–11.
- Reber, T., Dacke, M., Warrant, E. and Baird, E. (2016). Bumblebees perform well-controlled landings in dim light. *Frontiers in Behavioral Neuroscience* **10**, 1–10.
- Reber, T., Vähäkainu, A., Baird, E., Weckström, M., Warrant, E. and Dacke, M. (2015). Effect of light intensity on flight control and temporal properties of photoreceptors in bumblebees. *Journal of Experimental Biology* **218**, 1339–1346.
- Ribbands, C. R. (1949). The Foraging Method of Individual Honey-Bees. *The Journal of Animal Ecology* **18**, 47.
- Riley, J. R., Reynolds, D. R., Smith, A. D., Edwards, A. S., Osborne, J. L., Williams, I. H. and McCartney, H. A. (1999). Compensation for wind drift by bumble-bees. *Nature* **400**:6740 **400**, 126–126.
- Roderick, W. R. T., Cutkosky, M. R. and Lentink, D. (2017). Touchdown to take-off: at the interface of flight and surface locomotion. *Interface Focus* **7**.
- Rogers, B. (2021). Optic Flow: Perceiving and Acting in a 3-D World. *i-Perception* **12**.
- Rohrseitz, N. and Fry, S. N. (2011). Behavioural system identification of visual flight speed control in *Drosophila melanogaster*. *Journal of The Royal Society Interface* **8**, 171–185.
- Roth, E., Sponberg, S. and Cowan, N. J. (2014). A comparative approach to closed-loop computation. *Current Opinion in Neurobiology* **25**, 54–62.
- Serres, J. R., Masson, G. P., Ruffier, F. and Franceschini, N. (2008). A bee in the corridor: centering and wall-following. *Naturwissenschaften* **2008** *95*:12 **95**, 1181–1187.
- Serres, J. R. and Ruffier, F. (2017). Optic flow-based collision-free strategies: From insects to robots. *Arthropod Structure & Development* **46**, 703–717.
- Shackleton, K., Balfour, N. J., Toufaily, H. A., Alves, D. A., Bento, J. M. and Ratnieks, F. L. W. (2019). Unique nest entrance structure of *Partamona helleri* stingless bees leads to remarkable ‘crash-landing’ behaviour. *Insectes Sociaux* **2019** *66*:3 **66**, 471–477.
- Shyy, W., Kang, C.-k., Chirarattananon, P., Ravi, S. and Liu, H. (2016). Aerodynamics, sensing and control of insect-scale flapping-wing flight. *Proceedings of the Royal Society A: Mathematical, Physical and Engineering Science* **472**, 20150712.
- Southwick, E. E. and Southwick, A. K. (1986). Nectar characteristics and phenology of spring bee plants in northwestern New York. *Agriculture, Ecosystems & Environment* **16**, 55–62.
- Srinivasan, M. V. (2011a). Honeybees as a Model for the Study of Visually Guided Flight, Navigation, and Biologically Inspired Robotics. *Physiological Reviews* **91**, 413–460.
- Srinivasan, M. V. (2011b). Visual control of navigation in insects and its relevance for robotics. *Current Opinion in Neurobiology* **21**, 535–543.

- Stöckl, A. L., Kihlström, K., Chandler, S. and Sponberg, S. (2017). Comparative system identification of flower tracking performance in three hawkmoth species reveals adaptations for dim light vision. *Philosophical Transactions of the Royal Society B: Biological Sciences* **372**.
- Sun, M. (2014). Insect flight dynamics: Stability and control. *Reviews of Modern Physics* **86**, 615–646.
- Taylor, G. J., Luu, T., Ball, D. and Srinivasan, M. V. (2013). Vision and air flow combine to streamline flying honeybees. *Scientific Reports* **2013 3:1**, 1–11.
- Taylor, G. J., Ribí, W., Bech, M., Bodey, A. J., Rau, C., Steuwer, A., Warrant, E. J. and Baird, E. (2016). The dual function of orchid bee ocelli as revealed by X-ray microtomography. *Current Biology* **26**, 1319–1324.
- Taylor, G. K., Bacic, M., Bomphrey, R. J., Carruthers, A. C., Gillies, J., Walker, S. M. and Thomas, A. L. R. (2008). New experimental approaches to the biology of flight control systems. *Journal of Experimental Biology* **211**, 258–266.
- Taylor, G. K. and Krapp, H. G. (2007). Sensory Systems and Flight Stability: What do Insects Measure and Why? In *Insect Mechanics and Control*, volume 34, pp. 231–316. Academic Press.
- Tichit, P. (2021). *The visual ecology of bees - Tales of diverse eyes and behaviours*. Ph.D. thesis, Lund University.
- Tichit, P., Alves-dos Santos, I., Dacke, M. and Baird, E. (2020a). Accelerated landing in a stingless bee and its unexpected benefits for traffic congestion. *Proceedings of the Royal Society B* **287**, 20192720.
- Tichit, P., Alves-dos Santos, I., Dacke, M. and Baird, E. (2020b). Accelerated landings in stingless bees are triggered by visual threshold cues. *Biology letters* **16**, 20200437.
- Van Breugel, F. and Dickinson, M. H. (2012). The visual control of landing and obstacle avoidance in the fruit fly *Drosophila melanogaster*. *Journal of Experimental Biology* **215**, 1783–1798.
- Van den Hof, P. M. J. (2012). *System Identification - Data-Driven Modelling of Dynamic Systems*. February. Eindhoven University of Technology, 305 pp.
- Vance, J. T., Altshuler, D. L., Dickson, W. B., Dickinson, M. H. and Roberts, S. P. (2014). Hovering flight in the honeybee *Apis mellifera*: Kinematic mechanisms for varying aerodynamic forces. *Physiological and Biochemical Zoology* **87**, 870–881.
- Wagner, H. (1982). Flow-field variables trigger landing in flies. *Nature* **297**, 147–148.
- Warrant, E. J. (2007). Nocturnal bees. *Current Biology* **17**, R991–R992.
- Warrant, E. J. (2008). Seeing in the dark: vision and visual behaviour in nocturnal bees and wasps. *Journal of Experimental Biology* **211**, 1737–1746.
- Warrant, E. J., Kelber, A., Gislén, A., Greiner, B., Ribí, W. and Wcislo, W. T. (2004).

Nocturnal Vision and Landmark Orientation in a Tropical Halictid Bee. *Current Biology* **14**, 1309–1318.

Wcislo, W. T. and Tierney, S. M. (2009). Behavioural environments and niche construction: The evolution of dim-light foraging in bees. *Biological Reviews* **84**, 19–37.

Whitehead, J. G. (2020). *An examination of the kinematics and behavior of mallards (*Anas platyrhynchos*) during water landings*. Ph.D. thesis, Virginia Tech.

Willmer, P. (2011). *Pollination and Floral Ecology*. Princeton University Press.

Wilson, E. O. (1984). The superorganism. In *Biophilia*, pp. 23–38. Harvard University Press.



Chapter 2

Bumblebees land rapidly and robustly using a sophisticated modular flight control strategy

Pulkit Goyal¹, Antoine Cribellier¹, Guido C.H.E. de Croon², Martin J. Lankheet¹, Johan L. van Leeuwen¹, Remco P.M. Pieters¹, Florian T. Muijres¹

¹ Experimental Zoology Group, Wageningen University & Research, Wageningen, The Netherlands

² Control and Simulation, Faculty of Aerospace Engineering, Delft University of Technology, 2629 HS Delft, The Netherlands

Published as **Pulkit Goyal, Antoine Cribellier, Guido C.H.E. de Croon, Martin J. Lankheet, Johan L. van Leeuwen, Remco P.M. Pieters, Florian T. Muijres** (2021). Bumblebees land rapidly and robustly using a sophisticated modular flight control strategy. *iScience* 24(5), p. 102407. The text and figures were reformatted for this thesis.

Summary

When approaching a landing surface, many flying animals use visual feedback to control their landing. Here, we studied how foraging bumblebees (*Bombus terrestris*) use radial optic expansion cues to control in-flight decelerations during landing. By analysing the flight dynamics of 4, 672 landing maneuvers, we showed that landing bumblebees exhibit a series of deceleration bouts, unlike landing honeybees that continuously decelerate. During each bout, the bumblebee keeps its relative-rate-of-optical-expansion constant, and from one bout to the next, the bumblebee tends to shift to a higher, constant relative-rate-of-expansion. This modular landing strategy is relatively fast compared to the strategy described for honeybees, and results in approach dynamics that is strikingly similar to that of pigeons and hummingbirds. The here-discovered modular landing strategy of bumblebees helps explaining why these important pollinators in nature and horticulture can forage effectively in challenging conditions; moreover, it has potential for bio-inspired landing strategies in flying robots.

2.1 Introduction

Landing is essential for all flying animals, and successful landings require precise control of flight momentum to perform soft touchdown. This is particularly relevant for foraging animals that use flight to routinely collect food. For example, bumblebees can perform more than 1000 landing maneuvers on flowers per hour (Heinrich, 1979). For each landing, the animal uses its sensory-motor system to control deceleration in such a manner that its flight speed reduces to near zero at touchdown, thereby maximizing landing success and minimizing the risk of impact injuries (Foster and Cartar, 2011).

Many flying animals, including birds and insects, use visual motion cues to control approach speed during landings (Lee et al., 1991, 1993; Van Breugel and Dickinson, 2012; Baird et al., 2013; Chang et al., 2016). The animal's motion relative to the landing surface generates a radially expanding optic flow field, in which various features in the image appear to move radially outward from the center of expansion (Gibson, 1955; Edwards and Ibbotson, 2007). Flying animals can use this rate of optical expansion along with the retinal size of an object (Wagner, 1982) or angular position of features in the visual field (Baird et al., 2013) to compute the *relative-rate-of-expansion* (r), or its inverse the instantaneous *time-to-contact* ($\tau = 1/r$, referred to as parameter *tau* in literature) (Lee, 1976; Sun and Frost, 1998; Lee et al., 2009; Balebail et al., 2019). The relative-rate-of-expansion provides information about the ego-motion of the animal and equals the ratio between approach speed V and distance from the landing surface y ($r = V/y$); instantaneous time-to-contact equals the time until contact with the landing surface, should the animal continue to fly at its current flight speed ($\tau = y/V$). The animals can use this relative-rate-of-expansion (or time-to-contact) to gradually reduce their flight speed when approaching the landing surface, and touch down at near-zero speed (Lee et al., 1991, 1993, 2009; Baird et al., 2013).

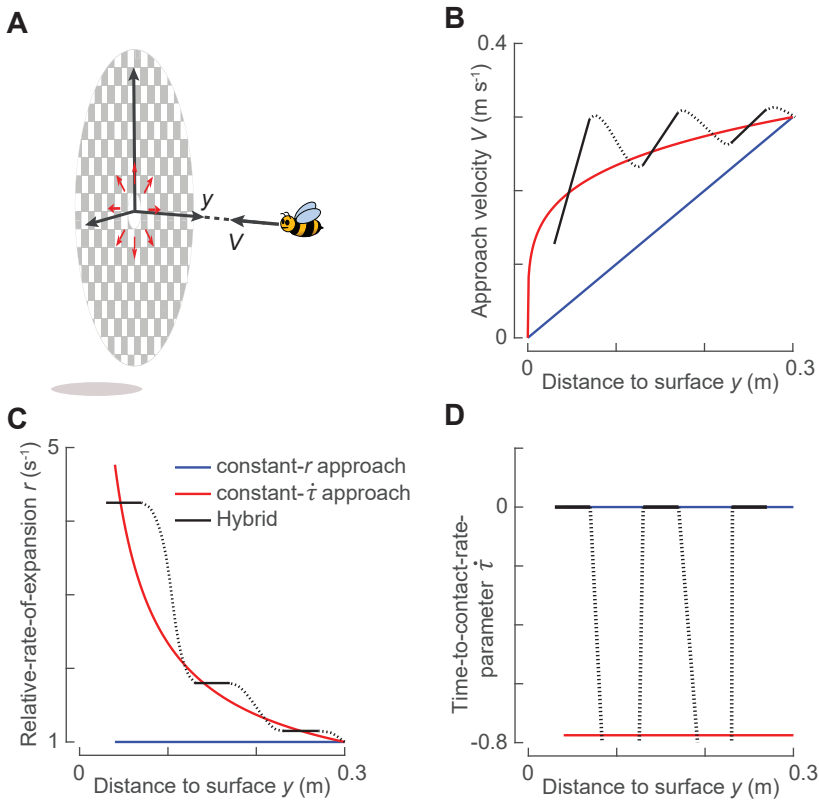


Figure 2.1: Illustration of landing strategies described in honeybees (blue) (Baird et al., 2013), birds (red) (Lee et al., 1991, 1993) and in bumblebees as observed in this study (black). (A) An animal that approaches a vertical landing platform along its axial direction experiences a relative optical expansion rate as symbolized by the red arrows. At time t , the animal is at distance y from the object, has an approach flight velocity V , experiences a relative-rate-of-expansion of $r = V/y$, and has an instantaneous time-to-contact $\tau = y/V$. (B–D) The variation with distance from the landing surface of (B) approach velocity V , (C) relative-rate-of-expansion r , and (D) time-to-contact-rate ($\dot{\tau} = d\tau/dt$) for the constant- r landing approach observed in honeybees (blue) (Baird et al., 2013), the constant- $\dot{\tau}$ landing approach of birds (red) (Lee et al., 1991, 1993), and the here-observed hybrid landing approach of bumblebees (black). The hybrid landing approach consists of constant- r segments (solid lines), separated by transition phases (dotted curves). All results, and particularly the transition phases, are of idealized cases. Because birds and insects differ in size, there are large differences in distances and velocities between these landing strategies. For comparative purpose, we here show idealized versions of the three landing strategies with speeds and distances typical for bumblebees and honeybees, as all landings start at 0.3 m distance from the landing surface with an approach velocity of 0.3 m s^{-1} .

Birds and insects decelerate during landing in different ways (Figure 2.1). Honeybees (*Apis mellifera ligustica*) have been shown to approach a landing surface (up until ~ 7 cm distance from the surface) by keeping the relative-rate-of-expansion constant at a particular set-point (Baird et al., 2013). By doing so, their approach speed decreases linearly with distance to the landing surface (Figure 2.1B). Fruit flies (*Drosophila melanogaster*) and bumblebees (*Bombus impatiens*) have been suggested to use similar strategies (Van Breugel

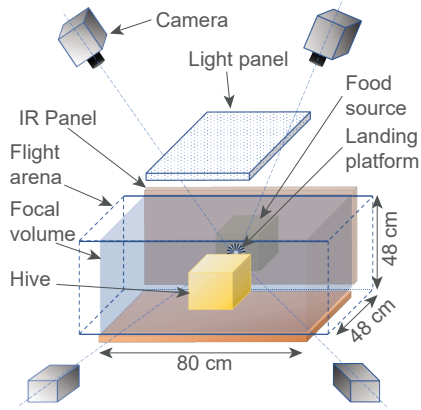
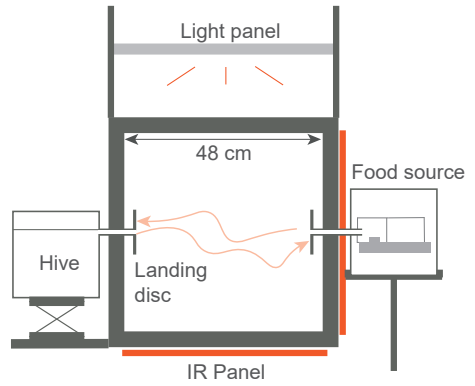
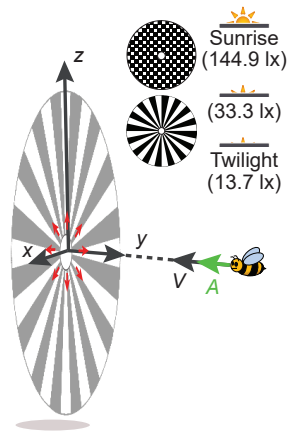
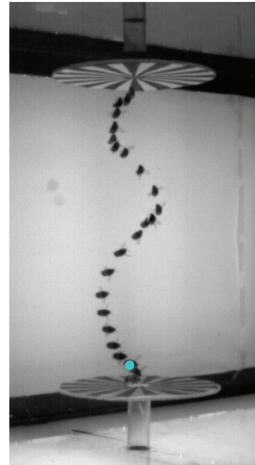
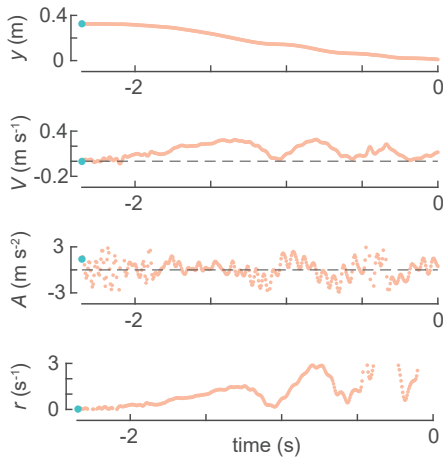
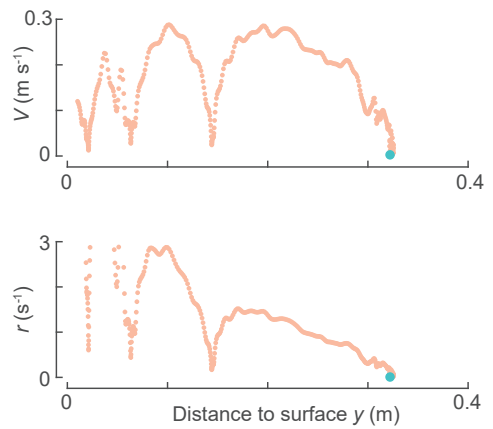
A**B****C****D****E****F***(Caption on the next page.)*

Figure 2.2: Experimental setup, definitions of the landing kinematics parameters, and temporal dynamics of a typical landing maneuver. (A,B) The experimental setup consists of a flight arena with a four-camera high-speed videography system for tracking flying bumblebees, two vertical landing platforms connected to a hive and food source (outside the arena), and a LED light panel for varying the light conditions. (C) The landing kinematics are described in a Cartesian coordinate system with its origin at the center of the landing platform, the z -axis vertically up, and the y -axis aligned along the axis of the disc and pointing into the flight arena. For each landing, we determined the temporal dynamics of approach distance y , velocity $V = -v_y$, and acceleration $A = -a_y$ along the y -axis. The different landing patterns and light conditions used in this study are also shown. (D–F) Flight dynamics of a bumblebee taking off and landing on a spokes landing platform; in all panels, the blue circle denotes the start of the flight sequence. (D) Photomontage from a downward-facing camera of the landing maneuver, at a time interval of ~ 0.1 s. (E) Temporal dynamics of the kinematics parameters (y , V , A) and the optical relative-rate-of-expansion $r = V/y$, where time $t = 0$ s at touchdown. (f) The variation of V and r with perpendicular distance from the platform y .

and Dickinson, 2012; Baird et al., 2013; Chang et al., 2016). Pigeons (*Columba livia*) and hummingbirds (*Colibri coruscans*), on the other hand, approach a landing surface by keeping the derivative of instantaneous time-to-contact constant (Figure 2.1B–D, at a negative value as per sign convention in Figure 2.1A) (Lee et al., 1991, 1993). This derivative of *time-to-contact* ($\dot{\tau}$) is hereafter referred to as *time-to-contact-rate*, and defines how fast the animal decreases its time-to-contact, or increases its relative-rate-of-expansion, during the landing maneuver (Figure 2.1C). Compared to honeybees, the avian landing strategy results in higher approach flight speeds, and hence faster landings (Figure 2.1B). From here on, we refer to the avian landing strategy as the constant- $\dot{\tau}$ strategy, and the honeybees landing strategy as the constant- r strategy. Note that the constant- r strategy is a special case of the constant- $\dot{\tau}$ strategy whereby $\dot{\tau}$ is maintained at a value of zero ($\dot{\tau} = 0$).

Here, we study the landing maneuver dynamics of bumblebees (*Bombus terrestris*). Bumblebees are important pollinators in both nature and horticulture (Fontaine et al., 2006; Velthuis and Doorn, 2006; Joar Hegland and Totland, 2008) owing to their ability to forage in a wide range of environmental conditions including relatively low temperatures (Corbet et al., 1993) and limited light conditions such as during twilight hours (Reber et al., 2015, 2016). Moreover, foraging bumblebees are efficient pollinators as they are able to visit more than 1000 flowers per hour (Heinrich, 1979). During such fast foraging actions, bumblebees tend to rapidly move from flower to flower in a single flower patch, followed by longer distance flights between patches. As a result, the average distance traveled between flowers in a fresh clover field is approximately 0.33 m (Heinrich, 1979).

To reproduce these foraging conditions, we trained bumblebees to routinely fly back and forth between two vertical landing platforms, one connected to their colony and the other to a food source (Figure 2.2A,B). We placed the landing platforms 0.34 m apart, which is similar to an average distance of 0.33 m traveled by bumblebees between landings when foraging on a fresh flower patch (Heinrich, 1979). The setup was placed in a large flight arena (Figure 2.2A,B), allowing the bumblebees to also exhibit the larger distance flights that resemble those between flower patches (Heinrich, 1979).

Using machine-vision techniques, we then tracked 10,005 landing maneuvers of bumblebees. This data set consists of 2792 landings performed directly after taking-off from the opposite platform or the ground, and 7213 landings following free-flight. Moreover, to test how environmental conditions affect these landings, we varied the light intensity in three steps from twilight to sunrise conditions, and used two landing platforms with relatively low and high optical expansion information (Figure 2.2C).

We used two approaches to analyze the temporal deceleration dynamics of the landings. First, we analyzed how the average of multiple landing approaches varied among treatments (light condition and landing platform type) and type of landing maneuvers (landing after take-off and from free-flight). This analysis strategy is similar to the one used previously to study the landing dynamics of bumblebees (*B. impatiens*) and honeybees (Baird et al., 2013; Chang et al., 2016). Second, we analyzed how the flight dynamics of individual landing maneuvers vary among the treatments and between landings after take-off and from free-flight. Hereafter, we refer to the former and the latter as the *average-per-treatment* and *per-track* analyses methods, respectively.

Our average-per-treatment analysis provides similar results as reported previously (Baird et al., 2013; Chang et al., 2016), showing that *on average* landing bumblebees decelerate linearly with reducing distance, in all tested conditions. This suggests that bumblebees use a constant- r landing strategy during both landings after take-off and from free-flight. In contrast, our per-track analysis shows that *individual bumblebees* do not do so, as they exhibit short intervals of deceleration at different set-points of relative-rate-of-expansion (Figure 2.1). During each set-point, bumblebees keep their relative-rate-of-expansion constant, and they increase their set-point value as they reach closer to the surface. In fact, this increase in set-points of relative-rate-of-expansion with decreasing distance from the landing surface is governed on an average by a constant- $\dot{\tau}$ law, with $\dot{\tau}$ values similar to that of birds. Thus on average, landing bumblebees approximate the landing strategies of birds by adjusting their constant- r set-point in discrete steps as they approach the landing surface. Hence, this modular landing strategy of bumblebees can best be characterized as a hybrid between the constant- r and constant- $\dot{\tau}$ strategies described for honeybees and birds, respectively.

2.2 Results

We trained a hive of bumblebees (*B. terrestris*) to forage for food in a flight arena equipped with a real-time automatic machine-vision based three-dimensional insect tracking system (Straw et al., 2011) (Figure 2.2A). We placed a food source and hive on either side of the flight arena, and connected them to two vertical landing platforms (0.18 m diameter). To collect food, the foraging bumblebees flew between the landing platforms and walked through the small aperture (0.02 m diameter) in the middle of the platform to access either the hive or the food source (Figure 2.2B).

During the experiments, we used landing platforms with either checkerboard or spoke patterns, as they provide a high and low amount of optical expansion flow information, respectively (Figure 2.2C). In addition, we varied the light intensity in the setup in three levels ranging from twilight to sunrise, referred to as low (13.7 lx), medium (33.3 lx) and high (144.9 lx) light conditions. Bumblebees continued to forage in all light conditions, allowing us to test how landing strategy varied throughout the natural variation of challenging light conditions experienced by foraging bumblebees (Figure 2.2C). Light and platform conditions were systematically varied such that all combinations were tested (Table S2.1).

We placed the two landing platforms 0.34 m apart from each other, such that it resembles the 0.33 m average distance travelled between flowers by bumblebees foraging in a fresh clover patch (Heinrich, 1979). The flight arena ($3 \times 0.48 \times 0.48$ m; length \times width \times height) was large enough to not only capture landings directly after take-off from the other platform, but also landings from free-flight (Figure S2.1). These landings represent those exhibited by bumblebees when travelling between flower patches, or when travelling between hive and foraging site.

We used the insect tracking system to determine the three-dimensional spatial-temporal dynamics of body location in 10,005 flight maneuvers of bumblebees approaching the landing platforms. Out of 10,005 landing approaches, 2792 landings followed after a take-off from the ground or the opposite platform (Figures 2.2D–F), and 7213 landings occurred after free flight (Figures 2.3A,B). Irrespective of how bumblebees initiated their landing, most approach flights consisted of both acceleration and deceleration phases (Figures 2.2E). We hereafter focussed only on the deceleration phases as we aimed to find out how bumblebees slowed down during their landing maneuver. For the landings following take-off, the flight speed at the start of the landing maneuver was $U_{\text{start}} = 0.11$ [0.04, 0.24] m s^{-1} (median [first quartile, third quartile], $n = 2792$ landings), and for landings following free-flight this was $U_{\text{start}} = 0.34$ [0.21, 0.49] m s^{-1} ($n = 7213$ landings) (Figure S2.2). The free-flight landings were thus initiated at flight speeds similar to those observed in previous bumblebee studies, and sometimes even surpassed them (Reber et al., 2015; Chang et al., 2016).

The average flight kinematics of all recorded landing maneuvers

For each landing approach, we calculated the temporal dynamics of the following state variables (Figure 2.2D–F): 3D-position ($x(t), y(t), z(t)$), approach velocity ($V(t) = -dy(t)/dt$) and approach acceleration ($A(t) = -d^2y(t)/dt^2$) perpendicular to the landing platform, and the relative-rate-of-expansion that a bumblebee experiences due to its motion perpendicular to the landing platform ($r(t) = V(t)/y(t)$).

On average, bumblebees performed the landing maneuver in a direction perpendicular to the platform (Figures 2.3A,B). During their mean landing maneuver, they advanced towards the platform by first gradually increasing their approach velocity (V), followed by

a deceleration phase during which they decreased their approach velocity ($0.04 \text{ m} \leq y \leq 0.11 \text{ m}$). As previously observed in honeybees (Baird et al., 2013) and suggested for bumblebees (*B. impatiens*) (Chang et al., 2016), the average decelerating bumblebee decreased its approach velocity approximately linearly with distance, thus keeping the relative-rate-of-expansion nearly constant at a set-point r^* (Figure 2.3C).

We used a linear mixed-effects model to test how this set-point of relative-rate-of-expansion r^* differed between tested treatments (light condition and landing platform) and between landings following take-off and free-flight (landing type) (see Methods). This showed that the set-point of relative-rate-of-expansion r^* differed significantly between both light conditions and landing type, but r^* did not differ between the landing patterns (Table S2.2). The relative-rate-of-expansion set-point was higher in brighter light conditions (Figures 2.3C,D and S2.3), and it was higher in landings after take-off than in landings from free-flight (Figure S2.3). It implies that, in the presence of brighter light conditions and when the landing followed take-off, bumblebees decelerated more quickly during the landing maneuver, thus allowing for higher approach velocities and more rapid landings.

The expansion-rate set-points of the landing maneuvers across all tested conditions were on average $r^* = 2.32 [0.24] \text{ s}^{-1}$ and $r^* = 3.02 [0.24] \text{ s}^{-1}$ for the free-flight landings and the landings following take-off, respectively (mean [standard error], $n = 6$ conditions). These values are similar to the expansion-rate set-points observed in landings of honeybees (Baird et al., 2013), and the set-points suggested for *Bombus impatiens* landings (Chang et al., 2016).

The flight kinematics of individual landing maneuvers

Although the average approach dynamics suggests that bumblebees use a constant relative-rate-of-expansion landing strategy as described previously (Chang et al., 2016), we observed that individual flight trajectories deviated often significantly from the average constant relative-rate-of-expansion track (Figure 2.3C). In fact, many landing maneuvers consisted of multiple deceleration phases (Figure 2.2D–F) instead of a single continuous one. To analyse these individual flight maneuvers separately, we used an in-house developed automatic detection algorithm to extract the segments of the landing maneuvers in which bumblebees kept the relative-rate-of-expansion constant (Figure 2.4A, see Methods for details).

Hereafter, we refer to the track segments identified using our detection algorithm as constant- r segments and characterize them by their average values of the four state variables (y^* , V^* , A^* , r^*), displacement normal to the platform (along y -axis) during a single constant- r segment (Δy_1) and displacement normal to the platform for a set of consecutive constant- r segments (Δy_2) (Δy_1 and Δy_2 are annotated in Figure 2.4A). We use r^* as an estimate of the set-point of relative-rate-of-expansion that the bumblebee aims to hold constant (see Methods for explanation).

The output of the constant- r detection algorithm depends on a setting parameter f ,

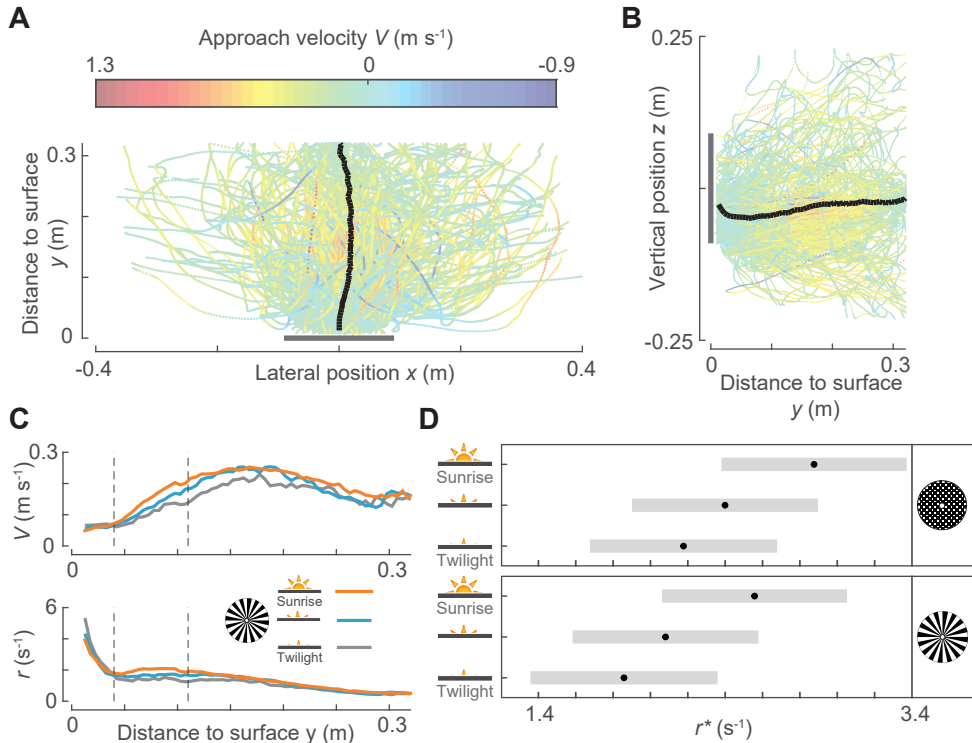


Figure 2.3: The average flight kinematics of bumblebees approaching a landing platform. (A,B) Top and side views of every 35th flight trajectory of all 10,005 recorded landing maneuvers ($n = 288$ tracks), color-coded with approach velocity V . The black curve shows the mean trajectory of all 10,005 recorded maneuvers, and the landing platform is shown in gray. (C,D) The average approach kinematics of bumblebees. (C) The approach velocity V and relative-rate-of-expansion r versus perpendicular distance from the platform y for bumblebees approaching a spoke pattern for landings initiated from free-flight in low, medium and high light conditions (in gray, blue and orange, respectively). The y -segment ($0.04 \text{ m} \leq y \leq 0.11 \text{ m}$) for which the data is used to find the mean relative-rate-of-expansion r^* is highlighted in dashed black lines. (D) r^* as predicted by the linear mixed-effects model for the three tested light conditions and two landing patterns for landings of free-flying bumblebees (see Methods). The mean relative-rate-of-expansion increases with increase in light intensity, but did not differ significantly between the two tested landing platforms (Table S2.2). Black dots depict estimated means and gray bars are 95% confidence intervals. (See also Figures S2.2, S2.3 and Table S2.2).

whereby higher f leads to the detection of more (and wider) constant- r segments, and thus fewer false negatives and more false positives (see Methods for details). We therefore performed a sensitivity analysis by systematically varying the factor f from 0.25 to 2.5 to determine its effect on the distribution of set-points identified and their dynamics with distance described later in this section (see Methods).

For $f = 1$, we identified 6,291 constant- r segments within the 4,672 landing maneuvers (1,359 and 3,313 landings starting from take-off and free-flight, respectively) out of a total of 10,005 maneuvers (Figures 2.4B–D and S2.1). For $f = 2.5$, the number of constant- r segments increased to 16,322 constant- r segments identified within 7,951

landing maneuvers. Although the number of constant- r segments increased with f , the distribution of constant- r segments (including their dynamics with distance) remained essentially unaltered throughout our tested range of f , so here we report all results for factor $f = 1$ (see Methods and Table S2.1 for results at the other f -values).

Landing maneuvers consist of multiple flight segments with constant- r

The set-points of relative-rate-of-expansion varied considerably among segments (Figures 2.4B and S2.4) and their observed distribution can be approximated by the gamma distribution (median $r^* = 2.15 \text{ s}^{-1}$, $a = 3.59 [3.47 - 3.71]$, $b = 0.65 [0.63 - 0.67]$, mean [95% confidence intervals], see Methods for details).

For the 6, 291 identified constant- r segments, the displacement during a single segment (Figure 2.4B) was $\Delta y_1 = 0.035 \pm 0.017 \text{ m}$ (mean \pm standard deviation), which consisted on average of only 13% of the total displacement (along y -direction) during the complete approach maneuver ($\Delta y = 0.266 \pm 0.063 \text{ m}$, Figure 2.4B). This suggests that bumblebees, while approaching a landing platform, do not fly at a single set-point of the relative-rate-of-expansion, like observed in the average-per-treatment analysis. Instead, they fly at a constant relative-rate-of-expansion for relatively short travel distances (0.035 m), after which they likely switch to a new set-point of relative-rate-of-expansion.

Landing bumblebees increase the constant- r set-points when approaching the landing platform

We tested how bumblebees adjusted these set-points of relative-rate-of-expansion within a landing approach by analysing the transitions from one set-point to the next, for all landing maneuvers in which we detected multiple constant- r segments (Figure 2.5). Out of 4, 672 landing maneuvers, 1015 maneuvers were identified with two constant- r segments (examples in Figures 2.5A,B), and 283 maneuvers with three or more constant- r segments (example in Figure 2.5C).

The displacement during two consecutive constant- r segments (Figure 2.4B) was on average $\Delta y_2 = 0.114 \pm 0.049 \text{ m}$ ($n = 1015$ landings), and thus explained on average 40% of the total approach displacement (Figure 2.3D). Because the mean approach displacement during a single constant- r segment (Δy_1) was 13%, bumblebees traversed approximately $1/3^{\text{rd}}$ of the displacement during two consecutive constant- r segments (Δy_2) while transitioning from one set-point to another. Of all transitions between two consecutive constant- r segments, 72% were from a lower constant- r set-point value to a higher value, and the average set-point increase was $r^* = 1.05 \pm 0.93 \text{ s}^{-1}$ ($n = 1050$ transitions). Thus, during a transition, bumblebees tend to increase the set-point of relative-rate-of-expansion (on average 113%), and a set of two consecutive constant- r segments represents a significant proportion (40%) of the total displacement during a landing maneuver. These

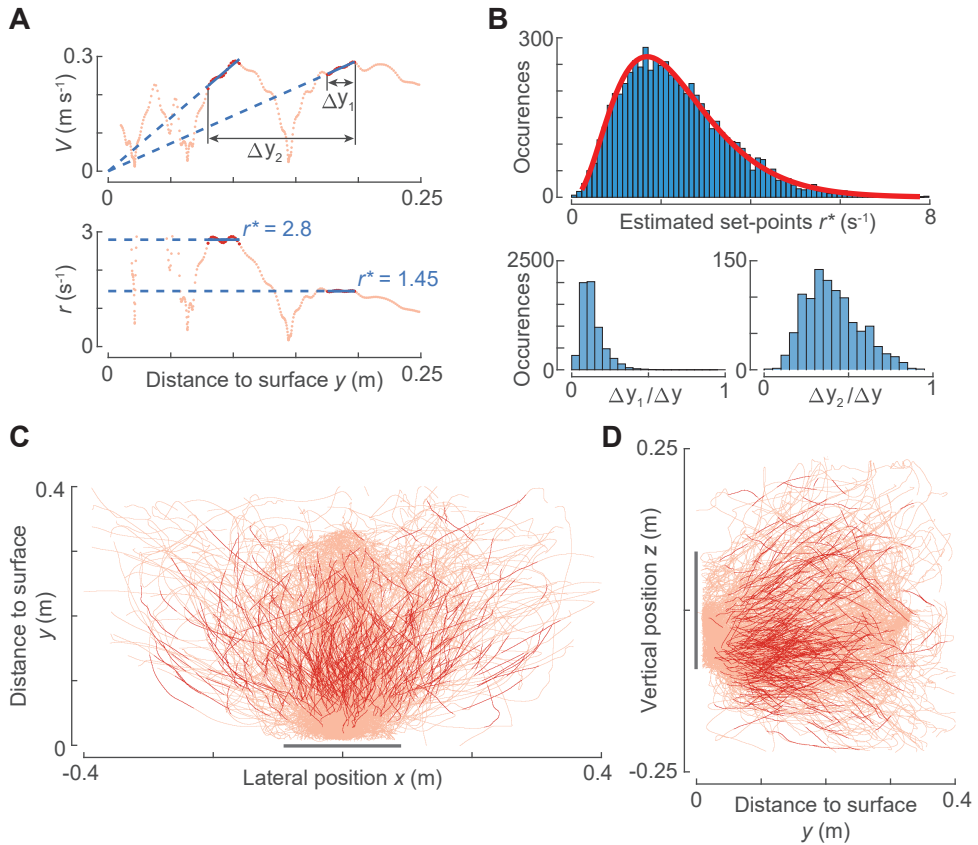


Figure 2.4: Landing bumblebees decelerate at a range of set-points of relative-rate-of-optical-expansion (r^*). (A) The variation of approach velocity V and relative-rate-of-expansion r with perpendicular distance from the platform y of the landing maneuver in Figures 2.2D–F. The segments in which r is identified as (nearly) constant are highlighted in dark red. The corresponding relative-rate-of-expansion set-points r^* are indicated by the dashed blue lines (as slope and ordinate values in the V - y and r - y graphs, respectively). (B) Top panel: histogram of the set-points of relative-rate-of-expansion r^* for all identified constant- r segments ($n = 6291$ segments). Bottom panels: histograms of the ratio of displacement travelled by bumblebees during constant- r segments (Δy_1 or Δy_2) to the total displacement normal to the landing platform (Δy). Left shows the relative distance travelled during a single constant- r segment $\Delta y_1/\Delta y$ ($n = 6291$ segments), and right shows the relative distance travelled during two consecutive constant- r segments $\Delta y_2/\Delta y$ ($n = 1015$ segments), as defined in the panel (A). (C,D) Top and side views of 470 tracks (every 10th of 4672 tracks) used to study the landing dynamics. The complete flight tracks are shown in orange, and the track segments in which the optical expansion rate is kept constant are highlighted in red. The landing platform is shown in gray. (See also Figures S2.1, S2.4 and Table S2.3).

results are consistently observed for each tested treatment and for both landing types (after take-off and from free flight) (Table S2.3).

The stepwise increase of the relative-rate-of-expansion set-points occurs at a constant time-to-contact-rate

The dynamics of increasing set-points of relative-rate-of-expansion with decreasing distance from the landing platform (Figure 2.5) resembles the trend observed in birds that use the constant- $\dot{\tau}$ landing strategy (Figure 2.1C). We tested whether bumblebees comply to this strategy by fitting a linear mixed-effects model (see Methods) to both the dataset with the maneuvers containing multiple constant- r segments (Figure 2.5D, Table S2.4, $n = 2917$ segments) and the complete dataset (Figure 2.6A–C, Table S2.5, $n = 6, 291$ segments). The model predicts an average time-to-contact-rate $\dot{\tau} = -0.78$ and $\dot{\tau} = -0.87$ for the reduced dataset and complete dataset, respectively. Thus, bumblebees increase the set-points of relative-rate-of-expansion while approaching the landing platform at a constant time-to-contact-rate. The resulting average time-to-contact-rate at which they do this is strikingly similar to that observed in birds ($\dot{\tau} = -0.76$ for hummingbirds (Lee et al., 1991) and $\dot{\tau} = -0.72$ for pigeons (Lee et al., 1993)).

Our linear mixed-effects model analysis also allowed us to test how the landing strategy differed with light intensity, optical expansion information of the landing platform, and between landings performed from free-flight and landings that followed take-off (Figure 2.6, Table S2.5). The minimal linear mixed-effects model included effects of all treatments and landing type, but no interactions between these (see Methods for details). Therefore, we here discuss the effects of light intensity, landing pattern and landing type consecutively.

In high light intensities, bumblebees approach the landing platform at higher speeds

Our linear mixed-effects model analysis shows that the relative-rate-of-expansion set-point differed significantly between all light conditions, but the set-point r^* did not differ significantly with the interaction between light intensity and y^* (Table S2.5). As a result, the model predicts that for an average landing maneuver, the relative-rate-of-expansion set-point at the average distance $y^* = 0.15$ m equals $r^* = 1.68 [0.05] \text{ s}^{-1}$, $r^* = 1.82 [0.05] \text{ s}^{-1}$ and $r^* = 1.99 [0.05] \text{ s}^{-1}$ in low, medium and high light condition, respectively (mean [standard error]). This corresponds to an average approach flight speed of $V^* = 0.25 [0.01] \text{ m s}^{-1}$, $V^* = 0.27 [0.01] \text{ m s}^{-1}$ and $V^* = 0.30 [0.01] \text{ m s}^{-1}$ in low, medium and high light condition, respectively. In contrast, the variation of r^* with y^* did not change with light condition, showing that the governing time-to-contact-rate for adjusting set-points with distance did not change with light intensity. Thus, bumblebees approached the landing platform on average 19% faster in the bright sunrise light conditions than in twilight, but the bumblebees slowed down at a similar rate in various light conditions.

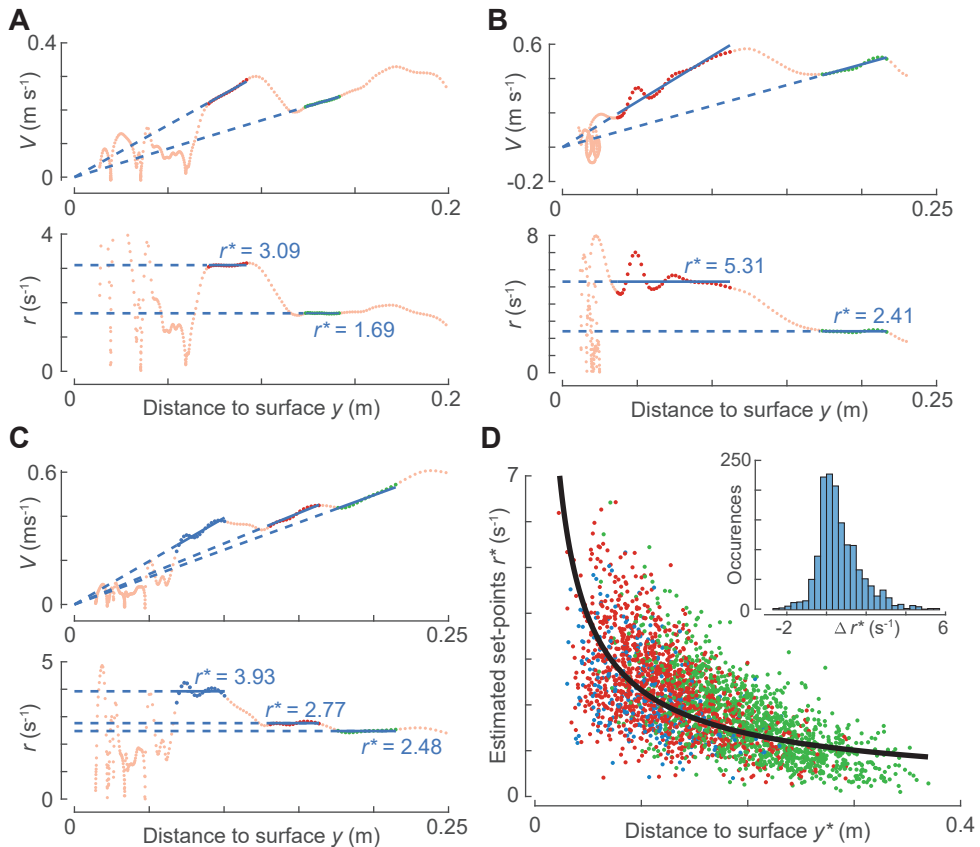


Figure 2.5: Bumblebees stepwise increase their set-points of relative-expansion-rate during a landing approach. (A–C) Examples of landing approaches that start from a free-flight condition and contain multiple set-points of relative-rate-of-expansion, as shown by the variation of approach velocity V and relative-rate-of-expansion r with perpendicular distance from the platform y . The track segments in which r is approximately constant are highlighted in green (first observed set-point), red (second set-point) and blue (third or higher set-point). The magnitude of the relative-rate-of-expansion set-points r^* are indicated by the dashed blue lines (as slope and ordinate values in the V - y and r - y graphs, respectively). (D) Variation of relative-rate-of-expansion set-point r^* with distance from the platform y^* for landing maneuvers with multiple constant- r segments. The first set-points in each track is shown in green, the second set-points in red, and third or higher set-points in blue. The average variation of r^* with y^* as estimated from the linear mixed-effects model is shown in black (see Methods). The inset shows a histogram of the change in relative-rate-of-expansion set-point between two consecutive constant- r segments Δr^* ($n = 1456$). (See also Table S2.3, S2.4).

Bumblebees brake more rapidly when landing on a platform with low optical expansion information

The statistical results related to the effect of landing platform pattern on the landing dynamics is opposite to that of light intensity: the relative-rate-of-expansion set-point at the mean distance $y^* = 0.15$ m did not differ significantly between landings on the different platforms, but did differ significantly with the interaction between landing pattern

and distance from the platform y^* ($p = 0.00025$, Table S2.5). Based on this, the statistical model predicts that, for an average bumblebee, the time-to-contact-rate is 11% smaller when approaching a checkerboard landing platform with high optical expansion information ($\dot{\tau} = -0.92 [0.02]$) than when approaching a spoke landing platform with low optical expansion information ($\dot{\tau} = -0.83 [0.02]$).

This shows that bumblebees approaching a spoke landing platform with low optical expansion cues slowed down more quickly (higher $\dot{\tau}$) than bumblebees landing on a checkerboard platform with high optical expansion information. This results in lower approach speeds close to the landing platform, suggesting that bumblebees land more carefully on the less conspicuous platform.

Bumblebees landing from free-flight brake more rapidly than bumblebees landing after take-off

We finally tested how the landing strategy differed between landings that were performed directly after taking-off and landings from free-flight. The linear mixed-effects model shows that the relative-rate-of-expansion set-point differed significantly with both landing type and the interaction between landing type and y^* ($p < 0.0001$, Table S2.5). The model predicts that an average bumblebee slowed down more quickly (higher $\dot{\tau}$) when landing from free-flight ($\dot{\tau} = -0.73 [0.01]$) than when landing after take-off ($\dot{\tau} = -1.01 [0.02]$) (Figure 2.6C). This shows that bumblebees that land from free-flight start their approach flight at a higher approach velocity, but because they decelerate more quickly, they end their approach at a lower approach velocity (Figure 2.6C). As a result of this rapid deceleration, the approach velocity close to the platform ($y^* = 0.05$ m) is 31% lower when landing from a free-flight ($V^* = 0.197 [0.006]$ m s⁻¹) than when landing after take-off ($V^* = 0.287 [0.010]$ m s⁻¹).

2.3 Discussion

Here we studied how bumblebees (*B. terrestris*) decelerate to land smoothly when performing foraging flights. This includes landings that directly follow after taking-off and landings that are initiated from a free-flight. These two landing types represent two common but possibly distinct landing maneuvers. The landing directly after take-off is performed by foraging bumblebees at rates of up to a 1000 times per hour when moving between flowers in a single flower patch (Heinrich, 1979); the landing from free-flight is commonly performed when moving between flower patches and the hive.

To study the landing dynamics of both types of maneuvers, we trained bumblebees to forage for food. They landed on two vertical platforms directly from free-flight (7, 213 landings) or after taking off from the opposite platform or ground (2, 792 landings). We placed the landing platforms 0.34 m apart, similar to the average 0.33 m distance between consecutively-visited fresh flowers by bumblebees within a patch (Heinrich, 1979).

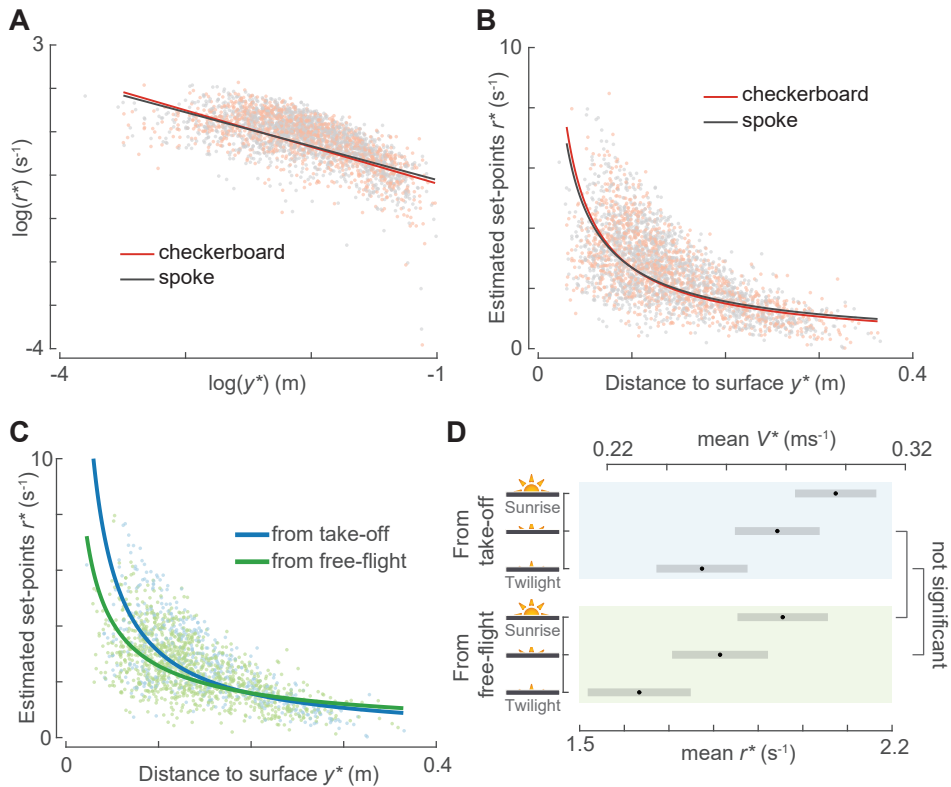


Figure 2.6: In all tested conditions, landing bumblebees stepwise increase their set-points of relative-expansion-rate such that they approximate a constant time-to-contact-rate landing strategy. (A,B) The set-points of relative-rate-of-expansion r^* versus perpendicular distance from the landing platform y^* , for all detected constant- r segments in landings of freely-flying bumblebees in sunrise light, when landing on a checkerboard platform (red) or a spoke platform (gray). Data are shown in the log-transformed domain (A) and the untransformed domain (B). (C) Variation of r^* with y^* for all detected constant- r segments of landings on a spoke landing platform in sunrise light, when initiated from take-off (blue) and from free-flight (green). (A–C) Data points show all detected constant- r segments in the condition defined by color, and the solid lines show the linear mixed-effects model fits in the log transformed domain for the same condition. (D) The relative-rate-of-expansion r^* and approach flight speed V^* at the average distance from the landing platform ($y^* = 0.15$ m), as predicted by the model for landings directly after take-off (top) and from free flight (bottom), and at low, medium and high light conditions. The approach speed at $y^* = 0.15$ m increases with increasing light intensity and is higher for landings initiated after take-off (Table S2.5 for p -values). Black dots depict estimated means and gray bars are 95% confidence intervals. Non-significant differences are indicated on the right. Equivalent data for the other combinations of environmental conditions and landing types is available in Table S2.5.

We systematically varied the visual pattern on the landing platforms (low and high optic expansion information), and we varied the environmental light intensities from twilight to sunrise conditions. Although we use vertical landing platforms, the deceleration strategy described in our study is based on an optic flow profile generated for landings on surfaces of any orientation and for any direction of approach (Baird et al., 2013).

Average landing approach kinematics versus approach kinematics of individual bumblebees

To examine how bumblebees decelerated during a landing approach, we use two different analysis methods, referred to as average-per-treatment and per-track analyses methods.

In the average-per-treatment method, we first analyzed the mean of all 10,005 approaches and selected a range of distance interval ($0.04 \text{ m} \leq y \leq 0.11 \text{ m}$) in which the approach velocity towards the platform decreased proportionately with distance. Within this distance range, we then analyzed how the mean relative-rate-of-expansion varied with tested treatment (landing pattern and light intensity), and between landing type (from take-off or from free flight).

In the per-track analysis method, we first extracted the segments in which a bumblebee kept its relative-rate-of-expansion constant (this constant is referred to as the relative-rate-of-expansion set-point) within each landing approach and then analyzed how the mean relative-rate-of-expansion of all identified segments vary with the distance to the landing surface, for different treatments, and between landing types. It should be noted that the per-track analysis is inclusive of average-per-treatment analysis i.e., if individual landing maneuvers are similar to the average landing approach, per-track analysis will identify constant- r segments only near the distance interval selected for the average-per-treatment analysis and will yield negligible dependence of set-point on distance.

Using the average-per-treatment analysis – a method used in the previous studies (Baird et al., 2013; Chang et al., 2016) – we found that bumblebees on average approached the platform by first increasing their velocity and then decelerated by decreasing their velocity linearly with distance to make a soft touchdown. This suggests that our bumblebees approach the landing platform by flying at a constant relative-rate-of-expansion, as has also been described in honeybees (Baird et al., 2013) and suggested in other bumblebees (Chang et al., 2016).

The mean set-point of relative-rate-of-expansion differed between light conditions and landing type, but not between landing platforms (Figures 2.3C,D and S2.3). At higher light intensities and for landings initiated from take-off, the rate-of-expansion set-point was higher, resulting in a higher mean approach velocity. As a result, landings after take-off were on average 30% faster than landings initiated from free flight, and landings in the highest light condition (sunrise) were on average 29% faster than in the lowest twilight condition.

The mean expansion-rate set-point at sunrise is similar to that of honeybees (8% lower for checkerboard pattern and 15% lower for spoke pattern) (Baird et al., 2013), but 34% lower than for bumblebees (*B. impatiens*, unreported and estimated from Figure 2A in Chang et al. 2016). This striking difference in expansion-rate set-point could be due to differences in light conditions, as we here showed that light intensity affects the relative-rate-of-expansion set-point. However, we cannot test this because light intensity was not

reported in the previous studies (Baird et al., 2013; Chang et al., 2016). A second explanation could be the differences in maximum distance available in front of the landing platform, which was 0.41 m in our set-up, 1.5 m for the honeybees study (Baird et al., 2013) and 6 m for the *B. impatiens* study (Chang et al., 2016). Although our free-flight landings are initiated at speeds similar to those of *B. impatiens* (Chang et al., 2016), a new study in which landing distance is varied systematically would be needed to test this.

The hybrid landing strategy of short-distance landing maneuvers in bumblebees

The average-per-treatment analysis provided a useful insight into the mean approach dynamics but failed to capture the approach dynamics of all individual landing maneuvers. Specifically, it missed the deceleration phases that were spread across a landing approach. To capture all deceleration phases, we used our custom-developed per-track analysis method. Using this analysis, we extracted 6, 291 segments (within the 4, 672 landings) in which individual bumblebees kept their relative-rate-of-expansion constant (constant- r segments); for each segment, we estimated the relative-rate-of-expansion set-point at which the animal flew. The distribution of these 6, 291 set-points reveals that landing bumblebees exhibit a skewed distribution of set-points in all tested treatments (Figures 2.4B and S2.4). The observed distribution of set-points encompasses the set-points from average-per-treatment analyses and the ones observed for honeybees and bumblebees in earlier studies (Baird et al., 2013; Chang et al., 2016).

To determine the switching dynamics of constant- r set-points within a landing approach, we analyzed the set-points variation with distance for 1, 298 approaches in which we detected more than one constant- r segment (Figure 2.5D). We found that, within a landing approach, bumblebees most often switched from a lower set-point of relative-rate-of-expansion to a higher one, as this was the case in 72% of all observed transitions, and the average set-point after transition was 113% higher than before. This shows that the observed wide range of set-points of relative-rate-of-expansion are not due to the individual differences between bumblebees, but that the bumblebees can exhibit more than one constant- r set-point within a single landing approach. Moreover, these dynamics are very similar between tested treatments and landing types (Table S2.3), indicating that the internal process of switching the set-points within a landing approach happens with the same probability irrespective of both environmental conditions and landing type.

To determine how bumblebees collectively adjusted their relative-rate-of-expansion set-points as they approached the landing platforms, we tested the variation of set-points of relative-rate-of-expansion (r^*) with distance to the platform (y^*) for the 6, 291 detected constant- r segments. We found a linear relationship between the log transformations of r^* and y^* , suggesting that bumblebees increase their set-points during deceleration at a constant time-to-contact-rate (Figures 2.1B,C and 2.6A). These estimates of time-to-contact-

rate in bumblebees varied from -0.690 to -1.054 for all tested treatments and landing types, and are thus similar to those observed in hummingbirds ($\dot{\tau} = -0.76$) (Lee et al., 1991) and pigeons ($\dot{\tau} = -0.72$) (Lee et al., 1993) (the reported time-to-contact-rates from literature are transformed to sign convention depicted in Figure 2.2C). The key difference between deceleration strategies of bumblebees and birds is that birds regulate their relative rate-of-expansion continuously at a negative time-to-contact rate, whereas bumblebees adjust the set-points of relative rate-of-expansion in steps at a negative time-to-contact-rate, thereby discretely approximating the constant- $\dot{\tau}$ strategy of birds (Figure 2.1).

The adjustment of set-points with distance is observed in datasets with landing maneuvers in which we detected only multiple constant- r segments (Table S2.4), only a single constant- r segment (Table S2.6) and when both datasets were pooled together (Table S2.5). This strongly indicates that tracks containing only one constant- r segment may also have more constant- r segments that were not detected due to the limitations of our constant- r extraction method. These limitations can occur due to the factor f that restricts the variation of r allowed in a constant- r segment (see Methods), or the fundamental basis of the per-track analysis methodology that detects only the set-points that bumblebees have been able to reach and follow in their trajectory. We overcome both of these limitations by using a large dataset with thousands of landing approaches.

Here, we conclude that bumblebees effectively use a hybrid between the constant- r landing strategy described in honeybees (Baird et al., 2013) and the constant- $\dot{\tau}$ landing strategy observed in birds (Lee et al., 1991, 1993), as they exhibit several segments of constant- r and regulate the set-points of these constant- r segments in a constant- $\dot{\tau}$ manner.

The hybrid landing strategy is faster than a constant- r landing strategy

It has been suggested that the constant- $\dot{\tau}$ deceleration strategy used by birds results in faster approach flights than the constant- r strategy used by honeybees (Baird et al., 2013). We tested how the here-described hybrid landing strategy compares to both strategies. For this, we calculated for the 1,008 landings with two consecutive constant- r segments, the hybrid-to-constant- r speed ratio and the hybrid-to-constant- $\dot{\tau}$ speed ratio as U_H/U_r and $U_H/U_{\dot{\tau}}$. Here, U_H is the average flight speed during the combined flight segment, and U_r and $U_{\dot{\tau}}$ are the equivalent speeds if the bumblebee would have used the constant- r and constant- $\dot{\tau}$ strategy, respectively (see Methods for details). The constant- r and constant- $\dot{\tau}$ are based on the first set-point in a set of two consecutive constant- r segments and average time-to-contact-rate observed in our dataset, respectively. For 1,008 landings with two detected constant- r segments, the hybrid-to-constant- r speed ratio is $U_H/U_r = 1.16 \pm 0.69$ and the hybrid-to-constant- $\dot{\tau}$ speed ratio is $U_H/U_{\dot{\tau}} = 0.88 \pm 0.55$. This shows that the here-described hybrid landing strategy of bumblebees is 16% faster than if the bumblebee would use the equivalent constant- r strategy, but 12% slower than if it would continuously

fly at a constant- $\dot{\tau}$. The reduction in effective flight speed relative to the true constant- $\dot{\tau}$ observed in birds is because bumblebees keep relative-rate-of-expansion constant for some time and experience transition dynamics between two consecutive set-points.

Robustness of the hybrid landing strategy of bumblebees

To test the robustness of hybrid strategy, we offered the bumblebees different light conditions ranging from twilight to sunrise and allowed them to land on two different landing platforms, one with a checkerboard pattern and one with a spoke pattern. We find that bumblebees robustly exhibit this strategy in all tested conditions, but with some differences.

During constant- r segments, our statistical model predicts that at the average distance from the landing platforms ($y^* = 0.15$ m), bumblebees fly slower at lower light conditions, with differences ranging from 8% to 18% among different tested light conditions and for two landing types (Figure 2.6D, Table S2.5). However, the slope ($\dot{\tau}$ estimates) of regulating the set-points (r^*) with distance (y^*) is not significantly different between light conditions. This shows that bumblebees tend to fly at lower speeds under lower light intensity, but that the governing set-point dynamics does not change with light condition. This finding is similar to the results from our average-per-treatment analysis (Figure 2.3D) and suggests that as light intensity falls, bumblebees possibly use neural temporal summation to improve the reliability of visual cues, and they fly slower to compensate for the resulting loss of temporal resolution (Baird et al., 2015; Reber et al., 2015). It is congruent with the observation in cruising flights of bumblebees (*B. terrestris*) (Reber et al., 2015) where they also reduce their mean flying speed with a decrease in light intensity.

In contrast to the negligible effect of light on set-point dynamics, the visual expansion information of the landing platform does affect the effective time-to-contact-rate at which the landing bumblebees change their set-points. When approaching the spokes landing platform with low visual expansion information, the bumblebees fly at 10% higher time-to-contact-rate than when approaching the checkerboard platform with high expansion information. As a result, bumblebees approaching a landing platform with limited optic expansion cues decelerate more rapidly, which results in a lower approach velocity when they reach the landing platform, thus reducing the chance of collision with the surface. Because theoretically r^* can be set in the brain of a bumblebee, independent of r (a sensory measurement), bumblebees slow down more quickly, and thus, perform a more careful landing when less visual expansion information is present. These results are similar to the behaviour described in honeybees where they approached a spoke landing platform at a 4% lower average relative-rate-of-expansion than a checkerboard pattern (Baird et al., 2013).

Differences in the landing strategy between landings from free flight and after take-off

In our study, we recorded two types of landing maneuvers, the landing directly after a take-off and the landing initiated from free flight. We tested how these two landing types that are both commonly performed by foraging bumblebees differ.

We find that, for both types of landing maneuvers, bumblebees use the here-described hybrid landing strategy, but especially the time-to-contact-rates that govern set-point adjustment with distance are strikingly different (Figure 2.6C). Bumblebees that land from free-flight exhibited on average a 28% higher time-to-contact-rate than when they landed directly after take-off. Moreover, bumblebees that land from free flight start their landing maneuver at a higher approach velocity, but because they decelerate more quickly (with 28% higher time-to-contact-rate), their approach velocity at landing is much lower than for the landings after take-off (31% lower speed at $y^* = 0.05$ m). This shows that landings from free flight are performed much more carefully than landings following take-off, similarly to landings on a platform with low and high visual expansion cues, respectively.

The fact that these rapid consecutive take-off and landing maneuvers are performed much more commonly by the foraging bumblebees could explain these differences, as bumblebees might have learned to perform such frequent landings both rapidly and safely. A similar type of learning has been described in foraging honeybees, where honeybees that forage in a unfamiliar environment improve their in-flight aerodynamic braking in time to increase their landing success (Muijres et al., 2020).

Differences in the landing strategy between honeybees and bumblebees

Considered together, our results describe a deceleration strategy of *Bombus terrestris* during landing that is different from the deceleration strategy suggested previously for *Bombus impatiens* (Chang et al., 2016) and observed in *Apis mellifera* (Baird et al., 2013). These differences could exist due to differences among species, tested light conditions, maximum distance available in front of the landing platform or analysis methods. It is unlikely that the differences in distance available in the front of the platform is the primary cause, because the bumblebees in our setup flew at approach velocities similar to the cruising speeds reported in previous bumblebee studies (Reber et al., 2015; Chang et al., 2016) (Figures 2.5A–C). Light condition could possibly explain differences in the magnitude of the relative-rate-of-expansion set-point, but it is unlikely that it explains the difference between the hybrid and constant- r landing strategy among studies. Thus, the differences among species and analysis method are the most likely candidates for explaining the occurrence of two distinct landing strategies. Because our per-track analysis is more comprehensive than the average-per-treatment analysis used in literature, it would therefore be interesting to apply our analysis method to the landing dynamics of *Apis mellifera ligustica* and *Bombus impatiens*, to

rule out any effect of analyses methods on observed deceleration strategies.

There is one previous honeybee landing study that used an individual track-based analysis method (Srinivasan et al., 2000). This study showed that when honeybees land on a horizontal surface, they reduce their forward flight speed linearly with distance to the surface, and thus do not make use of the here-described hybrid landing strategy. This suggests that the landing strategy difference between our study and those described in literature (Srinivasan et al., 2000; Baird et al., 2013; Chang et al., 2016) is due to differences in species. But note that forward flying honeybees land on horizontal surfaces by regulating front-to-back translatory optic flow, instead of optic expansion cues (Baird et al., 2013). Therefore, to conclusively determine the cause of the differences in landing strategies used by our bumblebees and honeybees, one would need to apply our analysis method to the landings that honeybees control using optical expansion cues.

How do bumblebees execute the hybrid landing strategy?

There is another important remaining question is: during the hybrid landing approach, what triggers switching from one constant- r set-point to another? This question is especially relevant because optical flow cues, such as visual expansion, capture the ratio of velocity and distance, but do not allow to disentangle these quantities. The dynamics of the transitions may provide a clue here. Most transitions look relatively smooth, but especially when closer to the landing surface, oscillations in r around the setpoint are evident (Figure 2.5). Moreover, among the 1,015 tracks containing two constant- r segments, as many as 23% of the transitions contained near-zero approach velocity ($V < 0.05 \text{ m s}^{-1}$). These observations point into the direction of a recent theory on monocular distance perception (de Croon, 2016), which postulates that insects can detect the instabilities that arise when performing closed-loop optical flow control. It was shown that (de Croon, 2016), given a fixed control system, these instabilities arise at specific distances from the target object, allowing to disentangle distance and speed. In the current case, the detection of instabilities could provide the bumblebee an estimate of distance to the surface which consequently could trigger the change in set-point. However, alternative explanations are possible, such as the use of other distance cues (de Croon et al., 2021) or parallax cues arising from lateral motion (Baird et al., 2021). More research is needed to shed further light on this essential part of the hybrid landing strategy.

How can bumblebees estimate the relative-rate-of-expansion?

The studies depicting neural measurements of relative-rate-of-expansion (or time-to-contact) are scarce and we are aware of only one example of computation of threshold time-to-contact value by the neural system in pigeons (Wang and Frost, 1992; Sun and Frost, 1998). However, when an animal approaches a surface, it can use some measure of absolute-rate-of-expansion (or simply, rate-of-expansion ρ) (e.g., ρ averaged over a part of visual field,

maximum ρ in the visual field) as a proxy for relative-rate-of-expansion (Baird *et al.*, 2013). Also, neural measurements of absolute-rate-of-expansion have been recorded in honeybees (Ibbotson *et al.*, 2017). It is therefore likely that certain neurons in bumblebees' visual neuropil also measure absolute-rate-of-expansion which could then be used as an alternate for relative-rate-of-expansion.

Conclusion

By using our custom-designed individual-track-based analysis method, we here described the deceleration strategy that bumblebees exhibit during landing. Specifically, we have shown that landing bumblebees decrease their velocity towards the landing platforms by holding the relative-rate-of-optic-expansion cue constant for only short bouts within the landing maneuver. From one bout to the next, they tend to increase the optic-expansion set-point at which they fly. This modular increase in set-points with reducing distance results in a discrete approximation of the deceleration strategy of birds. Birds use a constant time-to-contact-rate to regulate their expansion rate with distance, which results in relatively fast landings.

The landing strategy of bumblebees is observed in the presence of variable degrees of optic expansion cues and is exhibited by bumblebees landing both after take-off and from free-flight. Moreover, it occurs in a wide range of luminance levels, suggesting that bumblebees adequately control landing by using neural summation. Our results are a step towards detailed understanding of how bumblebees robustly control their landing approaches. Once sufficiently understood, these control strategies can provide bio-inspiration for the development of landing algorithms in autonomously flying robots.

Limitations of the study

Limitations of our relative-rate-of-expansion set-points analysis method

Our analyses assumes that the sensorimotor control system of landing bumblebees sets the set-points of relative-rate-of-expansion as a goal in the brain of the bumblebee. This assumption needs to be further investigated and supported by neuroethological studies that are aimed at identifying the neural circuits that underlie this sensorimotor control system. The response property of set-point identified in this study *i.e.*, its modulation with distance, can be useful for this purpose.

Based on the above assumption, we analyzed the landing dynamics of foraging bumblebees, using two analysis methods, namely the *average-per-treatment* method and the *per-track* analysis method. Both methods provide useful insights, but also have their specific limitations as described below.

Limitations of our analysis method based on the average landing dynamics

The average-per-treatment analysis method allows us to estimate the average set-points of relative-rate-of-expansion in each treatment group. This provided a useful insight into the mean approach dynamics of bumblebees, and allows testing of how this differs between conditions (treatments). In contrast, the method ignores the detailed landing dynamics exhibited by individual bumblebees. Specifically, it does not capture the rapid deceleration phases that occur in between phases at which the animal would aim to fly at a constant relative-rate-of-expansion. To analyse these detailed flight dynamics, we developed our analysis method based on the individual flight trajectories.

Limitations of our analysis method based on the individual flight trajectories

This per-track analysis method allowed us to identify the hybrid landing strategy described in this study, but the method has one primary limitation. Because the per-track analysis method identifies set-points of relative-rate-of-expansion in individual flight trajectories, a set-point can only be identified if the bumblebee flies at this set-point for a certain time period. Bumblebees can fail to reach a set-point for several reasons. For example, the animal can land before reaching it, the animal could switch to a new set-point before reaching the previous set-point, or a landing can be aborted prior to it. In our study, we identified 6, 291 set-points of relative-rate-of-expansion (for $f = 1$) within 10, 005 landing maneuvers, suggesting that bumblebees regularly do not fly at their expansion-rate set-point.

The ability to detect a set-point of relative-rate-of-expansion depends on the sensitivity of our per-track analysis method, set by the f -factor (see Methods). The number of identified set-point increases with f -factor, but also the number of false positive set-points increases. Based on our sensitivity analysis, we showed that the main conclusions of our study are relatively insensitive to the f -factor value (see Methods).

In conclusion, our per-track analysis method does not allow us to identify all set-point of relative-rate-of-expansion during a landing maneuver. But because our analysis is based on a large number of flights, this does not limit us in identifying and accurately describing the hybrid landing strategy of bumblebees.

Methods

All methods can be found in Section S2.3.

Data and code availability

The data gathered during experiments is available here: <http://dx.doi.org/10.17632/rrbjyhkm8z.1> and the code used in the analysis is available here: <https://github.com/rrbjyhkm8z/1>

Acknowledgements

This project is supported by the Nederlandse Organisatie voor Wetenschappelijk Onderzoek - Toegepaste en Technische Wetenschappen (NWO-TTW grant number 15039). We thank Emma Rietveld and Lana de Vries for useful discussions and help during the experiments, Henk Schipper for his help in organising the computational resources, and Andres Hagmayer for his help with the statistical analysis. We thank Remco Huvermann, Edwin Muijt and Anne Mathijssen from Koppert B.V. for providing the bumblebee colony. We also thank them together with Coby van Dooremalen for their advice on working with bumblebees.

Author contributions

Conceptualization, P.G., G.C.H.E.d.C., and F.T.M.; methodology, P.G. and F.T.M.; Software, P.G.; validation, P.G., M.J.L., and F.T.M.; formal analysis, P.G., J.L.v.L., and F.T.M.; investigation, P.G., A.C., and R.P.M.P.; resources, J.L.v.L., F.T.M.; data curation, P.G.; writing – original draft, P.G. and F.T.M.; writing – review & editing, P.G., A.C., G.C.H.E.d.C., M.J.L., J.L.v.L., R.P.M.P., and F.T.M.; visualization, P.G.; supervision, J.L.v.L. and F.T.M.; project administration, P.G. and F.T.M.; funding acquisition, G.C.H.E.d.C. and F.T.M..

Declaration of interests

The authors declare no competing interests.

References

- Baird, E., Boeddeker, N., Ibbotson, M. R. and Srinivasan, M. V. (2013). A universal strategy for visually guided landing. *Proceedings of the National Academy of Sciences of the United States of America* **110**, 18686–18691.
- Baird, E., Boeddeker, N. and Srinivasan, M. V. (2021). The effect of optic flow cues on honeybee flight control in wind. *Proceedings of the Royal Society B: Biological Sciences* **288**, 20203051.
- Baird, E., Fernandez, D. C., Wcislo, W. T. and Warrant, E. J. (2015). Flight control and landing precision in the nocturnal bee *Megalopta* is robust to large changes in light intensity. *Frontiers in Physiology* **6**, 1–7.
- Balebail, S., Raja, S. K. and Sane, S. P. (2019). Landing maneuvers of houseflies on vertical and inverted surfaces. *PLoS ONE* **14**, 1–17.
- Chang, J. J., Crall, J. D. and Combes, S. A. (2016). Wind alters landing dynamics in bumblebees. *The Journal of Experimental Biology* **219**, 2819–2822.

- Corbet, S. A., Fussell, M., Ake, R., Fraser, A., Gunson, C., Savage, A. and Smith, K. (1993). Temperature and the pollinating activity of social bees. *Ecological Entomology* 18, 17–30.
- de Croon, G. C. H. E. (2016). Monocular distance estimation with optical flow maneuvers and efference copies: a stability-based strategy. *Bioinspiration & Biomimetics* 11, 016004.
- de Croon, G. C. H. E., De Wagter, C. and Seidl, T. (2021). Enhancing optical-flow-based control by learning visual appearance cues for flying robots. *Nature Machine Intelligence* 3, 33–41.
- Edwards, M. and Ibbotson, M. R. (2007). Relative sensitivities to large-field optic-flow patterns varying in direction and speed. *Perception* 36, 113–124.
- Fontaine, C., Dajoz, I., Meriguet, J. and Loreau, M. (2006). Functional diversity of plant-pollinator interaction webs enhances the persistence of plant communities. *PLoS Biology* 4, 0129–0135.
- Foster, D. J. and Cartar, R. V. (2011). What causes wing wear in foraging bumble bees? *Journal of Experimental Biology* 214, 1896–1901.
- Gibson, J. J. (1955). The optical expansion-pattern in aerial locomotion. *The American journal of psychology* 68, 480–484.
- Heinrich, B. (1979). Resource heterogeneity and patterns of movement in foraging bumblebees. *Oecologia* 40, 235–245.
- Ibbotson, M. R., Hung, Y. S., Meffin, H., Boeddeker, N. and Srinivasan, M. V. (2017). Neural basis of forward flight control and landing in honeybees. *Scientific Reports* 7, 1–15.
- Joar Hegland, S. and Totland, Ø. (2008). Is the magnitude of pollen limitation in a plant community affected by pollinator visitation and plant species specialisation levels? *Oikos* 0, 080227085440234–0.
- Lee, D. N. (1976). A theory of visual control of braking based on information about time to collision. *Perception* 5, 437–459.
- Lee, D. N., Bootsma, R. J., Land, M., Regan, D. and Gray, R. (2009). Lee's 1976 Paper. *Perception* 38, 837–858.
- Lee, D. N., Davies, M. N. O., Green, P. R. and (Ruud). Van Der Weel, F. R. (1993). Visual control of velocity of approach by pigeons when landing. *Journal of Experimental Biology* 180, 85–104.
- Lee, D. N., Reddish, P. E. and Rand, D. T. (1991). Aerial docking by hummingbirds. *Naturwissenschaften* 78, 526–527.
- Muijres, F. T., van Dooremalen, C., Lankheet, M., Lugt, H., de Vries, L. J. and Van Langevelde, F. (2020). *Varroa destructor* infestation impairs the improvement of landing performance in foraging honeybees. *Royal Society Open Science* 7, 201222.

- Reber, T., Dacke, M., Warrant, E. and Baird, E. (2016). Bumblebees perform well-controlled landings in dim light. *Frontiers in Behavioral Neuroscience* **10**, 1–10.
- Reber, T., Vähäkainu, A., Baird, E., Weckström, M., Warrant, E. and Dacke, M. (2015). Effect of light intensity on flight control and temporal properties of photoreceptors in bumblebees. *Journal of Experimental Biology* **218**, 1339–1346.
- Srinivasan, M. V., Zhang, S. W., Chahl, J. S., Barth, E. and Venkatesh, S. (2000). How honeybees make grazing landings on flat surfaces. *Biological Cybernetics* **83**, 171–183.
- Straw, A. D., Branson, K., Neumann, T. R. and Dickinson, M. H. (2011). Multi-camera Real-time Three-dimensional Tracking of Multiple Flying Animals. *Journal of The Royal Society Interface* **8**, 395–409.
- Sun, H. and Frost, B. J. (1998). Computation of different optical variables of looming objects in pigeon nucleus rotundus neurons. *Nature Neuroscience* **1**, 296–303.
- Van Breugel, F. and Dickinson, M. H. (2012). The visual control of landing and obstacle avoidance in the fruit fly *Drosophila melanogaster*. *Journal of Experimental Biology* **215**, 1783–1798.
- Velthuis, H. W. and Doorn, A. V. (2006). A century of advances in bumblebee domestication and the economic and environmental aspects of its commercialization for pollination. *Apidologie* **37**, 421–451.
- Wagner, H. (1982). Flow-field variables trigger landing in flies. *Nature* **297**, 147–148.
- Wang, Y. and Frost, B. J. (1992). Time to collision is signalled by neurons in the nucleus rotundus of pigeons. *Nature* **356**, 236–238.

Supplemental information

2

Bumblebees land rapidly and robustly using a sophisticated modular flight control strategy

Pulkit Goyal, Antoine Cribellier, Guido C.H.E. de Croon, Martin J. Lankheet, Johan L. van Leeuwen, Remco P.M. Pieters, Florian T. Muijres

S2.1 Figures

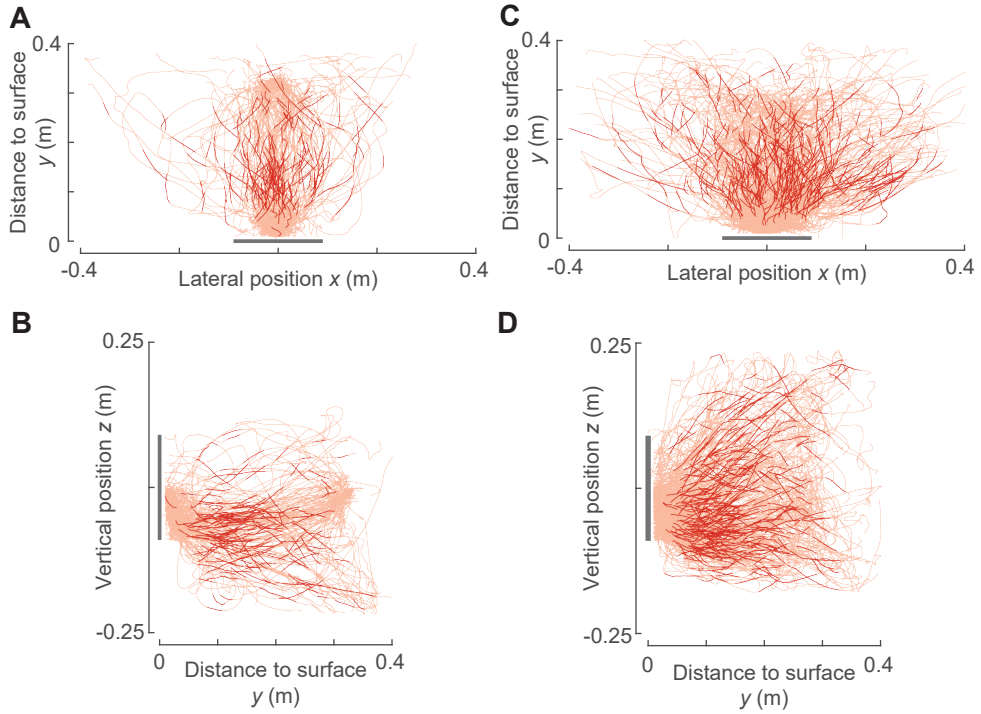


Figure S2.1: Flight trajectories of bumblebees landing directly after take-off (A,B) and from free-flight (C,D) (related to Figure 2.4). (A,B) Top and side views of 138 flight trajectories of bumblebees that landed immediately after taking-off from either the ground or the opposite platform (every 10th of 1359 flight tracks are shown). (C,D) Top and side views of 334 flight trajectories of bumblebees that initiated landing from a free-flight (every 10th track of 3313 recorded tracks are shown). (A–D) The flight tracks, landing platform, and the track segments in which optical expansion rate is kept constant are shown in orange, gray, and red, respectively.

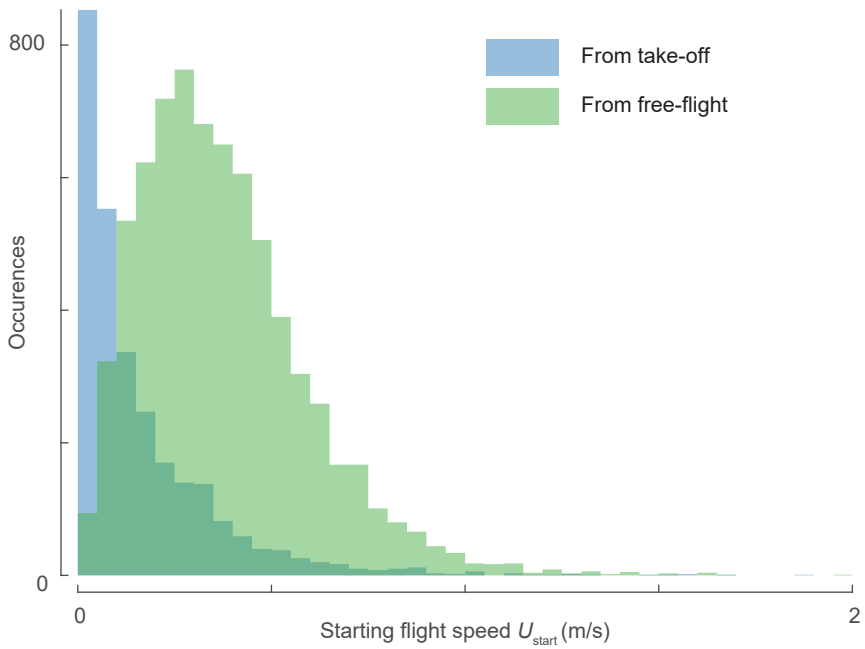


Figure S2.2: Histogram of flight speeds at the start of the landing maneuvers performed by bumblebees from take-off (blue, $n=2792$) and from free-flight (green, $n=7213$) (related to Figure 2.3).

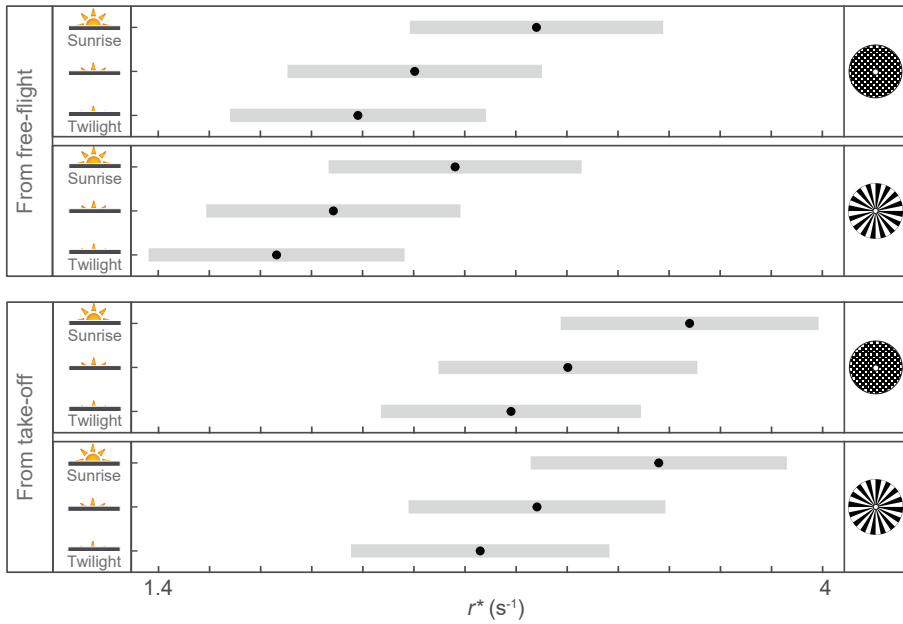


Figure S2.3: The mean relative-rate-of-expansion r^* as predicted by the linear mixed-effects model in three tested light conditions and two landing patterns for both landing types (from take-off and free-flight) using average-per-treatment analysis (related to Figure 2.3). The mean relative-rate-of-expansion increases with increase in light intensity and is higher when bumblebees initiate landing from take-off. It did not differ significantly between the two tested landing platforms (Table S5.1). Black dots depict estimated means and gray bars are 95% confidence intervals.

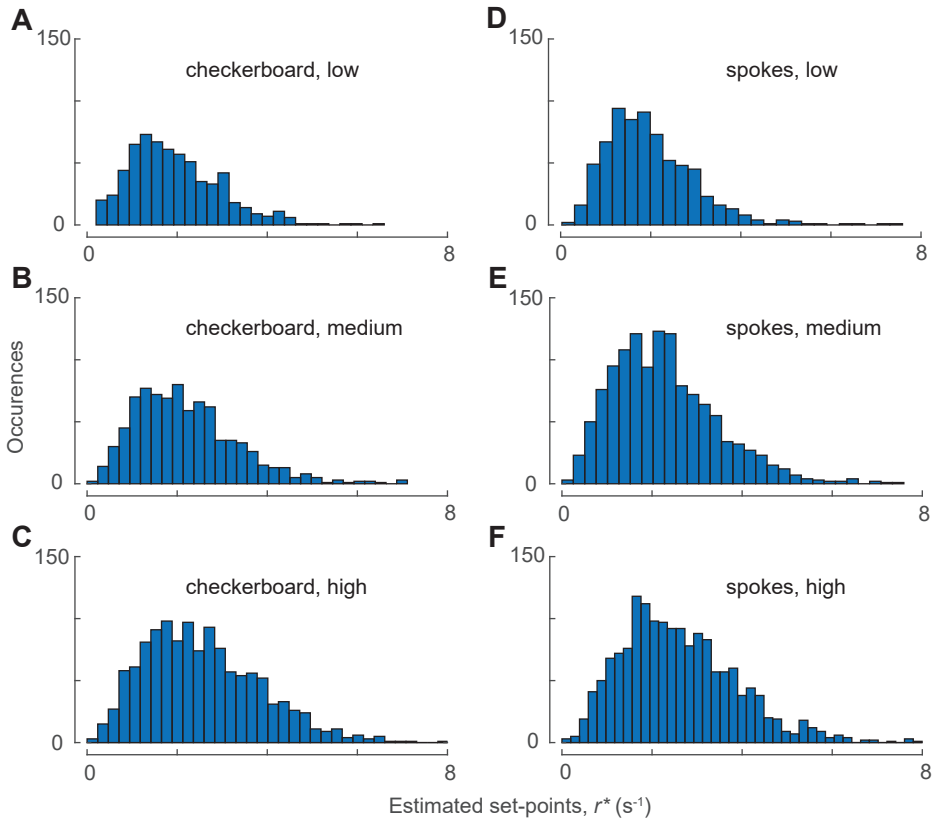


Figure S2.4: Histograms of the set-points of optical expansion rate r^* in all tested treatments (related to Figure 2.4). The conditions are: (A) checkerboard pattern, low light condition ($n=643$ segments), (B) checkerboard pattern, medium light condition ($n=847$ segments), (C) checkerboard pattern, high light condition ($n=1243$ segments), (D) spoke pattern, low light condition ($n=700$ segments), (E) spoke pattern, medium light condition ($n=1255$ segments), (F) spoke pattern, high light condition ($n=1603$ segments). (A–F) Each panel contains set-points for both landing types (landings initiated from take-off and free-flight).

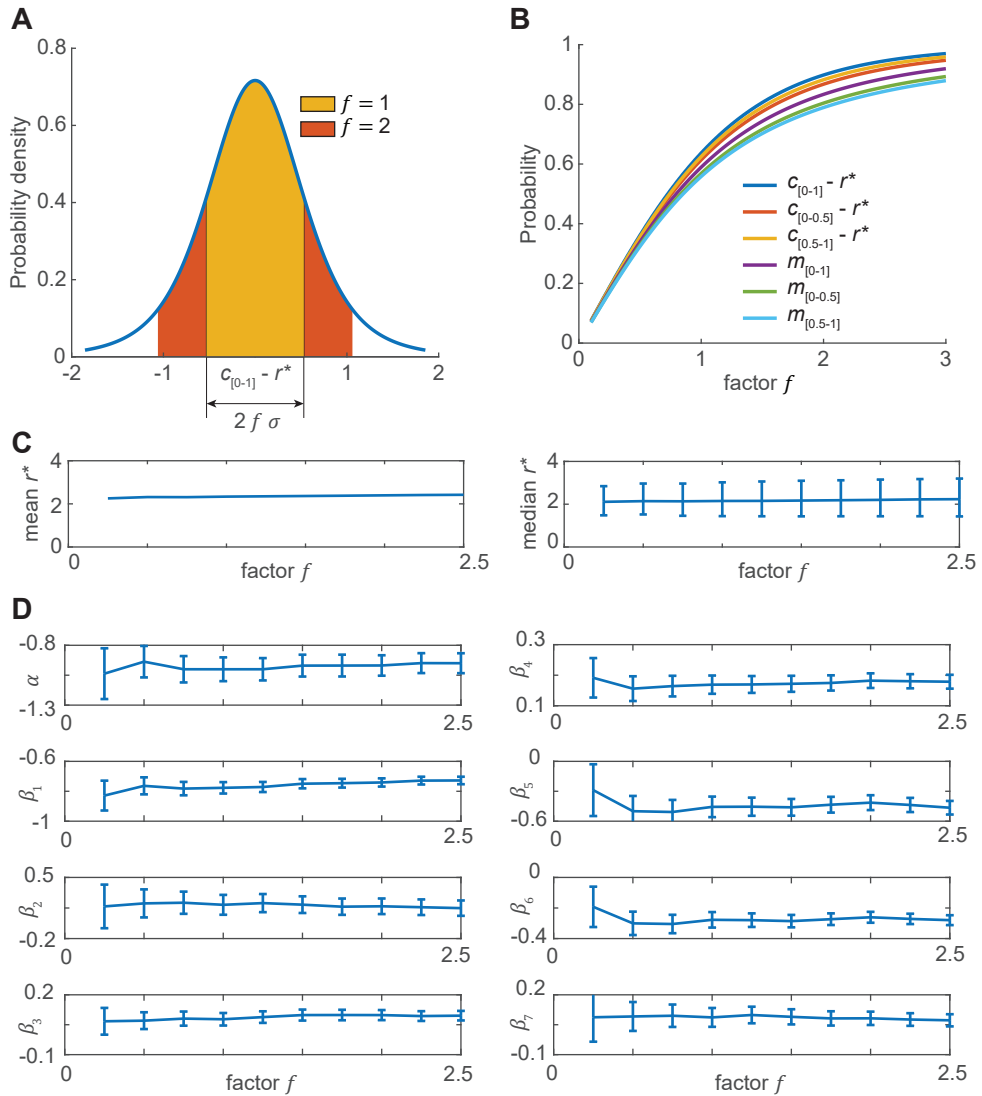


Figure S2.5: The effect of factor f on the results (related to Figures 2.4–2.6). (A) The threshold of variation allowed around the mean for $f = 1$ (yellow) and $f = 2$ (orange) for the probability density function of parameter $c_{[0-1]} - r^*$, $\sigma = 0.53$. (B) The probability of values that lie within f scale-parameter band around the mean of each parameter ($c_{[0-1]} - r^*$, $c_{[0-0.5]} - r^*$, $c_{[0.5-1]} - r^*$, $m_{[0-1]}$, $m_{[0-0.5]}$, and $m_{[0.5-1]}$). (C) The mean and median (25 percentile and 75 percentile) of the set-points of relative rate of expansion identified at various values of the factor f . (D) The dependence of r^* on distance from the platform (y^*) along with the effect of different environmental conditions (landing patterns and light conditions) and landing type (take-off or free-flight) as per Equation S2.2 for each factor ($\log(r_{i,d,a,s}^*) \sim N(\alpha + \alpha_d + \alpha_a + \alpha_s + \beta_1 \log(y_{i,d,a,s}^*) + \beta_2 \text{SPOKE}_{i,d,a,s} + \beta_3 \text{MEDIUMlight}_{i,d,a,s} + \beta_4 \text{HIGHlight}_{i,d,a,s} + \beta_5 \text{fromTakeoff}_{i,d,a,s} + \beta_6 \log(y_{i,d,a,s}) \times \text{fromTakeoff}_{i,d,a,s} + \beta_7 \log(y_{i,d,a,s}) \times \text{SPOKE}_{i,d,a,s}, \sigma^2)$, vertical bars for each coefficient indicate 95% confidence intervals).

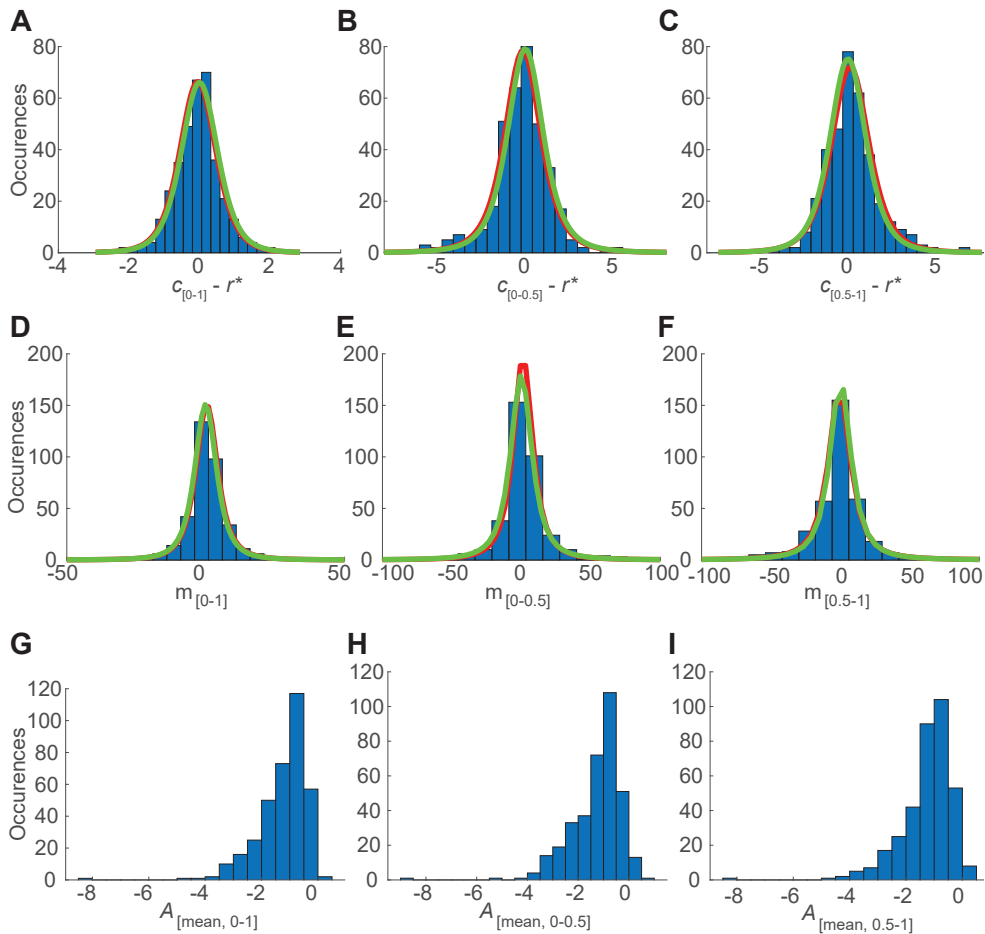


Figure S2.6: Distributions of nine parameters used in the constant- r extraction algorithm (related to Figures 2.4–2.6). (A) $c_{[0-1]} - r^*$, (B) $c_{[0-0.5]} - r^*$, (C) $c_{[0.5-1]} - r^*$, (D) $m_{[0-1]}$, (E) $m_{[0-0.5]}$, (F) $m_{[0.5-1]}$, (G) $A_{[\text{mean}, 0-1]}$, (H) $A_{[\text{mean}, 0-0.5]}$, and (I) $A_{[\text{mean}, 0.5-1]}$. In blue, histograms of nine parameters obtained from manual selection of 355 constant- r segments in 313 (out of first 532) landing maneuvers for high light condition and spoke landing pattern. In red, estimated probability density functions of first six parameters (generalized student's t -distributions, see Table S2.8 for parameter values). In green, the representative probability density functions of first six parameters used in constant- r extraction algorithm (location parameter μ for these six parameters is zero, scale parameter σ is σ_1 , $2\sigma_1$, σ_2 , $2\sigma_2$ and $2\sigma_2$ for panels (a)–(f), respectively (where $\sigma_1 = 0.53$ and $\sigma_2 = 4.22$) and shape parameter ν is same as in Table S2.8).

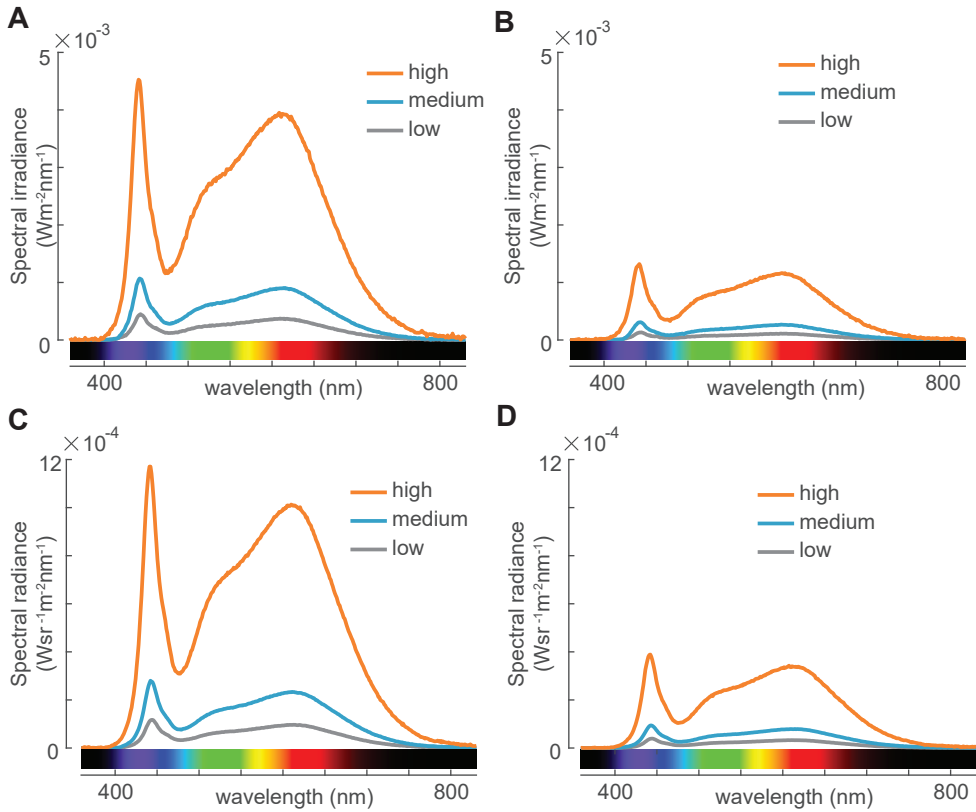


Figure S2.7: Light intensities for the low (gray), medium (blue) and high (orange) light conditions (related to Figure 2.2). Spectral irradiance (A) and spectral radiance (C) at the center of the flight arena. Spectral irradiance (B) and spectral radiance (D) at the centre of the landing platforms.

S2.2 Tables

Table S2.1: The number of landing maneuvers recorded in each tested treatment and the number of landing maneuvers that are identified with constant- r segments for different values of factor f (related to Figure 2.4).

Treatment (landing pattern, light condition)	Number of landing maneuvers	Factors f									
		0.25	0.5	0.75	1	1.25	1.5	1.75	2	2.25	2.5
From F											
L+	579	55	149	225	300	362	395	423	452	473	484
M+	923	71	221	358	472	545	605	649	687	719	744
H+	1886	94	327	541	729	871	988	1099	1188	1271	1347
Lx	520	70	162	241	303	348	380	405	431	449	461
Mx	1188	104	294	474	626	747	834	893	939	995	1027
Hx	2117	129	383	639	883	1065	1198	1325	1426	1521	1589
From T											
L+	242	26	79	125	152	163	182	191	200	208	216
M+	287	24	67	96	137	169	189	203	219	230	238
H+	554	35	99	164	229	271	312	343	377	406	422
Lx	298	30	88	123	166	196	224	234	250	266	271
Mx	593	52	149	237	296	359	402	435	454	476	492
Hx	818	62	179	283	379	449	512	549	596	629	660
Total landings	10005	752	2197	3506	4672	5545	6221	6749	7219	7643	7951

Free-flight (F), Take-off (T), Low (L), medium (M) and high (H) light conditions, checkerboard (+) and spoke (x) landing patterns.

Table S2.2: Analysis of mean relative-rate-of-expansion in different tested treatments (landing patterns, light conditions and starting conditions) for average-per-treatment analysis method (related to Figure 2.3). The data comprises of 10,005 landing approaches between $0.04 \text{ m} \leq y \leq 0.11 \text{ m}$, where y is the perpendicular distance to the platforms. Post-hoc tests compare differences between mean relative-rate-of-expansion observed in different tested conditions (statistical model as given by Equation S2.1: $r_{i,d,a,s} \sim N(\alpha + \alpha_d + \alpha_a + \alpha_s + \beta_1 \text{SPOKE}_{i,d,a,s} + \beta_2 \text{MEDIUMlight}_{i,d,a,s} + \beta_3 \text{HIGHlight}_{i,d,a,s} + \beta_4 \text{fromTakeoff}_{i,d,a,s} + \beta_5 \text{SPOKE}_{i,d,a,s} \times \text{fromTakeoff}_{i,d,a,s}, \sigma^2)$).

Fixed effect	Estimate	Std error	t value	Pr(> t)
α	2.18	0.26	8.51	0.034
β_1	-0.32	0.15	-2.17	0.056
β_2	0.22	0.05	4.07	$4.67 \cdot 10^{-5}$
β_3	0.70	0.05	13.90	$< 2 \cdot 10^{-16}$
β_4	0.60	0.06	9.64	$< 1 \cdot 10^{-16}$
β_5	0.20	0.08	2.44	0.015
Post-hoc contrasts*	Estimate	Std error	z ratio	p value
(H + F) - (L + F)	0.70	0.05	13.90	$4.1 \cdot 10^{-42}$
(H + F) - (M + F)	0.48	0.04	11.76	$3.95 \cdot 10^{-30}$
(H + F) - (H x F)	0.32	0.15	2.17	1
(H + F) - (L x F)	1.02	0.16	6.53	$4.3 \cdot 10^{-09}$
(H + F) - (M x F)	0.80	0.15	5.21	$1.24 \cdot 10^{-05}$
(L + F) - (M + F)	-0.22	0.05	-4.07	0.003
(L + F) - (H x F)	-0.38	0.16	-2.45	0.930
(L + F) - (L x F)	0.32	0.15	2.17	1
(L + F) - (M x F)	0.10	0.16	0.61	1
(M + F) - (H x F)	-0.16	0.15	-1.04	1
(M + F) - (L x F)	0.54	0.16	3.44	0.038
(M + F) - (M x F)	0.32	0.15	2.17	1
(H x F) - (L x F)	0.70	0.05	13.90	$4.1 \cdot 10^{-42}$
(H x F) - (M x F)	0.48	0.04	11.76	$3.95 \cdot 10^{-30}$
(L x F) - (M x F)	-0.22	0.05	-4.07	0.003

(Continued on next page.)

(Continued from previous page.)

Post-hoc contrasts*	Estimate	Std error	z ratio	p value
(H + T) - (L + T)	0.70	0.05	13.90	$4.1 \cdot 10^{-42}$
(H + T) - (M + T)	0.48	0.04	11.76	$3.95 \cdot 10^{-30}$
(H + T) - (H x T)	0.12	0.16	0.76	1
(H + T) - (L x T)	0.82	0.17	4.91	$6.12 \cdot 10^{-05}$
(H + T) - (M x T)	0.60	0.16	3.65	0.017
(L + T) - (M + T)	-0.22	0.05	-4.07	0.003
(L + T) - (H x T)	-0.58	0.17	-3.48	0.033
(L + T) - (L x T)	0.12	0.16	0.76	1
(L + T) - (M x T)	-0.10	0.17	-0.61	1
(M + T) - (H x T)	-0.36	0.16	-2.17	1
(M + T) - (L x T)	0.34	0.17	2.03	1
(M + T) - (M x T)	0.12	0.16	0.76	1
(H x T) - (L x T)	0.70	0.05	13.90	$4.1 \cdot 10^{-42}$
(H x T) - (M x T)	0.48	0.04	11.76	$3.95 \cdot 10^{-30}$
(L x T) - (M x T)	-0.22	0.05	-4.07	0.003

*Low (L), medium (M) and high (H) light conditions, checkerboard (+) and spoke (x) landing patterns, free-flight (F) and take-off (T) starting conditions.

*Comparisons among starting conditions also formed part of post-hoc test, but are not shown here.

Table S2.3: Number of landing maneuvers that contain more than one set-points of relative rate of expansion along with different characteristics (Δr^* , Δy_1 and Δy_2 , related to Figure 2.4 and 2.5) in different tested treatments (factor $f = 1$).

Treatment (pattern, light)	No. of landing tracks with constant- r segments	No. of constant- r segments	No. of man- euvers with > 1 constant- r segments	For 1298 maneuvers with more than one constant- r segments			For 1015 maneuvers with two constant- r segments			
				No. of constant- r segments	No. of jumps to a different r^*	% of jumps	For jumps to a higher r^*		Δy_1 (m) (mean [std-dev.])	Δy_2 (m) (mean [std-dev.])
							Δr^* (s^{-1}) (mean [std-dev.])			
From F										
L+	300	418	94	212	118	73.7%	0.740 [0.688]	0.030 [0.015]	0.099 [0.040]	
M+	472	667	148	343	195	72.3%	1.023 [0.964]	0.033 [0.016]	0.110 [0.044]	
H+	729	939	175	385	210	74.8%	1.394 [1.120]	0.037 [0.018]	0.116 [0.053]	
Lx	303	454	118	269	151	67.6%	0.778 [0.595]	0.030 [0.015]	0.107 [0.046]	
Mx	626	854	180	408	228	71.5%	1.047 [0.846]	0.034 [0.018]	0.111 [0.047]	
Hx	883	1103	187	407	220	75.0%	1.198 [0.964]	0.036 [0.017]	0.112 [0.047]	
From T										
L+	152	225	54	127	73	75.3%	0.986 [0.873]	0.033 [0.018]	0.132 [0.048]	
M+	137	180	37	80	43	74.4%	1.052 [1.065]	0.036 [0.019]	0.121 [0.060]	
H+	229	304	64	139	75	73.3%	1.305 [1.184]	0.037 [0.017]	0.114 [0.052]	
Lx	166	246	61	141	80	75.0%	0.854 [0.733]	0.035 [0.019]	0.120 [0.052]	
Mx	296	401	82	187	105	72.4%	0.967 [0.892]	0.036 [0.017]	0.122 [0.053]	
Hx	379	500	98	219	121	65.3%	1.221 [1.020]	0.039 [0.020]	0.128 [0.054]	

Free-flight (F), Take-off (T), Low (L), medium (M) and high (H) light conditions, checkerboard (+) and spoke (x) landing patterns.

Table S2.4: Analysis of relative-rate-of-expansion set-points (r^*) dependence on distance to the platform (y^*) in different tested treatments (landing patterns and light conditions) and with different starting conditions (take-off and free-flight) for per-track analysis method (related to Figure 2.5). The data comprises of r^* and y^* for 2,917 constant- r segments in 1,298 landing maneuvers that contain more than one constant- r segments (factor $f = 1$) (statistical model as given by Equation S2.2: $\log(r_{i,d,a,s}^*) \sim N(\alpha + \alpha_d + \alpha_a + \alpha_s + \beta_1 \log(y_{i,d,a,s}^*) + \beta_2 \text{SPOKE}_{i,d,a,s} + \beta_3 \text{MEDIUMlight}_{i,d,a,s} + \beta_4 \text{HIGHlight}_{i,d,a,s} + \beta_5 \text{fromTakeoff}_{i,d,a,s} + \beta_6 \log(y_{i,d,a,s}) \times \text{fromTakeoff}_{i,d,a,s} + \beta_7 \log(y_{i,d,a,s}) \times \text{SPOKE}_{i,d,a,s}, \sigma^2)$).

Fixed effect	Estimate	Std error	t value	Pr(> t)
α	-0.98	0.06	-17.64	$1.11E - 47$
β_1	-0.74	0.03	-28.88	$5.3E - 161$
β_2	0.18	0.07	2.62	0.009372
β_3	0.06	0.02	2.85	0.004463
β_4	0.17	0.02	8.00	$2.68E - 15$
β_5	-0.26	0.07	-3.76	0.000173
β_6	-0.16	0.03	-4.55	$5.54E - 06$
β_7	0.09	0.03	2.65	0.008201

Table S2.5: Analysis of relative-rate-of-expansion set-points (r^*) dependence on distance to the platform (y^*) in different tested treatments (landing patterns and light conditions) and with different starting conditions (take-off and free-flight) for per-track analysis method (related to Figure 2.6). The data comprises of r^* and y^* for 6,291 constant- r segments in 4,672 landing maneuvers. Post-hoc tests compare differences in $\log(r^*)$ observed at mean $y^* = 0.15m$ in the presence of different light conditions and landing platforms (factor $f = 1$) (statistical model as given by Equation S2.2: $\log(r_{i,d,a,s}^*) \sim N(\alpha + \alpha_d + \alpha_a + \alpha_s + \beta_1 \log(y_{i,d,a,s}^*) + \beta_2 \text{SPOKE}_{i,d,a,s} + \beta_3 \text{MEDIUMlight}_{i,d,a,s} + \beta_4 \text{HIGHLIGHT}_{i,d,a,s} + \beta_5 \text{fromTakeoff}_{i,d,a,s} + \beta_6 \log(y_{i,d,a,s}) \times \text{fromTakeoff}_{i,d,a,s} + \beta_7 \log(y_{i,d,a,s}) \times \text{SPOKE}_{i,d,a,s}, \sigma^2)$).

Fixed effect	Estimate	Std error	t value	Pr(> t)
α	-1.00	0.05	-20.13	1.53E - 17
β_1	-0.78	0.02	-40.76	0
β_2	0.19	0.06	3.28	0.001397
β_3	0.08	0.02	4.92	8.81E - 07
β_4	0.17	0.01	11.31	3.31E - 29
β_5	-0.46	0.05	-8.85	1.09E - 18
β_6	-0.28	0.03	-10.93	1.44E - 27
β_7	0.09	0.02	3.67	0.000248
Post-hoc constrasts* in $\log(r^*)$ at mean $y^* = 0.15m$	Estimate	Std error	z ratio	p value
L F - M F	-0.08	0.02	-4.92	1.27E - 05
L F - H F	-0.17	0.01	-11.31	1.72E - 28
L F - L T	-0.07	0.01	-5.58	3.68E - 07
L F - M T	-0.15	0.02	-7.13	1.53E - 11
L F - H T	-0.24	0.02	-11.94	1.14E - 31
M F - H F	-0.09	0.01	-7.17	1.1E - 11
M F - L T	0.01	0.02	0.35	1
M F - M T	-0.07	0.01	-5.58	3.68E - 07
M F - H T	-0.16	0.02	-9.08	1.63E - 18
H F - L T	0.10	0.02	5.17	3.46E - 06
H F - M T	0.02	0.02	1.17	1
H F - H T	-0.07	0.01	-5.58	3.68E - 07
L T - M T	-0.08	0.02	-4.92	1.27E - 05
L T - H T	-0.17	0.01	-11.31	1.72E - 28
M T - H T	-0.09	0.01	-7.17	1.1E - 11

*Low (L), medium (M) and high (H) light conditions, free-flight (F) and take-off (T) starting conditions.

The results are averaged over patterns because comparisons of r^ among landing patterns for each light condition and starting condition were similar.

Table S2.6: Analysis of relative-rate-of-expansion set-points (r^*) dependence on distance to the platform (y^*) in different tested treatments (landing patterns and light conditions) and with different starting conditions (take-off and free-flight) for per-track analysis method (related to Figures 2.5 and 2.6). The data comprises of r^* and y^* for 3,374 constant- r segments in 3,374 landing maneuvers, with one constant- r segment in each maneuver (factor $f = 1$) (statistical model as given by Equation S2.2: $\log(r_{i,d,a,s}^*) \sim N(\alpha + \alpha_d + \alpha_a + \alpha_s + \beta_1 \log(y_{i,d,a,s}^*) + \beta_2 \text{SPOKE}_{i,d,a,s} + \beta_3 \text{MEDIUMlight}_{i,d,a,s} + \beta_4 \text{HIGHlight}_{i,d,a,s} + \beta_5 \text{fromTakeoff}_{i,d,a,s} + \beta_6 \log(y_{i,d,a,s}) \times \text{fromTakeoff}_{i,d,a,s} + \beta_7 \log(y_{i,d,a,s}) \times \text{SPOKE}_{i,d,a,s}, \sigma^2)$).

Fixed effect	Estimate	Std error	t value	Pr(> t)
α	-0.97	0.07	-14.15	$2.68E - 17$
β_1	-0.79	0.03	-28.56	$8.2E - 161$
β_2	0.22	0.08	2.82	0.005261
β_3	0.08	0.02	3.49	0.000484
β_4	0.14	0.02	6.96	$4.2E - 12$
β_5	-0.67	0.07	-8.99	$4.16E - 19$
β_6	-0.40	0.04	-11.02	$8.71E - 28$
β_7	0.10	0.03	3.01	0.002627

Table S2.7: Pseudo-random treatment schedule followed during experiments (related to Figure 2.2).

Time (hours)		Days													
		1	2	3	4	5	6	7	8	9	10	11	12	13	14
start	end	1	2	3	4	5	6	7	8	9	10	11	12	13	14
80000	93000	M+	Lx	L+	Hx	L+	Hx	H+	Mx	H+	Mx	M+	Lx	M+	Lx
93000	110000	H+	Mx	H+	Mx	M+	Lx	M+	Lx	L+	Hx	L+	Hx	H+	Mx
110000	123000	L+	Hx	M+	Lx	H+	Mx	L+	Hx	M+	Lx	H+	Mx	L+	Hx
123000	140000	M+	Lx	L+	Hx	L+	Hx	H+	Mx	H+	Mx	M+	Lx	M+	Lx
140000	153000	H+	Mx	H+	Mx	M+	Lx	M+	Lx	L+	Hx	L+	Hx	H+	Mx
153000	170000	L+	Hx	M+	Lx	H+	Mx	L+	Hx	M+	Lx	H+	Mx	L+	Hx

Low (L), medium (M) and high (H) light conditions, checkerboard (+) and spoke (x) landing patterns.

Table S2.8: Estimated location parameter μ , scale parameter σ and shape parameter ν for six variables that together define the constancy of relative rate of expansion in a track segment (values are mean [95% confidence intervals]) (related to Figures 2.4 and S2.6).

Variables	μ	σ	ν
$c_{[0-1]} - r^*$	-0.05 [- 0.11, 0.02]	0.53 [0.46, 0.60]	5.02 [2.87, 8.77]
$c_{[0-0.5]} - r^*$	-0.14 [- 0.28, -0.00]	1.07 [0.93, 1.23]	3.24 [2.20, 4.76]
$c_{[0.5-1]} - r^*$	0.12 [- 0.02, 0.26]	1.11 [0.96, 1.27]	3.92 [2.47, 6.23]
$m_{[0-1]}$	0.39 [- 0.16, 0.95]	4.22 [3.63, 4.91]	2.30 [1.69, 3.13]
$m_{[0-0.5]}$	1.20 [0.16, 2.24]	7.67 [6.57, 8.95]	1.82 [1.41, 2.35]
$m_{[0.5-1]}$	-0.72 [- 1.93, 0.49]	8.85 [7.47, 10.48]	1.64 [1.27, 2.12]

S2.3 Transparent methods

S2.3.1 Experimental Animals

We used a commercially available hive of bumblebees (*Bombus terrestris*) from Koppert B.V. (Berkel en Rodenrijs, the Netherlands) for our experiments. The colony contained 50 – 70 worker bumblebees (female) that engaged in different activities required to maintain the hive. Among others, they performed foraging flights to collect artificial nectar (50% sugar solution obtained from Koppert B.V.) from a feeding platform. They had ad libitum access to the food source during the day and were given dried pollen directly in the hive at the end of each day. We placed the hive in an indoor laboratory where the temperature was maintained at $21 \pm 2^\circ\text{C}$ and the hive remained connected to our setup for the entire duration of the experiment.

S2.3.2 Experimental setup

The experimental setup consisted of a flight arena ($3 \times 0.48 \times 0.48$ m; length \times width \times height), with a bumblebee hive, food source, and a real-time machine-vision based videography system for tracking the flying bumblebees (Figure 2.2A,B). The top, bottom, and longitudinal side walls of the flight arena were made of transparent poly-carbonate sheets (thickness 0.01 m) and the far ends were closed with meshes. We installed the hive and a food source (containing sugar solution) outside the flight chamber and directly opposite to each other (Figure 2.2A). The hive and the food-source were connected to the longitudinal walls of the flight chamber near its middle section using Plexiglas tubes. These tubes extended 0.07 m inside the flight chamber and had vertical landing platforms attached at the end (Figure 2.2B). The landing discs were covered with either a checkerboard pattern (0.01 m black and white squares) or spoke pattern (32 spokes filled with alternating black and white colours) (Figure 2.2C) printed on a normal paper.

The flight chamber was illuminated with white broad-spectrum LED light panel (Lumihome 595×595 mm, 4800 lm, LED type: SMD2835, 4000K), powered with 300 W power supply (maximum 40 V and 1.1 A) (RS PRO RS6005P). This light panel was placed 50 cm above the chamber's top wall and right above the middle section of the flight arena (Figure 2.2A,B). The light panel could be set to three different light intensities by PWM dimming: a low light condition simulating dusk (13.7 lx), a medium light condition (33.3 lx), and a high light condition equivalent to sunrise (144.9 lx). Reported light intensities were the average at the centre of the flight arena and at the landing platforms, measured using a spectroradiometer (Specbos 1211 with JETI Lival software, Figure S2.7).

Flight movements of the foraging bumblebees were tracked in 3D using a real-time machine-vision based videography system. The system consisted of four synchronized high-speed cameras (one Basler acA1300 – 200um camera with 12 mm Fujinon lens and three Basler acA2040 – 90um cameras with 12.5 mm Kowa lenses), which viewed the central

portion of the arena from two orthogonal positions above the arena and two orthogonal positions from the side (Figure 2.2A). The cameras operated at 175 frames per second, image resolution was 504×504 pixels for Basler acA2040 – 90um cameras and 512×512 pixels for Basler acA1300 – 200um camera, and image depth was 8 bits. Exposure times were $260 \mu\text{s}$, $200 \mu\text{s}$, $400 \mu\text{s}$ and $900 \mu\text{s}$ for top-left (Basler acA2040 – 90um), top-right (Basler acA2040 – 90um), side-left (Basler acA2040 – 90um), and side-right (Basler acA1300 – 200um) cameras, respectively. All cameras were back-lit using custom-built arrays of infrared (IR) LED panels (centroid wavelength: 850 nm) to enhance the contrast of bumblebees with the background (19.25 V, 1 A).

When running, the real-time machine-vision based videography system estimated the three-dimensional position of all moving bumblebees at each recording time step. Based on these, movement trajectories for each bumblebee were constructed. To remove tracking noise from these trajectories, we filtered these using a low-pass second-order two-directional Butterworth filter (`filtfilt` in Matlab 2020a, MathWorks Inc) with a cut-off frequency of 20 Hz, and then stored in arrays with space-time vectors $\mathbf{X}_G = (x_G, y_G, z_G, t_G)$. Position was defined in the global coordinate system (not shown), and time resolution equalled that of the videography system (1/175 s). The software also had the option to automatically store video images to disc, based on tracking output. We calibrated the videography system four times throughout the experiments using Direct Linear Transformation; a correction for lens distortion was performed once (Svoboda et al., 2005; Straw et al., 2011).

S2.3.3 Experimental procedure

Before starting the experiments, we trained the bumblebees for 10 days to forage in the arena at the low light intensity condition. At the start of the training period, we directly connected the hive and food source with a bridge, allowing the bumblebees to walk to the food source; each day, we gradually increased the bridge gap until after 10 days the forager bumblebees would comfortably fly back and forth between hive and food source.

During training and experiments, we exposed bumblebees to a day-night cycle of 10 – 14 hours with day starting at 07:30h and ending at 17:30h. Sunrise (07:30h–08:00h) was simulated by gradually increasing the light intensity from zero to the light condition for the experiment (low, medium or high) or training (low). Similarly, sunset (17:00h–17:30h) was simulated by gradually reducing the last light condition of the day down to zero. During experiments, the rest of the day (08:00h–17:00h) was divided into 6 time-slots of 1.5 hours each. We changed the light condition in each time-slot and landing platform every day (Table S2.7).

Since the recorded landing maneuvers are likely to be highly stereotypical, we used a single hive in our study. The recorded landing maneuvers are thus pseudo-replications of foraging bumblebees that existed in the hive over a span of 14 consecutive days.

S2.3.4 Extraction of landing tracks

From all trajectory data of bumblebees inside the flight arena, we first selected the tracks in which bumblebees were flying, as tracks that were less than 5% of the time closer than 6 cm from the side walls or less than 0.1% of the time closer than 5 cm from the top and bottom surfaces. Among the resulting flight tracks, we then selected the tracks in which bumblebees approached one of the landing platforms. These landing approach tracks were defined as tracks that started at a normal distance (along y -axis) of at least 10 cm from the landing platform, and had a minimum normal distance to the platform of less than 2 cm. For each track that met those criteria, the landing approach maneuver was selected as the trajectory section between the distance furthest away from the landing platform and closest distance (up to 1 cm). Furthermore, the tracks starting close to either of the platforms (within 2.5 cm long cylinder around opposite disc) or the ground (less than 2 cm distance from ground) were labelled as the landing approaches starting from a take-off and the rest of the tracks were labelled as the landing approaches from free-flight condition.

The landing approaches were stored as space-time arrays $\mathbf{X} = (x, y, z, t)$, in the landing platform coordinate system (Figure 2.2C). This Cartesian coordinate system has its origin at the centre of the landing platform, y normal to the platform, and z upwards. Time t was set to zero at the end of the trajectory, i.e. when the bumblebee reached the closest distance to the platform. The corresponding velocity and acceleration vectors ($\mathbf{U} = (u, v, w)$ and $\mathbf{A} = (a_x, a_y, a_z)$, respectively) were computed by numerical differentiation using a second-order central differentiation scheme and stored. These approach sequences, referred to as landing maneuvers, were analysed in this study.

S2.3.5 Estimation of state variables and set-points of relative rate of expansion

To analyse the landing dynamics of bumblebees, we focused on the movement normal to the landing platform, which can be described by the state variables: normal distance from the platform $y(t)$, flight velocity towards the platform $V(t) = -v(t)$, and acceleration towards the platform $A(t) = -a_y(t)$. Based on these, we calculated the instantaneous relative rate of optical expansion throughout each landing approach track, as $r(t) = V(t)/y(t)$. In total, we thus used the temporal dynamics of four state variables (y, V, A, r) to describe the dynamics of bumblebees decelerating as they approach a surface for landing. A previous study suggested that bumblebees on an average hold the relative rate of expansion constant during a landing approach (Chang et al., 2016). Therefore, we developed a custom-made search algorithm for automatic identification of the landing approach segments in which the relative rate of expansion was close to a constant as bumblebees were decelerating.

The constant- r detection algorithm is based on six parameters that together define the constancy of r in a track segment. For an arbitrary track segment, these six parameters

are computed from three first-order linear regressions (one regression in full segment, and two regressions in two equal halves of the full segment) and they evaluate the deviations of these regressions from a constant r regression. To evaluate these deviations, we first find the expected probability distributions for each of these six parameters when bumblebees were flying with constant r , and then check whether the six parameters computed for an arbitrary segment lie within certain threshold around the expected mean of each parameter. This threshold is specified by a setting parameter f whose value can be changed to alter the variation allowed around the mean of each of the six linear regression parameters for an arbitrary segment to be identified as a constant- r segment. This f is thus similar to the number of standard deviations around the mean of a normally distributed variable that is included in the selection. Hence, by finding these parameters for different track segments in a landing maneuver, we could identify all track segments in which a bumblebee kept the variation of r below a threshold defined by a fixed value of factor f .

The identified track segments are called constant- r segments and are characterized by their average values of the four state variables (y^* , V^* , A^* , r^*). Here, r^* is a linear regression estimate from $r(t) = r^* + \epsilon$ (where ϵ denotes residuals) within a constant- r segment, and we use it as an estimate of the set-point of relative rate of expansion that the bumblebee aims to hold constant. This is because r^* for each constant- r track segment is very close to m , where m is a linear regression estimate of $V(t) = m \times y(t) + \epsilon$ (ϵ denotes residuals) in a constant- r segment (mean, median and maximum difference between the two values are 0.005, 0.002 and 0.096 s^{-1} , respectively). Moreover, the difference between the actual flight duration and the analytically computed flight duration if the bumblebees had followed exactly the estimated set-points of relative rate of expansion within identified constant- r segments is extremely low (maximum difference = 0.0086 s which is only 1.5 times $1/175$ s, the time resolution of the experimental apparatus). Additionally, we only consider the velocity perpendicular to the platforms as this component of the velocity was needed to be progressively built and later progressively reduced as bumblebees approached the platforms for landing. However, the deceleration strategy of adjusting these set-points with distance remains unchanged if 3D speed is considered.

S2.3.6 Statistical models

All statistical analyses were done in R 4.0.2 (R Foundation). We used `lmer` to develop different linear mixed-effects models for the two analysis methods. The landing patterns, light conditions, landing type (take-off and free-flight) along with their (significant) interactions are considered as fixed factors, and day of the experiment, landing side (whether the landing disc is located towards the hive or the food-source) and each landing approach are considered as random intercepts. We used model dredging to identify the minimal linear mixed-effects statistical model. For post-hoc tests, we used Bonferroni correction (using `emmeans` package in R) to adjust the statistical significance values for comparison of means

and covariates in different treatments (landing patterns and light conditions) and for different landing types. p -values < 0.05 were considered statistically significant. Unless stated otherwise, data-sets averages and distributions are given as mean \pm standard deviation, including sample size (n); statistical model predictions are given as mean [standard error], including p -values if relevant.

Specifically, the linear mixed-effects models were developed to determine (a) the set-points of relative rate of expansion (r^*) in average-per-treatment method, (b) the set-point variation with distance from the landing platforms (y^*) in per-track method, and (c) the effect of landing patterns, light conditions and landing type (landings starting from take-off or free-flight) in both analyses.

The average-per-treatment model

For the average-per-treatment analysis method, we computed the mean relative rate of expansion in each tested treatment by first using pattern, light, starting conditions along with all possible interactions as fixed factors and day of the experiment, landing approach number, and landing side (whether landing disc is located on the hive side or the food source side) as random factors. The model dredging revealed only *pattern* \times *startingCondition* as significant, therefore we used the reduced model (Equation S2.1).

$$r_{i,d,a,s} \sim N(\alpha + \alpha_d + \alpha_a + \alpha_s + \beta_1 \text{SPOKE}_{i,d,a,s} + \beta_2 \text{MEDIUMlight}_{i,d,a,s} + \beta_3 \text{HIGHlight}_{i,d,a,s} + \beta_4 \text{fromTakeoff}_{i,d,a,s} + \beta_5 \text{SPOKE}_{i,d,a,s} \times \text{fromTakeoff}_{i,d,a,s}, \sigma^2) \quad (\text{S2.1})$$

where $r_{i,d,a,s}$ is the relative rate of expansion for the i -th measurement from d -th day ($d \in \{1, 2, \dots, 14\}$), a -th landing approach ($a \in \{1, 2, \dots, 10005\}$) and s -th landing side ($s = 1$ for hive side and $s = 2$ for food-source side), α is the regression intercept for checkerboard pattern and low light condition (overall intercept), α_d is the day-specific intercept, α_a is the landing-approach-specific intercept, α_s is the landing-side-specific intercept, $\text{SPOKE}_{i,d,a,s}$, $\text{MEDIUMlight}_{i,d,a,s}$, $\text{HIGHlight}_{i,d,a,s}$ and $\text{fromTakeoff}_{i,d,a,s}$ indicate if spoke landing pattern, medium light condition, high light condition and take-off are present for the i -th measurement from d -th day, a -th landing approach and s -th landing side (0 = no, 1 = yes), $\beta_i \forall i \in \{1, 2, 3, 4, 5\}$ represent differences of fixed-effects and an interaction term from overall intercept, and σ is the residual standard deviation. The statistical output, along with post-hoc tests, from data of 10,005 landing approaches in the selected range of distance to the platforms ($0.04m \leq y \leq 0.11m$) is given in Table S2.2.

The per-track analysis model

For the per-track analysis method, the dependence of set-points of relative rate of expansion (r^*) on distance to the platform (y^*) was deemed based on the interdependence of r and y

for a constant- \dot{r} landing strategy (Equation S2.8b) i.e., a linear relationship between their log transformations. To adjust the dependence of r^* on y^* as per constant- \dot{r} law, we first constructed a full model with $\log(r^*)$ as response variable, $\log(y^*)$, landing patterns, light conditions, landing types along with all interactions as fixed factors, and day of the experiment, landing approach and landing side (whether landing disc is located on the hive side or the food source side) as random intercepts. Among all interaction terms, the model dredging revealed only $\log(y^*) \times pattern$ and $\log(y^*) \times startingCondition$ interaction terms as significant, therefore we used the following reduced model:

$$\log(r_{i,d,a,s}^*) \sim N(\alpha + \alpha_d + \alpha_a + \alpha_s + \beta_1 \log(y_{i,d,a,s}^*) + \beta_2 \text{SPOKE}_{i,d,a,s} + \beta_3 \text{MEDIUMlight}_{i,d,a,s} + \beta_4 \text{HIGHlight}_{i,d,a,s} + \beta_5 \text{fromTakeoff}_{i,d,a,s} + \beta_6 \log(y_{i,d,a,s}) \times \text{fromTakeoff}_{i,d,a,s} + \beta_7 \log(y_{i,d,a,s}) \times \text{SPOKE}_{i,d,a,s}, \sigma^2) \quad (\text{S2.2})$$

where $r_{i,d,a,s}^*$ and $y_{i,d,a,s}^*$ are set-point of relative rate of expansion and mean distance, respectively, for the i -th constant- r segment from d -th day ($d \in \{1, 2, \dots, 14\}$), a -th landing approach ($a \in \{1, 2, \dots, 4672\}$) and s -th landing side ($s = 1$ for hive side and $s = 2$ for food-source side), α is the regression intercept for checkerboard pattern, low light condition and free-flight starting condition (overall intercept), α_d is the day-specific intercept, α_a is the landing-approach-specific intercept, α_s is the landing-side-specific intercept, $\text{SPOKE}_{i,d,a,s}$, $\text{MEDIUMlight}_{i,d,a,s}$, $\text{HIGHlight}_{i,d,a,s}$ and $\text{fromTakeoff}_{i,d,a,s}$ indicate if spoke landing pattern, medium light condition, high light condition and take-off starting condition are present for the i -th measurement from d -th day, a -th landing approach and s -th landing side ($0 = \text{no}$, $1 = \text{yes}$), β_1 represents the regression slope for predictor $\log(y^*)$ (overall slope), $\beta_i \forall i \in \{2, 3, 4, 5, 6, 7\}$ represent differences of fixed-effects including an interaction from overall intercept and slope, and σ is the residual standard deviation. The statistical output, along with post-hoc tests, from data of 4, 672 landing maneuvers is given in Table S2.5.

S2.3.7 Algorithm for automatic extraction of set-points of relative rate of expansion

In order to automatically extract the segments of landing tracks in which bumblebees kept the relative rate of expansion constant (constant- r segments), we first define methods to estimate the set-points of relative rate of expansion and the variation of relative rate of expansion around its estimated set-point. We later use these defined methods to construct an algorithm for automatic search of constant- r segments in each landing approach.

S2.3.8 Estimation of a set-point of relative rate of expansion

For a track segment in which relative rate of expansion is held constant, we find a zeroth-order linear regression of r to obtain the set-point (r^*) at which r is held constant (Equations S2.3).

$$r(t) = r^* + \epsilon \quad (\text{S2.3a})$$

$$r^* = \frac{\sum_{i=1}^n r(t_i)}{n} \quad (\text{S2.3b})$$

where n denotes the number of data points in that track segment and ϵ denotes the residuals. The intercept (r^*) in the linear regression is an average of the relative rate of expansion observed within a constant- r segment and is used as an estimate of the set-point of r within that segment.

Identification of variation around the set-points

To find the expected variation of r around the set-points in constant- r segments, we began by identifying such segments in a smaller data-set using a custom-built Graphical User Interface (GUI) in Matlab 2020a. In this GUI, we plotted the computed state variables (V and r) against the perpendicular distance from the platform (y) and manually selected segment(s) of y (similar to the ones highlighted in red in Figure 2.4A) over which the instantaneous relative rate of expansion (or its mean) was observed to be nearly constant. For this purpose, we use first 532 landing maneuvers recorded for high light condition and spoke landing pattern. Out of 532 tracks, we identified 313 tracks with 355 constant- r segments (273 tracks with one segment, 38 tracks with two segments and 2 tracks with three segments) and estimated the set-point r^* using Equations S2.3 for each such segment.

To find the variation of r around the estimated set-points r^* , we estimated slopes and intercepts of three first-order linear fits in each such segment - one through the complete segment and two through its equal halves (Equations S2.4). Since, the relative rate of expansion is expected to be nearly constant in the full segment and also in its two halves, the variations of three slopes, along with differences between three intercepts and the corresponding estimated set-point for the full segment, are expected to be centered around zero. We use the two halves of the segments in addition to the full segment to avoid false positives segments being detected, namely in which bumblebees are either transitioning from acceleration to deceleration phase or vice-a-versa.

$$r_{[0-1]} = m_{[0-1]} y_{[0-1]} + c_{[0-1]} + \epsilon \quad (\text{S2.4a})$$

$$r_{[0-0.5]} = m_{[0-0.5]} y_{[0-0.5]} + c_{[0-0.5]} + \epsilon \quad (\text{S2.4b})$$

$$r_{[0.5-1]} = m_{[0.5-1]} y_{[0.5-1]} + c_{[0.5-1]} + \epsilon \quad (\text{S2.4c})$$

Subscripts $[0 - 1]$, $[0 - 0.5]$, and $[0.5 - 1]$ denote the full segment, first half, and second half of the segment, respectively, variables m and c denote the slope and intercept of a fit obtained using first-order linear regression and ϵ denotes the residuals in each case.

The distributions of three slopes ($m_{[0-1]}$, $m_{[0-0.5]}$ and $m_{[0.5-1]}$) and distributions of differences between three intercepts and the corresponding estimated set-point for the full segment ($c_{[0-1]} - r^*$, $c_{[0-0.5]} - r^*$ and $c_{[0.5-1]} - r^*$) are fitted using generalized student's t -distribution to identify their probability density functions (tLocationScaleDistribution in Matlab 2020a). Each such distribution is defined by a location parameter μ , scale parameter σ and shape parameter ν (σ dictates the spread of the distribution). As expected (Table S2.8), the location parameter (μ) for the distribution of six parameters is close to zero as the change in relative rate of expansion resulting due to estimated location parameters is very small for the distances covered during constant- r segments. Moreover, the estimated scale parameters (σ) of $m_{[0-0.5]}$ and $m_{[0.5-1]}$ distributions are approximately twice the scale parameter of $m_{[0-1]}$ distribution. Similarly, the scale parameters of $c_{[0-0.5]} - r^*$ and $c_{[0.5-1]} - r^*$ distributions are approximately twice the scale parameters of $c_{[0-1]} - r^*$ distribution. Therefore, we represent the location parameters for all six distributions with the expected value zero and scale parameters of $c_{[0-1]} - r^*$, $c_{[0-0.5]} - r^*$, $c_{[0.5-1]} - r^*$, $m_{[0-1]}$, $m_{[0-0.5]}$, and $m_{[0.5-1]}$ distributions as σ_1 , $2\sigma_1$, $2\sigma_1$, σ_2 , $2\sigma_2$ and $2\sigma_2$, respectively (where $\sigma_1 = 0.53$ and $\sigma_2 = 4.22$). We use the represented distributions in the constant- r extraction algorithm as they are very close to the estimated ones (Figure S2.6).

Along with aforementioned six parameters, we define three other parameters to calculate mean acceleration in the full segment ($A_{[\text{mean}, 0-1]}$) and its two equal halves ($A_{[\text{mean}, 0-0.5]}$ and $A_{[\text{mean}, 0.5-1]}$), where subscripts $[\text{mean}, 0 - 1]$, $[\text{mean}, 0 - 0.5]$ and $[\text{mean}, 0.5 - 1]$ denote the mean of the acceleration computed for a full segment, first half and second half of the segment, respectively. As these mean acceleration values are almost always negative for the manually-identified 355 constant- r segments (Figure S2.6), we use these three mean acceleration parameters to identify the track segments in which a bumblebee decelerated during its landing maneuver.

Algorithm for automatic extraction of segments with constant relative rate of expansion

To automatically identify the segments of constant relative rate of expansion in each landing track, we used the following algorithm:

1. Beginning with the first data point in each track, we looked at t_w time points ahead where $t_w \in \{15, 16, \dots, 49, 50\}$ and it denotes the size of different time-windows (or segments). We chose the minimum limit for the time points (15 data points) close to the median of time points observed in 355 manually-identified constant- r segments (18 data points). The maximum limit for the time points (50 data points) is chosen as the number of data points in most manually-identified constant- r seg-

ments (353 out of 355) were below 50. Note that any long deceleration phase with more than 65 data points will be captured as two (or more) segments, but that does not affect the results observed in our study.

2. We select all those segments which satisfy the following constraints:

$$\begin{aligned}
 |c_{[0-1]} - r^*| \leq f\sigma_1 \text{ and } |c_{[0-0.5]} - r^*| \leq 2f\sigma_1 \text{ and } |c_{[0.5-1]} - r^*| \leq 2f\sigma_1 \text{ and} \\
 |m_{[0-1]}| \leq f\sigma_2 \text{ and } |m_{[0-0.5]}| \leq 2f\sigma_2 \text{ and } |m_{[0.5-1]}| \leq 2f\sigma_2 \text{ and} \\
 A_{[\text{mean},0-1]} \leq 0 \text{ and } A_{[\text{mean},0-0.5]} \leq 0 \text{ and } A_{[\text{mean},0.5-1]} \leq 0
 \end{aligned}
 \tag{S2.5}$$

where f is a factor that decides the threshold on the variation allowed around the mean for first six parameters (see Section S2.3.8 for details). The first three constraints limit the variation allowed, around the constant r regression, for intercepts of first-order linear regressions in an arbitrary full segment and its two equal halves. Similarly, the next three constraints limit the variation allowed around zero for slopes of first-order linear regressions in a full segment and its two equal halves. The last three constraints helps in determining the track segments in which a bumblebee decelerates during its landing maneuver.

3. We repeat steps 1 and 2 for all data points in the landing track. The resulting set of selected segments contains segments that satisfy the constraint mentioned in Step 2 and may have some data points in common with other segments. Therefore, from the resulting set, we further find a subset of non-overlapping segments based on root mean square error (RMSE) in relative rate of expansion. For a segment containing n data points and estimated set-point r^* , RMSE error is calculated as given by Equation S2.6.

$$r_{\text{RMSE}} = \sqrt{\frac{\sum_{i=1}^n (r_i - r^*)^2}{n}}
 \tag{S2.6}$$

where r_i is the relative rate of expansion at i -th point in a segment. After computing r_{RMSE} for all selected segments, the subset of non-overlapping segments is found by first choosing the segment with lowest r_{RMSE} and discarding all other segments with which it has data points in common. The segment with lowest r_{RMSE} in the remaining set of segments is then chosen and the segments in the remaining set it overlaps with are discarded. This process is followed until there are no segments left to choose. The set of chosen segments are then all non-overlapping and satisfy the constraints given by Equation S2.5. We use RMSE error for this selection process as it favours the track segments with higher number of data-points.

The resulting non-overlapping segments in a landing track are identified as the constant- r segments.

Verification of results from automatic constant- r detection algorithm

To verify the results from constant- r detection algorithm, we compared the dependence of set-points of relative rate of expansion (r^*) with distance from the platform (y^*) for smaller data-set (313 landing maneuvers in which constant- r segments were manually identified) and complete data-set (4,672 landing maneuvers for factor $f = 1$). We observed that r^* increased significantly as y^* decreased with slope (time-to-contact-rate) estimate from regression for smaller data-set ($\dot{\tau} = -0.72$) being similar to the average slope (time-to-contact-rate) estimate for complete data-set ($\dot{\tau} = -0.81$).

Effect of factor f

Varying factor f has an effect similar to varying the number of standard deviations around the mean (e.g., 1 – 2 – 3 standard deviations for 68% – 95% – 99.7% empirical rule) of a normally distributed variable. Thus, increasing f leads to the detection of more false positives and fewer false negatives. Specifically, the factor f in Equation S2.5 determines following two aspects:

1. the threshold of the variation allowed around the mean for each parameter ($c_{[0-1]} - r^*$, $c_{[0-0.5]} - r^*$, $c_{[0.5-1]} - r^*$, $m_{[0-1]}$, $m_{[0-0.5]}$ and $m_{[0.5-1]}$) (Figure S2.5A)
2. the percentage of values of each parameter that lie within f scale-parameter band around the mean (Figure S2.5B)

Increase in f increases the threshold allowed in variation of r for a track segment to be identified as a constant- r segment, and hence, higher f can result in detection of new constant- r segments along with possible increase in the width of constant- r segments identified with lower f . However, increase in f beyond a certain value results in higher probability of detection of false positives without much increase in the true positives. We performed a sensitivity analysis by systematically varying f from 0.25 – 2.5 and analyzing its effect on distribution of set-points of relative rate of expansion (r^*) identified, r^* dynamics with distance to the platform (y^*) and effect of environmental conditions on this dynamics (Figure S2.5C,D). We observed that all of these results remain essentially unaltered in the tested wide-range of f .

S2.3.9 Calculation of relative approach speeds of the hybrid landing strategy

We tested how the here-described hybrid landing strategy compares to both the constant- r strategy and the constant- $\dot{\tau}$ strategy. For this, we calculated for each set of two consecutive constant- r segments, the hybrid-to-constant- r speed ratio and the hybrid-to-constant- $\dot{\tau}$ speed ratio as U_H/U_r and $U_H/U_{\dot{\tau}}$, respectively. Here, U_H is the average flight speed during the set of two consecutive constant- r segments, defined as $U_H = \Delta y_2 / \Delta t_2$, where

Δy_2 and Δt_2 are the distance travelled and flight duration, respectively (Figure 4a in the main text). U_r is the equivalent flight speed if the bumblebee would have used the constant- r strategy and continued to fly at its first set-point (r_1^*), and is defined as $U_r = 2/(r_1^*(y_{start} + y_{end}))$, where y_{start} and y_{end} are the distances from the platform at the start and end of the flight section. $U_{\dot{\tau}}$ is the equivalent speed if the bumblebee would have used the constant- $\dot{\tau}$ strategy to fly continuously at the average time-to-contact-rate observed in our data-set ($\dot{\tau} = -0.87$), with an initial approach speed equal to that at the start of a flight section. The resulting average speed $U_{\dot{\tau}}$ is then calculated as the average of approach velocities computed using Equation S2.8a. For this purpose, we used 1, 008 instead of 1, 015 landing maneuvers with two constant- r segments because remaining seven landing maneuvers corresponded to bumblebees flying away from the platforms in between the two consecutive constant- r segments.

S2.3.10 Governing equations for a constant time-to-contact-rate landing strategy

For an animal approaching a platform (Figure 2.1A), at time t , we denote its distance to the platform as $y(t)$, approach velocity as $V(t)$, relative rate of expansion as $r(t)$, time-to-contact parameter as $\tau(t)$, time-to-contact-rate parameter as $\dot{\tau}(t)$ and following holds:

$$V(t) = -\frac{dy(t)}{dt}, r(t) = \frac{1}{\tau(t)} = \frac{V(t)}{y(t)} \text{ and } \dot{\tau}(t) = \frac{d\tau(t)}{dt} \quad (\text{S2.7})$$

The equations that govern dependence of state variables r and V on y for a constant $\dot{\tau}$ landing strategy are derived elsewhere (Baird et al., 2013) and only final equations are depicted here (Equations S2.8).

$$V(t) = c_1 y(t)^{\dot{\tau}+1} \quad (\text{S2.8a})$$

$$r(t) = c_2 y(t)^{\dot{\tau}} \quad (\text{S2.8b})$$

where c_1 and c_2 are constants that depend on initial conditions of the state variables y , V and r .

S2.3.11 Parametrization of probability density functions used in this study

We use two probability density functions (pdf) in this study which are parametrized as follows:

- I. Gamma distribution (GammaDistribution in Matlab 2020a) - For a shape parameter a and scale parameter b , the pdf of the gamma distribution is

$$p(x | a, b) = \frac{1}{b^a \Gamma(a)} x^{a-1} e^{-\frac{x}{b}} \quad (\text{S2.9})$$

where $\Gamma(\cdot)$ is the Gamma function.

2. Generalized student's t -distribution (`tLocationScaleDistribution` in MATLAB 2020a) - For a location parameter μ , scale parameter σ and shape parameter ν , the pdf of generalized student's t -distribution is

$$p(x | \mu, \sigma, \nu) = \frac{\Gamma\left(\frac{\nu+1}{2}\right)}{\sigma\sqrt{\nu\pi}\Gamma\left(\frac{\nu}{2}\right)} \left[\frac{\nu + \left(\frac{x-\mu}{\sigma}\right)^2}{\nu} \right]^{-\left(\frac{\nu+1}{2}\right)} \quad (\text{S2.10})$$

where $\Gamma(\cdot)$ is the Gamma function.

S2.4 Movie

A video of a bumblebee taking off from one platform and landing on another is available at <https://doi.org/10.1016/j.isci.2021.102407>. This movie corresponds to the photomontage in Figure 2.2D and plays 5.83x slower than the actual speed.

References

- Baird, E., Boeddeker, N., Ibbotson, M. R. and Srinivasan, M. V. (2013). A universal strategy for visually guided landing. *Proceedings of the National Academy of Sciences of the United States of America* **110**, 18686–18691.
- Chang, J. J., Crall, J. D. and Combes, S. A. (2016). Wind alters landing dynamics in bumblebees. *The Journal of Experimental Biology* **219**, 2819–2822.
- Straw, A. D., Branson, K., Neumann, T. R. and Dickinson, M. H. (2011). Multi-camera Real-time Three-dimensional Tracking of Multiple Flying Animals. *Journal of The Royal Society Interface* **8**, 395–409.
- Svoboda, T., Martinec, D. and Pajdla, T. (2005). A convenient multicamera self-calibration for virtual environments. *Presence: Teleoperators and Virtual Environments* **14**, 407–422.



Chapter 3

Bumblebees land rapidly by robustly accelerating towards the surface during visually guided landings

Pulkit Goyal¹, Johan L. van Leeuwen¹, Florian T. Muijres¹

¹ Experimental Zoology Group, Wageningen University & Research, Wageningen, The Netherlands

Abstract

Many flying animals including insects parse visual feedback to decelerate during their landing approach. In addition to deceleration, some insects are also shown to accelerate during landing. Here, we study how landing bumblebees (*Bombus terrestris*) use visual cues to accelerate. Bumblebees use radial optic expansion cues to decelerate. They fly at a constant relative rate of expansion for brief intervals of time to reduce their approach velocity. This constant is referred to as a set-point and we analyze how their different subsystems (sensory system, controller and motor system) function together to reach these set-points in 10,005 landing maneuvers. Our results show that their closed-loop sensorimotor control system regulates the relative rate of expansion as bumblebees advance towards the landing surface. The track segments before and during a set-point are the transient and steady-state responses of such a control system. Bumblebees use the transient response to mostly accelerate towards the platform and steady-state response to always decelerate during landing. These results explain how bumblebees can land rapidly, allowing them to visit flowers very frequently (up to 1000 times in an hour), even in challenging environmental conditions. Based on our results, we propose a sensorimotor control system of bumblebees that facilitates rapid and robust execution of their modular landing strategy. Additionally, these results can provide inspiration for similar control systems in unmanned aerial vehicles.

3.1 Introduction

Bumblebees rely on the landing phase of their flight to visit flowers and gather nectar and pollen. It is essential for their survival and reproduction. They visit flowers very frequently (up to 1000 in an hour) (Heinrich, 1979), and for each visit, they accurately control their flight speed so that it reduces to near zero closer to the landing surface (Chang et al., 2016; Reber et al., 2016). Such a control ensures soft touchdown, and thus reduces the risk of damage that can be caused by high impact collisions (Foster and Cartar, 2011; Mountcastle and Combes, 2014; Rajabi et al., 2020).

Like many other flying animals (Lee et al., 1991, 1993; Srinivasan et al., 2000; Van Breugel and Dickinson, 2012; Baird et al., 2013; Liu et al., 2019; Tichit et al., 2020a), bumblebees use visual cues to accurately control their flight speed during landing (Chang et al., 2016; Goyal et al., 2021a). As they advance towards a surface for landing, their motion relative to the landing surface generates optical expansion cues in which various features in the visual field appear to move radially outward from the point that is being approached (Gibson, 1955; Edwards and Ibbotson, 2007). Bumblebees may use these optical expansion cues along with the retinal size of an object (Wagner, 1982) or angular position of features in the visual field (Baird et al., 2013) to measure the relative rate of expansion r . This relative rate of expansion encodes the ratio of approach velocity V and distance to the landing surface y as $r = V/y$ (Figure 3.1A).

Our previous study showed how bumblebees (*Bombus terrestris*) use this relative rate

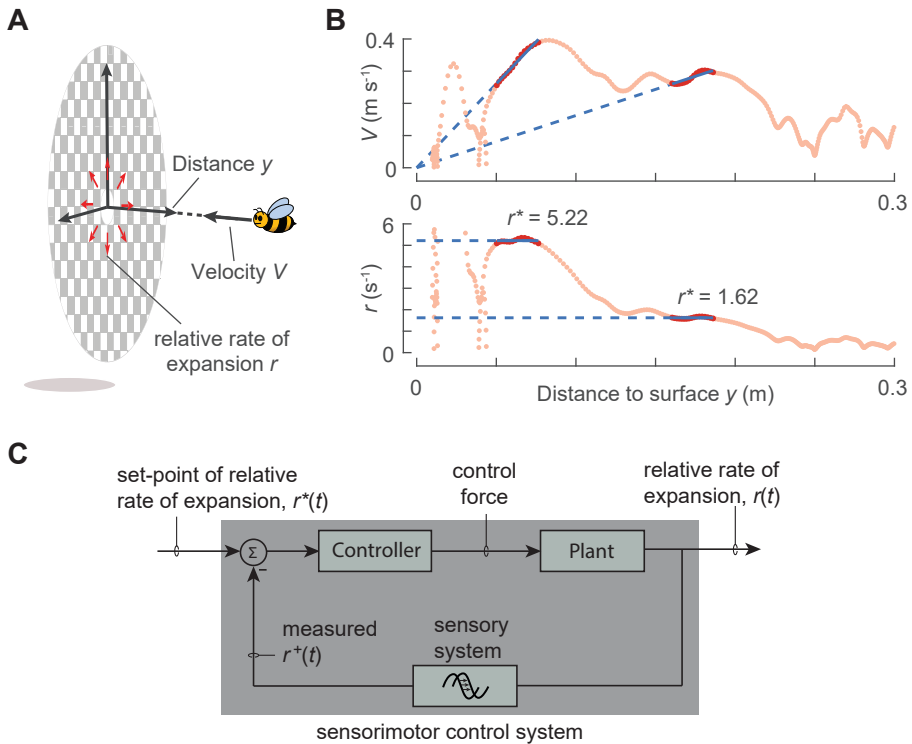


Figure 3.1: The landing strategy of bumblebees and hypothesized sensorimotor control system that bumblebees may use during landing. (A) A schematic of a bumblebee approaching a landing surface. Due to its motion perpendicular to the landing surface, the bumblebee flying at an approach velocity V and at a distance y experiences a relative optical rate of expansion $r = V/y$. (B) The variation of approach velocity V and relative rate of expansion r with perpendicular distance from the platform y for a typical landing maneuver of a bumblebee. The red sections show the periods when the landing bumblebee keeps the relative rate of expansion approximately constant. The constant r values are referred to as set-points of the relative rate of expansion r^* and are indicated by the dashed blue lines (as slope and ordinate values in the V - y and r - y graphs, respectively). (C) The closed-loop sensorimotor control system that we hypothesize bumblebees use during landing. As a bumblebee approaches a landing surface, the relative rate of expansion measured by the sensory system is compared with the desired set-point to generate an error-input for the controller; the controller would then convert this input into changes in the body and wing beat kinematics to modulate aerodynamic forces (control forces) that act on the animal (represented as 'plant'). This way, the expansion rate r converges towards the preferred set-point value r^* . This feedback control loop is similar to the forward flight speed controller in *Drosophila*, based on front-to-back optic flow (Fry et al., 2009; Rohrseitz and Fry, 2011; Medici and Fry, 2012).

of expansion to decrease their approach velocity as they reach closer to the landing surface (Goyal et al., 2021a). They decelerate in multiple bouts during their landing approach. During each bout, a bumblebee flies by approximately holding constant the relative rate of expansion; this constant is referred to as a set-point of relative rate of expansion. From one bout to the next, bumblebees tend to increase this set-point (Figure 3.1B). There are other studies that describe the landing strategies of honeybees (Baird et al., 2013), bumblebees

(*Bombus impatiens*) (Chang et al., 2016), fruit flies (Van Breugel and Dickinson, 2012; Baird et al., 2013), pigeons (Lee et al., 1993), hummingbirds (Lee et al., 1991), and mallard ducks (Whitehead, 2020). Though these studies depict the strategies these animals use to land, we do not yet know how these animals perform high-level sensorimotor control to execute these strategies.

To study the sensorimotor control of flying animals, principles from control theory are often used. With this theory, the complex physiological mechanisms of the sensorimotor control pathways that animals employ to exhibit a wide range of behaviors are often abstracted using a system level approach (for reviews, see Taylor et al., 2008; Cowan et al., 2014; Roth et al., 2014; Dickinson and Muijres, 2016; for some individual examples, see Dickson et al., 2008; Fry et al., 2009; Rohrseitz and Fry, 2011; Lehmann et al., 2012; Medici and Fry, 2012; Fuller et al., 2014; Sun, 2014; Stöckl et al., 2017; Wang et al., 2017). In this context, a set-point reaching behavior in animals is analogous to the negative feedback loops commonly applied in control engineering (Figure 3.1C) (Ogata, 2010). Here, the measured output of a system is compared to its input, the preferred value (or a set-point), to generate an error-input for the controller. Based on this input, the controller generates an appropriate motor command so that the output of the system converges to the desired goal. For example, to fly at a particular forward flight speed, fruit flies (*Drosophila melanogaster*) use the front-to-back translatory optic flow (Fry et al., 2009; Rohrseitz and Fry, 2011; Medici and Fry, 2012). They compare the translatory optic flow measured by the visual sensors with the its desired set-point and generate an error-input for the controller. The controller in turn converts this input into a change in wingbeat and body kinematics of the animal. These changes, in turn, produce forces that act on the animal (in control terminology ‘plant’) so that the translatory optic flow it is experiencing during its flight converges to its desired set-point.

Here, we investigate the sensorimotor control system of landing bumblebees and show how they use it to advance towards the landing surface. For this purpose, we use a database of 10, 005 maneuvers of bumblebees where they landed on two vertical platforms. These maneuvers corresponded to bumblebees landing directly after a take-off and from a free-flight condition (Figure 3.2A,B) (Goyal et al., 2021b). Both these landing types resemble landings of bumblebees in nature that occur within short distances (e.g., within a flower patch) and long distances (e.g., between flower patches and the hive), respectively. In these landing maneuvers, the different set-points of relative rate of expansion that bumblebees flew at were identified using an algorithm described in Goyal et al. (2021a).

We hypothesize that bumblebees exhibit a set-point reaching behavior during landing i.e., their sensorimotor control mechanism during landing uses the relative rate of expansion as a control variable; bumblebees obtain it as a sensory measurement and produce accelerations to reach its particular value - the set-point. To provide evidence in the support of this hypothesis, we study the overall closed-loop response of bumblebees as they transitioned from one set-point to the next. Specifically, we analyze the track segments

before they reached the set-points, hereafter referred to as *entry* segments, during which bumblebees accelerate (Figure 3.2D), decelerate (Figure 3.2E), or both (Figure 3.2F) to reach their set-point. Using a system identification approach from control theory, we show that the observed time course of relative rate of expansion in track segments leading up to the set-points is the transient response of the sensorimotor control system that is aiming to reach the desired set-points. This suggests that landing bumblebees use a control loop that is based on the relative rate of expansion r .

To also understand how bumblebees use the transient response of this r -based control loop to advance towards the landing platform, we first characterize their transient response as a motion at a constant expansion-acceleration (\dot{r}). The expansion-acceleration is the time-derivative of relative rate of expansion and defines how fast the animal increases or decreases its relative rate of expansion. Using this expansion-acceleration, we then identify how bumblebees regulate their transient response. This shows that this regulation of the transient response helps bumblebees to robustly accelerate towards the surface during their landing approach. These surprising acceleration phases allow bumblebees to land more rapidly than if they would perform more careful non-accelerated landings.

We also test how environmental conditions affect the transient response of the sensorimotor control system of bumblebees by analyzing their landing maneuvers from the database in the presence of different light conditions and optic expansion cues (Goyal et al., 2021b). During these landing maneuvers, bumblebees experienced three different levels of light intensities varying from twilight to sunrise, and two landing patterns that contain relatively high (a checkerboard pattern) and low optical expansion (a spoke pattern) information.

3.2 Materials and Methods

In this study, we analyze the landing maneuvers of bumblebees to elucidate the dynamic characteristics of the closed-loop sensorimotor control system that bumblebees use during landing. The in-depth details of the experimental set-up and the estimation of relevant state variables that are used to capture these landing maneuvers is provided elsewhere (Goyal et al., 2021a); therefore, we here present these aspects succinctly. The other methods are explained in detail.

Experimental animals and set-up

The experimental setup consisted of a bumblebee hive, food-source, a flight arena and a real-time machine-vision based videography system (Figure 3.2A,B). We used a commercially available hive of bumblebees (*Bombus terrestris*) from Koppert B.V. (Berkel en Rodenrijs, the Netherlands) along with their 50% sugar solution as food-source. The hive and food-source were placed opposite to each other with a flight arena ($3 \times 0.48 \times 0.48$ m; length \times width \times height) in between. Each of them was connected to a transparent Plexi-

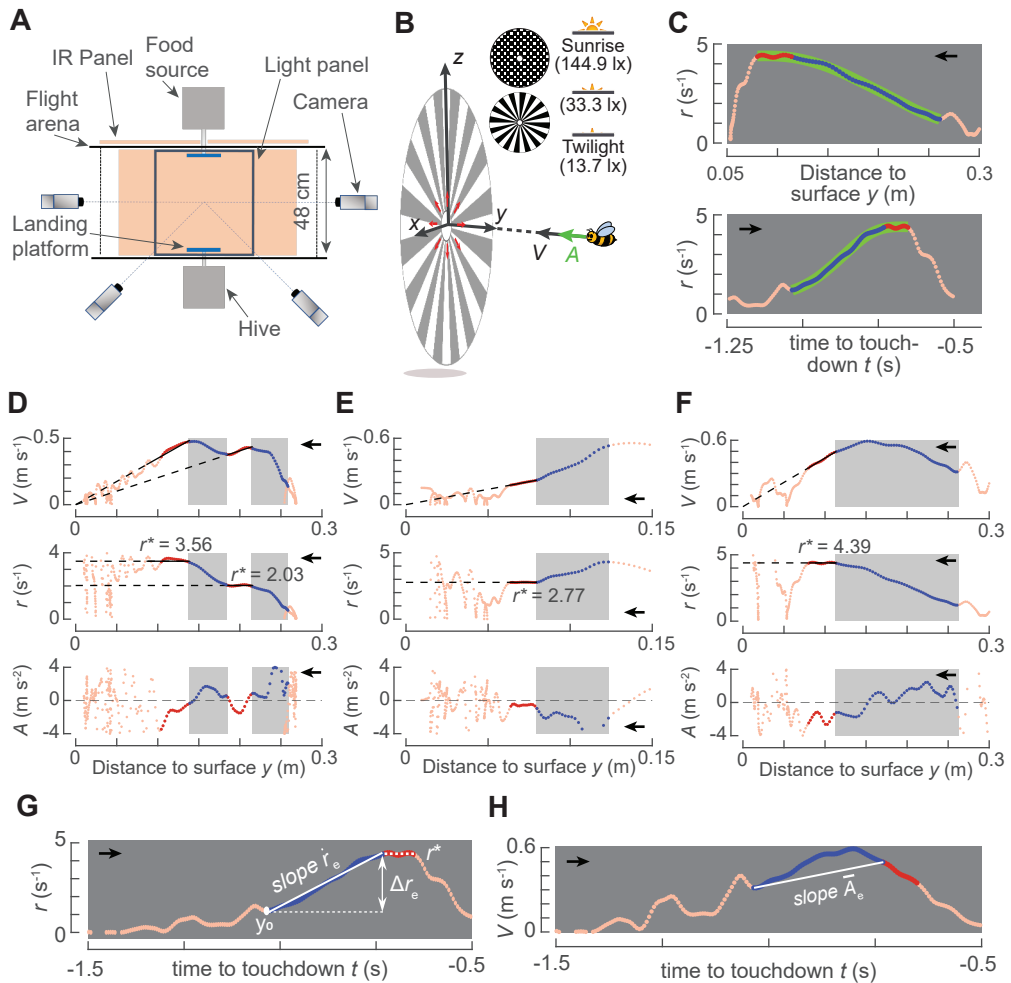


Figure 3.2: Experimental setup and conditions, the flight kinematics of typical landing maneuvers of foraging bumblebees, and definitions of the parameters used to analyze the landing dynamics.

(A) Top view of the experimental setup consisting of two vertical landing discs connected to a hive and food-source, a four-camera videography system for tracking bumblebees, and a LED light panel to vary light intensity (Goyal et al., 2021a,b). (B) Each landing is described in a Cartesian coordinate system with its origin at the center of the landing disc, z -axis vertically up, and y -axis normal to the disc and pointing into the flight arena. Four parameters describe the landing kinematics: approach distance y , approach velocity $V = -dy/dt$, approach acceleration $A = -d^2y/dt^2$ and the relative rate of optical expansion $r = V/y$ (red arrows). The different visual patterns on the landing disc and tested light intensities are also shown. (C) The variation of r with approach distance y and time t for a typical bumblebee landing maneuver. The landing maneuver includes a constant- r segment (red) and an entry segment directly preceding the constant- r segment (blue). For the entry segment and constant- r segment combined, we determined the low-pass filtered variation of $r(t)$ as $r_f(t)$ (light green). The temporal dynamics of $r_f(t)$ is modelled using the closed-loop sensorimotor control system depicted in Figure 3.1C.

(Caption continued on the next page.)

(D–F) The variation of the parameter set (V, A, r) with y for landings initiated from free-flight (D,E) and take-off (F) in the presence of a spoke landing pattern and sunrise light condition. During the entry segments (blue data, highlighted in grey), bumblebees accelerate (D), decelerate (E), or do both (F) to reach their set-point of relative rate of expansion (r^*). (G,H) The entry segments are characterized using five parameters: the derivative of relative rate of expansion referred to as expansion acceleration (\dot{r}_e), the required step change in relative rate of expansion (Δr_e), the associated set-point (r^*), the initial approach distance at which the entry segment starts (y_0), and the average acceleration during the entry segment (\bar{A}_e). (C–H) The black arrow indicates the direction in which abscissa data varies as a bumblebee approaches the landing disc.

glass tube that extended 0.07 m inside the flight arena and had a vertical landing disc (0.18 m diameter) attached at the end. These landing platforms were covered with either a checkerboard pattern (0.01 m squares) or a spoke pattern (32 spokes); both filled with alternating black and white colors. Moreover, the flight arena was illuminated by a white broad-spectrum LED light panel that was set to provide three different levels of environmental light intensity: a low-light condition depicting twilight (13.7 lx), a medium light condition (33.3 lx), and a high light condition depicting sunrise (144.9 lx). During experiments, the landing pattern was changed every day and bumblebees were exposed to all three light conditions twice a day, following a pseudo-random treatment schedule (see Goyal et al., 2021a for details) (Figure 3.2A,B).

The landing maneuvers of bumblebees in the flight arena were tracked using a real-time machine-vision based videography system that included four synchronized cameras operating at 175 frames per second. The recorded maneuvers corresponded to bumblebees that were initially flying freely in the arena and then landed on a platform, or bumblebees that just took off either from the ground or the opposite platform, and subsequently landed on the other platform.

The landing maneuvers were expressed in a Cartesian coordinate system (Figure 3.2B) which has its origin at the center of the landing platform, y -axis normal to the platform and z -axis vertically upwards. To reduce tracking noise, landing maneuvers were filtered using a low-pass second-order two-directional Butterworth filter (`filtfilt` in Matlab 2020a) with a cut-off frequency of 20 Hz. We then stored these maneuvers as space-time arrays $\mathbf{X} = (x, y, z, t)$ with time t set to zero when the bumblebee reached the closest distance to the platform. We also computed the corresponding velocity and acceleration vectors ($\mathbf{U} = (u, v, w)$ and $\mathbf{A} = (a_x, a_y, a_z)$, respectively) by numerically differentiating the space-time arrays \mathbf{X} using a second-order central differencing scheme.

Estimation of state variables and set-points of relative rate of expansion

To analyze the landing dynamics of bumblebees, we first computed the temporal dynamics of four state variables for each maneuver: normal distance from the platform $y(t)$, flight velocity towards the platform $V(t) = -v(t)$, acceleration towards the platform

$A(t) = -a_y(t)$, and instantaneous relative rate of expansion $r(t) = V(t)/y(t)$ that a bumblebee experienced due to its motion normal to the landing platform. Afterwards, using the algorithm from Goyal et al. (2021a), we identify the track segments in which bumblebees kept the relative rate of expansion nearly constant (Figure 3.2C–F). We refer to these segments as constant- r segments and characterize them with the average values of their state variables (y^* , V^* , A^* , r^*). We refer to r^* as a set-point of relative rate of expansion that the bumblebees possibly aim to reach and fly at using their sensorimotor control system (Goyal et al., 2021a).

The output of the set-point detection algorithm used to identify constant- r segments depends on a threshold factor f that limits the variation around the mean of six linear regression parameters in terms of number of scale parameter of a t -distribution (Goyal et al., 2021a). This is similar to the number of standard deviations around the mean of a normally distributed variable. Higher f leads to more and wider constant- r segments, but also increases the possibility of detecting false-positives (Goyal et al., 2021a). We performed a sensitivity analysis by systematically varying the factor f in a wide range of ($0.25 \leq f \leq 2.5$) and assessed its effect on all our results (Figure S3.1). We found that minimum threshold factor that gives the robust results is $f = 1.5$ and therefore, we here present the results for $f = 1.5$. For factor $f = 1.5$, the set-point detection algorithm identified 9, 957 constant- r segments within 6, 221 landing maneuvers out of a total of 10, 005 maneuvers.

Note that the set-point detection algorithm does not capture all of the set-points that bumblebees exhibit during landing. It misses the set-points at which bumblebees fly for some time-period, but the variation in r in the corresponding flight segments is higher than what can be captured by f . Additionally, it also misses the set-points that a bumblebee does not reach. This can happen e.g., when a bumblebee changes its set-point before reaching its previous set-point, or when it aborts the landing before reaching its set-point. Despite these limitations, the distribution of set-points and their adjustment with distance can be accurately captured by using thousands of landing maneuvers (Goyal et al., 2021a).

Extraction of entry segments (track segments leading up to constant- r segments)

During their landing maneuver, bumblebees hold the relative rate of expansion constant only for brief periods of time (Goyal et al., 2021a). To analyze their underlying closed-loop sensorimotor control system, we extracted the track segments leading up to these brief constant- r segments. Such segments are hereafter referred to as entry segments, as they potentially correspond to the moments when a bumblebee uses its sensorimotor control system to regulate optical expansion rate and reach the desired set-point.

For each constant- r segment, we identified a corresponding entry segment if there was a monotonic variation (either increase or decrease) of relative rate of expansion in the track segment before the constant- r segment (Figure 3.2C–H). For the purpose of analysis, the

entry segment starts where the monotonic variation of relative rate of expansion starts or from $r = 0.5 \text{ s}^{-1}$ (a low value of relative rate of expansion), whichever occurs later in time. The entry segment ends where the constant- r segment begins.

Note that not all of the constant- r segments were linked to a respective entry segment. This is because either the complete width of a constant- r segment had not been captured with the choice of factor f , or due to oscillations in r , the monotonic variation was absent before the constant- r segments. Since we use thousands of landing maneuvers, these limitations do not restrict us in accurately describing the closed-loop dynamics of sensorimotor control system of the landing bumblebees.

For factor $f = 1.5$, our entry-segment detection procedure was able to link 2, 776 out of 9, 957 constant- r segments with the corresponding entry segments.

Transfer-function based system identification

To find out if bumblebees regulate the optical expansion rate to reach the identified set-points, we analyzed the dynamics of all identified entry segments in conjunction with their corresponding constant- r segments. Specifically, we tested if the variation of relative rate of expansion (r) with time (t) during the entry segments can be captured as transient phases of a dynamic system aimed at reaching its steady-state – the corresponding set-point of relative rate of expansion (r^*).

We used a transfer-function based black-box system identification method to find a dynamic system that can capture the variation of relative rate of expansion (r) with time (t) in each combined pair of entry segment and constant- r segment. Note that, we denote the concatenated temporal variation of r in both segments as $r_c(t)$. Using system identification, we aim to capture only the ‘mean variation’ in $r_c(t)$ and not the oscillations around it. This mean variation is characterized by the low-frequency content in the $r_c(t)$ signal (Figure 3.2C). Therefore, we filtered each $r_c(t)$ using a second-order two-directional Butterworth filter (`filtfilt` in Matlab 2020a) with a cut-off frequency of 5 Hz and stored it as $r_f(t)$. Note that the high frequency content is likely a result of noise in the tracking measurements, or due to oscillations identified in a r -based control scheme (de Croon, 2016).

For the black-box system identification method, the set-point value r^* acted as input to the dynamic system. It was constant over time and denoted as $r^*(t)$ (Figure 3.1C). The desired variation of relative rate of expansion $r_f(t)$ that needed to be captured using the dynamic system was used as its output. A system identification process then involves parametrization of the dynamic system into a model structure of selected order, and the estimation of these parameters using optimization over the defined input-output data (Ljung, 1999).

We used a standard transfer-function-based system identification approach which characterizes a dynamic system as a system of linear time-invariant differential equations. The

coefficients of derivatives in these differential equations are parameters that are estimated using an iterative search algorithm that minimizes a quadratic prediction error criterion. This approach works in the frequency domain where such differential equations are represented as ratio of output to input polynomials. These polynomials are expressed as a function of a Laplacian variable s , and the ratio of these polynomials form a transfer function of the dynamic system.

We use a standard algorithm available in Matlab (v. 2020a, function `tfest`) to estimate a transfer function (Equation 3.1) from time-domain descriptions of input ($r^*(t)$) and output ($r_f(t)$) signals. For each combination of $r^*(t)$ and $r_f(t)$, we identified transfer functions of the first order to third order. In our results, we use second order transfer functions which are parameterized as follows:

$$\frac{r_f(s)}{r^*(s)} = \frac{K w^2}{s^2 + 2Dws + w^2} \quad (3.1)$$

Here $r^*(s)$ and $r_f(s)$ are Laplace transforms of input $r^*(t)$ and output $r_f(t)$, respectively; K (gain), D (damping ratio), and w (natural frequency) are parameters whose values are identified using system identification. The identified transfer functions were then simulated to produce the so-called simulated relative rate of expansion $r_s(t)$. Consequently, we computed fit-percentage F to compare the model output ($r_s(t)$) with the output $r_f(t)$ used for system identification. This is done to select the model order. The fit-percentage F is calculated as follows:

$$F = 100 \left(1 - \frac{\|r_f(t) - r_s(t)\|}{\|r_f(t) - \text{mean}(r_f(t))\|} \right) \quad (3.2)$$

Here $\|r_f(t) - r_s(t)\|$ and $\|r_f(t) - \text{mean}(r_f(t))\|$ indicate the Euclidean norm of the time-series signals. The fit-percent F can vary between $-\infty$ (bad fit) to 100 (perfect fit); a value of zero indicates that the model is no better than a straight line equal to the mean of the $r_f(t)$.

Characterization of entry segments

For our modelling purpose, we assume that bumblebees keep the derivative of relative rate of expansion in each entry segment approximately constant. We refer to this constant as expansion-acceleration (\dot{r}_e) and estimate it from the linear regression $r(t) = \dot{r}_e t + c + \epsilon$ (where c and ϵ denote intercept and residuals, respectively).

We tested this assumption by calculating the coefficient of determination (R^2) for the aforementioned linear regression in each entry segment which was very high (0.980 [0.961 0.990], median [interquartile range]). This also holds for all tested treatments and both landing types (Figure S3.2). Moreover, the difference between the actual flight distance

covered and the analytically computed flight distance if the bumblebees had performed the motion exactly at the estimated expansion-acceleration within the identified entry segments was also very low (0.0007 m [−0.0010 m, 0.0026 m], median [interquartile range]). Thus, the motion of landing bumblebees during the entry segments can be well approximated by a motion at a constant expansion-acceleration.

In addition to the slope of relative rate of expansion \dot{r}_e , we also identify the following three variables that are associated with an entry segment (Figure 3.2G): the change in relative rate of expansion that is required during an entry segment (Δr_e), the associated set-point value that a bumblebee aspires to reach during the entry segment (r^*), and the initial distance from the landing platform at which the entry segment starts (y_0). Note that $\Delta r_e = r^* - r_0$, where r_0 is the relative rate of expansion at the start of the entry segment.

We use the slope of relative rate of expansion (expansion-acceleration \dot{r}_e) as a performance measure for the closed-loop sensorimotor control system of bumblebees during landing. At the moment of switching the set-point, bumblebees can vary this slope depending upon the new set-point itself (r^*), the required step towards the new set-point (Δr_e) and the distance between the animal and the landing platform (y_0). Bumblebees are expected to exhibit higher slopes for higher set-points, larger step-changes in r and closer to the landing surface. This is because higher slopes will enable them to reach the desired set-point, and eventually the landing surface, more quickly. Additionally, this response rate \dot{r}_e can also potentially vary with the environmental light intensity, optical expansion cues available from the surface (landing patterns), or between the landings from free-flight and after take-off (the landing type).

In an entry segment, bumblebees either increase or decrease their relative rate of expansion to reach their set-point. As bumblebees advance towards the landing surface, the only way bumblebees can reduce their relative rate of expansion during an entry segment is by reducing their approach velocity, i.e., by decelerating. On the other hand, to increase their relative rate of expansion during an entry segment, bumblebees can potentially choose from several possibilities: fly at a constant approach velocity, weakly decelerate while approaching the platform, accelerate towards the landing surface or use a combination of these.

In order to find out how bumblebees use the transient response of their sensorimotor control system to advance towards the landing surface, we compute the mean acceleration \bar{A}_e during each entry segment (Figure 3.2H). This mean acceleration equals to the ratio of change in approach velocity ΔV that occurred in an entry segment and the corresponding time duration of the entry segment Δt ($\bar{A}_e = \Delta V / \Delta t$). Note that the positive value of mean acceleration in an entry segment occurs for segments in which bumblebees only accelerate towards the platform (Figure 3.2D) or accelerate more than they decelerate (Figure 3.2F).

Thus, we compute five parameters for each entry segment: ($\dot{r}_e, \Delta r_e, r^*, r_0, \bar{A}_e$). Out of these, the four variables $\dot{r}_e, \Delta r_e, r^*, y_0$ together completely characterize the motion at a

constant expansion-acceleration (Section S3.3.2) and \bar{A}_e is the mean acceleration resulting due to such a motion.

Statistical modelling

We tested how expansion-acceleration \dot{r}_e and the resulting mean acceleration \bar{A}_e in an entry segment varies with the factors that can potentially influence them. We developed linear mixed-effects statistical models for both the expansion-acceleration \dot{r}_e and the mean acceleration \bar{A}_e in R 4.0.2 (R Foundation). Initially, the models had r^* , Δr_e , y_0 , *light intensity*, *platform pattern*, *landing type* along with interactions among these as fixed factors and the day of the experiment, the approach sequence and the landing side (whether the landing platform was located towards the hive side or the food-source) as random intercepts. Afterwards, we used model dredging to find the minimal linear mixed-effects model. We used Bonferroni correction to adjust significance values during post-hoc tests. All statistical models and the corresponding results can be found in Section S3.3.1 and Tables S3.1, S3.2.

3.3 Results

Our previous study showed that bumblebees hold the relative rate of expansion constant at a desired set-point only for brief time intervals (Goyal et al., 2021a). Bumblebees step-wise regulate this set-point as they reach closer to the landing platform. Here, we used the temporal dynamics of relative rate of expansion resulting due to this step-wise regulation of set-points to understand the underlying closed-loop sensorimotor control dynamics.

Track segments leading up to the constant- r segments are the transient phases of reaching the steady state set-point

In each of the 2,776 combined pairs of entry segment and constant- r segment, we used the low-pass filtered temporal dynamics of relative rate of expansion ($r_f(t)$) to identify first order to third order transfer functions that can explain the variation of $r_f(t)$ with $r^*(t)$ as an input. Here, $r^*(t)$ is a signal constant at a desired set-point value. Among the different orders of transfer functions, we chose the second-order transfer functions to describe the observed $r_f(t)$ dynamics as they captured more variation than the first order transfer functions, and a similar variation as third order transfer functions (fit percentage, F values for first, second and third order transfer functions are 87.9% [84.3% 90.2%], 98.2% [94.6% 99.1%] and 98.8% [96.7% 99.5%], respectively, median [interquartile range]).

The identified transfer functions captured the dynamics of relative rate of expansion in different cases e.g., when bumblebees were accelerating (Figure 3.3A), decelerating (Figure 3.3B) or both (Figure 3.3C) during their entry segments. These transfer functions also captured the dynamics of relative rate of expansion during entry and constant- r segments

when bumblebees landed in the presence of different landing patterns (checkerboard and spoke) and light conditions (twilight to sunrise), or when they landed from a free-flight or immediately after a take-off (Figure 3.3D).

For a pair of entry and constant- r segment, these results show that the low-pass filtered temporal dynamics of relative rate of expansion in the entry segment can be described by a second-order dynamic process that is aiming to reach the steady-state set-point of optical expansion rate. Hence, entry and constant- r segments contain transient and steady-state responses of the closed-loop sensorimotor control system of bumblebees, respectively. This suggests that bumblebees use optical expansion rate r as a control variable in their sensorimotor control loop during landing.

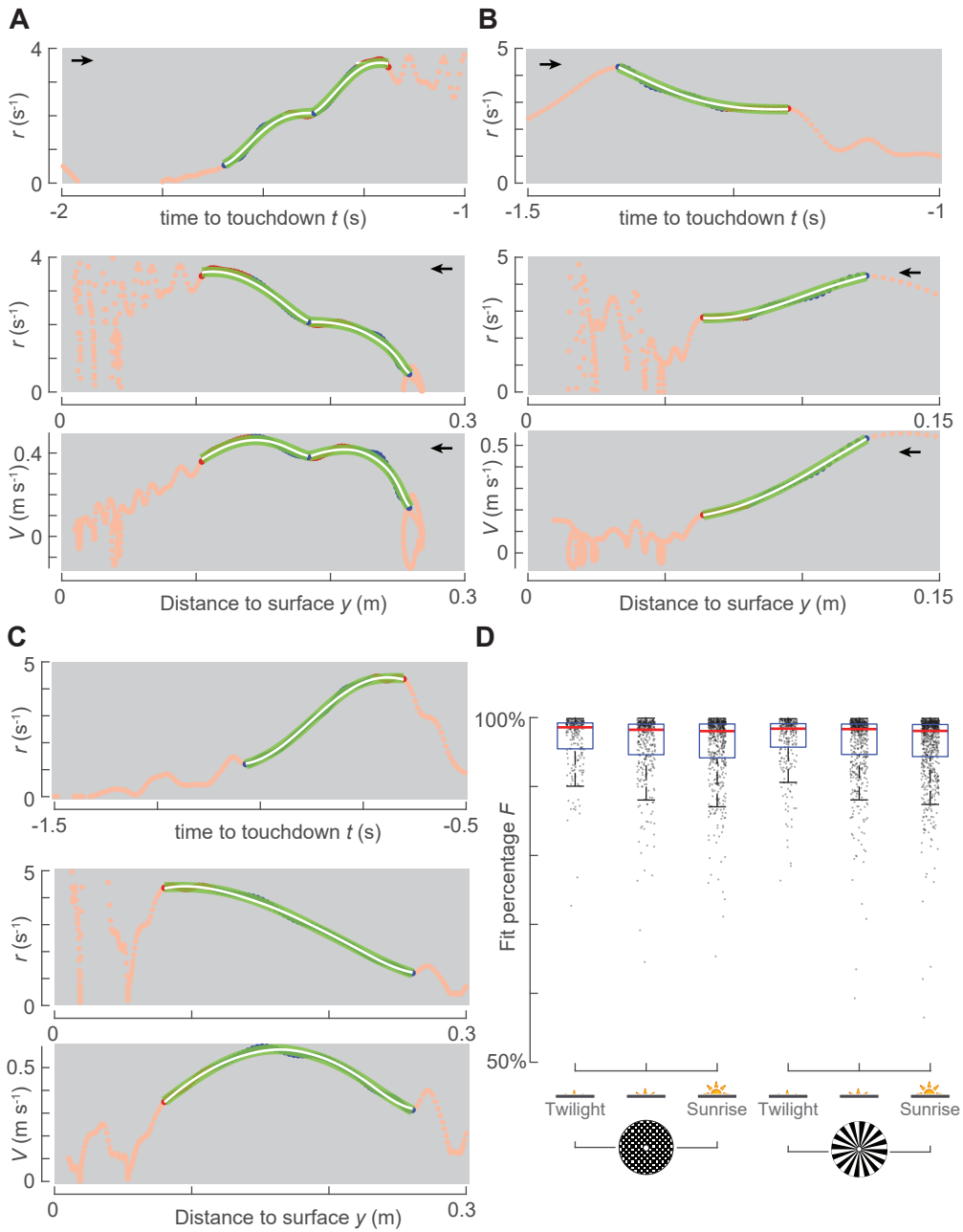
Bumblebees modulate the transient response of their sensorimotor control system during their landing approach

To model the transient response of the sensorimotor control system of landing bumblebees, we estimated the expansion-acceleration \dot{r}_e in each entry segment. It is a measure of how fast the sensorimotor control system of bumblebees is capable of reaching the set-point. In 2, 651 out of 2, 776 entry segments, bumblebees started with a relative rate of expansion lower than their set-point and therefore, exhibited positive expansion-acceleration. In the remaining 125 entry segments, bumblebees started with a higher relative rate of expansion than their set-point and thus, exhibited negative expansion-acceleration. Since, bumblebees mostly (95.5% of the time) increased their relative rate of expansion, we further focus only on these 2, 651 entry segments.

The estimated optical-expansion-acceleration (\dot{r}_e) varied considerably among entry segments (Figure 3.4A). The observed distribution of \dot{r}_e can be approximated by the gamma distribution (median $\dot{r}_e = 11.07 \text{ s}^{-2}$, $a = 4.8 [4.5, 5.0]$, $b = 2.5 [2.4, 2.7]$, mean [95% confidence intervals]) (Evans et al., 2000).

We further used linear mixed-effects model to test how the observed optical-expansion-acceleration (\dot{r}_e) varied with the initial distance from the landing surface (y_0), the step change required in the relative rate of expansion during an entry segment (Δr_e) and the set-point of relative rate of expansion that a bumblebee aims to reach at the end of an entry segment (r^*) (Figure 3.4B). We found linear variation between the logarithmic transformations of y_0 , Δr_e , r^* and \dot{r}_e (Section S3.3.1, Table S3.1). Moreover, we found that there were no significant interactions among these covariates except between y_0 and Δr_e . Therefore, we first describe the effects of y_0 and Δr_e together, and then afterwards the effects of r^* .

The linear mixed-effects model analysis shows that bumblebees reached their set-points at a higher rate i.e., exhibited higher optical-expansion-acceleration \dot{r}_e , when they were closer to the landing surface (lower y_0) and when their set-point r^* was further away from their initial relative rate of expansion r_0 (higher Δr_e) (see Table S3.1 for p -values). However, due to the presence of significant interaction between y_0 and Δr_e , the differences in \dot{r}_e due



(Caption on the next page.)

Figure 3.3: The time-evolution of relative rate of expansion in a combined entry and constant- r segment can be captured by a single dynamic system. (A–C) Three examples of approach flights of bumblebees landing on a spoke landing platform in the sunrise light condition. The landings were initiated from free-flight (A,B) and after take-off (C), and in all landing maneuvers, the bumblebees reached the desired optical expansion set-point r^* at least once (red). The top subpanel shows the variation of relative rate of expansion r with time to touchdown t , and the middle and bottom subpanels show the variation with distance to the landing surface y of r and approach velocity V , respectively. Each panel shows the complete track (orange), the constant- r segment (red), the transient entry segment (blue), the low-pass filtered signal used for system identification $r_f(t)$ (light green), and the estimated output from the simulation of identified second-order transfer functions $r_s(t)$ (white). The black arrow indicates the direction in which abscissa data varies as a bumblebee approaches the landing disc. (D) The goodness of the fit of the model simulation result $r_s(t)$ with the low-pass filtered signal $r_f(t)$, defined as the fit percentage of the normalized root mean square errors (Equation 3.2), for all six tested treatment conditions. For each condition, we show a box plot and the fit percentage for pairs of entry and constant- r segments (dots).

to these trends depend on the actual values of y_0 and Δr_e (Figure 3.4E). The bumblebees increased their expansion-acceleration \dot{r}_e with the required step-change Δr_e at a higher rate when they were closer to the landing surface, than when they were further away from it. In an average landing maneuver, the bumblebee reached its set-point at a 78% higher rate when they were at $y_0 = 0.1$ m than $y_0 = 0.3$ m from the landing surface ($\dot{r}_e = 17.1 [0.5]$ s^{-2} and $\dot{r}_e = 9.6 [0.3]$ s^{-2} , respectively) (mean [standard-error]). Similarly, in an average landing maneuver, bumblebees exhibited 31% higher expansion-acceleration when their set-point was twice as far from their initial set-point (for $\Delta r_e = 2$ s^{-1} , $\dot{r}_e = 11.6 [0.3]$ s^{-2} and for $\Delta r_e = 1$ s^{-1} , $\dot{r}_e = 8.9 [0.3]$ s^{-2}) (mean [standard-error]).

The model also predicted that bumblebees approach their set-point at a higher rate (\dot{r}_e) for higher set-points (p -value $< 2 \times 10^{-16}$, Table S3.1) (Figure 3.4F). An average bumblebee exhibits 14% higher expansion acceleration when $r^* = 3$ s^{-1} ($\dot{r}_e = 11.3 [0.3]$ s^{-2}) as compared to $r^* = 2$ s^{-1} ($\dot{r}_e = 10.0 [0.3]$ s^{-2}) (mean [standard-error]).

These results show that the sensorimotor control system of bumblebees responds faster when (a) they are closer to the surface, (b) they have a higher goal (set-point) or (c) their goal is further away from the relative rate of expansion at the start of the entry segment.

Bumblebees exhibit slower sensorimotor control response in low light intensities

The aforementioned linear mixed-effects model also allowed us to predict how bumblebees adapt the response of their sensorimotor control system with the changes in the environmental conditions (expansion cues and light intensity). The model shows that the closed-loop transient response of bumblebees, expressed as expansion-acceleration \dot{r}_e , is statistically similar in the presence of both strong (checkerboard) and weak expansion (spoke) cues (p -value = 0.19). It implies that the sensorimotor control system of bumblebees is robust to the tested variation in expansion cues and exhibits similar performance in the presence of both landing patterns.

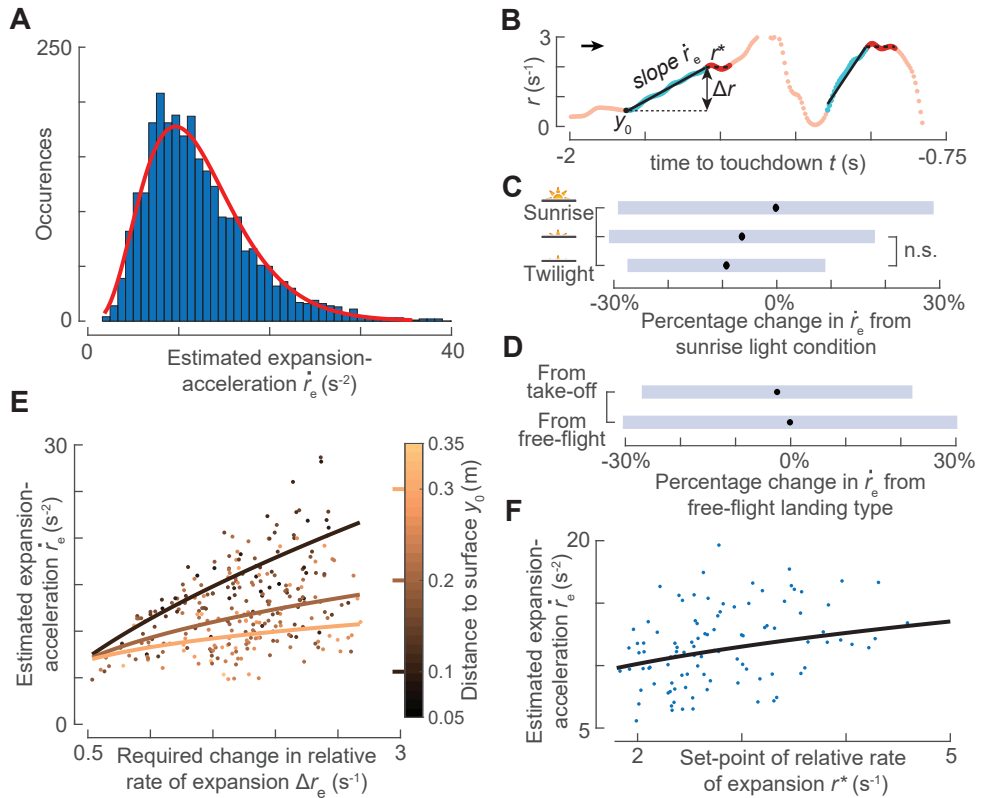


Figure 3.4: Bumblebees modulate the optical expansion-acceleration during the transient phase of their landing maneuvers with environmental conditions. (A) Histogram of estimated expansion-acceleration \dot{r}_e during the all transient phases in which bumblebees increased their expansion rate ($n = 2,651$ segments, red curve indicates the fitted gamma distribution). (B) An example track depicting the flight parameters that define the kinematics of a transient segment when converging to the optic expansion set-point r^* , and that we used for our linear mixed model analysis. (B–F) In our model, we correlated the change in the expansion-acceleration \dot{r}_e during entry segments with five covariates (light intensity; landing type (landing from take-off or free flight); required step change in relative rate of expansion Δr_e ; the set-point of relative rate of expansion r^* , the starting distance of the entry segment y_0). See Table S3.1 for statistical model output. (C,D) The effect of light conditions (C) and landing type (D) on the expansion-acceleration Δr_e during the transient phase of the landing maneuvers of bumblebees, as determined by our linear mixed model. Black dots depict the estimated means, blue bars are 95% confidence intervals and non-significant differences are indicated on the right. (C) On average, bumblebees flying in the sunrise light condition converge to the desired set-points at significantly higher expansion-accelerations than in the other lower light intensities. (D) Equivalently, bumblebees landing directly after take-off reach their set-points at slightly lower expansion-accelerations than when landings were initiated from free-flight. (E,F) The effect of the landing condition parameter set (Δr_e , r^* , y_0) on the expansion-acceleration \dot{r}_e during the transient phase of the landing maneuvers of bumblebees, as determined by our linear mixed model. Here, we show the model results for landings initiated from free-flight in the sunrise light condition; see Figures S3.5 and S3.6 for landings that follow take-off, and for other light conditions.

(Caption continued on the next page.)

(E) The effect of Δr_e and y_0 on \dot{r}_e , showing that bumblebees converge to r^* at higher expansion-accelerations when flying closer to the landing platform (lower y_0) and when they need to achieve a larger change in optical expansion value (larger Δr_e). Curves depict the statistical model output for the median value $r^* = 2.78 \text{ s}^{-1}$, and data points are shown for the interval $r^* \in [2.28, 3.28] \text{ s}^{-1}$ centered around the median value. (F) The expansion-acceleration \dot{r}_e increases with the set-point value r^* , independent of other conditional variables (no significant interaction). This shows that bumblebees converge more rapidly \dot{r}_e to higher r^* than to lower values of r^* . The curve shows the model prediction of \dot{r}_e versus r^* at the median values of Δr_e and y_0 ; data points are plotted for the intervals $\Delta r_e \in [1.28, 2.08] \text{ s}^{-1}$ and $y_0 \in [0.18, 0.24] \text{ m}$ around these median values.

In contrast to the effect of landing patterns, the decrease in light intensity diminishes the transient response characteristic of the vision-based sensorimotor control system of bumblebees. The average bumblebee reached its set-point at a 9% lower expansion acceleration in twilight condition than in sunrise light condition (Figure 3.4C). This reduction in \dot{r}_e with light intensity holds for all values of y_0 , Δr_e , r^* (Table S3.1). This shows that, starting from an initial value of relative rate of expansion, bumblebees take more time to reach a set-point in lower light intensity as compared to a higher light intensity.

Bumblebees landing after take-off reach their set-points slightly slower than bumblebees landing from free-flight

Using the same linear mixed-effects model, we also tested how the rate at which the bumblebees reached their set-points differed between the landings from free-flight and the landings that were performed directly after taking off. The model shows that the bumblebees reached their set-point only at a 3% lower rate (\dot{r}_e) when they landed after take-off than when they landed from free-flight (Figure 3.4D). This also holds for all values of y_0 , Δr_e , r^* (p -value = 0.047, Table S3.1). This shows that the sensorimotor control response of bumblebees does not depend much on how they initiate their landing.

Bumblebees use the transient response of their sensorimotor control system to mostly accelerate towards the landing surface

To study how the sensorimotor control response affects the flight dynamics, we further looked at the average acceleration \bar{A}_e that bumblebees exhibited during these entry segments (Figure 3.5). The average acceleration provides information about how bumblebees modulated their motor control. Note that the positive average acceleration ($\bar{A}_e > 0$) corresponds to bumblebees only accelerating towards the platform (Figure 3.2D), or mostly accelerating (Figure 3.2F) during their entry segments.

As expected, in the 125 entry segments with negative Δr_e , bumblebees decelerated towards the surface ($\bar{A}_e < 0$) to decrease their relative rate of expansion and reach the desired set-point ($\dot{r}_e < 0$). In the 2,651 entry segments with positive Δr_e , bumblebees mostly accelerated ($\bar{A}_e > 0$) towards the landing surface (2,620 times) and few times

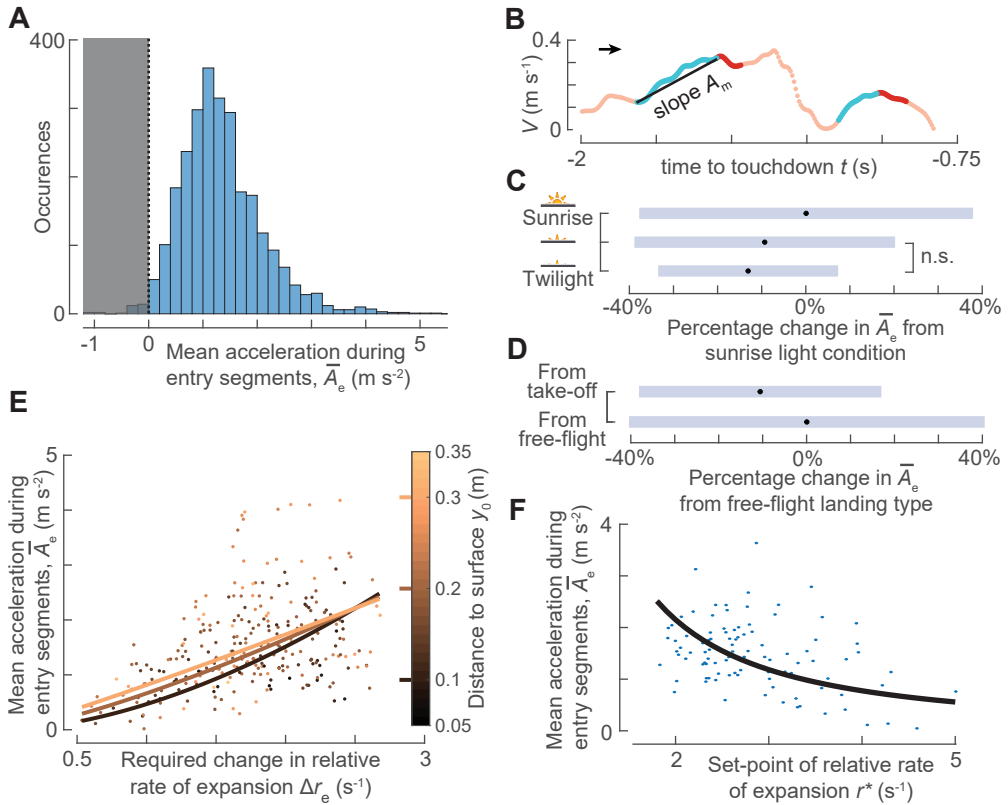


Figure 3.5: To reach their required optical expansion set-point, bumblebees robustly accelerate towards the landing surface during the transient phases of their landing maneuver. (A) Histogram of mean acceleration of the bumblebee towards the landing platforms \bar{A}_e during all identified entry segments ($n = 2651$ segments). During 99% of the entry segments, bumblebees accelerated towards the platform ($\bar{A}_e > 0$) and only 1% decelerated during the transient flight phase. (B) An example track depicting the mean acceleration of the bumblebee \bar{A}_e during the entry segment; positive values thus depict an acceleration towards the landing platform. (C–F) The results of our linear mixed model, in which we correlated the mean acceleration of the bumblebee \bar{A}_e during the entry segments with five conditional parameters (light intensity; landing type (landing from take-off or free flight); required step change in relative rate of expansion Δr_e ; the set-point of relative rate of expansion r^* , the starting distance of the entry segment y_0). See Table S3.2 for statistical model output. (C, D) The effect of light intensity (C) and landing type (D) on the acceleration of the bumblebee \bar{A}_e during the entry segments. Black dots depict the estimated means, blue bars are 95% confidence intervals and non-significant differences are indicated on the right. (C) On average, bumblebees flying in the sunrise light condition accelerated faster towards the landing platform during the transient phase than in the lower light intensities. (D) Bumblebees also accelerated less quickly towards the platform when they landed following a take-off than from a free-flight condition. (E, F) The effect of the landing condition parameter set (Δr_e , r^* , y_0) on the acceleration of the bumblebee \bar{A}_e during the entry segments, as determined by our linear mixed model. Results are shown for landings initiated from free-flight and in the sunrise light condition; see Figures S3.7 and S3.8 for the equivalent results for landings that follow take-off, and for other light conditions.

(Caption continued on the next page.)

(E) The effect of change required in the expansion rate Δr_e and distance from the platform y_0 on body acceleration \bar{A}_e . The curves depict the statistical model output at the median value $r^* = 2.78 \text{ s}^{-1}$, and data points are shown for the interval $r^* \in [2.28, 3.28] \text{ s}^{-1}$. The model shows that the body acceleration are higher when the bumblebee needs to achieve a larger change in optical expansion value (larger Δr_e); although significant, body accelerations vary only little with distance from the platform (y_0). (F) Body accelerations towards the platform \bar{A}_e decrease with an increase in the relative rate of expansion set-point r^* , independent of all other parameters. The curve shows the model prediction of \bar{A}_e versus r^* at the median values of Δr_e and y_0 ; data points are plotted for the intervals $\Delta r_e \in [1.28, 2.08] \text{ s}^{-1}$ and $y_0 \in [0.18, 0.24] \text{ m}$ around these median values.

slowly decelerated (31 times) to increase their relative rate of expansion. Hence, it can be concluded that bumblebees use the transient response of their sensorimotor control system to mostly (94.4%) accelerate towards the landing surface.

We further tested how the positive average acceleration \bar{A}_e varied with the distance to the landing surface (y_0), the step change required in the relative rate of expansion during an entry segment (Δr_e) and the set-point (r^*) (Figure 3.5B).

In general, the linear mixed-effects model shows that the average bumblebee exhibited higher acceleration for higher step change Δr_e and at a distance y_0 further away from the landing surface (see Table S3.2 for p -values). However, note that there is a significant interaction between y_0 and Δr_e ; these trends depend on the actual values of y_0 and Δr_e (Figure 3.5E). For an average landing maneuver, the bumblebee exhibited only 14% lower average acceleration at 0.1 m ($\bar{A}_e = 1.07 [0.05] \text{ m s}^{-2}$) from the landing platform than at 0.3 m ($\bar{A}_e = 1.25 [0.05] \text{ m s}^{-2}$) (mean [standard-error]). In contrast with y_0 , bumblebees showed stronger variation in average acceleration with the required step change Δr_e in an entry segment. For an average landing maneuver, bumblebees exhibited 142% higher average acceleration when the required step change Δr_e is doubled from $\Delta r_e = 1 \text{ s}^{-1}$ ($\bar{A}_e = 0.51 [0.02] \text{ m s}^{-2}$) to $\Delta r_e = 2 \text{ s}^{-1}$ ($\bar{A}_e = 1.23 [0.05] \text{ m s}^{-2}$) (mean [standard-error]). This shows that bumblebees accelerate towards the landing surface, albeit with smaller acceleration, even when they are close to the landing surface. Moreover, the average acceleration with which bumblebees advance towards the landing surface is strongly dependent on the required step change in the relative rate of expansion in an entry segment.

The linear mixed-effects \bar{A}_e model also predicted that the bumblebees exhibited a decrease in the average acceleration with an increase in set-point (r^*) (p -value $< 2 \times 10^{-16}$, Table S3.2, Figure 3.5F). An average bumblebee exhibits 45% lower average acceleration when $r^* = 3 \text{ s}^{-1}$ ($\bar{A}_e = 1.26 [0.05] \text{ m s}^{-2}$) as compared to $r^* = 2 \text{ s}^{-1}$ ($\bar{A}_e = 2.29 [0.1] \text{ m s}^{-2}$) (mean [standard-error]). This decrease in \bar{A}_e with increase in set-point is observed because bumblebees decelerate more in an entry segment with higher set-point.

Similar to the expansion-acceleration \dot{r}_e , we also assessed how the strength of optic expansion cues, light intensity or landing type affected the mean acceleration \bar{A}_e during an entry segment. We found that bumblebees accelerated during entry segments in a similar manner in the presence of both strong (checkerboard) and weak (spoke) expansion cues. Moreover, bumblebees accelerated with 13% lower acceleration in twilight as com-

pared to the sunrise light condition (Figure 3.5C). Additionally, bumblebees exhibited 10% lower accelerations when they landed directly after a take-off than from a free-flight condition (Figure 3.5D). These results hold for all y_0 , Δr_e and r^* (Table S3.2). This shows that bumblebees use the transient response of their sensorimotor control system to accelerate towards the landing surface in the presence of different expansion cues, light conditions and when they land after a take-off or directly from a free-flight.

3.4 Discussion

Here, we study the sensorimotor control system of landing bumblebees and how they use it to advance towards a vertical landing surface. For this purpose, we used 10,005 previously recorded landing maneuvers of bumblebees that resemble their landings in nature e.g., when they fly from one flower to another within a flower patch, or between flower patches and the hive (Heinrich, 1979; Goyal et al., 2021a,b). We also find how they adapt their sensorimotor control response when they land, after a take-off or from free-flight condition, in the presence of different expansion cues and light intensity.

Bumblebees use their sensorimotor control system during landing to regulate relative rate of expansion and produce motor actions to reach a desired set-point

To investigate the underlying sensorimotor control system of landing bumblebees, we used the natural excitation of this dynamic system that they offer during landing. Bumblebees exhibit different set-points of relative rate of expansion during their landing approach (Goyal et al., 2021a). When they regulate the relative rate of expansion during landing, the step-wise modulation in the set-points means that bumblebees fly not only at the set-point, but must also exhibit a transient entry phase to reach their set-point — a typical attribute of a step-response (Ogata, 2010). Moreover, during these transient phases, bumblebees should produce motor output to bring their relative rate of expansion closer to the desired set-point.

To validate this, we showed that the time evolution of relative rate of expansion, both in entry and constant- r segments, can be captured by a single dynamic system (Figure 3.3). We also showed that bumblebees tended to decelerate during an entry segment when they had to reduce their relative rate of expansion, and mostly accelerated to increase it. This means that bumblebees produce motor output in a direction that is consistent with the requirement of increasing or decreasing their relative rate of expansion in an entry segment. Moreover, our results also show that bumblebees exhibited higher mean acceleration in an entry segment when they started with a relative rate of expansion further away from their set-point (i.e., higher Δr_e) (Figure 3.5E). This shows that the motor output produced by bumblebees is dependent on the step change of optical expansion rate required in an entry segment.

We also performed an additional analysis to check how the instantaneous motor output produced by the bumblebees in an entry segment is correlated with the difference between the desired set-point and the instantaneous relative rate of expansion ($\Delta r(t) = r^* - r(t)$). For this purpose, we computed a new acceleration vector $A_e(t)$ by simulating a constant expansion-acceleration motion in an entry segment as the acceleration vector $A(t)$ (obtained from double differentiation of position vector) was noisy. We found a high and statistically significant correlation between $A_e(t)$ and $\Delta r(t)$ for all 2,776 entry segments (correlation coefficient: 0.988 [0.976 0.994], median [interquartile range], all p -values $< 2.8 \times 10^{-5}$).

Considered together, all these results show that the sensorimotor control system of landing bumblebees regulates the relative rate of expansion to advance towards the landing surface i.e., they produce motor output based on the difference between the instantaneous relative rate of expansion and the current set-point.

Using a system identification approach, we found that the second order transfer functions adequately captured the dynamics of bumblebees in both entry and constant- r segments. This is similar to classical mechanics where motions can be captured using second order derivatives. In bumblebees, second-order models are also found to be adequate for modelling the lift response (Tanaka and Kawachi, 2006).

The median values of parameters identified from system identification are close to each other (Figure S3.3), but we could not use the identified parameters to test how bumblebees adjust their sensorimotor control in different conditions. This is because several sets of parameter combinations can approximate the temporal dynamics of r during a combined pair of entry and constant- r segments, and the line search algorithms used during optimization could find these parameter combinations as local minima. Therefore, we used system identification only to capture the approximate (low-frequency) dynamics, and provide evidence that the dynamics of r during entry segments is the response of sensorimotor control system when a bumblebee is away from its steady-state. For understanding how bumblebees modulate their transient response, we use another method where we approximate their transient response as a motion at a constant expansion-acceleration \dot{r}_e .

How do bumblebees modulate the transient response of their sensorimotor control system during landing?

During entry segments, we found that the transient response of the sensorimotor control system of bumblebees can be modelled as a motion at a constant expansion acceleration \dot{r}_e (Figure S3.2). This response is similar to the classic attribute of step response of linear controllers (Ljung, 1999; Ogata, 2010) that are identified in animal flight (for review, see Taylor et al., 2008; Cowan et al., 2014; Roth et al., 2014; Dickinson and Muijres, 2016 and for examples of step-response in flight, see Baird, 2005; Fry et al., 2009; Rohrseitz and Fry, 2011; Fuller et al., 2014).

We further tested the dependency of the response of sensorimotor control (\dot{r}_e) on three other parameters that together with \dot{r}_e describe a motion at a constant expansion-acceleration (Figure 3.4). These parameters are: starting distance from the landing platform (y_0), the required step-change in relative rate of expansion (Δr_e), and the final set-point to reach (r^*). We found that bumblebees approached their goal at a higher rate as their goal and step-change required to reach the goal increased. Moreover, they also exhibited higher rate at shorter distances to the landing surface. This modulation of the transient response enables bumblebees to reach their set-point rapidly, especially when close to the platform.

The modulation of the transient response can be advantageous for bumblebees as flying at a set-point ensures deceleration, and can provide the animal an estimate of the distance to the platform based on which a change in the set-point could be triggered (de Croon, 2016; Goyal et al., 2021a).

The observed modulation in response rate \dot{r}_e with aforementioned parameters can occur due to two possible reasons. First, it can be due to the active adjustment of the underlying dynamic system e.g., by changing the controller gains with distance to the platform to delay the occurrence of instabilities (de Croon, 2016). Physiologically, changes in controller gains would translate to changes into wingbeat and body kinematics in such a way that higher aerodynamic forces are produced in case of higher \dot{r}_e for a given set-point and instantaneous optical expansion rate. Second, it can occur as it is an inherent characteristic of a closed-loop control with relative rate of expansion as a control variable e.g., an increase in the transient slope with the set-point (Ogata, 2010) or proximity to the landing surface (Corke and Good, 1992). A new study, possibly involving open-loop characterization of sub-systems (sensory system, controller and motor system), is needed to identify the contribution of each cause to the observed response modulation.

The sensorimotor control system of bumblebees compensates for low light conditions by responding slowly

We also tested how the change in expansion cues available from the landing platform and light intensity affected the closed-loop sensorimotor response of bumblebees. We found that the transient response of bumblebees is robust to the tested variation in expansion cues. However, bumblebees exhibited on average a 9% lower expansion-acceleration in twilight than in sunrise light condition. It shows that in a low light condition, bumblebees not only exhibit lower set-points (Goyal et al., 2021a), but also the slope at which they reach this set-point is lower. These results are in agreement with the findings from literature where animals, including bumblebees, are shown to fly slowly in low light intensity due to a loss in the temporal resolution of visual cues (Rose and Menzel, 1981; Spiewok and Schmolz, 2006; Reber et al., 2015, 2016; Sponberg et al., 2015).

In principle, the diminishing transient response with light intensity can occur due to two reasons. First, it can be due to a decrease in the response speed of photoreceptors (Re-

ber et al., 2015) and a consequent expected increase in the latency of relative rate of expansion measurement in low light intensity. Second, it can be due to the active adjustment of the closed-loop dynamic system by bumblebees as vision becomes less reliable in low light intensity. Irrespective of the cause, our results show that diminishing response in lower light intensity lead to bumblebees on average exhibiting lower average accelerations towards the landing surface (Figure 3.5C). This signifies that bumblebees use a more cautious landing approach in lower light intensities.

Bumblebees use the transient response of their sensorimotor control system to mostly accelerate and steady-state response to always decelerate during landing

We analyzed how the transient response observed during entry segments influenced the average acceleration \bar{A}_e during entry segments (Figure 3.5). We did this because the accelerations would be the result of changes in aerodynamic forces produced by the motor response (wingbeat and body kinematics) based on how far is the instantaneous relative rate of expansion from the set-point.

The linear mixed-effects model predicts that the mean acceleration is less when landing after a take-off than from a free-flight. This is because bumblebees when landing from take-off more often exhibited a transient phase in which they decelerated for a brief period after accelerating (Figure S3.4). This deceleration during entry segments results in lower mean accelerations. The same reason holds for the reduction of the mean acceleration as the set-point increases (Figure S3.4). Indeed, the instantaneous acceleration towards the landing surface \bar{A}_e increased with the other explanatory variables (y_0 , Δr_e and light intensity).

On average, bumblebees mostly (98.8%) accelerated towards the landing surface as they increased their instantaneous optical expansion rate to reach their set-point. They accelerated towards the surface during entry segments when they landed after a take-off or from a free-flight, and in the presence of different expansion cues and light intensities. They even accelerated when they were close to the landing surface. These results help us understand how foraging bumblebees visit flowers at a very rapid rate with up to 1000 times in an hour (Heinrich, 1979). Moreover, the acceleration phases during landing are also found in other bees (Shackleton et al., 2019; Tichit et al., 2020a,b) and flies (Liu et al., 2019), making it likely to be found in other flying insects as well.

In our previous study, we showed that bumblebees decelerate during constant- r segments (Goyal et al., 2021a). In this study, we show that bumblebees accelerated towards the landing surface during entry segments, and the entry and constant- r segments are the transient and steady-state response of a system aiming to reach its desired value. Considered together, these results show that bumblebees use the transient and steady-state response of their sensorimotor control system, which is based on the optical expansion rate, to accelerate and decelerate as they advance towards the landing surface, respectively.

How do bumblebees perform their flight control during landing?

In particular, what actions bumblebees could be performing during flight to produce accelerations (or decelerations) for reaching their set-points. Flies regulate their ground speed by using the translatory optic flow and are shown to reach their preferred set-point of translatory optic flow by regulating the tilt of the body to reorient their aerodynamic thrust vector (David, 1978; Rohrseitz and Fry, 2011; Medici and Fry, 2012). For bumblebees, the pitch angle of their body is associated with determining the thrust angle and forward flight speed (Dudley and Ellington, 1990). Therefore, bumblebees, similar to flies, could also use pitch angle of their body as a high level control to mediate acceleration during landing in a nested loop architecture (Medici and Fry, 2012).

Conclusion

In this study, we investigated how bumblebees land using a modular landing strategy. We analyse the closed-loop response of their sensorimotor control system that parses visual cues. We found that bumblebees use such a system to reach and fly at their desired set-point of optical expansion rate. Such a system offers a way of both accelerating and decelerating towards the landing surface robustly in different environmental conditions, and can thus be considered as a functional mechanism that bumblebees possess to perform rapid landings. This finding can be used to implement a bio-inspired landing control system onboard man-made flying machines (Shyy et al., 2016; Karásek et al., 2018). An onboard controller which uses the optical expansion rate as a control variable can be modified to use the step-wise modulation of optical expansion rate which would lead to rapid landings (de Croon, 2016; Ho et al., 2017).

Data and code availability

This study uses the public database of landing maneuvers of bumblebees which are available at: <http://dx.doi.org/10.17632/rrbjyhkm8z.1> and the code used for the analysis is available at: <https://github.com/kaku289/nimble-bbee-analysis/tree/entryTransients>.

Acknowledgements

This project is supported by the Nederlandse Organisatie voor Wetenschappelijk Onderzoek - Toegepaste en Technische Wetenschappen (NWO-TTW grant number 15039).

Author contributions

Conceptualization, P.G.; methodology, P.G.; Software, P.G.; validation, P.G.; formal analysis, P.G.; investigation, P.G., and F.T.M.; resources, J.L.v.L., F.T.M.; data curation, P.G.;

writing – original draft, P.G.; writing – review & editing, P.G., J.L.v.L., and F.T.M.; visualization, P.G.; supervision, J.L.v.L. and F.T.M.; project administration, P.G.; funding acquisition, F.T.M..

Declaration of interests

The authors declare no competing interests.

References

- Baird, E. (2005). Visual control of flight speed in honeybees. *Journal of Experimental Biology* **208**, 3895–3905.
- Baird, E., Boeddeker, N., Ibbotson, M. R. and Srinivasan, M. V. (2013). A universal strategy for visually guided landing. *Proceedings of the National Academy of Sciences of the United States of America* **110**, 18686–18691.
- Chang, J. J., Crall, J. D. and Combes, S. A. (2016). Wind alters landing dynamics in bumblebees. *The Journal of Experimental Biology* **219**, 2819–2822.
- Corke, P. I. and Good, M. C. (1992). Dynamic effects in high-performance visual servoing. *Proceedings - IEEE International Conference on Robotics and Automation* **2**, 1838–1843.
- Cowan, N. J., Ankarali, M. M., Dyhr, J. P., Madhav, M. S., Roth, E., Sefati, S., Sponberg, S., Stamper, S. A., Fortune, E. S. and Daniel, T. L. (2014). Feedback control as a framework for understanding tradeoffs in biology. *Integrative and Comparative Biology* **54**, 223–237.
- David, C. T. (1978). The relationship between body angle and flight speed in free-flying *Drosophila*. *Physiological Entomology* **3**, 191–195.
- de Croon, G. C. H. E. (2016). Monocular distance estimation with optical flow maneuvers and efference copies: a stability-based strategy. *Bioinspiration & Biomimetics* **11**, 016004.
- Dickinson, M. H. and Muijres, F. T. (2016). The aerodynamics and control of free flight manoeuvres in *Drosophila*. *Philosophical Transactions of the Royal Society B: Biological Sciences* **371**, 20150388.
- Dickson, W. B., Straw, A. D. and Dickinson, M. H. (2008). Integrative Model of *Drosophila* Flight. *AIAA Journal* **46**, 2150–2164.
- Dudley, R. and Ellington, C. P. (1990). Mechanics of Forward Flight in Bumblebees: I. Kinematics and Morphology. *Journal of Experimental Biology* **148**, 19–52.
- Edwards, M. and Ibbotson, M. R. (2007). Relative sensitivities to large-field optic-flow patterns varying in direction and speed. *Perception* **36**, 113–124.
- Evans, M., Hastings, N. and Peacock, B. (2000). *Statistical Distributions*. Wiley Series in Probability and Statistics. Wiley.

- Foster, D. J. and Cartar, R. V. (2011). What causes wing wear in foraging bumble bees? *Journal of Experimental Biology* 214, 1896–1901.
- Fry, S. N., Rohrseitz, N., Straw, A. D. and Dickinson, M. H. (2009). Visual control of flight speed in *Drosophila melanogaster*. *Journal of Experimental Biology* 212, 1120–1130.
- Fuller, S. B., Straw, A. D., Peek, M. Y., Murray, R. M. and Dickinson, M. H. (2014). Flying *Drosophila* stabilize their vision-based velocity controller by sensing wind with their antennae. *Proceedings of the National Academy of Sciences* 111, E1182–E1191.
- Gibson, J. J. (1955). The optical expansion-pattern in aerial locomotion. *The American journal of psychology* 68, 480–484.
- Goyal, P., Cribellier, A., de Croon, G. C. H. E., Lankheet, M. J., van Leeuwen, J. L., Pieters, R. P. M. and Muijres, F. T. (2021a). Bumblebees land rapidly and robustly using a sophisticated modular flight control strategy. *iScience* 24, 102407.
- Goyal, P., Cribellier, A., de Croon, G. C. H. E., Lankheet, M. J., van Leeuwen, J. L., Pieters, R. P. M. and Muijres, F. T. (2021b). Landing manoeuvres of bumblebees. *Mendeley Data Version 1*.
- Heinrich, B. (1979). Resource heterogeneity and patterns of movement in foraging bumblebees. *Oecologia* 40, 235–245.
- Ho, H. W., de Croon, G. C. and Chu, Q. (2017). Distance and velocity estimation using optical flow from a monocular camera. *International Journal of Micro Air Vehicles* 9, 198–208.
- Karásek, M., Muijres, F. T., Wagter, C. D., Remes, B. D. W. and de Croon, G. C. H. E. (2018). A tailless aerial robotic flapper reveals that flies use torque coupling in rapid banked turns. *Science* 361, 1089–1094.
- Lee, D. N., Davies, M. N. O., Green, P. R. and (Ruud). Van Der Weel, F. R. (1993). Visual control of velocity of approach by pigeons when landing. *Journal of Experimental Biology* 180, 85–104.
- Lee, D. N., Reddish, P. E. and Rand, D. T. (1991). Aerial docking by hummingbirds. *Naturwissenschaften* 78, 526–527.
- Lehmann, F.-O., Schützner, P. and Wang, H. (2012). *Visual motion sensing and flight path control in flies*. Vienna: Springer Vienna, 129–141 pp.
- Liu, P., Sane, S. P., Mongeau, J. M., Zhao, J. and Cheng, B. (2019). Flies land upside down on a ceiling using rapid visually mediated rotational maneuvers. *Science Advances* 5.
- Ljung, L. (1999). *System Identification: Theory for the User*. Prentice Hall information and system sciences series. Prentice Hall PTR.
- Medici, V. and Fry, S. N. (2012). Embodied linearity of speed control in *Drosophila melanogaster*. *Journal of The Royal Society Interface* 9, 3260–3267.

- Mountcastle, A. M. and Combes, S. A.** (2014). Biomechanical strategies for mitigating collision damage in insect wings: Structural design versus embedded elastic materials. *Journal of Experimental Biology* **217**, 1108–1115.
- Ogata, K.** (2010). *Modern Control Engineering*. Instrumentation and controls series. Prentice Hall.
- Rajabi, H., Dirks, J. H. and Gorb, S. N.** (2020). Insect wing damage: Causes, consequences and compensatory mechanisms. *Journal of Experimental Biology* **223**.
- Reber, T., Dacke, M., Warrant, E. and Baird, E.** (2016). Bumblebees perform well-controlled landings in dim light. *Frontiers in Behavioral Neuroscience* **10**, 1–10.
- Reber, T., Vähäkainu, A., Baird, E., Weckström, M., Warrant, E. and Dacke, M.** (2015). Effect of light intensity on flight control and temporal properties of photoreceptors in bumblebees. *Journal of Experimental Biology* **218**, 1339–1346.
- Rohrseitz, N. and Fry, S. N.** (2011). Behavioural system identification of visual flight speed control in *Drosophila melanogaster*. *Journal of The Royal Society Interface* **8**, 171–185.
- Rose, R. and Menzel, R.** (1981). Luminance dependence of pigment color discrimination in bees. *Journal of comparative physiology* **141**, 379–388.
- Roth, E., Sponberg, S. and Cowan, N. J.** (2014). A comparative approach to closed-loop computation. *Current Opinion in Neurobiology* **25**, 54–62.
- Shackleton, K., Balfour, N. J., Toufaily, H. A., Alves, D. A., Bento, J. M. and Ratnieks, F. L. W.** (2019). Unique nest entrance structure of *Pardosa helleri* stingless bees leads to remarkable ‘crash-landing’ behaviour. *Insectes Sociaux 2019 66:3* **66**, 471–477.
- Shyy, W., Kang, C.-k., Chirarattananon, P., Ravi, S. and Liu, H.** (2016). Aerodynamics, sensing and control of insect-scale flapping-wing flight. *Proceedings of the Royal Society A: Mathematical, Physical and Engineering Science* **472**, 20150712.
- Spiewok, S. and Schmolz, E.** (2006). Changes in temperature and light alter the flight speed of hornets (*Vespa crabro* L.). *Physiological and biochemical zoology: PBZ* **79**, 188–193.
- Sponberg, S., Dyhr, J. P., Hall, R. W. and Daniel, T. L.** (2015). Luminance-dependent visual processing enables moth flight in low light. *Science (New York, N.Y.)* **348**, 1245–1248.
- Srinivasan, M. V., Zhang, S. W., Chahl, J. S., Barth, E. and Venkatesh, S.** (2000). How honeybees make grazing landings on flat surfaces. *Biological Cybernetics* **83**, 171–183.
- Stöckl, A. L., Kihlström, K., Chandler, S. and Sponberg, S.** (2017). Comparative system identification of flower tracking performance in three hawkmoth species reveals adaptations for dim light vision. *Philosophical Transactions of the Royal Society B: Biological Sciences* **372**.
- Sun, M.** (2014). Insect flight dynamics: Stability and control. *Reviews of Modern Physics*

86, 615–646.

- Tanaka, K. and Kawachi, K.** (2006). Response characteristics of visual altitude control system in *Bombus terrestris*. *Journal of Experimental Biology* **209**, 4533–4545.
- Taylor, G. K., Bacic, M., Bomphrey, R. J., Carruthers, A. C., Gillies, J., Walker, S. M. and Thomas, A. L. R.** (2008). New experimental approaches to the biology of flight control systems. *Journal of Experimental Biology* **211**, 258–266.
- Tichit, P., Alves-dos Santos, I., Dacke, M. and Baird, E.** (2020a). Accelerated landing in a stingless bee and its unexpected benefits for traffic congestion. *Proceedings of the Royal Society B* **287**, 20192720.
- Tichit, P., Alves-dos Santos, I., Dacke, M. and Baird, E.** (2020b). Accelerated landings in stingless bees are triggered by visual threshold cues. *Biology letters* **16**, 20200437.
- Van Breugel, F. and Dickinson, M. H.** (2012). The visual control of landing and obstacle avoidance in the fruit fly *Drosophila melanogaster*. *Journal of Experimental Biology* **215**, 1783–1798.
- Wagner, H.** (1982). Flow-field variables trigger landing in flies. *Nature* **297**, 147–148.
- Wang, H., Ando, N., Takahashi, H. and Kanzaki, R.** (2017). Visuomotor Response to Object Expansion in Free-Flying Bumble Bees. *Journal of Insect Behavior* pp. 1–20.
- Whitehead, J. G.** (2020). *An examination of the kinematics and behavior of mallards (*Anas platyrhynchos*) during water landings*. Ph.D. thesis, Virginia Tech.

Supplemental information

Bumblebees land rapidly by robustly accelerating towards the surface during visually guided landings

Pulkit Goyal, Johan L. van Leeuwen, Florian T. Muijres

S3.1 Figures

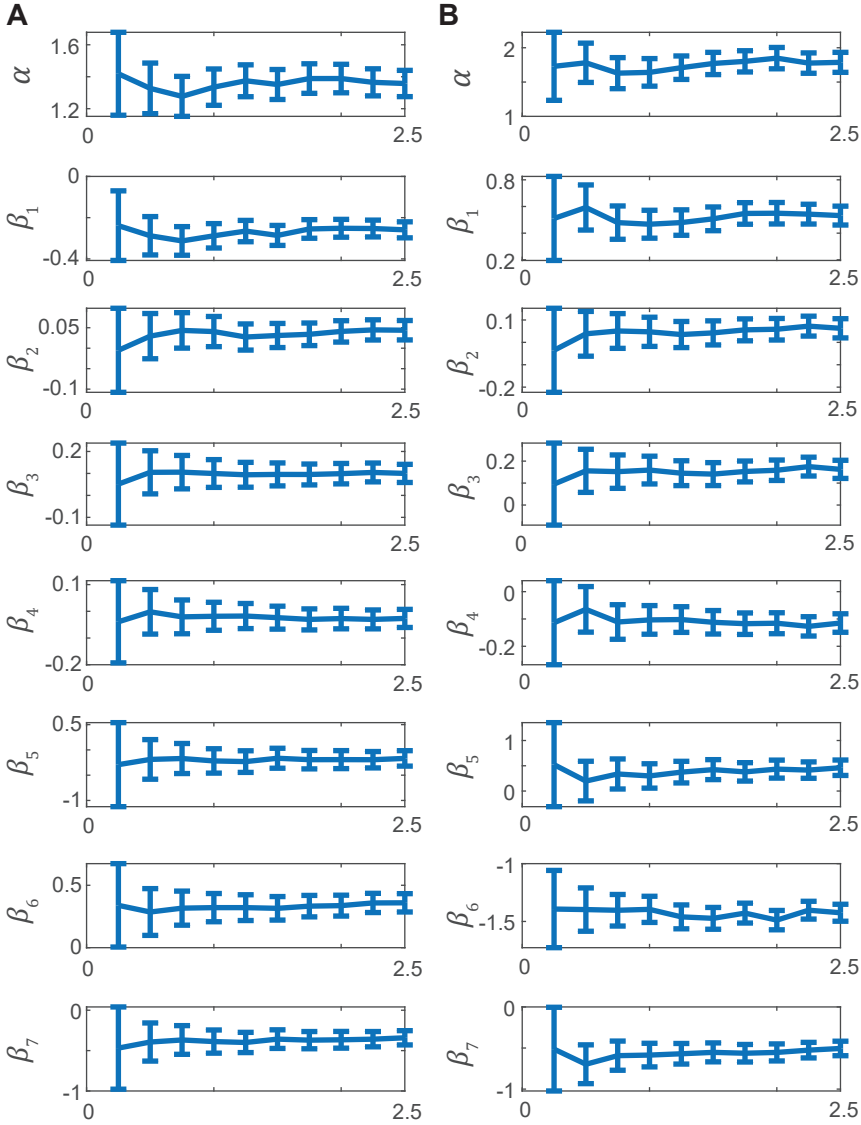


Figure S3.1: The effect of factor f on the results. (A,B) The dependence of expansion-acceleration r_e (A) and mean acceleration \bar{A}_e (B) on distance from the landing surface (y_0), step-change of relative rate of expansion required in an entry segment Δr_e , the set-point r^* , environmental light intensity and landing type (landing after a take-off or from a free-flight) for different factors f (Equation S3.1: $\log(r_e) \sim N(\alpha + \alpha_d + \alpha_a + \alpha_s + \beta_1 \log(y_0_{i,d,a,s}) + \beta_2 \text{MEDIUMlight}_{i,d,a,s} + \beta_3 \text{HIGHLIGHT}_{i,d,a,s} + \beta_4 \text{fromTakeoff}_{i,d,a,s} + \beta_5 \log(\Delta r_{e,i,d,a,s}) + \beta_6 \log(r^*_{i,d,a,s}) + \beta_7 \log(y_0_{i,d,a,s}) \times \log(\Delta r_{e,i,d,a,s}), \sigma^2)$, similar equation holds for \bar{A}_e). The vertical bars for each coefficient indicate 95% confidence intervals.

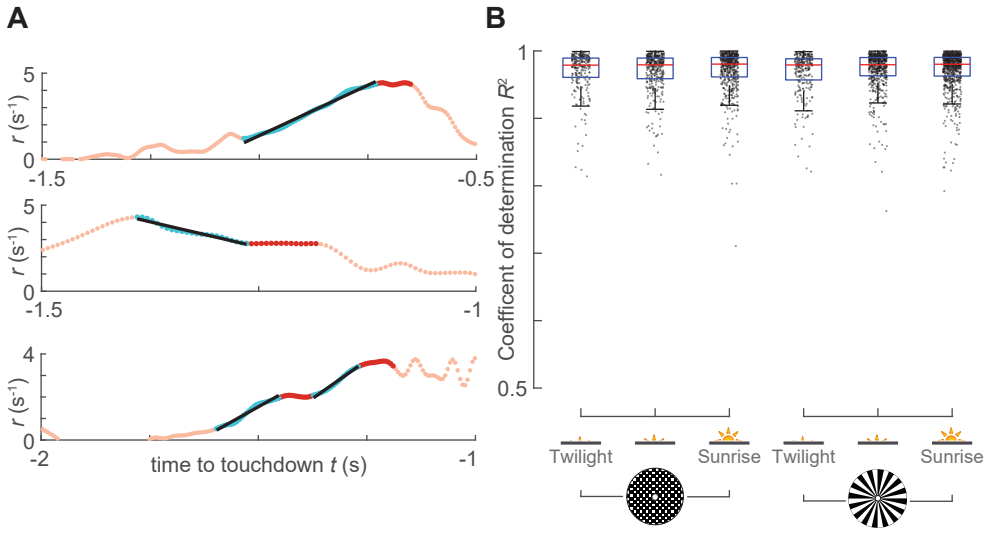


Figure S3.2: During the transient phases of a landing approach, bumblebees keep the expansion acceleration \dot{r}_e approximately constant. (A) Three examples of landing approaches in which the variation of relative rate of expansion r during entry segments (blue) is fitted with time-to-touchdown t using a linear regression (black). This linear regression approximates the optic expansion acceleration with a constant value. The constant- r segment is shown in red and the black arrow indicates the variation of abscissa data as a bumblebee approaches the landing disc. (d) The goodness of fit of the linear regression model for all identified transient phases, in the six experimental conditions, as defined by the coefficient of determination (R^2). At each condition, we show a box plot and the coefficient of determination (R^2) at all transient phases (dots). The median coefficient of determination is above 0.98 in all tested treatments.

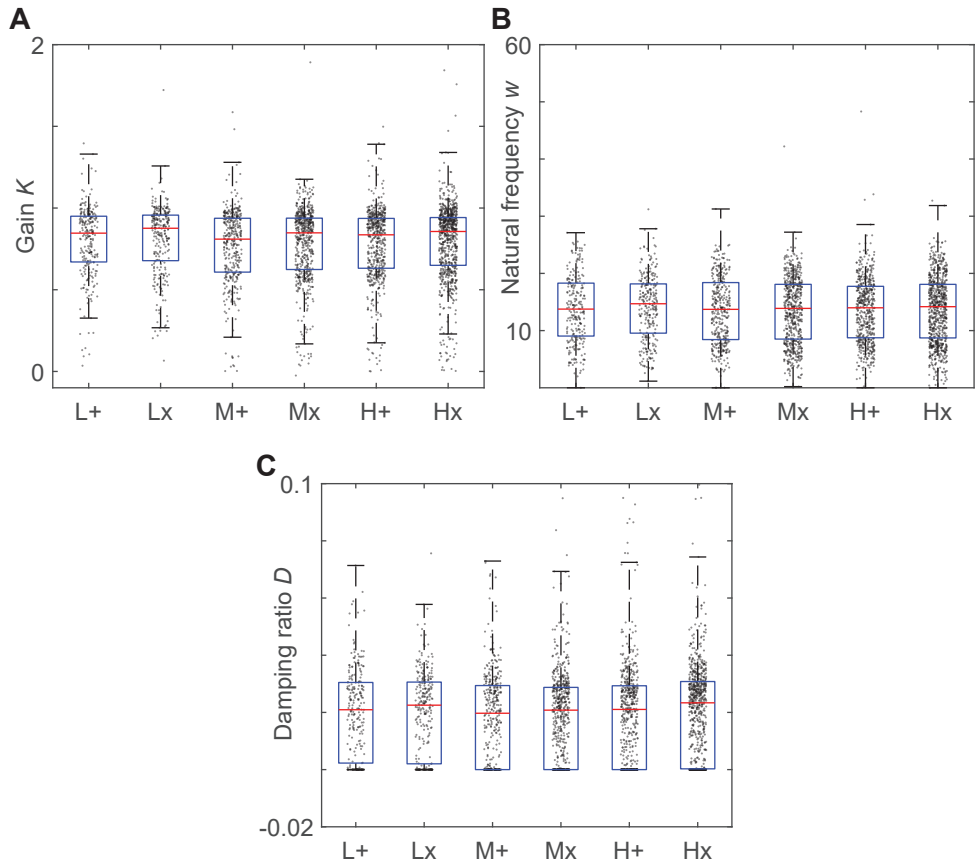


Figure S3.3: The parameters identified using system identification. (a) Gain K , (b) natural frequency w and (c) damping ratio D . For each treatment, the data from different landing types (landings initiated from free-flight or take-off) are shown together. The blue box indicates interquartile range, and black lines indicate the maximum and minimum, respectively. The values that lie 1.5 times the interquartile range away from the top or the bottom of the blue box are labelled as outliers (Low (L), medium (M) and high (H) light conditions, checkerboard (+) and spoke (x) landing patterns).

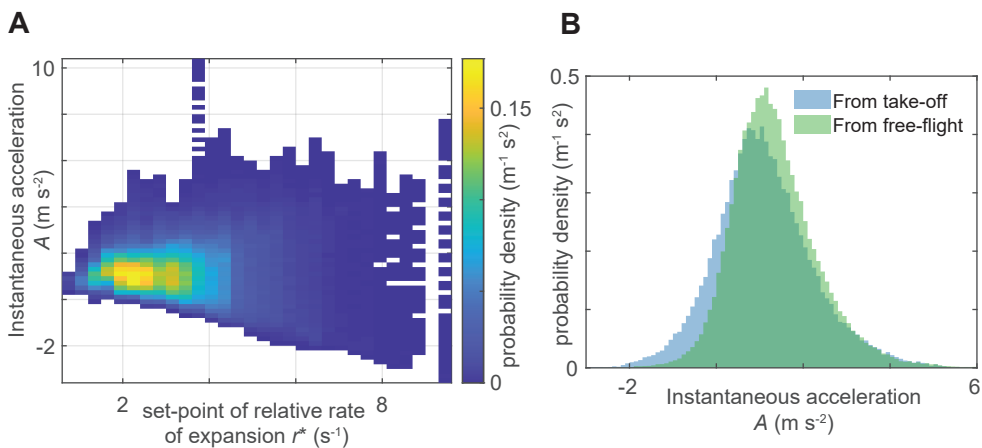


Figure S3.4: The variation of instantaneous acceleration $A(t)$ during entry segments with the set-point of relative rate of expansion r^* and landing type (landing from a free-flight or after take-off). The data plotted here corresponds to 2,620 entry segments in which bumblebees exhibited positive mean acceleration ($\bar{A}_e > 0$).

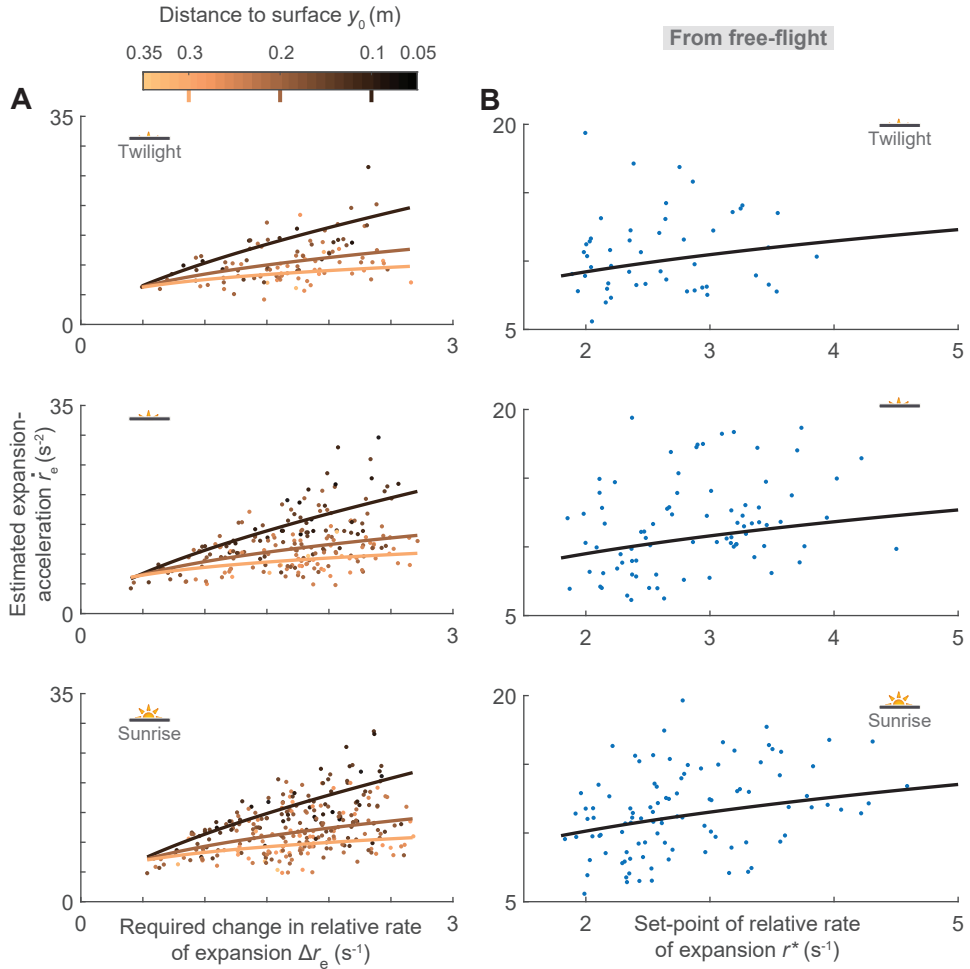


Figure S3.5: The depiction of how bumblebees modulate their sensorimotor control response \dot{r}_e in different light conditions when they landed from free-flight. (A) Effect of required step-change in relative rate of expansion in an entry segment Δr_e and distance from the landing platform y_0 on \dot{r}_e , data points are shown for $r^* \in [2.28, 3.28] \text{ s}^{-1}$, solid curves depict statistical model output, and are plotted for $r^* = 2.78 \text{ s}^{-1}$ (the median value). (B) Effect of set-point of relative rate of expansion r^* on \dot{r}_e , data points are plotted for $\Delta r_e \in [1.28, 2.08] \text{ s}^{-1}$ and $y_0 \in [0.18, 0.24] \text{ m}$ (these intervals are centered around their median values). See Table S3.1 for statistical model output. (A,B) Top, middle and bottom panels correspond to low, medium and high light conditions, respectively.

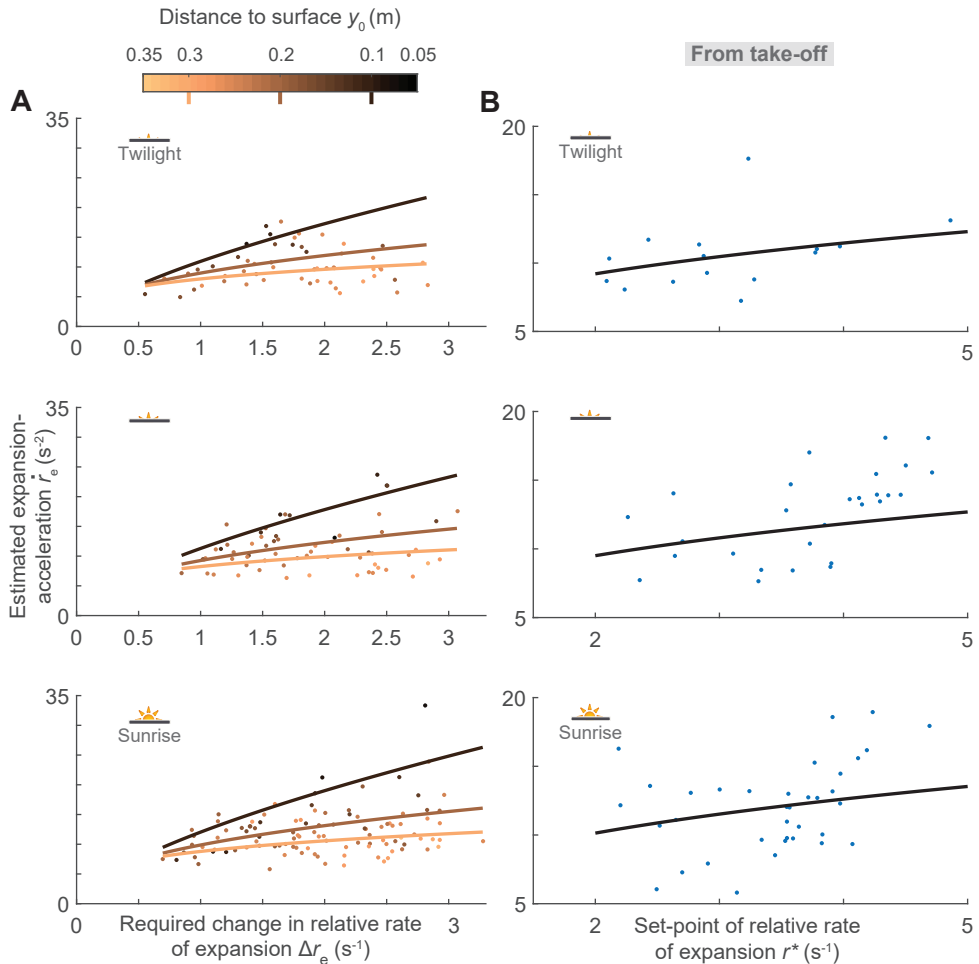


Figure S3.6: The depiction of how bumblebees modulate their sensorimotor control response \dot{r}_e in different light conditions when they landed after take-off. (A) Effect of required step-change in relative rate of expansion in an entry segment Δr_e and distance from the landing platform y_0 on \dot{r}_e , data points are shown for $r^* \in [2.28, 3.28] s^{-1}$, solid curves depict statistical model output, and are plotted for $r^* = 2.78 s^{-1}$ (the median value). (B) Effect of set-point of relative rate of expansion r^* on \dot{r}_e , data points are plotted for $\Delta r_e \in [1.28, 2.08] s^{-1}$ and $y_0 \in [0.18, 0.24] m$ (these intervals are centered around their median values). See Table S3.1 for statistical model output. (A,B) Top, middle and bottom panels correspond to low, medium and high light conditions, respectively.

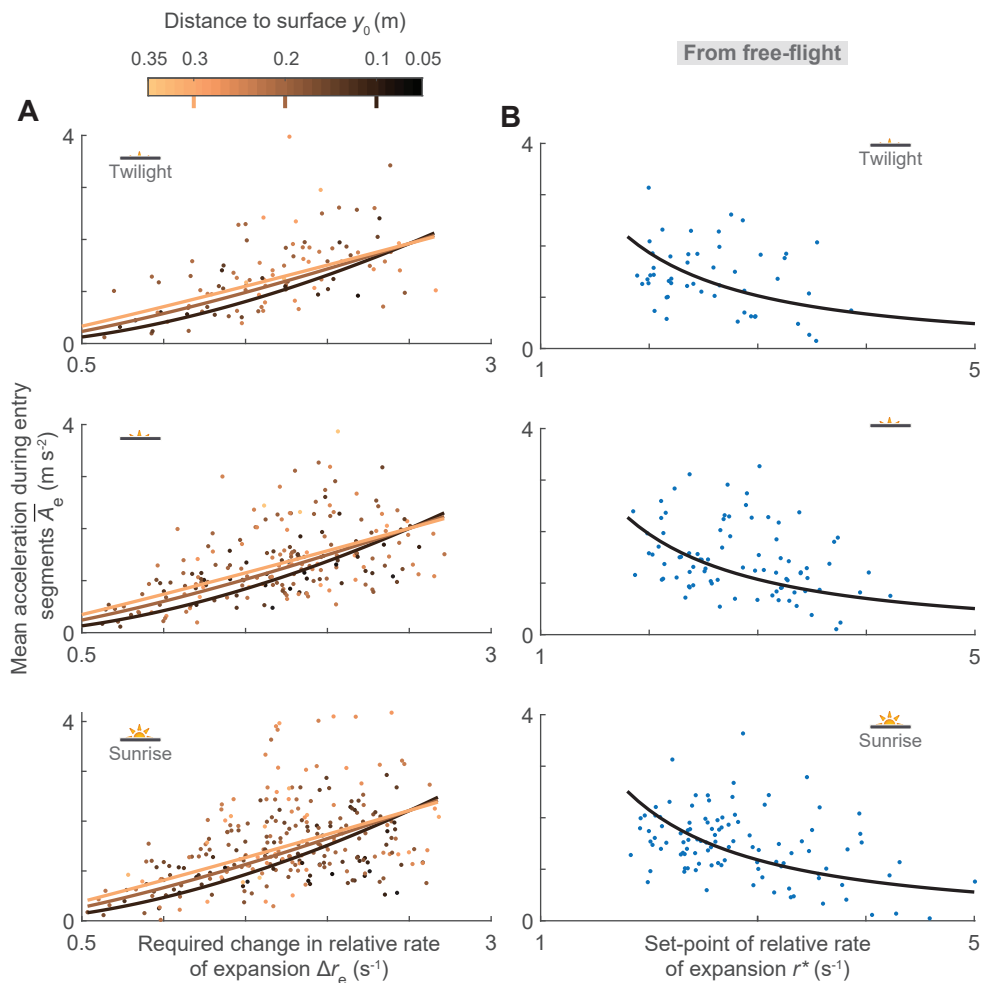


Figure S3.7: The depiction of how bumblebees modulate their mean acceleration \bar{A}_e during an entry segment in different light conditions when they landed from free-flight. (A) Effect of required step-change in relative rate of expansion in an entry segment Δr_e and distance from the landing platform y_0 on \bar{A}_e , data points are shown for $r^* \in [2.28, 3.28] \text{ s}^{-1}$, solid curves depict statistical model output, and are plotted for $r^* = 2.78 \text{ s}^{-1}$ (the median value). (B) Effect of set-point of relative rate of expansion r^* on \bar{A}_e , data points are plotted for $\Delta r_e \in [1.28, 2.08] \text{ s}^{-1}$ and $y_0 \in [0.18, 0.24] \text{ m}$ (these intervals are centered around their median values). See Table S3.2 for statistical model output. (A,B) Top, middle and bottom panels correspond to low, medium and high light conditions, respectively.

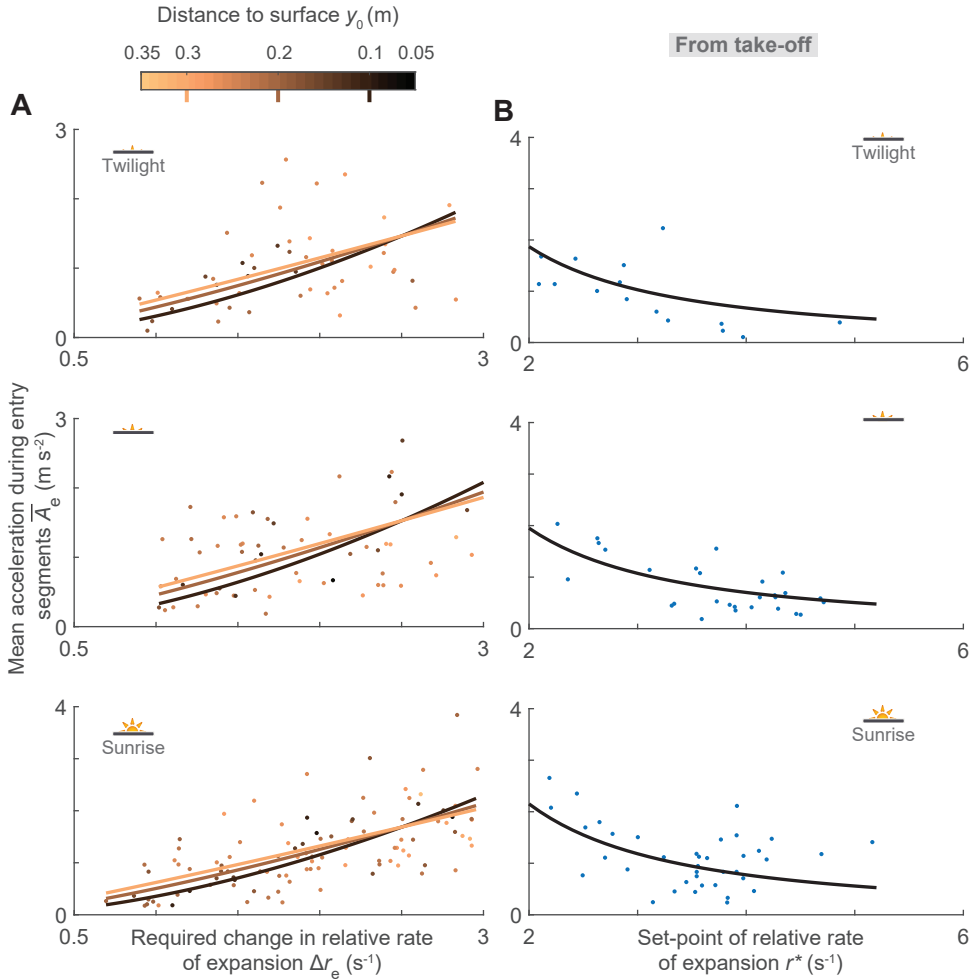


Figure S3.8: The depiction of how bumblebees modulate their mean acceleration \bar{A}_e during an entry segment in different light conditions when they landed after take-off. (A) Effect of required step-change in relative rate of expansion in an entry segment Δr_e and distance from the landing platform y_0 on \bar{A}_e , data points are shown for $r^* \in [2.28, 3.28] \text{ s}^{-1}$, solid curves depict statistical model output, and are plotted for $r^* = 2.78 \text{ s}^{-1}$ (the median value). (B) Effect of set-point of relative rate of expansion r^* on \bar{A}_e , data points are plotted for $\Delta r_e \in [1.28, 2.08] \text{ s}^{-1}$ and $y_0 \in [0.18, 0.24] \text{ m}$ (these intervals are centered around their median values). See Table S3.2 for statistical model output. (A,B) Top, middle and bottom panels correspond to low, medium and high light conditions, respectively.

S3.2 Tables

Table S3.1: Analysis of how bumblebees modulate the expansion-acceleration (\dot{r}_e) during entry segments with the starting distance from the landing surface (y_0), the required step-change in relative rate of expansion (Δr_e), the final set-point to reach (r^*), light conditions and the landing type. The data comprises of 2,651 entry segments identified in 2,511 landing maneuvers of bumblebees (statistical model as given by Equation S3.1: $\log(\dot{r}_{e\ i,d,a,s}) \sim N(\alpha + \alpha_d + \alpha_a + \alpha_s + \beta_1 \log(y_{0\ i,d,a,s}) + \beta_2 \text{MEDIUMlight}_{i,d,a,s} + \beta_3 \text{HIGHlight}_{i,d,a,s} + \beta_4 \text{fromTakeoff}_{i,d,a,s} + \beta_5 \log(\Delta r_{e\ i,d,a,s}) + \beta_6 \log(r_{i,d,a,s}^*) + \beta_7 \log(y_{0\ i,d,a,s}) \times \log(\Delta r_{e\ i,d,a,s}), \sigma^2)$).

Fixed effect	Estimate	Std error	t value	Pr(> t)
α	1.35	0.05	28.24	$1.91E - 10$
β_1	-0.29	0.02	-11.57	$3.06E - 30$
β_2	0.03	0.02	2.07	0.039
β_3	0.10	0.01	6.55	$7.08E - 11$
β_4	-0.02	0.01	-1.99	0.047
β_5	-0.16	0.05	-3.01	0.003
β_6	0.32	0.03	12.48	$9.43E - 35$
β_7	-0.36	0.03	-11.17	$2.43E - 28$

Table S3.2: Analysis of how the mean acceleration of bumblebees in an entry segment (\bar{A}_e) varies with the starting distance from the landing surface (y_0), the required step-change in relative rate of expansion (Δr_e), the final set-point to reach (r^*), light conditions and the landing type. The data comprises of 2,620 entry segments identified in 2,485 landing maneuvers of bumblebees (statistical model as given by Equation S3.1: $\log(\bar{A}_{e\ i,d,a,s}) \sim N(\alpha + \alpha_d + \alpha_a + \alpha_s + \beta_1 \log(y_{0\ i,d,a,s}) + \beta_2 \text{MEDIUMlight}_{i,d,a,s} + \beta_3 \text{HIGHlight}_{i,d,a,s} + \beta_4 \text{fromTakeoff}_{i,d,a,s} + \beta_5 \log(\Delta r_{e\ i,d,a,s}) + \beta_6 \log(r_{i,d,a,s}^*) + \beta_7 \log(y_{0\ i,d,a,s}) \times \log(\Delta r_{e\ i,d,a,s}), \sigma^2)$).

Fixed effect	Estimate	Std error	t value	Pr(> t)
α	1.77	0.08	21.42	$3.12E - 15$
β_1	0.51	0.05	11.17	$2.38E - 28$
β_2	0.04	0.03	1.54	0.123
β_3	0.14	0.03	5.28	$1.38E - 07$
β_4	-0.11	0.02	-5.12	$3.37E - 07$
β_5	0.42	0.10	4.20	$2.72E - 05$
β_6	-1.47	0.05	-30.63	$2.9E - 176$
β_7	-0.55	0.06	-9.40	$1.12E - 20$

S3.3 Supporting text

S3.3.1 Statistical models

We developed linear mixed-effects models to find how the transient response of the sensorimotor control system of landing bumblebees (\dot{r}_e) and the resulting mean accelerations (\bar{A}_e) varied with the starting distance from the landing surface (y_0), the required step-change in relative rate of expansion (Δr_e), the final set-point to reach (r^*), landing patterns (checkerboard and spoke), environmental light intensities, and the starting condition of the landing maneuver (whether the landing is from a free-flight or after a take-off). We first constructed a full model with aforementioned variables along with their interactions as fixed factors, and with the day of the experiment, the landing approach and the landing side (whether landing disc is located on the hive side or the food source side) as random intercepts. The model dredging revealed that the landing patterns did not affect either of the response variables (\dot{r}_e or \bar{A}_e). Moreover, among all interaction terms, only $\log(y_0) \times \log(\Delta r_e)$ term was found to be significant, therefore we used the following reduced model:

$$\log(\dot{r}_{e\ i,d,a,s}) \sim N(\alpha + \alpha_d + \alpha_a + \alpha_s + \beta_1 \log(y_{0\ i,d,a,s}) + \beta_2 \text{MEDIUMlight}_{i,d,a,s} + \beta_3 \text{HIGHlight}_{i,d,a,s} + \beta_4 \text{fromTakeoff}_{i,d,a,s} + \beta_5 \log(\Delta r_{e\ i,d,a,s}) + \beta_6 \log(r_{i,d,a,s}^*) + \beta_7 \log(y_{0\ i,d,a,s}) \times \log(\Delta r_{e\ i,d,a,s}), \sigma^2) \quad (\text{S3.1})$$

where $\dot{r}_{e\ i,d,a,s}$, $y_{0\ i,d,a,s}$, $\Delta r_{e\ i,d,a,s}$, and $r_{i,d,a,s}^*$ are the measurements from the i -th entry segment from d -th day, a -th landing approach and s -th landing side, α is the regression intercept for the low light intensity and free-flight starting condition (overall intercept), α_d is the day-specific intercept, α_a is the landing-approach-specific intercept, α_s is the landing-side-specific intercept, $\text{MEDIUMlight}_{i,d,a,s}$, $\text{HIGHlight}_{i,d,a,s}$ and $\text{fromTakeoff}_{i,d,a,s}$ indicate if medium light condition, high light condition and take-off starting condition are present for the i -th measurement from d -th day, a -th landing approach and s -th landing side (0 = no, 1 = yes), $\beta_i \forall i \in \{2, 3, 4\}$ represent differences of fixed-effects from the overall intercept, $\beta_i \forall i \in \{1, 5, 6, 7\}$ represent the slopes of different covariates along with an interaction, and σ is the residual standard deviation. The similar formula holds for the mean acceleration \bar{A}_e as well. The statistical outputs are given in Tables S3.1 and S3.2.

S3.3.2 Governing equations for motion at a constant expansion-acceleration

During entry segments, the motion of an animal towards the landing surface can be well approximated by a motion at a constant expansion-acceleration (\dot{r}). Such a motion is de-

scribed by a following system of equations:

$$V(t) = -\frac{dy(t)}{dt} \quad (\text{S3.2a})$$

$$A(t) = \frac{dV(t)}{dt} = \dot{r} y(t) - \frac{V^2(t)}{y(t)} \quad (\text{S3.2b})$$

$$y(t_0) = y_0, \text{ and } V(t_0) = (r^* - \Delta r) y_0 \quad (\text{S3.2c})$$

where $y(t)$, $V(t)$, and $A(t)$ are the distance (in a direction normal to the landing surface), velocity and acceleration of an animal at time t , and r^* and Δr_e are the new set-point and the required step-change in relative rate of expansion at the moment of switching the set-point (t_0).



Chapter 4

Bumblebees actively compensate for the adverse effects of steady sidewinds during visually guided landings

Pulkit Goyal¹, Johan L. van Leeuwen¹, Florian T. Muijres¹

¹ Experimental Zoology Group, Wageningen University & Research, Wageningen, The Netherlands

Abstract

Flying animals often encounter winds during their visually guided landings. However, how winds affect their flight control strategy during landing remains unknown. Here, we investigated the effect of steady sidewinds on the landing strategy, sensorimotor control dynamics and landing performance of foraging bumblebees (*Bombus terrestris*). We trained a hive of bumblebees to forage in a wind tunnel and used high speed stereoscopic imaging to record 19,421 landing approaches of bumblebees in six windspeeds that they often encounter in nature ($0 - 3.41 \text{ m s}^{-1}$). We found that bumblebees landed less often as wind speed increased. Moreover, our results show that the landing strategy and the sensorimotor control response of bumblebees in these wind conditions is similar to the still air condition, but bumblebees exhibited some important adaptations in winds. Compared to the still air, bumblebees more often exhibited low approach velocity phases ($V < 0.05 \text{ m s}^{-1}$) in higher winds. This can lead to an increase in the travel time and hence, can adversely affect their foraging efficiency. But, bumblebees also modulated their landing strategy and sensorimotor control response in higher winds that enabled them to travel faster towards the landing surface. This in turn allowed bumblebees to compensate for the increase in travel time that would otherwise occur due to more low approach velocity phases in higher winds. In addition to revealing the adverse effects of winds and the compensation mechanism of bumblebees during landing, we also use the natural excitation that landing bumblebees offered to propose how they integrate information from the wind-mediated mechanosensory modality with their vision-based flight control loop. This can be useful to implement similar control strategies onboard man-made flying systems.

4.1 Introduction

Wind is an important characteristic of the natural world that affects both ecological interactions and biomechanics of flying insects. Wind affects their migration and dispersal in an environment (Mikkola, 1986; Pasek, 1988; Hu et al., 2016a,b), their interaction with plants and flowers (Alcorn et al., 2012; Alma et al., 2017; Hennessy et al., 2021), and floral visitation rates (Crall et al., 2020; Hennessy et al., 2021). During flight, wind imposes significant maneuverability challenges (Ortega-Jimenez et al., 2013; Ravi et al., 2013; Ortega-Jimenez et al., 2014; Mountcastle et al., 2015; Ravi et al., 2016; Chang et al., 2016; Jakobi et al., 2018; Matthews and Sponberg, 2018; Burnett et al., 2020) and can lead to high energetic costs (Combes and Dudley, 2009; Crall et al., 2017). Understanding how flying insects cope with the effects of winds can help us understand their ecology, as well as provide guiding principles for the development of wind mitigation strategies in man-made aerial vehicles.

For flying animals, landing is an important behavior, especially for foraging animals, such as bumblebees, that rely on it to gather food essential for their survival and reproduction (Michener, 2007; Goulson, 2010). A successful landing requires precise control of flight speed as an animal draws closer to the surface (Srinivasan et al., 2000; Baird et al., 2013;

Goyal et al., 2021a). Foraging bumblebees perform these landings very frequently with up to a thousand times in an hour while visiting flowers (Duncan, 1974; Heinrich, 1979) and often in a wide range of wind conditions (Riley et al., 1999; Peat and Goulson, 2005; Crall et al., 2017).

In the absence of wind, bumblebees use visual feedback cues to control their flight speed as they advance towards the landing surface and achieve a soft touchdown (Chang et al., 2016; Reber et al., 2016; Goyal et al., 2021a), similar to many other flying animals (Lee et al., 1991, 1993; Srinivasan et al., 2000; Van Breugel and Dickinson, 2012; Baird et al., 2013; Balebail et al., 2019; Liu et al., 2019; Shackleton et al., 2019; Tichit et al., 2020; Whitehead, 2020). Their motion relative to the landing surface generates optical expansion cues in which various features in the visual image appear to move radially outward from the point that is being approached (Gibson, 1955; Edwards and Ibbotson, 2007). Bumblebees can use this optical flow relative to the retinal image size of an object (Wagner, 1982) or the angular position of features in the image (Baird et al., 2013) to measure optical expansion rate, also known as relative rate of expansion (Lee et al., 2009). The instantaneous optical expansion rate r is equal to the ratio of approach velocity V of the bumblebee and its distance y from the surface ($r = V/y$) (Figure 4.1A). Bumblebees use this optical expansion rate to control their flight during landing (Chang et al., 2016; Goyal et al., 2021a).

As bumblebees approach a landing surface in still air, they exhibit a series of bouts (Figure 4.1B) (Goyal et al., 2021a). In each bout, a bumblebee regulates the optical expansion rate and uses its sensorimotor control system to produce the motor output needed to reach a particular value of the optical expansion rate, also known as a set-point (Figure 4.1C) (Chapter 3). From one bout to the next, bumblebees tend to increase their set-point. This stepwise modulation of set-points allows them to both accelerate and decelerate towards the landing surface. In addition to the acceleration and deceleration phases, bumblebees sometimes also exhibit a low-velocity phase, also known as hover phases in literature (Reber et al., 2016; de Vries et al., 2020; Goyal et al., 2021a). These low velocity phases are likely a result of an instability arising out of a flight controller that uses optical expansion rate as a control variable (de Croon, 2016).

During their landing approach in wind, bumblebees experience different air speeds around their wings and body as compared to the still air. As this airspeed influences the aerodynamic forces and torques that bumblebees produce with their flapping wings (Sane, 2003; Sun, 2014), it becomes mandatory for the bumblebees to adapt their sensorimotor control response for successful landings. This adaptation can be based on the active measurement of airspeed, possibly with their antennae (Taylor and Krapp, 2007; Jakobi et al., 2018), and must generate forces and torques that can compensate the effects of winds as well as enable them to advance towards the surface (Dickinson et al., 2000).

Winds in the natural world are often characterized as a combination of mean wind and the fluctuations around it (Stull, 1988; Garratt, 1994). While the effect of mean wind and the fluctuations on the locomotion and performance has been the subject of investigation

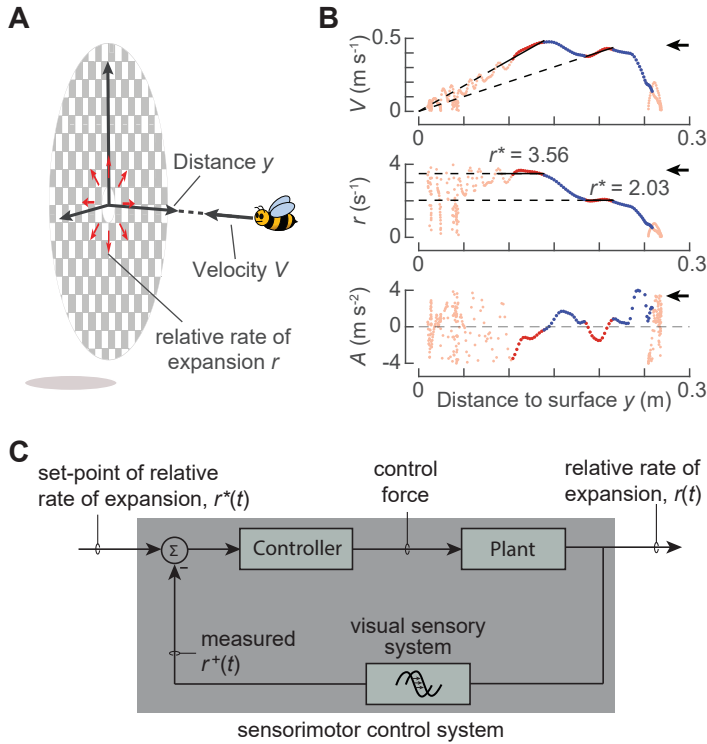


Figure 4.1: The visually-guided strategy and the sensorimotor control system of landing bumblebees in quiescent air. (A) A representation of a bumblebee approaching a landing surface. A bumblebee flying with approach velocity V at a distance y experiences a relative rate of optical expansion $r = V/y$. (B) The kinematic parameters during a typical landing maneuver of a bumblebee. In orange, we show the variation of approach velocity V (top), relative rate of expansion r (middle), and approach acceleration A (bottom) with perpendicular distance from the platform y . The black arrow indicates the direction in which abscissa data varies as a bumblebee approaches the landing surface. (C) The proposed closed-loop sensorimotor control system that bumblebees use during landing. (B,C) Bumblebees land by keeping the relative rate of expansion approximately constant for brief periods as indicated in Goyal et al. (2021a) (red). These constants are referred to as set-points r^* and are depicted by the dashed blue lines as slope and ordinate values in the $V - y$ and $r - y$ graphs, respectively. During landing, bumblebees stepwise modulate this set-point. This results in them exhibiting phases during which they converge towards their set-point; these phases are referred to as transient phases (blue) (Chapter 3). During these transient phases, bumblebees are proposed to measure the optical expansion rate r with their visual sensors, compare it against the set-point and produce a control force (by changing the wing and body kinematics) that acts on the animal (represented as “plant” in control terminology) to bring the measured optical expansion rate r^+ closer to the set-point r^* (Chapter 3).

for freely flying insects (Barron and Srinivasan, 2006; Fuller et al., 2014; Ravi et al., 2015; Engels et al., 2016; Shepard et al., 2016; Crall et al., 2017; Baird et al., 2021; Laurent et al., 2021), their effects during the landing behavior has received relatively little attention. To our knowledge, there is only one study that suggests that winds influence the landing dynamics of bumblebees (Chang et al., 2016), but it still remains unknown how bumblebees achieve flight control during landing in winds. To address this knowledge gap, we here in-

investigate the landing dynamics of bumblebees in the presence of different steady sidewinds.

Specifically, we study how the vision-based modular guidance strategy and the sensorimotor control of landing bumblebees (Goyal et al., 2021a; Chapter 3) is affected by the mean sidewinds and how bumblebees cope with their effects. For this purpose, we introduced bumblebees to six different steady horizontal winds ranging from $0 - 3.41 \text{ m s}^{-1}$ in the direction parallel to the landing surface. These steady conditions correspond to the mean wind speed that bumblebees experience in nature (Crall et al., 2017). Moreover, we offered these conditions in the sideways direction as bumblebees often encounter crosswinds during flight (Riley et al., 1999) and flying insects, including bumblebees, are most sensitive to the aerial disturbances along the lateral axis (Ravi et al., 2013, 2016; Vance et al., 2013). These steady sidewinds also ensure constant wind-induced mechanosensory input throughout the landing approach (except very close to the surface), which is useful in understanding the effects of winds on the sensorimotor control dynamics of landing bumblebees.

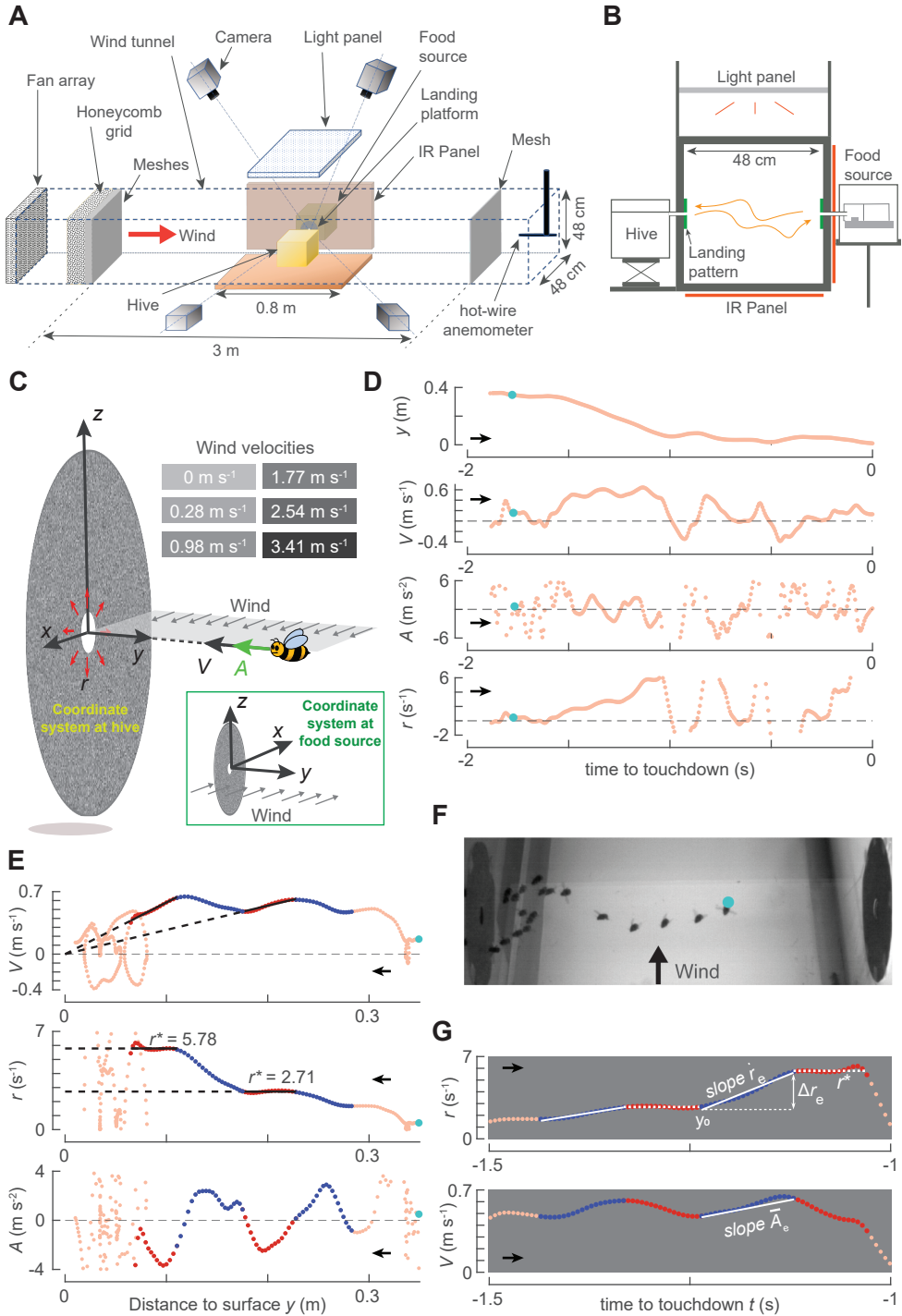
Using high speed stereoscopic imaging, we first recorded 19,421 landing approaches of bumblebees. The landings comprised of bumblebees landing directly after a take-off or from a free-flight condition. These landings are similar to the landings of bumblebees in nature when they visit flowers within a flower patch, or move between the patches and the hive, respectively. We then analyzed the individual landing approaches of bumblebees to find how bumblebees landed in the presence of winds and how they coped with their adverse effect during landing. Furthermore, we also took advantage of the natural excitation of the sensorimotor control that landing bumblebees offered during the stepwise regulation of set-point to propose how they integrate information from the mechanoreceptors measuring airspeed with their visual feedback loop.

4.2 Materials and Methods

Animals, experimental setup and procedure

We carried out experiments in an indoor facility where temperature was maintained at $21 \pm 2^\circ\text{C}$. For our experiments, we used a hive of bumblebees (*Bombus terrestris*) commercially available from Koppert B.V. (Berkel en Rodenrijs, the Netherlands). The colony contained more than 50 worker bumblebees (female) which performed flights to gather food (50% sugar solution) from a feeder. They were provided dried pollen directly in the hive every day.

Our experimental setup consisted of a wind tunnel, the bumblebee hive, a feeder, and a real-time machine-vision based videography system (Figure 4.2A). The hive and the feeder were placed across from each other near the middle section of the wind tunnel ($3 \times 0.48 \times 0.48 \text{ m}$; length \times width \times height). Both were connected to the longitudinal walls of the wind tunnel (transparent poly-carbonate 0.01 m thick sheets) using Plexiglass tubes (0.02 m diameter). These tubes were flush with the inside of longitudinal walls. We attached



(Caption on the next page.)

Figure 4.2: Experimental setup, wind conditions, flight kinematics of a typical landing maneuver of foraging bumblebees, and definitions of the parameters used to find the effect of wind on the landing dynamics. (A) The experimental setup consisted of a wind tunnel, two vertically placed circular landing surfaces connected to a hive and a food-source, respectively, a four-camera videography system for tracking bumblebees (Goyal et al., 2021a), and a LED light panel to illuminate the set-up (Goyal et al., 2021a). (B) The cross-sectional view of the middle section of the wind tunnel. Bumblebees landed on a landing surface either from a free-flight condition or directly after a take-off from the opposite surface or the ground. (C) Each landing is described in a Cartesian coordinate system with its origin at the center of the landing surface, z -axis vertically up, y -axis normal to the disc and x -axis in the downstream direction of the winds. The coordinate systems attached to the landing surface at the hive and food-source are right-handed and left-handed (inset) coordinate systems. Wind conditions that bumblebees are subjected to are also shown. (D–F) A typical maneuver of a bumblebee landing from free-flight in 3.41 m s^{-1} sidewind. The blue dot denotes the same time instant in all panels. Four parameters describe the landing kinematics: approach distance y , and approach ground-velocity $V = -dy(t)/dt$, approach acceleration $A = -d^2y(t)/dt^2$ and relative rate of optical expansion $r = V/y$. (D) The variation of these parameters with time to touchdown. (E) The variation of (V, r, A) with approach distance y . To study the landing dynamics, we determine constant- r segments (red) and transient segments (blue) (transient segments are also referred to as entry segments). (F) Photomontage from a top-view camera at a time interval of $\sim 0.1 \text{ s}$. (G) Parameters used to describe the motion during transient segments: optical-expansion acceleration (\dot{r}_e), required step-change in optical expansion rate (Δr_e), associated set-point (r^*), the initial approach distance at which the transient segment starts (y_0), and average acceleration (\bar{A}_e). (D,E,G) The black arrow indicates the direction in which abscissa data varies as a bumblebee approaches the landing surface.

graphical landing patterns around these flush openings (Figure 4.2B). These landing patterns (0.18 m diameter) consisted of squares ($1 \times 1 \text{ mm}$) filled with random grayscale values and were located 0.48 m apart from each other. The set-up was illuminated with a white broad-spectrum LED light panel to produce light intensities similar to the overcast day in a natural environment (1823 lx, Figure S4.1) (for details about the light panel, see Goyal et al., 2021a).

To generate different steady wind conditions in the wind tunnel, we built two fan-grids of conventional DC cooling fans. Each fan-grid contained 36 fans of one type (San Ace 80 9GA0812P7S001 or 9GV0812P4K03, Sanyo Denki Co., Japan), arranged in a 6×6 grid, and was powered with a 480 W power supply (Mean Well SP-480-12, Mean Well Co., Taiwan). In our setup, the air flow generated by a fan-grid travelled through a honeycomb structure (Tubes core PC, diameter 6 mm, 100 mm thickness, Tubus Bauer GmbH, Germany) and a sequence of four meshes (FG1814F Fiberglass mosquito netting, $1.17 \times 1.59 \text{ mm}$ aperture, 68% transparency, Wire Waving Dinxperlo, The Netherlands) before it reached the bumblebees in the wind tunnel. This was done to breakdown any vortices generated by fans and reduce turbulence in the flow.

Before starting our experiments, we characterized the air flow in the wind tunnel using a hot-wire CTA Anemometer (Dantec 55P16 wire probe and 54T42 MiniCTA, Dantec Dynamics, Denmark). We found that the wind velocities up until 4 cm distance from the walls were within 94% of the mean wind velocity observed at the center of the wind tunnel. This was detected at the middle cross-section of the wind tunnel and 0.20 m downstream and upstream of it. Additionally, the wind velocities measured at a cross-section (located

1.75 m downstream of the middle section) over a span of eleven days during the experiments had a maximum 2% difference from each other. Moreover, the turbulence intensity (standard deviation of the flow velocity divided by the mean velocity) of the air flow in our set-up was less than 3% at all measured locations and for all tested wind speeds. Hence, it can be concluded that bumblebees in our set-up experienced nearly uniform wind conditions with very low turbulence (at distances more than 0.04 m away from the walls).

We here investigate the landing dynamics of bumblebees in six steady wind conditions that span the range of mean wind speeds bumblebees experience in nature (Crall et al., 2017): 0, 0.28, 0.98, 1.77, 2.54, 3.41 m s⁻¹. To generate these wind conditions, we controlled either of the two fan-grids using pulse-width modulation (San Ace 80 9GA0812P7-S001 fan-grid for 0.28 and 0.98 m s⁻¹ winds and San Ace 80 9GV0812P4K03 fan-grid for 1.77, 2.54 and 3.41 m s⁻¹ winds), and for simulating zero wind condition (still air), we turned off the power supply to the fan-grid.

Before starting the experiments, we trained the hive for four days to forage in still air. During training and experiments, bumblebees experienced a day-night cycle of 10 – 14 hours. Each day, light intensity was gradually increased (from zero to 1823 lx) and decreased (from 1823 lx to zero) to simulate sunrise (07 : 30 – 08 : 00 h) and sunset (17 : 00 – 17 : 30 h), respectively. During these time-slots, bumblebees were exposed to zero wind condition. During experiments, we divided the rest of the day (08 : 00 – 17 : 00 h) into six 1.5 hour time-slots and bumblebees were exposed to one wind condition in each time-slot following a pseudo-random schedule spanning over eleven days (Table S4.1).

During experiments, we used a customized machine-vision based videography system (Straw et al., 2011). It consisted of four high-speed cameras along with a custom-built arrays of infrared LED panels (see Goyal et al., 2021a for details) and recorded the three-dimensional position of moving bumblebees in real-time at 175 Hz. Based on these position coordinates, we constructed the movement trajectories of each bumblebee and stored them as space-time vectors in a global Cartesian coordinate system (not shown). After performing a correction for lens distortion, we calibrated the videography system twice during experiments using Direct Linear Transformation (Svoboda et al., 2005; Straw et al., 2011).

Estimation of state variables

From the stored movement trajectories, we extracted the tracks in which bumblebees were landing using a selection process described in (Goyal et al., 2021a). These tracks corresponded to bumblebees landing on the surface either from a free-flight, or immediately after taking off from the opposite surface or the ground. In this study, we refer to these two kinds of landing tracks as landing types.

These landing tracks were defined in a Cartesian coordinate system attached to the center of the landing surface, with the y -axis pointing outward and normal to it, the z -axis vertically upward and the x -axis in the downstream direction of the air flow (Figure 4.2C).

This axes definition results in different coordinate systems at the hive and the food-source. The landing coordinate system at hive is right-handed system whereas the landing coordinate system at the food-source is left-handed system (Figure 4.2C). We filtered these tracks using a low-pass second-order two-directional Butterworth filter (cut-off frequency = 20 Hz, `filtfilt` in Matlab 2020a) and stored them as space-time arrays $\mathbf{X} = (x, y, z, t)$ with time t set to zero at the end of the landing maneuver (i.e., when a bumblebee was closest to the surface). We also computed the corresponding velocity of the bumblebee relative to the ground, the ‘ground-velocity’ $\mathbf{U}_G = (u_G, v_G, w_G)$ and acceleration vectors $\mathbf{A} = (a_x, a_y, a_z)$ at each recorded time-step by numerical differentiation using a second-order central differencing scheme (Figure 4.2D).

In addition to the ground-velocity vector \mathbf{U}_G , we also record at each time-step the wind-velocity $\mathbf{U}_W = (u_W, 0, 0)$ and air-velocity $\mathbf{U}_A = (u_A, v_A, w_A)$ in the landing-platform coordinate system. Here, u_W is the wind velocity with magnitude equal to one of the six wind speeds used in the experiments and direction aligned along the x -axis of the landing-platform coordinate system. It remains constant throughout the landing maneuver (until a bumblebee reaches 4 cm distance from the surface). However, the air-velocity vector is the air velocity relative to the bumblebee (ignoring the effect of the bumblebee on the air motion), which depends on both the ground and wind velocities, and thus it changes with time: $\mathbf{U}_A = (u_A, v_A, w_A) = (u_G - u_W, v_G, w_G)$. The magnitude of the air velocity vector \mathbf{U}_A is denoted as airspeed U_A .

To describe the approach of bumblebees towards the landing surface, we compute four state variables: approach distance from the surface $y(t)$, approach velocity $V(t) = -v_G(t)$, approach acceleration $A(t) = -a_y(t)$, and the relative rate of optical expansion that a bumblebee experiences due to its motion normal to the landing surface $r(r) = V(t)/y(t)$ (Figures 4.2D–F). Here, we use the velocity perpendicular to the surface for the computation of relative rate of expansion as bumblebees are shown to progressively increase and decrease this component as they advance towards the landing surface in still air (Goyal et al., 2021a; Chapter 3).

Extraction and characterization of constant- r and transient segments

To determine if bumblebees in the presence of winds use a modular landing strategy similar to the still air (Goyal et al., 2021a), we used an algorithm from Goyal et al. (2021a). This algorithm finds the track segments in which bumblebees kept the relative rate of expansion nearly constant. We refer to these identified segments as constant- r segments and characterize each segment with the average values of the state variables (y^* , V^* , A^* , r^*) (Figure 4.2E). The r^* is referred to as a set-point of relative rate of expansion. It is an estimate of the value of optical expansion rate that bumblebees aim to reach and fly at using their sensorimotor control system.

The set-point extraction algorithm we use to identify the constant- r segments depends on a factor f . It restricts the variation allowed around the mean r^* for a segment to be identified as a constant- r segment. The factor f has an effect analogous to the numbers 1, 2 and 3 that are multiplied with the standard deviation σ for the 68 – 95 – 99.7% empirical rule in a normal distribution. In this algorithm, instead of a normal distribution, generalized t -distributions are used, and factor f is multiplied by a scale parameter σ of these distributions to obtain the plausible intervals of variables that determine the constancy of r in a track segment (see Goyal et al., 2021a for details). Here, we present the results for factor $f = 1$, but our results remain similar for a wide range of factor f ($0.25 \leq f \leq 2.5$).

To analyze the sensorimotor control response of bumblebees in different wind conditions, we used an algorithm from Chapter 3. This algorithm identifies the track segments that precede a constant- r segment and contain a monotonic variation (increase or decrease) of relative rate of expansion (Figure 4.2E). In still air, this monotonic variation of r is the transient response of the sensorimotor control system resulting due to the step-wise modulation of set-point (Chapter 3). We refer to these segments as transient or entry segments, and characterize each entry segment with six variables: optical expansion-acceleration \dot{r}_e , mean body acceleration \bar{A}_e , the required step-change in relative rate of expansion Δr_e , the associated set-point r^* , the initial approach distance at which it starts y_0 (Figure 4.2G) and the mean airspeed a bumblebee experienced \bar{U}_{Ae} .

Here, we use the optical expansion-acceleration \dot{r}_e as a performance measure of the sensorimotor control response of landing bumblebees as it dictates how fast a bumblebee is able to reach the set-point. For each entry segment, it is estimated from a linear regression: $r(t) = \dot{r}_e t + c + \epsilon$ (where c and ϵ denote intercept and residuals, respectively). Similar to the bumblebee landings in still air (Chapter 3), this linear regression captured well the motion during entry segments in all tested wind conditions (Section S4.3.1, Figures 4.2G, 4.6A).

The mean body acceleration \bar{A}_e for each entry segment is computed as a ratio of change in approach velocity and travel-time during an entry segment. A positive acceleration ($\bar{A}_e > 0$) indicates that bumblebees use the transient response to accelerate towards the surface.

Note that the algorithms we use to extract the constant- r and entry segments do not capture all the set-points or the transient phases that bumblebees exhibit during landing (see Goyal et al., 2021a and Chapter 3 for limitations of each algorithm). We overcome these limitations by using thousands of landing maneuvers to describe the influence of winds on the landing dynamics of bumblebees.

Characterization of bumblebees exhibiting a low-velocity phase

During landing, bumblebees also sometimes exhibit one or more low-velocity phases ($V < 0.05 \text{ m s}^{-1}$) (Figure 4.2E). These low-velocity phases are similar to the hover phases described in literature (Reber et al., 2016; de Vries et al., 2020; Goyal et al., 2021a). During

these phases, bumblebees hover or sometimes even fly away from the landing surface for a short-while. To characterize how often bumblebees exhibited this low-velocity phase during their landing in different wind conditions, we first divided the approach distance y into four regions of equal size: y_1 ($0.05 \text{ m} < y \leq 0.10 \text{ m}$), y_2 ($0.10 \text{ m} < y \leq 0.15 \text{ m}$), y_3 ($0.15 \text{ m} < y \leq 0.20 \text{ m}$) and y_4 ($0.20 \text{ m} < y \leq 0.25 \text{ m}$). For each landing maneuver that started beyond $y = 0.25 \text{ m}$, we then checked if a bumblebee exhibited a low-velocity phase i.e., $V < 0.05 \text{ m s}^{-1}$ or not. To reduce the effect of instances when bumblebees started their landing maneuver with a low velocity, we ignored the initial 0.05 m travelled perpendicular to the landing surface. We then tested how the probability of occurrence of low-velocity phases $P_{\text{low } V}$ varied among different y -regions, wind conditions and landing types (whether a bumblebee landed after a take-off or from a free-flight). The dependence on distance to the surface is considered here because these low-velocity phases are likely due to the r -based closed-loop control (Goyal et al., 2021a) and thus, can occur more often at distances closer to the surface (de Croon, 2016).

Quantification of the landing performance of bumblebees

To assess the overall landing performance of bumblebees flying in different wind conditions and for two landing types, we computed the travel time Δt of bumblebees. We used travel time as it depicts how long bumblebees remain airborne which influences energetic cost and therefore, can be a driving factor of the approach dynamics of bumblebees in different conditions.

The travel time Δt was computed as the time that a bumblebee takes to cover 0.2 m approach distance from $y = 0.25 \text{ m}$ to $y = 0.05 \text{ m}$. It was computed for all landing maneuvers that started beyond $y = 0.25 \text{ m}$.

Statistical analysis

We used R 4.0.3 (The R Foundation, Austria) for statistical analyses. For this purpose, we developed linear mixed-effects models and a generalized linear mixed-effects model (using functions `lmer` and `glmer`, respectively, in R). Wherever relevant, we used the approach sequence, the landing side (whether a bumblebee landed on the hive side or the feeder side), the day of the experiment, and the time-slot during the day as random intercepts in all statistical models. The p -values < 0.05 were considered statistically significant. For post-hoc comparisons, we used Bonferroni correction (using the `emmeans` package in R) to adjust the statistical significance values. The details of all statistical models and associated results can be found in Section S4.3.2 and Tables S4.2–S4.8, respectively.

4.3 Results

Using our experimental setup, we recorded 19,421 landing approaches of bumblebees in six mean wind speeds (0, 0.28, 0.98, 1.77, 2.54, 3.41 m s⁻¹). Among these, 16,374 and 3,047 landing approaches corresponded to bumblebees landing from a free-flight or after a take-off, respectively.

Bumblebees land less often at higher wind speeds

We first tested how winds influenced the landing frequency of bumblebees. For this purpose, we used two linear mixed models to find how the average number of landing approaches per hour (N) varied with the wind conditions. The two models correspond to two landing types (landing from a free-flight, or after a take-off from the opposite surface or ground) (Section S4.3.2, Table S4.2). Note that the bumblebees experienced each wind condition for 90 minutes every day.

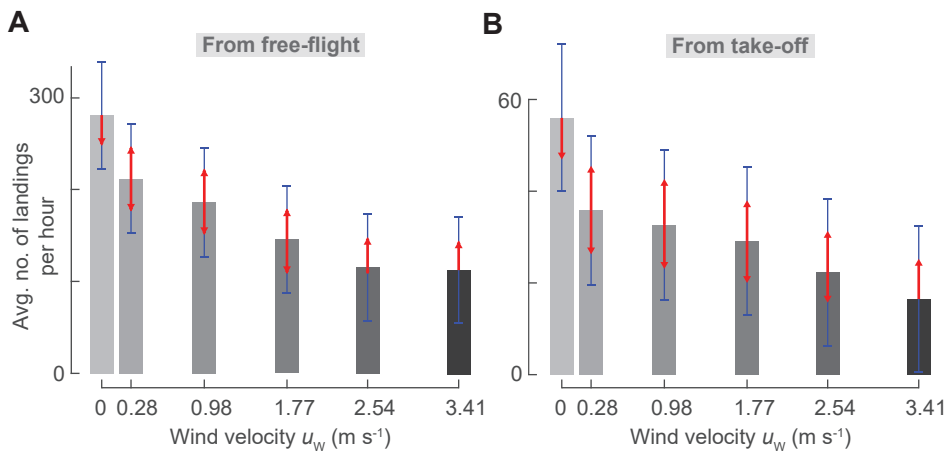


Figure 4.3: The bumblebees perform fewer landings in faster winds. (A,B) The average number of landing maneuvers per hour (grey) in the presence of different wind conditions for landings from a free-flight condition (A), or directly after a take-off (B) from the opposite platform or ground. Vertical blue intervals are 95% confidence intervals and red arrows show whether the average number of landings per hour differs significantly among different wind conditions for each landing type (no overlap indicates statistically significant differences) (see Section S4.3.2, Table S4.2 for statistical model and results, respectively).

We found that the bumblebees landed less often in faster winds (Figure 4.3). For landings from a free-flight condition, bumblebees reduced their landing frequency by 60% in the presence of fastest wind ($N = 112.2 [27.8]$, $U_W = 3.41$ m s⁻¹) as compared to the still air ($N = 280.8 [28.3]$, $U_W = 0$ m s⁻¹) (Figure 4.3A, Table S4.2). For landings after a take-off, bumblebees reduced their landing frequency from still air ($N =$

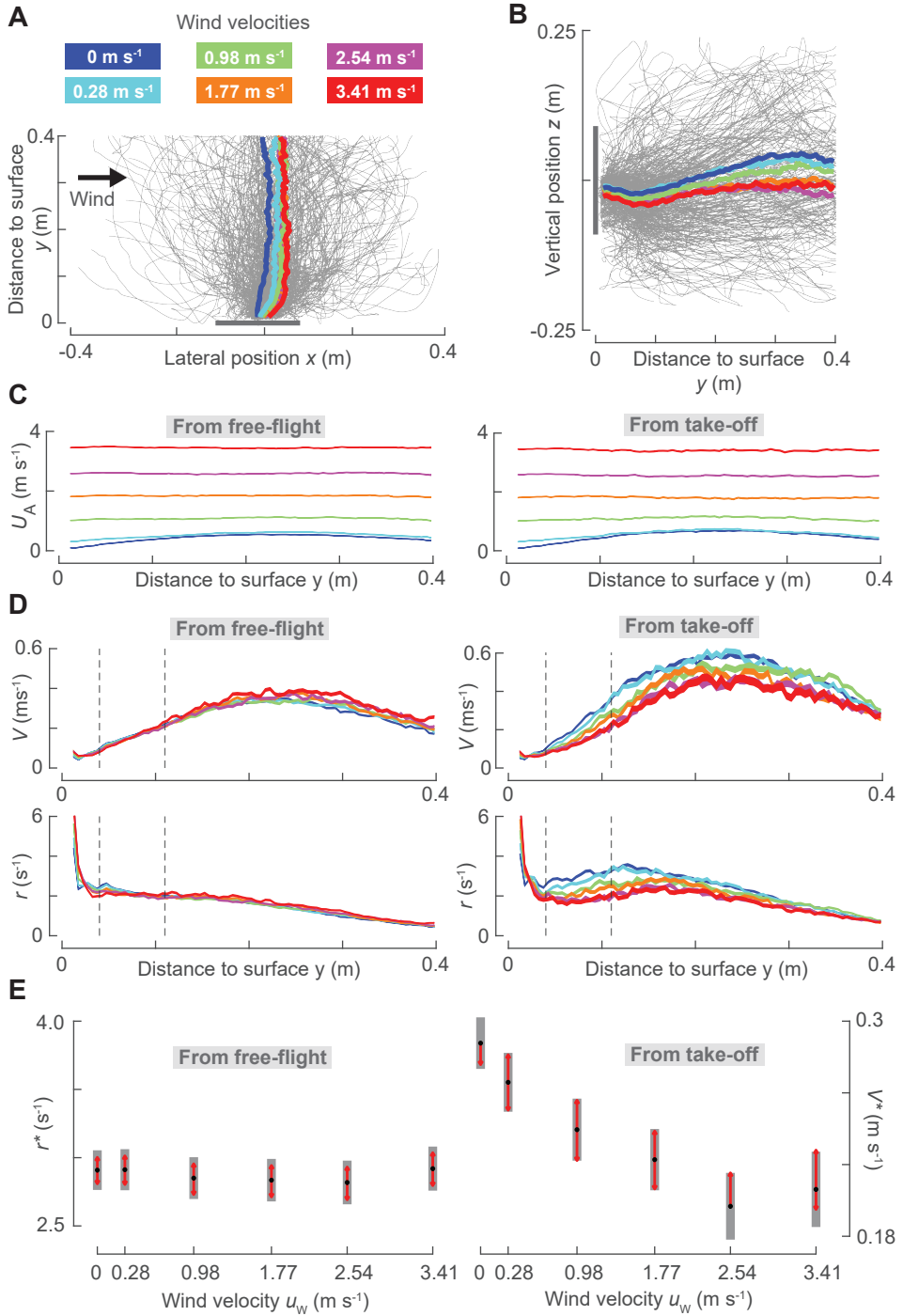
56.0 [7.8], $U_W = 0 \text{ m s}^{-1}$) to fastest wind ($N = 16.5 [7.7]$, $U_W = 3.41 \text{ m s}^{-1}$) by 70% (Figure 4.3B, Table S4.2, mean [standard-error]). Thus, it can be concluded that winds adversely affect the landing frequency of foraging bumblebees.

Average landing approach in different wind conditions

In all tested steady sidewinds, bumblebees, on average, flew approximately perpendicular to the landing surface (Figures 4.4A and 4.4B). The bumblebees experienced higher air-speeds (their speed relative to the surrounding air) in higher wind speeds (Figure 4.4C) and thus they had to generate higher compensatory forces and torques during their landing approach. Specifically, they needed to compensate for the additional drag force in the lateral direction due to winds and any changes in the aerodynamic forces and torques these winds had caused in other directions. On average, they were able to do this for all tested wind conditions, though with a slight lateral drift in the wind direction and a small loss of height (Figures 4.4A and 4.4B).

During their average landing approach, bumblebees first gradually increased and then gradually decreased their approach velocity (V) as they approached the surface (Figure 4.4D). During their deceleration phase ($0.04 \text{ m} \leq y \leq 0.11 \text{ m}$), on average they approximately flew at a constant set-point of optical expansion rate r^* — a behavior described before in honeybees (Baird et al., 2013) and bumblebees (Chang et al., 2016; Goyal et al., 2021a). Please note that individual flight paths tend to deviate substantially from the average behavior (Figures 4.2E, 4.5A,B).

We used a linear mixed model to find how this average set-point r^* during the deceleration phase varied in different wind conditions and landing types (landing from free-flight or take-off) (Section S4.3.2). We found that, when bumblebees landed from free-flight, they had similar set-points in all wind conditions ($r^* = 2.89 [0.08] \text{ s}^{-1}$, $U_W = 0 \text{ m s}^{-1}$ and $r^* = 2.90 [0.08] \text{ s}^{-1}$, $U_W = 3.41 \text{ m s}^{-1}$), and thus similar approach velocities throughout the deceleration phase. In contrast, when they landed shortly after a take-off, they decreased their set-point r^* with increasing wind speed ($r^* = 3.84 [0.10] \text{ s}^{-1}$, $U_W = 0 \text{ m s}^{-1}$ and $r^* = 2.75 [0.14] \text{ s}^{-1}$, $U_W = 3.41 \text{ m s}^{-1}$, mean [standard-error], Figure 4.4E, Table S4.3). ‘From take-off landings’ had higher set points at low wind speeds ($U_W < 1.7 \text{ m s}^{-1}$) than those of landings from free-flight. In still air, bumblebees, on average, had higher set-points and flew faster towards the surface when they landed from a take-off as compared to a free-flight condition, which agrees with previous findings (Goyal et al., 2021a). But, as wind speed increased, they approached the surface with similar and lower ground velocities while landing from take-off compared to those of the free-flight condition.



(Caption on the next page.)

Figure 4.4: The effect of steady lateral winds on the average approach kinematics of landing bumblebees. (A,B) Top and side views of landing maneuvers of bumblebees in all tested wind conditions. In gray, we show every 70th landing maneuver of all 19,421 recorded maneuvers ($n = 281$ tracks). The mean landing maneuvers in different wind conditions are shown in thick solid lines, and the landing platform is shown in gray. (C,D,E) The variation of mean airspeed U_A with perpendicular distance to the surface y (C) and the average approach kinematics (D,E) of bumblebees landing from free-flight (left) and after take-off (right) in different wind conditions. (D) The variation of approach ground-velocity V and relative rate of expansion r with distance to the surface y (the thickness of curves represents the standard error of the means). (E) The mean set-point of relative rate of expansion r^* and resulting approach ground-velocity V^* at distance $y = 0.075$ m, as predicted by linear mixed model (Section S4.3.2, Table S4.3). The y -segment ($0.04 \text{ m} \leq y \leq 0.11 \text{ m}$) for which the data is used to find r^* is indicated with two vertical dashed gray lines in panel (D). The analysis based on the average of the landing maneuvers suggests that bumblebees exhibited similar set-point r^* in all wind conditions while landing from free-flight. In contrast, they exhibited lower setpoint r^* in faster winds when landing after a take-off. Black dots depict estimated means, gray bars are 95% confidence intervals and red arrows indicate whether estimated means differ significantly from each other (no overlap indicates statistically significant differences). (A–E) The curves for 0, 0.28, 0.98, 1.77, 2.54, 3.41 m s^{-1} wind velocities are shown in dark-blue, light-blue, green, orange, pink and red, respectively.

In all wind conditions, individual bumblebees stepwise modulate their set-point of optical expansion rate during their landing approach

Though the analysis of the average of landing maneuvers is useful, it has previously failed to capture the detailed landing dynamics of individual bumblebees in still air (Goyal et al., 2021a). Therefore, we also analyze the individual landing maneuvers using the analyses techniques described in Goyal et al. (2021a) and Chapter 3 to understand how bumblebees land in the presence of winds.

Using the set-point extraction algorithm, we identified 12,338 constant- r segments in 9,097 out of 19,421 landing tracks (for factor $f = 1$) (Figure 4.5A,B). The observed distribution of identified set-points of relative rate of expansion r^* in these constant- r segments can be approximated by a gamma distribution (median $r^* = 2.41 \text{ s}^{-1}$, $a = 3.74$ [3.65 – 3.83], $b = 0.69$ [0.68 – 0.71], mean [95% confidence intervals]) (Figure 4.5C) (Evans et al., 2000). This distribution is similar to the one identified before for bumblebees (Goyal et al., 2021a) and for honeybees (Chapter 5).

Out of the 9,097 landing tracks with constant- r segments, 2,632 had more than one constant- r segments (Figure 4.5A,B shows examples of such events). In these tracks, bumblebees switched from one set-point to another 3,241 times, and which occurred in all wind conditions. Out of a total 3,241 set-point transitions, they switched to a higher set-point 76% of the time which resulted in an average increase of $\Delta r^* = 1.24$ [1.09] s^{-1} in their set-point. For the rest, 24% of the transitions, they switched to a lower set-point with an average reduction of $\Delta r^* = -0.48$ [0.48] s^{-1} in their set-point (mean [std. dev.]) (Figure 4.5D). These results are similar to our previous study on the bumblebees in which we analyzed their landings recorded in the same flight arena with quiescent air and different environmental conditions (Goyal et al., 2021a). Thus, it can be said that landing bumble-

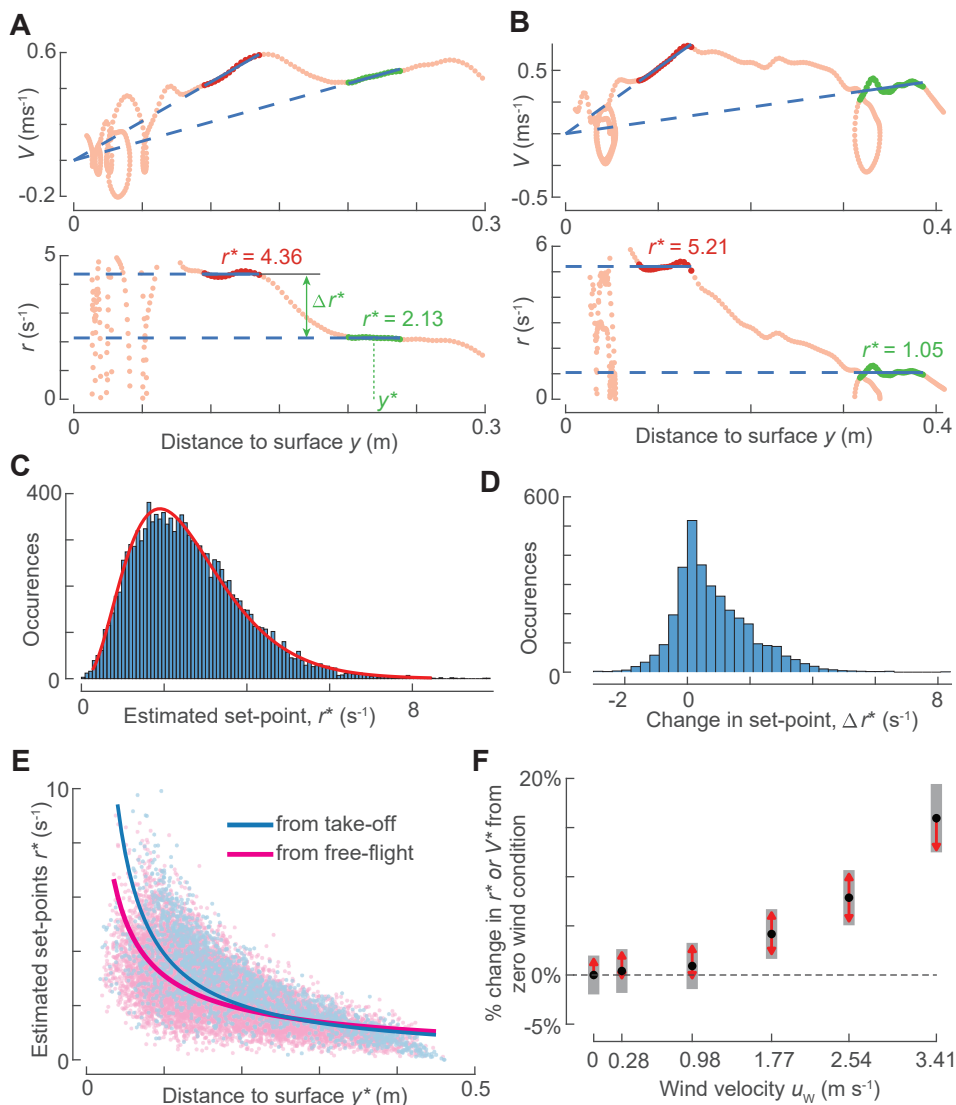


Figure 4.5: In the presence of steady lateral winds, bumblebees step-wise modulate the set-point of optical expansion rate during their landing approach; they exhibit higher set-points in higher winds. (A,B) The variation of approach ground-velocity V and relative rate of expansion r with perpendicular distance to the surface y for bumblebees landing in 3.41 m s⁻¹ sidewind after a take-off (A) and from free-flight (B). The first and second set-points of optical expansion rate r^* (slopes and ordinate values in top and bottom panel, respectively) identified in these landing maneuvers are shown in green and red, respectively. (C) Histogram of all identified set-points r^* ($n = 12,338$) (gamma distribution fit in red). (D) Histogram of change in set-point Δr^* between two consecutive set-points in a landing maneuver, as defined in panel (A) ($n = 3,241$).

(Caption continued on the next page.)

(E) The variation of set-point r^* with corresponding distance to the surface y^* (defined in panel (A)) for bumblebees landing after take-off (blue) and from free-flight (pink). Solid lines depict output of linear mixed model (Table S4.4). (F) The effect of wind on set-point r^* or corresponding approach ground-velocity V^* . In faster winds, bumblebees on average increased their set-point, thus flew faster towards the landing surface. Black dots depict estimated means, gray bars are 95% confidence intervals and red arrows indicate whether estimated means differ significantly from each other (no overlap indicates statistically significant differences).

bees more often switched to a higher set-point even in the presence of winds.

In the 9, 097 landing tracks, we then tested how bumblebees adjusted their set-point of relative rate of expansion with distance to the surface. We found a linear relationship between the logarithmic transformations of the set-point r^* and their corresponding distance to the surface y^* (Figures S4.2 and 4.5E, Section S4.3.2, Table S4.4). We used a linear mixed-effects model to find an estimate of the slope m of this linear variation. The model predicted that bumblebees, on average, increased their set-point with decreasing distance to the surface at a rate $m = -0.727 [0.008]$ and $m = -0.960 [0.017]$ while landing from free-flight and take-off, respectively (mean [std. error]). This step-wise modulation of set-point resulted in bumblebees exhibiting higher set-points closer to the landing surface – in all wind conditions. In still air, bumblebees have been previously shown to exhibit similar values of m for the two landing types (Goyal et al., 2021a). Note that this m is equivalent to the time-to-contact-rate $\dot{\tau}$ parameter identified in literature for the landing strategy of birds (Lee et al., 1991, 1993; Baird et al., 2013; Whitehead, 2020; Goyal et al., 2021a).

Surprisingly, the variation of set-point r^* with distance to the surface y^* was independent of wind speed for both landing types (Tables S4.4).

Bumblebees approach the landing surface at a higher set-point, and hence higher speeds, in faster winds

In contrast, our linear mixed model did predict that relative to the still air bumblebees exhibited a constant increase in set-points for each wind speed (Figure 4.5F). This increase in set-point relative to the still air was observed at all distances to the surface by bumblebees landing from both free-flight or take-off condition. At 3.41 m s^{-1} wind, they exhibited 16% increase in set-point relative to the still air whereas it was 8% for 2.54 m s^{-1} wind ($r_{3.41}^* = 1.16 r_0^*$ and $r_{2.54}^* = 1.08 r_0^*$; subscript denotes wind velocity in m s^{-1}) (Figure 4.5F, Table S4.4). These results show that bumblebees exhibited higher set-points in faster winds, and thus flew faster towards the surface in faster winds.

Bumblebees exhibit faster sensorimotor control response in faster winds

The step-wise modulation of the set-point of optical expansion rate in all wind conditions results intermediate track segments that precede these constant- r segments and contain the

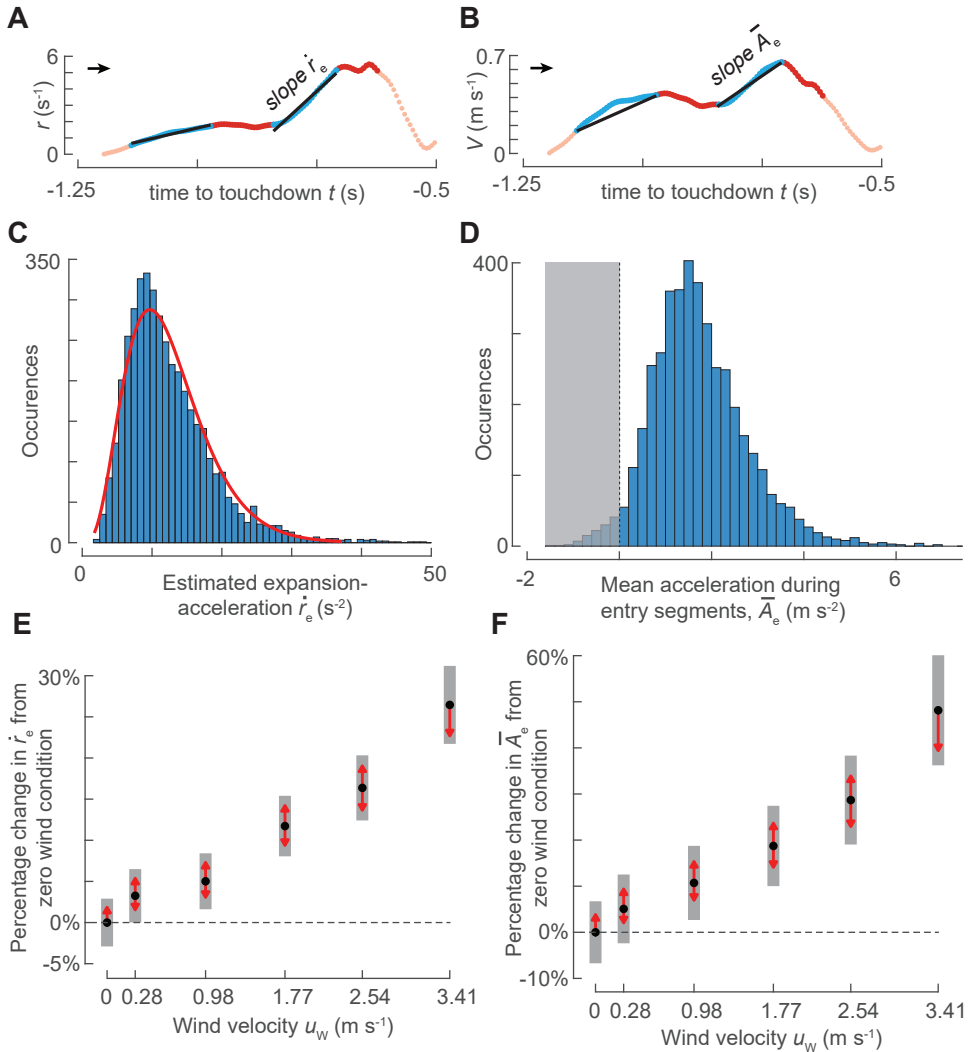


Figure 4.6: Bumblebees use the transient response of their sensorimotor control system to accelerate towards the surface in the presence of all tested steady sidewinds; moreover they accelerate faster in higher winds. The effect of wind speed on the transient response of the sensorimotor control system (A,C,E) and the resulting motor output (body accelerations) (B,D,F) during entry segments. (A,B) An example track depicting the estimation of expansion-acceleration \dot{r}_e (A) and mean acceleration \bar{A}_e (B) in an entry segment. (C,D) Histograms of \dot{r}_e (fitted gamma distribution in red) and \bar{A}_e (for both $n = 4, 221$) during entry segments in which bumblebees increased their optical expansion rate. During these transient phases, bumblebees accelerated 97% of the times towards the landing surface ($\bar{A}_e > 0$). (E,F) On average, bumblebees converged to their set-point faster in higher winds (E) by accelerating faster towards the surface in higher winds (F). This behavior is present for all step changes in relative rate of expansion in an entry segment Δr_e ; the set-point of relative rate of expansion r^* , the starting distance of the entry segment y_0 and both landing types (from take-off or free-flight) (Δr_e , r^* and y_0 are parameters defined for an entry segment, see Figure 4.2G, Tables S4.5 and S4.6). Black dots depict estimated means, gray bars are 95% confidence intervals and red arrows indicate whether the estimated means differ significantly from each other (no overlap indicates statistically significant differences).

transient response of their sensorimotor control system. We refer to these segments as entry or transient segments and extract them using an algorithm from Chapter 3 (see Methods).

Out of 12,338 constant- r segments, the entry-segment extraction algorithm linked 4,374 constant- r segments with a respective transient segment. We modelled the sensorimotor control response of bumblebees during these transient segments as a motion at a constant optical-expansion-acceleration \dot{r}_e (Figure 4.6A) (see Methods). The expansion-acceleration \dot{r}_e defines how fast the bumblebees are capable of reaching their set-point.

Among these 4,374 identified transient segments, bumblebees increased and decreased their optical expansion rate 4,221 and 153 times, respectively, to reach their set-points. Because bumblebees mostly increased their optical expansion rate during entry segments (96.5% of the time), we further focus only on analyzing the sensorimotor control response in them.

In 4,221 entry segments, the observed distribution of expansion-acceleration \dot{r}_e in the presence of all winds can be approximated by a gamma distribution (median $\dot{r}_e = 11.07 \text{ s}^{-2}$, $a = 4.55 [4.4, 4.7]$, $b = 2.7 [2.6, 2.9]$, mean [95% confidence intervals]) (Figure 4.6C) (Evans et al., 2000). This distribution is similar to the one identified for the sensorimotor control response of bumblebees in still air (Chapter 3).

We further used a linear mixed model to test how the observed optical expansion-acceleration (\dot{r}_e) during an entry segment varied in different tested wind conditions. In addition to wind, this model also had other co-variates associated with an entry segment: y_0 , Δr_e , r^* and the landing type (landing from a free-flight or after a take-off) (Figure 4.2G, see methods for their definition). In the presence of winds, the variation in expansion-acceleration \dot{r}_e with these co-variates (Table S4.5) was found to be similar to still air, which is described elsewhere (Chapter 3). Therefore, we here only describe the effect of winds on the optical expansion-acceleration \dot{r}_e .

Our model predicts that bumblebees increased the optical expansion-acceleration with wind velocity. They reached their set-points at a higher rate when the wind velocity was higher (Figure 4.6E). For example, in 3.41 m s^{-1} wind, bumblebees reached their set-point 26.5% faster than still air, and in 2.54 m s^{-1} wind, 16.4% faster (Figure 4.6E, Table S4.5). This wind effect was observed independently of all covariates (y_0 , Δr_e , r^* and landing type). These results show that winds augmented the transient response of the sensorimotor control system of landing bumblebees. This in turn led to bumblebees reaching their set-point faster in faster sidewinds.

Bumblebees accelerate faster towards the landing surface in faster winds

In still air, our previous study (Chapter 3) shows that bumblebees mostly use the transient response of their sensorimotor control system to accelerate towards the landing surface. To understand how bumblebees use this transient response in the presence of winds, we

computed the mean body acceleration \bar{A}_e in each entry segment (Figure 4.6B).

In 153 out of 4374 transient segments, bumblebees decelerated towards the surface ($\bar{A}_e < 0$) when they had to decrease their optical expansion rate for reaching the desired set-point ($\dot{r}_e < 0$). In the remaining 4,221 entry segments, bumblebees, on average, accelerated ($\bar{A}_e > 0$) towards the landing surface 4,102 times and weakly decelerated ($\bar{A}_e < 0$) 119 times to increase their optical expansion rate (Figure 4.6D). Hence, it can be concluded that bumblebees in the presence of winds used the transient response of their sensorimotor control system to mostly (93.7%) accelerate towards the landing surface. Moreover, they produced accelerations and decelerations towards the surface (by changing wing and body kinematics) in the directions that are consistent with the requirement of increasing or decreasing their relative rate of expansion in an entry segment. This is similar to their behavior in the still air condition (Chapter 3).

Using a linear mixed model, we further tested how the positive average acceleration \bar{A}_e varied in different wind conditions. This model also had covariates (y_0 , Δr_e , r^* and landing type) and we found that their effect in the presence of all winds were similar to still air described before (Table S4.6) (Chapter 3). Therefore, we here discuss only the effect of different winds on the body acceleration \bar{A}_e .

Our model predicts that bumblebees accelerated faster towards the landing surface in faster winds (Figure 4.6F). Bumblebees exhibited this behavior independent of all covariates (y_0 , Δr_e , r^* and landing type). For example, in 3.41 m s^{-1} wind, bumblebees exhibited 48% faster mean acceleration than still air, and in 2.54 m s^{-1} wind, 29% faster (Figure 4.6F, Table S4.6).

Bumblebees more often exhibit low velocity phase when they are closer to the landing surface and as wind velocity increases

In still air, as bumblebees approach a surface for landing, they occasionally exhibit moments of near-zero or negative approach velocity V ($V < 0.05 \text{ m s}^{-1}$) (Figure 4.7A) (Reber et al., 2016; de Vries et al., 2020; Goyal et al., 2021a). We refer to these phases as low velocity phases, but they are often called hover phases in literature. These phases are potentially unfavorable while advancing towards the landing surface (except at the start of the landing maneuver and at distances closer to the surface when they can be essential) as they force bumblebees to fly for longer duration. Flying for more time is an energetically costlier affair (Reinhold, 1999) — can be even more so in the presence of winds (Shepard et al., 2016). Moreover, for foraging bees, increase in landing time can negatively impact their floral visitation rate and hence, their energy gain as well (Roubik, 1978; Hansen et al., 2002).

We used a generalized linear mixed model to test how the probability of occurrence of the low velocity phase $P_{\text{low } V}$ varies with wind speeds, landing type (landing from free-flight or take-off) and distance to the surface y (divided into four regions: y_1 ($0.05 \text{ m} <$

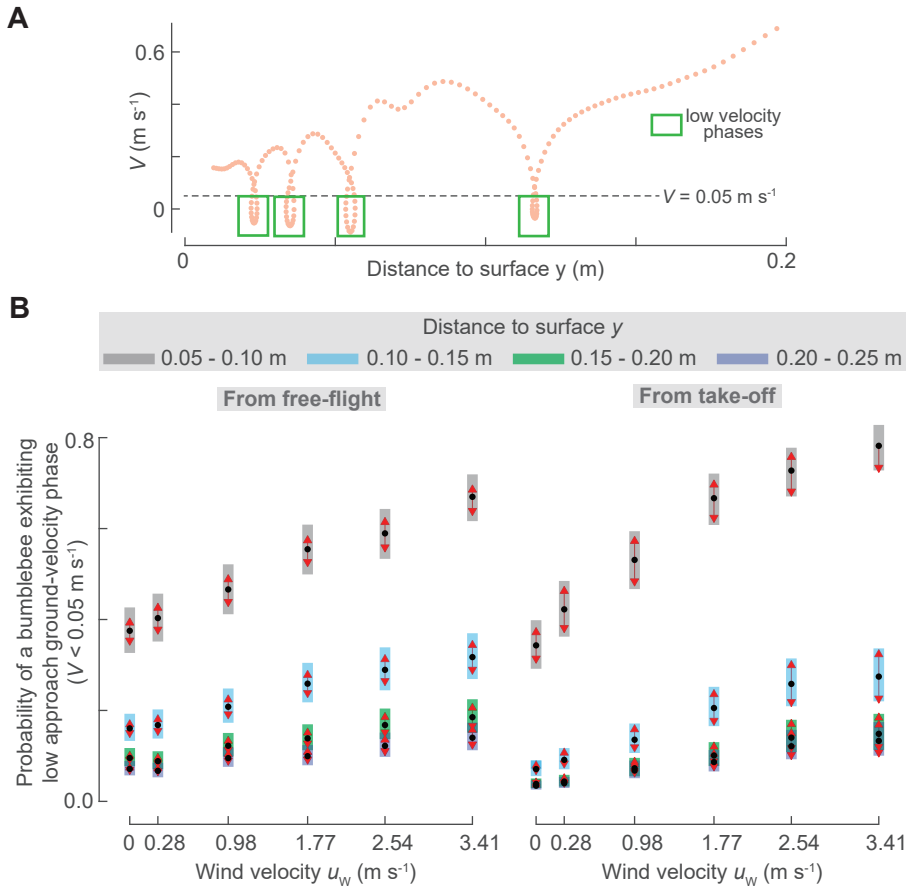


Figure 4.7: The landing bumblebees exhibit a low ground-velocity phase ($V < 0.05 \text{ m s}^{-1}$) more often when they were closer to the surface and when they were flying in higher winds. (A) An example track depicting low approach ground-velocity phases ($V < 0.05 \text{ m s}^{-1}$) during a landing maneuver of a bumblebee. (B) The estimated probabilities that a bumblebee slows down ($V < 0.05 \text{ m s}^{-1}$) at different distances from the surface y , wind speeds and for two landing types (landing from a free-flight or after a take-off) (see Table S4.7 for the output of the used generalized linear mixed model). Black dots depict estimated means, gray bars are 95% confidence intervals and red arrows indicate whether the estimated means differ significantly from each other (no overlap indicates statistically significant differences).

$y \leq 0.10 \text{ m}$), y_2 ($0.10 \text{ m} < y \leq 0.15 \text{ m}$), y_3 ($0.15 \text{ m} < y \leq 0.20 \text{ m}$) and y_4 ($0.20 \text{ m} < y \leq 0.25 \text{ m}$)) (Section S4.3.2). We found that the two-way interactions among these explanatory variables were statistically significant (Table S4.7). Therefore, we successively discuss the effect of each interaction.

Effect of y regions and landing type: In each tested wind condition, bumblebees more often exhibited a low velocity phase as their distance to the surface reduced during a landing approach (Figure 4.7B). When landing from a free-flight, the probability of exhibiting a low velocity phase closer to the landing surface was 5.3 times the probability further away

from it ($P_{\text{low } V} = 0.51 [0.03]$ for $0.05 < y \leq 0.10$ m and $P_{\text{low } V} = 0.10 [0.01]$ for $0.20 < y \leq 0.25$ m). Similarly, when landing after a take-off, the probability $P_{\text{low } V}$ closer to the landing surface was 8.2 times the probability further away from it ($P_{\text{low } V} = 0.59 [0.03]$ for $0.05 < y \leq 0.10$ m and $P_{\text{low } V} = 0.07 [0.01]$ for $0.20 < y \leq 0.25$ m) (mean [standard-error], results are averaged over wind conditions, Table S4.7).

Furthermore, bumblebees more often exhibited low velocity phases in faster winds (Figure 4.7B). This holds for all distance ranges to the surface and landing types (landing from free-flight or take-off). But, the increase in the probability $P_{\text{low } V}$ in different wind conditions is influenced by its interactions with the other covariates.

Effect of y regions and wind conditions: At the furthest tested distance region y_4 ($0.20 < y \leq 0.25$ m), the probability of occurrence of low velocity phase in the fastest tested wind condition $P_{\text{low } V}$ was 2.7 times the probability in still air ($P_{\text{low } V} = 0.14 [0.02]$, $U_W = 3.41 \text{ m s}^{-1}$ and $P_{\text{low } V} = 0.05 [0.01]$, $U_W = 0 \text{ m s}^{-1}$). Similarly, at the closest tested distance region y_1 ($0.05 < y \leq 0.10$ m), this probability in the fastest wind condition was 2 times the probability in still air ($P_{\text{low } V} = 0.73 [0.02]$, $U_W = 3.41 \text{ m s}^{-1}$ and $P_{\text{low } V} = 0.36 [0.02]$, $U_W = 0 \text{ m s}^{-1}$) (mean [standard-error], results are averaged over landing type, Table S4.7).

Effect of landing type and wind conditions: When landing from a free-flight, the probability of bumblebees undergoing a low velocity phase in the fastest tested wind condition was 2 times the probability in still air ($P_{\text{low } V} = 0.30 [0.02]$, $U_W = 3.41 \text{ m s}^{-1}$ and $P_{\text{low } V} = 0.15 [0.01]$, $U_W = 0 \text{ m s}^{-1}$). Similarly, when landing after a take-off, this probability in the fastest tested wind condition was 3.8 times the probability in still air ($P_{\text{low } V} = 0.30 [0.03]$, $U_W = 3.41 \text{ m s}^{-1}$ and $P_{\text{low } V} = 0.08 [0.01]$, $U_W = 0 \text{ m s}^{-1}$). Even though, bumblebees have similar average probability in the fastest wind condition for the two landing types, the increase in $P_{\text{low } V}$ relative to the still air is higher for landings after take-off than free-flight. This is because in still air, bumblebees experienced a low velocity phase (approximately) only half of the time during landings from take-off as compared to the free-flight condition (mean [standard-error], results are averaged over all distance regions, Table S4.7).

These results show that bumblebees exhibited low ground-velocity ($V < 0.05 \text{ m s}^{-1}$) phases more often as their distance to the surface reduced and when they experienced faster winds during a landing approach. Moreover, among two landing types, their landings from take-off were more adversely affected by winds as compared to the landings from free-flight. This is because landings from take-off in a sidewind had a higher increase in the probability of occurrence of a low velocity phase relative to the still air.

Bumblebees in fast winds compensate for the increase in travel time that would occur due to the increase in occurrence of low-velocity phases; they fully or partly compensate depending upon the landing type

We further tested how travelling faster during landing (higher set-points and higher expansion-accelerations) and exhibiting low-velocity phases more often in winds affected the landing performance of bumblebees. We used a linear mixed model to determine how the travel time Δt of landing bumblebees varied in different wind conditions and for two landing types (landing from free-flight and take-off) (Figure 4.8, Table S4.8).

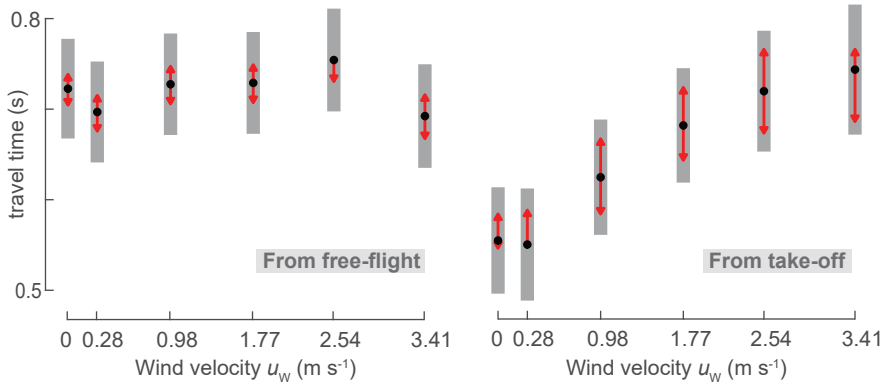


Figure 4.8: The travel time of bumblebees in all wind velocities is similar to quiescent air when they land from free-flight, whereas it increases with wind velocity when they land after a take-off. The travel time Δt of bumblebees to cover 0.2 m approach distance y (from $y = 0.25$ m to $y = 0.05$ m from the landing platform) in different wind conditions and landing types (landing directly after a take-off or from a free-flight condition). Black dots depict estimated means, gray bars are 95% confidence intervals, and red arrows show whether the travel time differs significantly among different conditions (no overlap indicates statistically significant differences). (see Table S4.8 for statistical results).

We found that the travel time of bumblebees landing from free-flight remained similar to the still air in all winds ($\Delta t = 0.72 [0.03]$ s, $U_W = 0$ m s⁻¹ and $\Delta t = 0.69 [0.03]$ s, $U_W = 3.41$ m s⁻¹). In contrast, it increased in stronger winds when they landed after a take-off with a 35% increase in the fastest wind as compared to the still air ($\Delta t = 0.55 [0.03]$ s, $U_W = 0$ m s⁻¹ and $\Delta t = 0.74 [0.04]$ s, $U_W = 3.41$ m s⁻¹) (mean [standard-error], Figure 4.8, Table S4.8). This shows that bumblebees landing from a free-flight fully compensated for the loss in travel time that occurred due to an increase in the occurrence of low velocity phases in faster winds. They achieved this compensation by exhibiting higher set-points and expedited sensorimotor control response in faster winds. But, when landing after a take-off, they could only partly compensate for the loss in travel time. This is observed because the percentage increase of occurrence of low velocity phases relative to the still air

was 2.7 times higher for the landings from take-off (280%, $P_{\text{low } V} = 0.30 [0.03]$, $U_W = 3.41 \text{ m s}^{-1}$ and $P_{\text{low } V} = 0.08 [0.01]$, $U_W = 0 \text{ m s}^{-1}$) as compared to the landings from free-flight (103%, $P_{\text{low } V} = 0.30 [0.02]$, $U_W = 3.41 \text{ m s}^{-1}$ and $P_{\text{low } V} = 0.15 [0.01]$, $U_W = 0 \text{ m s}^{-1}$). In contrast, the percentage increase of set-points and optical expansion-acceleration remained same for both landing types in different wind conditions.

4.4 Discussion

Winds are one of the ubiquitous characteristic of the natural environment which bumblebees often encounter during their foraging trips (Crall et al., 2017). We here investigated how bumblebees execute the landing phase of their flight in the presence of steady sidewinds. For this purpose, we recorded 19,421 landings approaches of bumblebees towards a vertical surface in six different levels of steady sidewinds produced by a wind tunnel (0, 0.28, 0.98, 1.77, 2.54, 3.41 m s^{-1}). These winds correspond to the mean wind conditions that foraging bumblebees experience in nature (Riley et al., 1999; Crall et al., 2017).

The landing strategy of bumblebees in steady sidewinds

We analyzed the individual landing maneuvers of bumblebees using techniques from Goyal et al., 2021a and Chapter 3. Using these methods, we found that, in all tested wind conditions, bumblebees advanced towards the surface by keeping the optical expansion rate approximately constant for brief periods of time (constant- r segments) (Figure 4.5). We refer to this constant as a set-point of optical expansion rate. Bumblebees tended to step-wise increase this set-point as they reached closer to the landing surface. This trend of increasing set-point with reducing distance is captured by a linear relationship with average slope $m = -0.843 [0.01]$ between their logarithmic transformations (Figure S4.2, Table S4.4, mean [std. error]). This slope is the same in all wind conditions. This suggests that the underlying mechanism that results in the set-point adjustment with distance remained unaffected by tested sidewinds.

Moreover, this slope m is also similar to the one previously observed for bumblebees when they landed in different environmental conditions (landing patterns and light intensities) with quiescent air (Goyal et al., 2021a,b). Moreover, it is also similar to the average slope of logarithmic transformations of optical expansion rate and distance to the surface observed during the landings of pigeons ($m = -0.72$) (Lee et al., 1993), hummingbirds ($m = -0.76$) (Lee et al., 1991) and mallards ($m = -0.90$) (Whitehead, 2020). Although these slopes are similar for birds and bumblebees, there is one major difference between their landing strategies. Birds continuously increase their optical expansion rate with reducing distance to the surface as per this slope m , whereas bumblebees only do it discretely (during constant- r segments).

The step-wise modulation of set-point of optical expansion rate in all wind conditions during landing ensured that bumblebees flew not only temporarily at the set-point, but

also exhibited the time-evolution of optical expansion rate as it converged towards the set-point – a typical attribute of a step-response (Ogata, 2010). In still air, these time-evolutions (captured as entry segments) have been previously shown to be the transient response of a sensorimotor control system which regulates the optical expansion rate (Chapter 3). This system produces accelerations (or decelerations) during these transient phases that are consistent with bringing the optical expansion rate closer to the desired set-point (Chapter 3). In this study, we showed that bumblebees exhibited similar behavior in all tested wind conditions. Moreover, we also showed that bumblebees in steady sidewinds continued to use the transient response (entry segments) of their sensorimotor control system to mostly accelerate towards the landing surface and the set-point response (constant- r segments) to always decelerate. This suggests that bumblebees while landing in the steady sidewinds continue to use the visual feedback loop same as still air. This can be helpful in future studies that are aimed at understanding the influence of fluctuations in mean winds on the landing dynamics of bumblebees.

Hence, we here conclude that bumblebees, even in the presence of steady lateral winds, approach a landing surface in multiple bouts. During each bout, they use their sensorimotor control system to regulate optical expansion rate and reach its particular set-point. From one bout to the next, they step-wise increase their set-point as they reach closer to the landing surface. Consequently, this results in bumblebees accelerating and decelerating towards the surface.

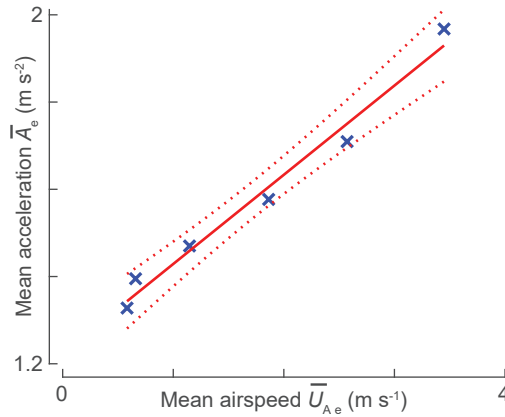
How winds affect the landing dynamics of bumblebees

In addition to the transient and steady-state phases of their sensorimotor control system, landing bumblebees also occasionally exhibited low velocity phases which results in them hovering or even briefly flying away from the surface. Here, we discuss the effects of winds on each of these phases in the following order: (1) transient, (2) low velocity, and (3) set-point phase. Afterwards, we also discuss the effect winds on the overall landing performance (travel time).

(1) Interaction of airspeed measuring mechanosensory modality with the vision-based control system of landing bumblebees

Our results show that bumblebees exhibited faster transient response (expressed as expansion-acceleration \dot{r}_e) and higher mean accelerations (\bar{A}_e) in faster winds (or higher airspeeds). This holds for all values of covariates that influence the transient response of bumblebees (distance from the landing surface (y_0), the required step-change in optical expansion rate (Δr_e) and the associated set-point of optical expansion rate (r^*)). The faster expansion-acceleration and higher mean accelerations during the transient response are indicative of higher control forces that are produced by bumblebees. Hence, it can be said that the airspeed measuring mechanosensory modality in bumblebees has an additive effect on the

A



B

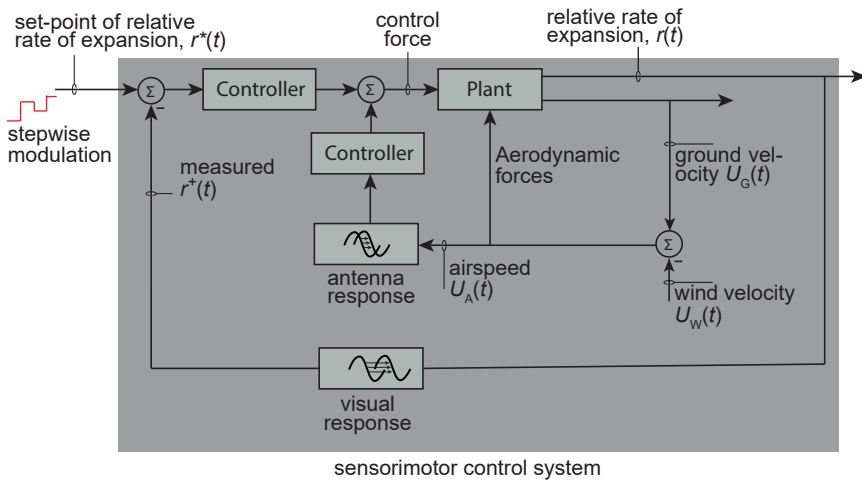


Figure 4.9: The proposed model of integration of airspeed measuring mechanosensory modality with the visual feedback loop in landing bumblebees. (A) The mean acceleration \bar{A}_e increases approximately linearly with the mean airspeed \bar{U}_{A_e} during the transient phase of the landing maneuver. The \bar{A}_e values are first predicted by the linear mixed model for each wind condition at the median values of covariates: $y_0 = 0.29$ m, $\Delta r_e = 1.88$ s $^{-1}$, $r^* = 3.0$ s $^{-1}$ and averaged over landing types (landing from free-flight and take-off) (Table S4.6). The \bar{A}_e variation is then modelled against the median values of mean airspeed \bar{U}_{A_e} during the transient phases in different wind conditions (blue - data points, solid red line - linear fit, dotted lines - 95% confidence intervals, coefficient of determination $R^2 = 0.98$). (B) The proposed model of multimodal sensory integration in landing bumblebees that can explain the linear increase of \bar{A}_e (mean control force per unit mass) with \bar{U}_{A_e} during entry segments. Bumblebees possibly use their antennae to measure the wind induced mechanosensory input (airspeed) and integrate it with a positive feedback in their vision-based closed-loop sensorimotor control (explained in Figure 4.1C). This fast positive feedback can provide active damping that counteracts the unstable oscillations of a visual feedback loop. A similar multimodal sensory integration is also proposed in the forward flight of *Drosophila* (Fuller et al., 2014).

force produced by bumblebees during the transient responses.

To assess this effect, we tested how the mean acceleration (\bar{A}_e , mean force per unit mass) varied with the mean airspeed \bar{U}_{Ae} that bumblebees experienced during these transient phases in different wind conditions. We found that a linear relationship captures well (slope = 0.204 [0.015] s^{-1} , mean [std. error], coefficient of determination $R^2 = 0.98$) the increase in mean accelerations with airspeed (or winds) during entry segments (Figure 4.9A). This linear relationship is indicative of a positive feedback with a constant gain from the airspeed measuring mechanosensory modality to the vision-based regulator of landing bumblebees (Figure 4.9B). A similar multi-sensor feedback architecture is also suggested for free-flying *Drosophila* (Fuller et al., 2014).

Mechanoreceptors on the bumblebee's antennae (Taylor and Krapp, 2007; Jakobi et al., 2018) likely detect the changes in airspeed in different wind conditions. As the neural processing time of information from antennae (~ 20 ms) is much shorter than the visual system ($\sim 50 - 100$ ms), a positive feedback from the antennal system can provide active damping to any vision based regulator (Fuller et al., 2014). In the event of sudden disturbances such as wind, an active damping can stabilize the oscillations of a slow visual feedback loop, e.g., as observed in free-flying *Drosophila* (Fuller et al., 2014). Active damping is also implicated in stabilizing the dynamics of insect locomotion in multiple other scenarios (Cowan et al., 2006; Hedrick et al., 2009; Cheng and Deng, 2011; Hedrick, 2011; Elzinga et al., 2012; Dyhr et al., 2013; Taylor et al., 2013; Sun, 2014).

Based on these observations, we here propose that the airspeed sensing mechanosensory modality has a positive feedback (with constant gain) to the vision-based control of landing bumblebees. In the event of sudden wind disturbances, this fast mechanosensory feedback would stabilize the oscillations of a slow visual control loop.

(2) Interaction of airspeed measuring mechanosensory modality with the vision-based feedback loop likely causes bumblebees to more often undergo the low velocity phase in faster winds

Why do bumblebees more often exhibit low velocity phase in faster winds? This question is especially relevant because more low velocity phases can result in more landing time, which in turn can negatively impact their foraging efficiency (Balfour et al., 2021). The increase in the transient response of the sensorimotor control system with wind velocity, independent of all other covariates, is analogous to bumblebees operating their visual feedback loop at a higher gain in still air. This higher gain in the r -based control loop will result in instabilities occurring at distances further away from the landing surface (de Croon, 2016). This means that the characteristics of the low velocity phases that bumblebees earlier exhibited closer to the landing surface in still air will be observed at distances further away from it in the presence of winds. This is consistent with our results which show that (a) in still air, bumblebees more often exhibited a low velocity phase when they were closer to the

landing surface, and (b) as wind velocity increased, bumblebees more-often underwent a low velocity phase ($V < 0.05 \text{ m s}^{-1}$) at each tested distance region from the surface. This suggests that the low-velocity phases in landing bumblebees are caused by the interaction of airspeed feedback with the vision-based control loop.

(3) Influence of winds on the set-point

Our results also show that the landing bumblebees exhibited higher set-points of optical expansion rate in faster winds. This is similar to the free-flight of honeybees where the mean set-point of translational optic flow is higher in the presence of higher headwinds (Baird et al., 2021). This shows that the airspeed measuring mechanosensory modality, in addition to the sensorimotor control system, also influences the set-point that it aims to reach. During landing, both of these positive influences of winds enabled bumblebees to compensate for the loss in travel time that occurred due to the low velocity phases during landing.

Note that the analysis of average landing maneuvers failed to capture the increase of set-points in faster winds (Figure 4.4). It instead predicted that bumblebees either kept the set-point of optical expansion rate same (for landings from free-flight) or lowered it (for landings from take-off) in faster winds. Moreover, as previously shown (Goyal et al., 2021a), it also failed to capture a series of acceleration and deceleration bouts during a landing maneuver (Figure 4.5), and instead predicted that landing bumblebees exhibited one acceleration and deceleration phase. Thus, it can be concluded that analysis of average maneuvers hides important features of the landing dynamics of bumblebees in the presence of tested winds.

(4) Influence of winds on the travel time

Our results also show that bumblebees fully compensated for the likely increase in travel distance due to low-velocity flight phases while landing from free-flight, but not when they landed after a take-off. In fact, they exhibited up to 35% more travel time when they landed after a take-off in winds. This result is in contrast to the results obtained for honeybees where increase in wind speeds did not affect the inter-flower flight duration (Hennessy et al., 2020, 2021). The direct comparison is difficult here because flowers in these studies were situated more closely than our study (48 cm in our study, maximum 20 cm distance between two flowers in Hennessy et al., 2020 and unknown in Hennessy et al., 2021, but many flowers were present within a patch of size $160 \times 60 \text{ cm}$). Moreover, honeybees in those studies likely experienced slower and more variable winds in the wakes of the flowers as compared to the uniform winds in our study.

Energetic costs while landing in winds

Our results suggest that winds can influence the total food influx into a bumblebee colony. In our set-up, bumblebees took more time to travel when they landed after a take-off. This can negatively influence their foraging efficiency within a flower patch (Balfour et al., 2021). Moreover, bumblebees in our setup performed up to 70% less landings in the fastest tested wind condition (3.41 m s^{-1}). Similar results are observed in the (semi) field studies (Pinzauti, 1986; Vicens and Bosch, 2000; Hennessy et al., 2020, 2021) where the presence of winds negatively impacted the foraging rate of honeybees.

These results suggest that the winds can have detrimental effects on the colonies of insect pollinators (Riessberger and Crailsheim, 1997), and their pollination services (Tuell and Isaacs, 2010). Understanding these effects is crucial as insect pollinators support biodiversity (Ollerton et al., 2011) and global food productivity (Klein et al., 2006). This is even more pertinent with a predicted increase in wind speeds due to climate change in some areas of the world (Hosking et al., 2018). Future work in this direction can ascertain the direct effect of winds on the colony fitness and pollination dynamics.

Conclusion

Wind is an important yet understudied environmental influence on the flight control strategy of insects during landing. Here, we present how bumblebees use visual cues and potentially airflow cues to advance towards the surface in the presence of steady lateral winds and how they compensate for the effect of those winds on their landing approach. We have shown that bumblebees in these winds continue to approach a landing surface using a visually-guided strategy similar to still air, but with some key differences. Similar to still air, they advanced towards the landing surface by regulating optical expansion rate and exhibiting bouts of acceleration and deceleration phases, along with the occasional low velocity phases ($V < 0.05 \text{ m s}^{-1}$). In contrast to still air, they travelled faster towards the landing surface, but also more often exhibited low velocity phases with increasing wind speed. The occurrence of more low velocity phases can negatively impact their foraging efficiency as it will result in bumblebees taking longer time to land. But, by travelling faster towards the surface, bumblebees fully or partly compensated for this potential increase in travel time depending upon whether they landed from a free-flight or after a take-off, respectively.

In addition to understanding these positive and negative effects of winds on the landing dynamics of bumblebees, our results also enable us to propose how bumblebees integrate information from their airspeed measuring mechanosensors with the vision-based control loop. Our results suggest that bumblebees have a positive feedback from their airspeed measuring mechanosensors to their visual feedback loop. Such a control architecture is also proposed for flying *Drosophila* (Fuller et al., 2014) and can provide active damping to the unstable oscillations of the visual feedback loop in the event of external disturbances.

In nature, winds can have both direct and indirect influences on the landing dynamics

of bumblebees. The direct influence corresponds to the effects of mean wind speeds and the fluctuations around these speeds on the landing dynamics. The indirect influence corresponds to the impact on the visual information that bumblebees perceive due to swaying of flowers in winds (Kapustjansky et al., 2009; Hennessy et al., 2020). Out of these, our study investigates the effects of mean winds on the landing dynamics of bumblebees and therefore, is a step towards better understanding the exemplary ability of bumblebees to mitigate the effect of winds.

Data and code availability

The landing maneuvers of bumblebees gathered in this study will be publicly available as a data repository and the code used for the analysis is available at: https://github.com/kaku289/nimble-bbee-analysis/tree/landing_steady_winds.

Acknowledgements

This project is supported by the Nederlandse Organisatie voor Wetenschappelijk Onderzoek - Toegepaste en Technische Wetenschappen (NWO-TTW grant number 15039). We thank Wouter van Veen, Cees Voeselek and Antoine Cribellier for useful discussions and Remco P.M. Pieters for his help in building the experimental set-up.

Author contributions

Conceptualization, P.G., J.L.v.L., and F.T.M.; methodology, P.G.; Software, P.G.; validation, P.G.; formal analysis, P.G.; investigation, P.G.; resources, J.L.v.L., F.T.M.; data curation, P.G.; writing – original draft, P.G.; writing – review & editing, P.G., J.L.v.L., and F.T.M.; visualization, P.G.; supervision, J.L.v.L. and F.T.M.; project administration, P.G.; funding acquisition, F.T.M..

Declaration of interests

The authors declare no competing interests.

References

- Alcorn, K., Whitney, H. and Glover, B. (2012). Flower movement increases pollinator preference for flowers with better grip. *Functional Ecology* **26**, 941–947.
- Alma, A. M., Farji-Brener, A. G. and Elizalde, L. (2017). A breath of fresh air in foraging theory: The importance of wind for food size selection in a central-place forager. *American Naturalist* **190**, 410–419.
- Baird, E., Boeddeker, N., Ibbotson, M. R. and Srinivasan, M. V. (2013). A universal strategy for visually guided landing. *Proceedings of the National Academy of Sciences of the United States of America* **110**, 18686–18691.

- Baird, E., Boeddeker, N. and Srinivasan, M. V. (2021). The effect of optic flow cues on honeybee flight control in wind. *Proceedings of the Royal Society B: Biological Sciences* 288, 20203051.
- Balebail, S., Raja, S. K. and Sane, S. P. (2019). Landing maneuvers of houseflies on vertical and inverted surfaces. *PLoS ONE* 14, 1–17.
- Balfour, N. J., Shackleton, K., Arscott, N. A., Roll-Baldwin, K., Bracuti, A., Toselli, G. and Ratnieks, F. L. (2021). Energetic efficiency of foraging mediates bee niche partitioning. *Ecology* 102, e03285.
- Barron, A. and Srinivasan, M. V. (2006). Visual regulation of ground speed and headwind compensation in freely flying honey bees (*Apis mellifera* L.). *Journal of Experimental Biology* 209, 978–984.
- Burnett, N. P., Badger, M. A. and Combes, S. A. (2020). Wind and obstacle motion affect honeybee flight strategies in cluttered environments. *Journal of Experimental Biology* 223.
- Chang, J. J., Crall, J. D. and Combes, S. A. (2016). Wind alters landing dynamics in bumblebees. *The Journal of Experimental Biology* 219, 2819–2822.
- Cheng, B. and Deng, X. (2011). Translational and rotational damping of flapping flight and its dynamics and stability at hovering. *IEEE Trans Robot* 27, 849–864.
- Combes, S. A. and Dudley, R. (2009). Turbulence-driven instabilities limit insect flight performance. *Proceedings of the National Academy of Sciences* 106, 9105–9108.
- Cowan, N., Lee, J. and Full, R. (2006). Task-level control of rapid wall following in the American cockroach. *Journal of Experimental Biology* 209, 1617–1629.
- Crall, J. D., Brokaw, J., Gagliardi, S. F., Mendenhall, C. D., Pierce, N. E. and Combes, S. A. (2020). Wind drives temporal variation in pollinator visitation in a fragmented tropical forest. *Biology letters* 16, 20200103.
- Crall, J. D., Chang, J. J., Oppenheimer, R. L. and Combes, S. A. (2017). Foraging in an unsteady world: Bumblebee flight performance in fieldrealistic turbulence. *Interface Focus* 7.
- de Croon, G. C. H. E. (2016). Monocular distance estimation with optical flow maneuvers and efference copies: a stability-based strategy. *Bioinspiration & Biomimetics* 11, 016004.
- de Vries, L. J., van Langevelde, F., van Dooremalen, C., Kornegoor, I. G., Lankheet, M. J., van Leeuwen, J. L., Naguib, M. and Muijres, F. T. (2020). Bumblebees land remarkably well in redâ€“blue greenhouse LED light conditions. *Biology Open* 9.
- Dickinson, M. H., Farley, C. T., Full, R. J., Koehl, M. A., Kram, R. and Lehman, S. (2000). How animals move: An integrative view. *Science* 288, 100–106.
- Duncan, C. D. C. (1974). *The social behavior of the bees : a comparative study*. Cambridge, Mass. SE - xii, 404 pages : illustrations ; 26 cm: Belknap Press of Harvard University

Press.

- Dyhr, J. P., Morgansen, K. A., Daniel, T. L. and Cowan, N. J. (2013). Flexible strategies for flight control: an active role for the abdomen. *Journal of Experimental Biology* **216**, 1523–1536.
- Edwards, M. and Ibbotson, M. R. (2007). Relative sensitivities to large-field optic-flow patterns varying in direction and speed. *Perception* **36**, 113–124.
- Elzinga, M., Dickson, W. and Dickinson, M. (2012). The influence of sensory delay on the yaw dynamics of a flapping insect. *J R Soc Interface* **9**, 1685–1696.
- Engels, T., Kolomenskiy, D., Schneider, K., Lehmann, F. O. and Sesterhenn, J. (2016). Bumblebee flight in Heavy Turbulence. *Physical Review Letters* **116**, 1–5.
- Evans, M., Hastings, N. and Peacock, B. (2000). *Statistical Distributions*. Wiley Series in Probability and Statistics. Wiley.
- Fuller, S. B., Straw, A. D., Peek, M. Y., Murray, R. M. and Dickinson, M. H. (2014). Flying *Drosophila* stabilize their vision-based velocity controller by sensing wind with their antennae. *Proceedings of the National Academy of Sciences* **111**, E1182—E1191.
- Garratt, J. R. (1994). The atmospheric boundary layer. *Earth-Science Reviews* **37**, 89–134.
- Gibson, J. J. (1955). The optical expansion-pattern in aerial locomotion. *The American journal of psychology* **68**, 480–484.
- Goulson, D. (2010). *Bumblebees: Behaviour, Ecology, and Conservation*. Oxford biology. OUP Oxford.
- Goyal, P., Cribellier, A., de Croon, G. C. H. E., Lankheet, M. J., van Leeuwen, J. L., Pieters, R. P. M. and Muijres, F. T. (2021a). Bumblebees land rapidly and robustly using a sophisticated modular flight control strategy. *iScience* **24**, 102407.
- Goyal, P., Cribellier, A., de Croon, G. C. H. E., Lankheet, M. J., van Leeuwen, J. L., Pieters, R. P. M. and Muijres, F. T. (2021b). Landing manoeuvres of bumblebees. *Mendeley Data Version 1*.
- Hansen, D. M., Olesen, J. M. and Jones, C. G. (2002). Trees, birds and bees in Mauritius: exploitative competition between introduced honey bees and endemic nectarivorous birds? *Journal of Biogeography* **29**, 721–734.
- Hedrick, T. (2011). Damping in flapping flight and its implications for manoeuvring, scaling and evolution. *Journal of Experimental Biology* **214**, 4073–4081.
- Hedrick, T., Cheng, B. and Deng, X. (2009). Wingbeat Time and the Scaling of Passive Rotational Damping in Flapping Flight. *Science* **324**, 252–255.
- Heinrich, B. (1979). Resource heterogeneity and patterns of movement in foraging bumblebees. *Oecologia* **40**, 235–245.
- Hennessy, G., Harris, C., Eaton, C., Wright, P., Jackson, E., Goulson, D. and Rat-

- nieks, F. F. (2020). Gone with the wind: effects of wind on honey bee visit rate and foraging behaviour. *Animal Behaviour* **161**, 23–31.
- Hennessy, G., Harris, C., Pirot, L., Lefter, A., Goulson, D. and Ratnieks, F. L. (2021). Wind slows play: increasing wind speed reduces flower visiting rate in honey bees. *Animal Behaviour* **178**, 87–93.
- Hosking, J. S., MacLeod, D., Phillips, T., Holmes, C. R., Watson, P., Shuckburgh, E. F. and Mitchell, D. (2018). Changes in European wind energy generation potential within a 1.5°C warmer world. *Environmental Research Letters* **13**, 054032.
- Hu, G., Lim, K. S., Horvitz, N., Clark, S. J., Reynolds, D. R., Sapir, N. and Chapman, J. W. (2016a). Mass seasonal bioflows of high-flying insect migrants. *Science (New York, N.Y.)* **354**, 1584–1587.
- Hu, G., Lim, K. S., Reynolds, D. R., Reynolds, A. M. and Chapman, J. W. (2016b). Wind-Related Orientation Patterns in Diurnal, Crepuscular and Nocturnal High-Altitude Insect Migrants. *Frontiers in behavioral neuroscience* **10**, 32.
- Jakobi, T., Kolomenskiy, D., Ikeda, T., Watkins, S., Fisher, A., Liu, H. and Ravi, S. (2018). Bees with attitude: the effects of directed gusts on flight trajectories. *Biology Open* **7**.
- Kapustjansky, A., Chittka, L. and Spaethe, J. (2009). Bees use three-dimensional information to improve target detection. *Naturwissenschaften* **2009** 97:2 **97**, 229–233.
- Klein, A.-M., Vaissire, B. E., Cane, J. H., Steffan-Dewenter, I., Cunningham, S. A., Kremen, C. and Tscharntke, T. (2006). Importance of pollinators in changing landscapes for world crops. *Proceedings of the Royal Society B: Biological Sciences* **274**, 303–313.
- Laurent, K. M., Fogg, B., Ginsburg, T., Halverson, C., Lanzone, M. J., Miller, T. A., Winkler, D. W. and Bewley, G. P. (2021). Turbulence explains the accelerations of an eagle in natural flight. *Proceedings of the National Academy of Sciences of the United States of America* **118**.
- Lee, D. N., Bootsma, R. J., Land, M., Regan, D. and Gray, R. (2009). Lee's 1976 Paper. *Perception* **38**, 837–858.
- Lee, D. N., Davies, M. N. O., Green, P. R. and (Ruud). Van Der Weel, F. R. (1993). Visual control of velocity of approach by pigeons when landing. *Journal of Experimental Biology* **180**, 85–104.
- Lee, D. N., Reddish, P. E. and Rand, D. T. (1991). Aerial docking by hummingbirds. *Naturwissenschaften* **78**, 526–527.
- Liu, P., Sane, S. P., Mongeau, J. M., Zhao, J. and Cheng, B. (2019). Flies land upside down on a ceiling using rapid visually mediated rotational maneuvers. *Science Advances* **5**.
- Matthews, M. and Sponberg, S. (2018). Hawkmoth flight in the unsteady wakes of

- flowers. *Journal of Experimental Biology* **221**.
- Michener, C. D.** (2007). *The Bees of the World*. Johns Hopkins University Press.
- Mikkola, K.** (1986). Direction of Insect Migrations in Relation to the Wind. In *Insect Flight* (ed. W. Danthanarayana), pp. 152–171. Berlin, Heidelberg: Springer Berlin Heidelberg.
- Mountcastle, A. M., Ravi, S. and Combes, S. A.** (2015). Nectar vs. pollen loading affects the tradeoff between flight stability and maneuverability in bumblebees. *Proceedings of the National Academy of Sciences* **112**, 10527–10532.
- Ogata, K.** (2010). *Modern Control Engineering*. Instrumentation and controls series. Prentice Hall.
- Ollerton, J., Winfree, R. and Tarrant, S.** (2011). How many flowering plants are pollinated by animals? *Oikos* **120**, 321–326.
- Ortega-Jimenez, V. M., Greeter, J. S., Mittal, R. and Hedrick, T. L.** (2013). Hawkmoth flight stability in turbulent vortex streets. *Journal of Experimental Biology* **216**, 4567–4579.
- Ortega-Jimenez, V. M., Mittal, R. and Hedrick, T. L.** (2014). Hawkmoth flight performance in tornado-like whirlwind vortices. *Bioinspiration & Biomimetics* **9**, 025003.
- Pasek, J. E.** (1988). Influence of wind and windbreaks on local dispersal of insects. *Agriculture, Ecosystems & Environment* **22-23**, 539–554.
- Peat, J. and Goulson, D.** (2005). Effects of Experience and Weather on Foraging Rate and Pollen versus Nectar Collection in the Bumblebee, *Bombus terrestris*. *Behavioral Ecology and Sociobiology* **58**, 152–156.
- Pinzauti, M.** (1986). The influence of the wind on nectar secretion from the melon and on the flight of bees: The use of an artificial wind-break. *Apidologie* **17**, 63–72.
- Ravi, S., Crall, J. D., Fisher, A. and Combes, S. A.** (2013). Rolling with the flow: bumblebees flying in unsteady wakes. *Journal of Experimental Biology* **216**, 4299–4309.
- Ravi, S., Crall, J. D., McNeilly, L., Gagliardi, S. F., Biewener, A. A. and Combes, S. A.** (2015). Hummingbird flight stability and control in freestream turbulent winds. *Journal of Experimental Biology* **218**, 1444–1452.
- Ravi, S., Kolomenskiy, D., Engels, T., Schneider, K., Wang, C., Sesterhenn, J. and Liu, H.** (2016). Bumblebees minimize control challenges by combining active and passive modes in unsteady winds - Supplement material. *Scientific Reports* **6**, 1–11.
- Reber, T., Baird, E. and Dacke, M.** (2016). The final moments of landing in bumblebees, *Bombus terrestris*. *Journal of Comparative Physiology A: Neuroethology, Sensory, Neural, and Behavioral Physiology* **202**, 277–285.
- Reinhold, K.** (1999). Energetically costly behaviour and the evolution of resting metabolic rate in insects. *Functional Ecology* **13**, 217–224.

- Riessberger, U. and Crailsheim, K. (1997). Short-term effect of different weather conditions upon the behaviour of forager and nurse honey bees (*Apis mellifera carnica* Pollmann). *Apidologie* **28**, 411–426.
- Riley, J. R., Reynolds, D. R., Smith, A. D., Edwards, A. S., Osborne, J. L., Williams, I. H. and McCartney, H. A. (1999). Compensation for wind drift by bumble-bees. *Nature* *1999 400:6740* **400**, 126–126.
- Roubik, D. W. (1978). Competitive interactions between neotropical pollinators and Africanized honey bees. *Science* **201**, 1030–1032.
- Sane, S. P. (2003). The aerodynamics of insect flight. *Journal of Experimental Biology* **206**, 4191–4208.
- Shackleton, K., Balfour, N. J., Toufalia, H. A., Alves, D. A., Bento, J. M. and Ratnieks, F. L. W. (2019). Unique nest entrance structure of *Partamona helleri* stingless bees leads to remarkable ‘crash-landing’ behaviour. *Insectes Sociaux* *2019 66:3* **66**, 471–477.
- Shepard, E. L. C., Ross, A. N. and Portugal, S. J. (2016). Moving in a moving medium: new perspectives on flight. *Philosophical Transactions of the Royal Society B: Biological Sciences* **371**.
- Srinivasan, M. V., Zhang, S. W., Chahl, J. S., Barth, E. and Venkatesh, S. (2000). How honeybees make grazing landings on flat surfaces. *Biological Cybernetics* **83**, 171–183.
- Straw, A. D., Branson, K., Neumann, T. R. and Dickinson, M. H. (2011). Multi-camera Real-time Three-dimensional Tracking of Multiple Flying Animals. *Journal of The Royal Society Interface* **8**, 395–409.
- Stull, R. B. (1988). *An introduction to boundary layer meteorology*, volume 13. Springer Science & Business Media.
- Sun, M. (2014). Insect flight dynamics: Stability and control. *Reviews of Modern Physics* **86**, 615–646.
- Svoboda, T., Martinec, D. and Pajdla, T. (2005). A convenient multicamera self-calibration for virtual environments. *Presence: Teleoperators and Virtual Environments* **14**, 407–422.
- Taylor, G. J., Luu, T., Ball, D. and Srinivasan, M. V. (2013). Vision and air flow combine to streamline flying honeybees - Supplement material. *Scientific Reports* **3**, 1–37.
- Taylor, G. K. and Krapp, H. G. (2007). Sensory Systems and Flight Stability: What do Insects Measure and Why? In *Insect Mechanics and Control*, volume 34, pp. 231–316. Academic Press.
- Tichit, P., Alves-dos Santos, I., Dacke, M. and Baird, E. (2020). Accelerated landing in a stingless bee and its unexpected benefits for traffic congestion. *Proceedings of the Royal Society B* **287**, 20192720.
- Tuell, J. K. and Isaacs, R. (2010). Weather during bloom affects pollination and yield of

- highbush blueberry. *Journal of Economic Entomology* **103**, 557–562.
- Van Breugel, F. and Dickinson, M. H.** (2012). The visual control of landing and obstacle avoidance in the fruit fly *Drosophila melanogaster*. *Journal of Experimental Biology* **215**, 1783–1798.
- Vance, J. T., Faruque, I. and Humbert, J. S.** (2013). Kinematic strategies for mitigating gust perturbations in insects. *Bioinspiration and Biomimetics* **8**.
- Vicens, N. and Bosch, J.** (2000). Weather-dependent pollinator activity in an apple orchard, with special reference to *Osmia cornuta* and *Apis mellifera* (Hymenoptera: Megachilidae and Apidae). *Environmental Entomology* **29**, 413–420.
- Wagner, H.** (1982). Flow-field variables trigger landing in flies. *Nature* **297**, 147–148.
- Whitehead, J. G.** (2020). *An examination of the kinematics and behavior of mallards (*Anas platyrhynchos*) during water landings*. Ph.D. thesis, Virginia Tech.

Supplemental information

Bumblebees actively compensate for the adverse effects of steady sidewinds during visually guided landings

Pulkit Goyal, Johan L. van Leeuwen, Florian T. Muijres

S4.1 Figures

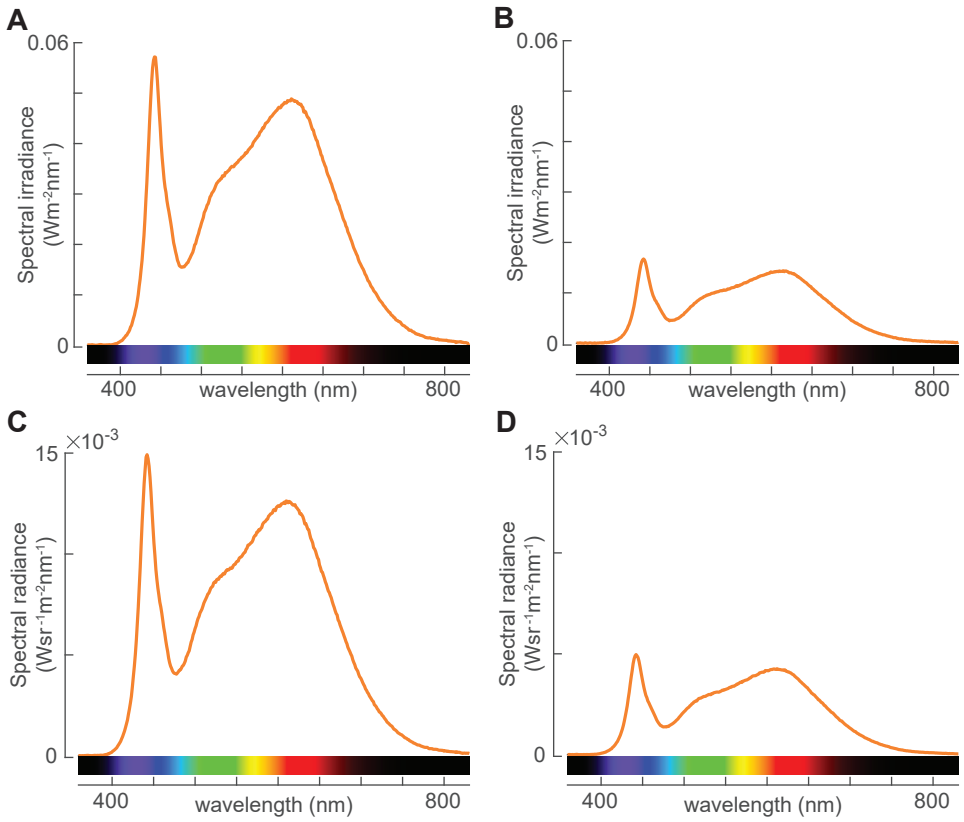


Figure S4.1: Light spectrum used in the experiments. Spectral irradiance (A) and spectral radiance (C) at the center of the flight arena. Spectral irradiance (B) and spectral radiance (D) at the centre of the landing platforms.

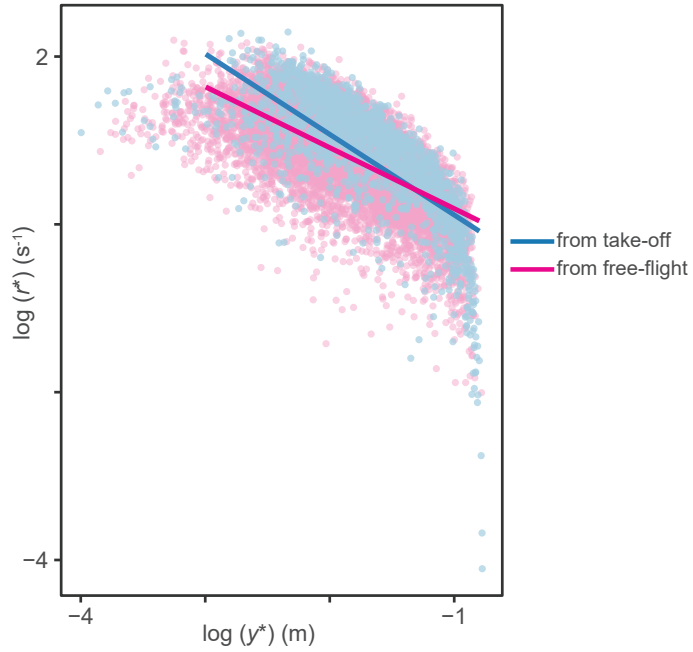


Figure S4.2: The variation of set-point of optical expansion rate τ^* with distance to the surface y^* in the logarithmic domain as identified by the linear mixed-effects model in Equation S4.3 (Table S4.4).

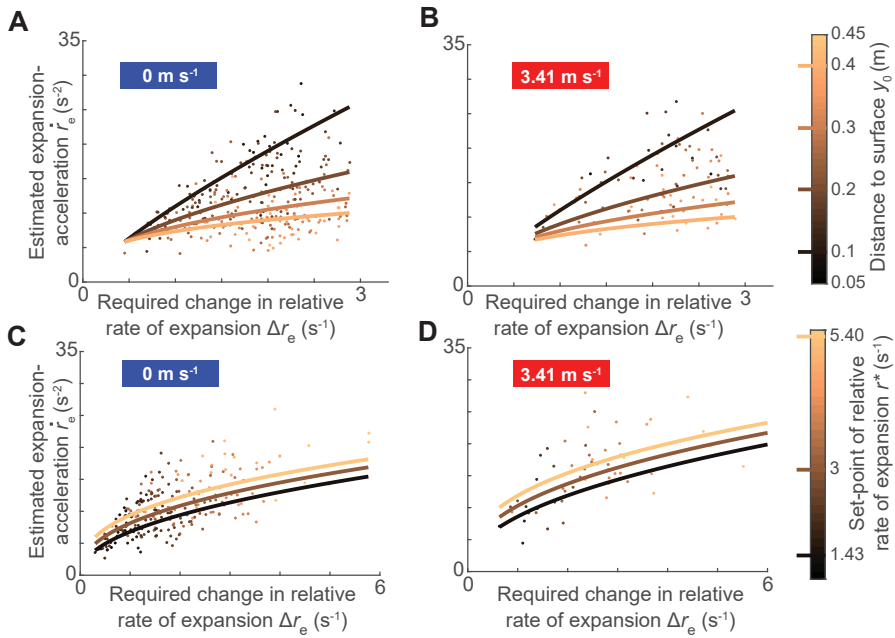


Figure S4.3: The variation of optical expansion-acceleration \hat{r}_e with explanatory variables as identified by the linear mixed-effects model in Equation S4.4 (Table S4.5). (A,B) The variation of expansion-acceleration \hat{r}_e due to the interaction between the required step-change in relative rate of expansion (Δr_e) and the starting distance of the entry segment from the landing surface (y_0) in still air (A) and fastest tested wind speed (B). (C,D) The variation of expansion-acceleration \hat{r}_e due to the interaction between the required step-change in relative rate of expansion (Δr_e) and the final set-point to reach (r^*) in an entry segment for still air (C) and fastest tested wind speed (D). (A,B) The curves depict the statistical model output at the median value $r^* = 2.98 \text{ s}^{-1}$, and data points are shown for the interval $r^* \in [2.48, 3.48] \text{ s}^{-1}$. (C,D) The curves depict the statistical model output at the median value $y_0 = 0.28 \text{ m}$, and data points are shown for the interval $y_0 \in [0.255, 0.305] \text{ m}$.

S4.2 Tables

Table S4.2: The analysis of landing frequency of bumblebees in different wind speeds. The post-hoc tests compare differences between the number of landings per hour N in different wind conditions (statistical model as given by Equation S4.1: $N_{\text{takeoff},i,d,t}$ or $N_{\text{freeflight},i,d,t} \sim N(\alpha_0 + \alpha_d + \alpha_t + \sum_{j=1}^5 \beta_j \text{WIND}_{j,i,d,t}, \sigma^2)$).

Effect on $N_{\text{freeflight},i,d,t}$				
Fixed effect	Estimate	Std error	t value	Pr(> t)
α	280.83	28.22	9.95	$8.34E - 09$
β_1	-69.41	22.47	-3.09	0.0038
β_2	-94.72	22.68	-4.18	0.0002
β_3	-135.19	21.44	-6.31	$2.48E - 07$
β_4	-165.55	21.79	-7.60	$4.31E - 09$
β_5	-168.61	21.17	-7.97	$1.4E - 09$
Post-hoc contrasts*	Estimate	Std error	z ratio	p value
0 - 1	69.41	22.55	3.08	0.057264
0 - 2	94.72	22.88	4.14	0.002631
0 - 3	135.19	21.48	6.29	$3.27E - 06$
0 - 4	165.55	21.88	7.56	$5.58E - 08$
0 - 5	168.61	21.27	7.93	$1.81E - 08$
1 - 2	25.32	23.06	1.10	1
1 - 3	65.79	22.54	2.92	0.087547
1 - 4	96.15	22.24	4.32	0.001572
1 - 5	99.20	22.12	4.49	0.000929
2 - 3	40.47	22.98	1.76	1
2 - 4	70.83	22.28	3.18	0.043664
2 - 5	73.88	22.09	3.34	0.027328
3 - 4	30.36	22.09	1.37	1
3 - 5	33.41	21.57	1.55	1
4 - 5	3.05	21.14	0.14	1

*0, 1, 2, 3, 4, and 5 correspond to wind speeds 0, 0.28, 0.98, 1.77, 2.54, and 3.41 m s^{-1} , respectively.

(Continued on next page.)

Effect on $N_{\text{takeoff},i,d,t}$

Fixed effect	Estimate	Std error	t value	Pr(> t)
α	55.986	7.803	7.175	$4.39E - 07$
β_1	-20.145	6.256	-3.220	0.002645
β_2	-23.300	6.332	-3.680	0.000717
β_3	-26.808	5.969	-4.491	$6.67E - 05$
β_4	-33.637	6.071	-5.541	$2.51E - 06$
β_5	-39.508	5.900	-6.696	$6.75E - 08$

Post-hoc contrasts*	Estimate	Std error	z ratio	p value
0 - 1	20.14	6.27	3.21	0.03988
0 - 2	23.30	6.37	3.66	0.011189
0 - 3	26.81	5.97	4.49	0.000967
0 - 4	33.64	6.09	5.52	$3.64E - 05$
0 - 5	39.51	5.92	6.68	$9.46E - 07$
1 - 2	3.16	6.41	0.49	1
1 - 3	6.66	6.27	1.06	1
1 - 4	13.49	6.19	2.18	0.53075
1 - 5	19.36	6.15	3.15	0.047411
2 - 3	3.51	6.40	0.55	1
2 - 4	10.34	6.20	1.67	1
2 - 5	16.21	6.15	2.64	0.179731
3 - 4	6.83	6.15	1.11	1
3 - 5	12.70	6.00	2.12	0.610922
4 - 5	5.87	5.88	1.00	1

*0, 1, 2, 3, 4, and 5 correspond to wind speeds 0, 0.28, 0.98, 1.77, 2.54, and 3.41 m s^{-1} , respectively.

Table S4.3: Analysis of mean relative-rate-of-expansion in different tested treatments (wind speeds and starting conditions) for average-per-treatment analysis method. The data comprises of 19,421 landing approaches between $0.04 \text{ m} \leq y \leq 0.11 \text{ m}$, where y is the perpendicular distance to the platforms. Post-hoc tests compare differences between mean relative-rate-of-expansion observed in different tested conditions (statistical model as given by Equation S4.3: $r_{i,d,a,s} \sim N(\alpha + \alpha_d + \alpha_a + \alpha_s + \sum_{j=1}^5 \beta_j \text{WIND}_{j,i,d,a,s} + \beta_6 \text{fromTakeoff}_{i,d,a,s} + \sum_{j=7}^{11} \beta_j \text{WIND}_{j,i,d,a,s} \times \text{fromTakeoff}_{i,d,a,s}, \sigma^2)$).

Fixed effect	Estimate	Std error	t value	Pr(> t)
α	2.892	0.075	38.439	0.003595
β_1	0.003	0.049	0.062	0.950452
β_2	-0.059	0.051	-1.168	0.242655
β_3	-0.075	0.053	-1.416	0.156752
β_4	-0.092	0.056	-1.634	0.102325
β_5	0.011	0.057	0.196	0.844827
β_6	0.945	0.077	12.323	$9.62E - 35$
β_7	-0.294	0.122	-2.412	0.015855
β_8	-0.584	0.128	-4.547	$5.47E - 06$
β_9	-0.792	0.128	-6.185	$6.34E - 10$
β_{10}	-1.122	0.139	-8.068	$7.62E - 16$
β_{11}	-1.099	0.154	-7.120	$1.12E - 12$
Post-hoc contrasts*	Estimate	Std error	z ratio	p value
o - 1	0.291	0.112	2.600	0.13995
o - 2	0.644	0.118	5.440	$7.98E - 07$
o - 3	0.867	0.117	7.431	$1.62E - 12$
o - 4	1.213	0.127	9.532	$2.31E - 20$
o - 5	1.088	0.143	7.585	$4.97E - 13$
1 - 2	0.352	0.130	2.710	0.100911
1 - 3	0.575	0.128	4.479	0.000112
1 - 4	0.922	0.138	6.676	$3.68E - 10$
1 - 5	0.796	0.153	5.202	$2.95E - 06$
2 - 3	0.223	0.134	1.667	1
2 - 4	0.570	0.143	3.977	0.001046
2 - 5	0.444	0.158	2.816	0.072967
3 - 4	0.347	0.142	2.444	0.217702
3 - 5	0.221	0.156	1.413	1
4 - 5	-0.126	0.165	-0.764	1

*o, 1, 2, 3, 4, and 5 correspond to wind speeds 0, 0.28, 0.98, 1.77, 2.54, and 3.41 m s^{-1} , respectively.

*These post-hoc tests correspond to landings after a take-off. For landings from a free-flight, all comparisons among wind speeds were statistically insignificant.

Table S4.4: Analysis of dependence of relative-rate-of-expansion set-points (r^*) on distance to the platform (y^*), different wind speeds and two starting conditions (take-off and free-flight). The data comprises of r^* and y^* for 12,338 constant- r segments in 9,097 landing manoeuvres. Post-hoc tests compare differences in $\log(r^*)$ observed at mean $y^* = 0.185\text{ m}$ in the presence of different wind speeds (factor $f = 1$) (statistical model as given by Equation S4.3: $\log(r_{i,d,a,s}^*) \sim N(\alpha + \alpha_d + \alpha_a + \alpha_s + \beta_1 \log(y_{i,d,a,s}^*) + \sum_{j=2}^6 \beta_j \text{WIND}_{j,i,d,a,s} + \beta_7 \text{fromTakeoff}_{i,d,a,s} + \beta_8 \log(y_{i,d,a,s}) \times \text{fromTakeoff}_{i,d,a,s} + \dots)$).

Fixed effect	Estimate	Std error	t value	Pr(> t)
α	-0.539	0.018	-30.237	1.77E - 89
β_1	-0.727	0.008	-89.275	0
β_2	0.004	0.011	0.361	0.718181
β_3	0.009	0.012	0.769	0.441659
β_4	0.041	0.012	3.302	0.000966
β_5	0.076	0.013	5.691	1.31E - 08
β_6	0.148	0.015	9.727	3E - 22
β_7	-0.309	0.035	-8.849	1.01E - 18
β_8	-0.234	0.019	-12.238	3.1E - 34
Post-hoc constrasts* in $\log(r^*)$ at mean $y^* = 0.185\text{ m}$	Estimate	Std error	z ratio	p value
0 - 1	-0.004	0.011	-0.361	1
0 - 2	-0.009	0.012	-0.769	1
0 - 3	-0.041	0.012	-3.302	0.01442
0 - 4	-0.076	0.013	-5.691	1.9E - 07
0 - 5	-0.148	0.015	-9.727	3.47E - 21
1 - 2	-0.005	0.013	-0.392	1
1 - 3	-0.037	0.013	-2.748	0.089829
1 - 4	-0.072	0.014	-5.051	6.6E - 06
1 - 5	-0.144	0.016	-8.984	3.9E - 18
2 - 3	-0.032	0.014	-2.274	0.34472
2 - 4	-0.067	0.015	-4.503	0.000101
2 - 5	-0.139	0.017	-8.394	7.04E - 16
3 - 4	-0.035	0.015	-2.299	0.322887
3 - 5	-0.107	0.017	-6.356	3.11E - 09
4 - 5	-0.072	0.018	-4.121	0.000565

*0, 1, 2, 3, 4, and 5 correspond to wind speeds 0, 0.28, 0.98, 1.77, 2.54, and 3.41 $m\ s^{-1}$, respectively.

*The results are averaged over landing types because wind speeds had similar effect on both landing types.

Table S4.5: Analysis of how bumblebees modulate the expansion-acceleration (\dot{r}_e) during entry segments with the starting distance from the landing surface (y_0), the required step-change in relative rate of expansion (Δr_e), the final set-point to reach (r^*), wind speeds and the landing type. The data comprises of 4,221 entry segments with $\dot{r}_e > 0$ identified in 4,038 landing maneuvers of bumblebees (statistical model as given by Equation S4.4: $\log(\dot{r}_{e,i,d,a,s}) \sim N(\alpha + \alpha_d + \alpha_a + \alpha_s + \beta_1 \log(y_{0,i,d,a,s}) + \sum_{j=2}^6 \beta_j \text{WIND}_{j,i,d,a,s} + \beta_7 \text{fromTakeoff}_{i,d,a,s} + \beta_8 \log(\Delta r_{e,i,d,a,s}) + \beta_9 \log(r_{i,d,a,s}^*) + \beta_{10} \log(\Delta r_{e,i,d,a,s}) \times \log(y_{0,i,d,a,s}), \sigma^2) + \beta_{11} \log(\Delta r_{e,i,d,a,s}) \times \log(r_{i,d,a,s}^*), \sigma^2)$).

Fixed effect	Estimate	Std error	t value	Pr(> t)
α	1.466	0.030	48.337	6.77E - 33
β_1	-0.289	0.022	-12.896	2.41E - 37
β_2	0.032	0.012	2.606	0.009182
β_3	0.049	0.013	3.782	0.000158
β_4	0.111	0.013	8.253	2.04E - 16
β_5	0.152	0.014	10.678	2.78E - 26
β_6	0.235	0.016	14.488	1.86E - 46
β_7	-0.035	0.012	-3.055	0.002262
β_8	0.034	0.036	0.941	0.346987
β_9	0.243	0.021	11.354	1.9E - 29
β_{10}	-0.362	0.025	-14.681	1.26E - 47
β_{11}	-0.069	0.015	-4.770	1.9E - 06

Table S4.6: Analysis of how the mean acceleration of bumblebees in an entry segment (\bar{A}_e) varies with the starting distance from the landing surface (y_0), the required step-change in relative rate of expansion (Δr_e), the final set-point to reach (r^*), light conditions and the landing type. The data comprises of 4,102 entry segments identified in 3,933 landing maneuvers of bumblebees (statistical model as given by Equation S4.4: $\log(\bar{A}_{e\ i,d,a,s}) \sim N(\alpha + \alpha_d + \alpha_a + \alpha_s + \beta_1 \log(y_{0\ i,d,a,s}) + \sum_{j=2}^6 \beta_j \text{WIND}_{j,i,d,a,s} + \beta_7 \text{fromTakeoff}_{i,d,a,s} + \beta_8 \log(\Delta r_{e\ i,d,a,s}) + \beta_9 \log(r_{i,d,a,s}^*) + \beta_{10} \log(\Delta r_{e\ i,d,a,s}) \times \log(y_{0\ i,d,a,s}, \sigma^2) + \beta_{11} \log(\Delta r_{e\ i,d,a,s}) \times \log(r_{i,d,a,s}^*, \sigma^2))$).

Fixed effect	Estimate	Std error	t value	Pr(> t)
α	1.973	0.058	34.030	9.27E - 56
β_1	0.529	0.043	12.425	8.04E - 35
β_2	0.049	0.023	2.113	0.03465
β_3	0.102	0.025	4.140	3.57E - 05
β_4	0.172	0.025	6.757	1.63E - 11
β_5	0.253	0.027	9.445	6.29E - 21
β_6	0.393	0.030	12.897	3.32E - 37
β_7	-0.138	0.022	-6.272	4.01E - 10
β_8	0.590	0.069	8.567	1.49E - 17
β_9	-1.632	0.044	-36.770	2.5E - 255
β_{10}	-0.679	0.047	-14.490	1.95E - 46
β_{11}	-0.103	0.027	-3.754	0.000176

Table S4.7: The analysis of how often a bumblebee exhibits a low velocity phase ($V < 0.05 \text{ m s}^{-1}$). It depends upon the wind speed, the landing type (landing from free-flight or take-off) and distance to the surface y . There are six wind speeds (m s^{-1} : $w_0 = 0$, $w_1 = 0.28$, $w_2 = 0.98$, $w_3 = 1.77$, $w_4 = 2.54$, $w_5 = 3.41$) and four distance regions ($y_1(0.05 \text{ m} < y \leq 0.10 \text{ m})$, $y_2(0.10 \text{ m} < y \leq 0.15 \text{ m})$, $y_3(0.15 \text{ m} < y \leq 0.20 \text{ m})$ and $y_4(0.20 \text{ m} < y \leq 0.25 \text{ m})$) (statistical model as given by Equation S4.5: $P \sim y_{\text{Region}} + \text{wind} + \text{hasTakeoff} + \text{hasTakeoff} \times \text{wind} + y_{\text{Region}} \times \text{hasTakeoff} + \text{wind} \times y_{\text{Region}} + (1|_{\text{day}}) + (1|_{\text{approach}}) + (1|_{\text{landingSide}})$, estimate of effects is in *logit* scale).

Fixed effect	Estimate	Std error	z value	Pr(> t)
Intercept	-0.51	0.11	-4.66	$3.09E - 06$
y_2	-1.14	0.06	-19.25	$1.45E - 82$
y_3	-1.74	0.07	-25.45	$6.3E - 143$
y_4	-2.06	0.07	-27.69	$8.7E - 169$
w_1	0.12	0.06	1.99	0.046167
w_2	0.37	0.06	6.15	$7.96E - 10$
w_3	0.73	0.06	11.85	$2.04E - 32$
w_4	0.87	0.07	13.13	$2.12E - 39$
w_5	1.22	0.07	17.06	$2.75E - 65$
hasTakeoff	-0.14	0.07	-1.97	0.049158
$w_1 : \text{hasTakeoff}$	0.22	0.10	2.15	0.031574
$w_2 : \text{hasTakeoff}$	0.40	0.10	3.92	$8.72E - 05$
$w_3 : \text{hasTakeoff}$	0.61	0.10	6.23	$4.61E - 10$
$w_4 : \text{hasTakeoff}$	0.76	0.11	7.20	$6E - 13$
$w_5 : \text{hasTakeoff}$	0.71	0.12	6.05	$1.46E - 09$
$y_2 : \text{hasTakeoff}$	-0.78	0.08	-10.22	$1.59E - 24$
$y_3 : \text{hasTakeoff}$	-0.83	0.09	-9.27	$1.88E - 20$
$y_4 : \text{hasTakeoff}$	-0.63	0.09	-6.69	$2.17E - 11$
$y_2 : w_1$	-0.06	0.09	-0.72	0.471313
$y_3 : w_1$	-0.20	0.11	-1.91	0.056157
$y_4 : w_1$	-0.18	0.11	-1.59	0.111079
$y_2 : w_2$	-0.06	0.09	-0.63	0.531825
$y_3 : w_2$	-0.10	0.10	-0.93	0.35172
$y_4 : w_2$	-0.06	0.11	-0.55	0.58055
$y_2 : w_3$	-0.13	0.09	-1.42	0.156609
$y_3 : w_3$	-0.31	0.10	-3.00	0.00269
$y_4 : w_3$	-0.37	0.11	-3.30	0.000952
$y_2 : w_4$	-0.12	0.10	-1.23	0.220355
$y_3 : w_4$	-0.22	0.11	-2.10	0.035948
$y_4 : w_4$	-0.28	0.11	-2.43	0.01494
$y_2 : w_5$	-0.33	0.10	-3.28	0.00104
$y_3 : w_5$	-0.45	0.11	-4.04	$5.34E - 05$
$y_4 : w_5$	-0.47	0.12	-3.92	$8.69E - 05$

Table S4.8: The analysis of how travel time of landing bumblebees (Δt) depends on the wind speeds and two landing types (landing after a take-off or from a free-flight). The data comprises of travel time Δt of bumblebees that they took to cover 0.2 m approach distance y (from $y = 0.25$ m to $y = 0.05$ m from the landing platform) in all landing maneuvers that started beyond $y = 0.25$ m. (statistical model as given by Equation S4.6: $\Delta t_{i,d,s} \sim N(\alpha + \alpha_d + \alpha_s + \sum_{j=1}^5 \beta_j \text{WIND}_{j,i,d,s} + \beta_6 \text{fromTakeoff}_{i,d,s} + \sum_{j=7}^{11} \beta_j \text{WIND}_{j,i,d,s} \times \text{fromTakeoff}_{i,d,s})$).

Fixed effect	Estimate	Std error	t value	Pr(> t)
α	0.723	0.028	25.742	0.00903
β_1	-0.026	0.011	-2.389	0.016917
β_2	0.005	0.011	0.435	0.663802
β_3	0.006	0.011	0.561	0.574797
β_4	0.032	0.012	2.607	0.00915
β_5	-0.030	0.013	-2.407	0.016084
β_6	-0.175	0.014	-12.217	$3.81E - 34$
β_7	0.021	0.023	0.930	0.352305
β_8	0.065	0.024	2.673	0.007518
β_9	0.121	0.024	5.019	$5.26E - 07$
β_{10}	0.133	0.027	4.975	$6.6E - 07$
β_{11}	0.219	0.030	7.250	$4.39E - 13$

S4.3 Supporting text

S4.3.1 Characterization of transient segments

We approximated the motion of bumblebees during transient (entry) segments with motion at a constant expansion-acceleration. In each transient segment, we estimated this constant using a linear regression $r(t) = \dot{r}_e t + c + \epsilon$ (where c and ϵ denote intercept and residuals, respectively). We tested this assumption by calculating the coefficient of determination (R^2) for the aforementioned linear regression in each entry segment which was very high (0.980 [0.960-99], median [interquartile range]). The similar values of R^2 also hold for all tested wind conditions and both landing types (landings from a free-flight or directly after a take-off). Moreover, the difference between the actual flight distance covered and the analytically computed flight distance if the bumblebees had performed the motion exactly at the estimated expansion-acceleration within the identified entry segments was also very low (0.0011 m [-0.0015 m, 0.0042 m], median [interquartile range]). Thus, the motion of landing bumblebees during the entry segments can be well approximated by a motion at a constant expansion-acceleration.

S4.3.2 Statistical models

All statistical analyses were done in R 4.0.2 (R Foundation). We used `lmer` and `glmer` to develop different linear mixed-effects models.

The landing frequency in different wind speeds

To test how winds influenced the landing frequency of bumblebees, we used two linear mixed models to find how the average number of landing approaches per hour N varied with the wind conditions. The two models correspond to two landing types (landing from a free-flight or directly after a take-off) and had the time of the day and the day of the experiment as random factors. The statistical model developed can be expressed as follows:

$$N_{\text{takeoff},i,d,t} \text{ or } N_{\text{freeflight},i,d,t} \sim N\left(\alpha + \alpha_d + \alpha_t + \sum_{j=1}^5 \beta_j \text{WIND}_{j,i,d,t}, \sigma^2\right) \quad (\text{S4.1})$$

where $N_{\text{takeoff},i,d,t}$ and $N_{\text{freeflight},i,d,t}$ are the i -th measurements of the number of landing maneuvers per hour for landing from free-flight and after take-off, respectively, from the d -th day and t -th time-slot, α is the regression intercept for zero wind speed (overall intercept), α_d is the day-specific intercept, α_t is the time-slot-specific intercept, WIND_j indicates j -th wind in the set $\{0.28, 0.98, 1.77, 2.54, 3.41\}$, $\text{WIND}_{j,i,d,t}$ indicates if j -th wind condition is present for the d -th day and t -th time-slot ($0 = \text{no}$, $1 = \text{yes}$), $\beta_j \forall j \in \{1, 2, \dots, 5\}$ represent the differences of fixed-effects (wind conditions) from the overall intercept, and σ is the residual standard deviation. The statistical output and the results from post-hoc tests are given in Table S4.2.

The analysis of average of multiple landing maneuvers

For analyzing the average of multiple landing maneuvers, we computed the mean relative rate of expansion in each tested treatment by using wind speed, landing type along with all possible interactions as fixed factors and day of the experiment, landing approach number, and landing side (whether landing disc is located on the hive side or the food source side) as random factors. We used the following model.

$$r_{i,d,a,s} \sim N\left(\alpha + \alpha_d + \alpha_a + \alpha_s + \sum_{j=1}^5 \beta_j \text{WIND}_{j,i,d,a,s} + \beta_6 \text{fromTakeoff}_{i,d,a,s} + \sum_{j=7}^{11} \beta_j \text{WIND}_{j,i,d,a,s} \times \text{fromTakeoff}_{i,d,a,s}, \sigma^2\right) \quad (\text{S4.2})$$

where $r_{i,d,a,s}$ is the relative rate of expansion for the i -th measurement from d -th day ($d \in \{1, 2, \dots, 11\}$), a -th landing approach ($a \in \{1, 2, \dots, 19421\}$) and s -th landing side ($s = 1$ for hive side and $s = 2$ for food-source side), α is the regression intercept for

zero wind speed and landing from free-flight (overall intercept), α_d is the day-specific intercept, α_a is the landing-approach-specific intercept, α_s is the landing-side-specific intercept, WIND_j indicates j -th wind in the set $\{0.28, 0.98, 1.77, 2.54, 3.41\}$, $\text{WIND}_{j,i,d,t}$ and $\text{fromTakeoff}_{i,d,a,s}$ indicate if j -th wind speed and take-off are present for the i -th measurement from d -th day, a -th landing approach and s -th landing side (0 = no, 1 = yes), $\beta_i \forall i \in \{1, 2, \dots, 11\}$ represent the differences of the fixed-effects and interaction terms from overall intercept, and σ is the residual standard deviation. The statistical output, along with post-hoc tests, from data of 19, 421 landing approaches in the selected range of distance to the platforms ($0.04m \leq y \leq 0.11m$) is given in Table S4.3.

The analysis of individual landing maneuvers

1. During set-point phase: To find how bumblebees adjusted their set-point (r^*) with distance to the platform (y^*) and landing types (landing from a free-flight or after a take-off), we used a linear mixed model between their log transformations (similar to Chapter 2). We first constructed a full model with $\log(r^*)$ as a response variable, $\log(y^*)$, wind speeds, landing types along with all interactions as fixed factors, and day of the experiment, landing approach and landing side as random intercepts. Among all interaction terms, the model dredging revealed only $\log(y^*) \times \text{landingType}$ interaction terms as significant, therefore we used the following reduced model:

$$\log(r_{i,d,a,s}^*) \sim N\left(\alpha + \alpha_d + \alpha_a + \alpha_s + \beta_1 \log(y_{i,d,a,s}^*) + \sum_{j=2}^6 \beta_j \text{WIND}_{j,i,d,a,s} + \beta_7 \text{fromTakeoff}_{i,d,a,s} + \beta_8 \log(y_{i,d,a,s}) \times \text{fromTakeoff}_{i,d,a,s} + \right) \quad (\text{S4.3})$$

where $r_{i,d,a,s}^*$ and $y_{i,d,a,s}^*$ are set-point of relative rate of expansion and mean distance, respectively. The definition of other parameters here is similar to the model for analysis of average landing maneuver (Equation S4.2). The statistical output, along with post-hoc tests, from data of 9, 097 landing maneuvers is given in Table S4.4.

2. We used linear mixed-effects models to find how the transient response of the sensorimotor control system of landing bumblebees (\dot{r}_e) and the resulting mean accelerations (\bar{A}_e) varied with the starting distance from the landing surface (y_0), the required step-change in relative rate of expansion (Δr_e), the final set-point to reach (r^*), wind speeds, and the starting condition of the landing maneuver (whether the landing is from a free-flight or after a take-off). We first constructed a full model with aforementioned variables along with their interactions as fixed factors, and with the day of the experiment, the landing approach and the landing side (whether landing disc is located on the hive side or the food source side) as random intercepts. The model dredging revealed that, among all interaction terms, only $\log(\Delta r_e) \times \log(y_0)$ and $\log(\Delta r_e) \times \log(r^*)$ terms were found to be significant, therefore we used the

following reduced model:

$$\begin{aligned} \log(\dot{r}_{e\ i,d,a,s}) \sim N(& \alpha + \alpha_d + \alpha_a + \alpha_s + \beta_1 \log(y_{0\ i,d,a,s}) + \\ & \sum_{j=2}^6 \beta_j \text{WIND}_{j,i,d,a,s} + \beta_7 \text{fromTakeoff}_{i,d,a,s} + \\ & \beta_8 \log(\Delta r_{e\ i,d,a,s}) + \beta_9 \log(r_{i,d,a,s}^*) + \\ & \beta_{10} \log(\Delta r_{e\ i,d,a,s}) \times \log(y_{0\ i,d,a,s}), \sigma^2) + \\ & \beta_{11} \log(\Delta r_{e\ i,d,a,s}) \times \log(r_{i,d,a,s}^*), \sigma^2) \end{aligned} \quad (\text{S4.4})$$

where definition of parameters here is similar to the model for the analysis of average landing maneuver (Equation S4.2). The similar formula holds for the mean acceleration \bar{A}_e as well. The statistical outputs are given in Tables S4.5 and S4.6. Note that the statistical results for covariates ($y_0, \Delta r_e, r^*$) for both response variables are similar to as identified in Chapter 3 except $\log(\Delta r_e) \times \log(r^*)$ term. This term was not found to be statistically significant for the results in Chapter 3 likely because the dataset in Chapter 3 is smaller in size as compared to this dataset. Despite its statistical significance, this interaction term has a little effect on the response variables (Figure S4.3).

3. We used a generalized linear mixed model to test how the probability of occurrence of a low velocity phase $P_{\text{low } V}$ varied with wind speed, landing type (landing from free-flight or take-off) and distance to the surface y (divided into four regions: $y_1(0.05\text{ m} < y \leq 0.10\text{ m}), y_2(0.10\text{ m} < y \leq 0.15\text{ m}), y_3(0.15\text{ m} < y \leq 0.20\text{ m})$ and $y_4(0.20\text{ m} < y \leq 0.25\text{ m})$). A low velocity phase corresponds to $V < 0.05\text{ m s}^{-1}$. The model dredging revealed that two-way interactions between these explanatory variables were significant. Therefore, we used the following model (in *R* code):

$$\begin{aligned} P \sim & \text{yRegion} + \text{wind} + \text{hasTakeoff} + \text{hasTakeoff} \times \text{wind} + \\ & \text{yRegion} \times \text{hasTakeoff} + \text{wind} \times \text{yRegion} + \\ & (1|\text{day}) + (1|\text{approach}) + (1|\text{landingSide}) \end{aligned} \quad (\text{S4.5})$$

The statistical output is given in Table S4.7.

4. We used a linear mixed model to test how the travel time of bumblebees Δt varied with wind speed and the landing type (landing from free-flight or take-off). In this model, day of the experiment and landing side (whether landing disc is located on the hive side or the food source side) are used as random factors. The model dredging revealed that two-way interaction between the explanatory variables were significant. Therefore, we used the following model:

$$\begin{aligned} \Delta t_{i,d,s} \sim N(& \alpha + \alpha_d + \alpha_s + \sum_{j=1}^5 \beta_j \text{WIND}_{j,i,d,s} + \\ & \beta_6 \text{fromTakeoff}_{i,d,a,s} + \\ & \sum_{j=7}^{11} \beta_j \text{WIND}_{j,i,d,s} \times \text{fromTakeoff}_{i,d,s} \end{aligned} \quad (\text{S4.6})$$

where definition of parameters here is similar to the model for the analysis of average landing maneuver (Equation S4.2). The statistical output is given in Table S4.8.



Chapter 5

Visual guidance of landing approaches in honeybees

Pulkit Goyal^{1,a}, Emily Baird^{2,a}, Mandyam V. Srinivasan³, Florian T. Muijres¹

¹ Experimental Zoology Group, Wageningen University & Research, Wageningen, The Netherlands

² Department of Zoology, Stockholm University, 114 18 Stockholm, Sweden

³ Queensland Brain Institute, The University of Queensland, QLD 4072 St. Lucia, Australia

^a Both authors contributed equally to the work

Abstract

Landing is an important flight phase during which many animals use visual cues to accurately control flight speed and touchdown. Foraging honeybees rely on this phase to collect food, which is essential for the survival and reproduction of their colony. Here, we study how honeybees use optical expansion cues to control their approach towards the landing surface while decreasing their flight speed. Honeybees, on average, land by keeping their optical expansion rate constant, which results in a linear decrease of their velocity with distance. But, do individual honeybees also exhibit this strategy during the complete landing maneuver? To answer this question, we analyzed the flight dynamics of individual honeybees landing on vertical platforms with varying optical expansion cues. We show that, unlike the landing strategy suggested by the average analysis, individual honeybees land by holding the optic expansion rate constant for short periods within the maneuver, and that they tend to vary the magnitude of optic expansion rate between these phases in a stepwise manner. Hereby, honeybees flying at relatively low optic expansion rates tended to stepwise upregulate their optic expansion rate set-point, whereas honeybees flying at high optic expansions tended to downregulate their set-point. This modular landing control system allows honeybees to land robustly for a large range of initial flight conditions and visual landing platform patterns. This landing strategy is strikingly similar to that of bumblebees, and is thus likely to be also found in other flying animals. Moreover, it can be used as bioinspiration for guidance systems of flying robots.

5.1 Introduction

Landing is a critical phase of animal flight as it requires precise control of flight speed with reducing distance to the surface. Poor control can result in high-impact collisions which can be detrimental for an animal, especially for honeybees as they perform landings very frequently (up to a thousand landings in an hour) (Ribbands, 1949). During each landing, honeybees use visual cues to regulate their speed and to ensure a safe touchdown (Srinivasan et al., 2000; Baird et al., 2013), but how they use these cues during landing is not completely understood.

As honeybees approach a landing surface, their motion relative to the surface generates optical expansion cues (Baird et al., 2013). These cues consist of different features in the visual field moving radially outwards from the point that is being approached (Gibson, 1955; Edwards and Ibbotson, 2007). Such cues are generated irrespective of the surface orientation and the direction of approach (Baird et al., 2013), and can be used to measure the relative rate of expansion, which signifies how fast the features appear to radially expand relative to the retinal size of an object or their angular position in the visual field (Lee, 1976; Wagner, 1982; Baird et al., 2013). This relative rate of expansion (r) is equal to the ratio of velocity (V) with which an animal is approaching a landing surface and its distance to that surface (y) ($r = V/y$). Flying animals such as insects and birds have been shown to use

this expansion rate to reduce their approach velocity while approaching a landing surface, such that it is close to zero near the landing surface (Lee et al., 1991, 1993; Van Breugel and Dickinson, 2012; Baird et al., 2013; Chang et al., 2016; Shackleton et al., 2019; Baird et al., 2020; Whitehead, 2020; Tichit et al., 2020a,b; Goyal et al., 2021).

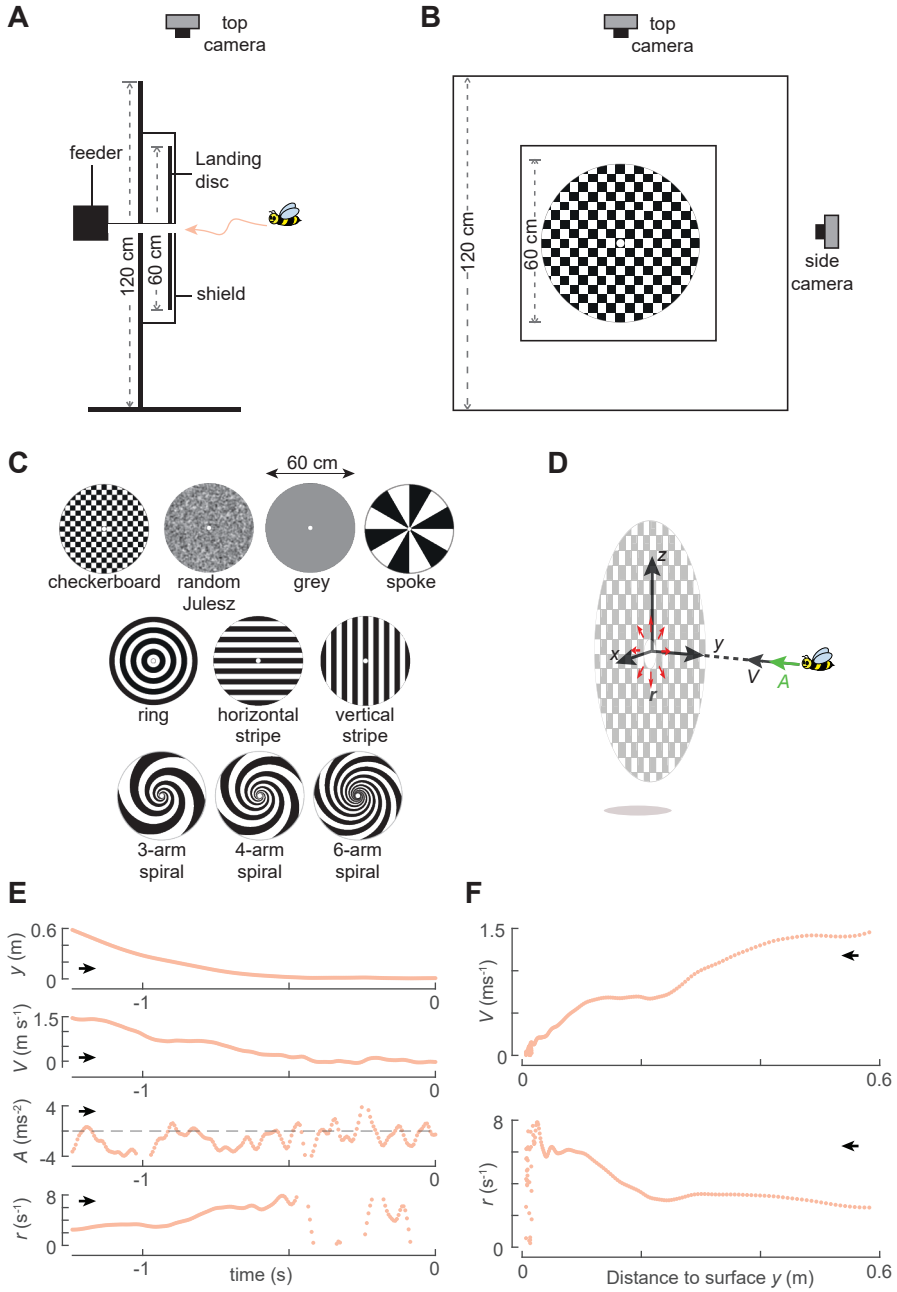
These studies have identified different strategies that animals use for reducing the approach velocity as they draw closer to the surface. By averaging the landing kinematics of a collection of landing maneuvers, it has been shown that honeybees (Baird et al., 2013), bumblebees (Chang et al., 2016; Goyal et al., 2021) and possibly also fruit flies (Van Breugel and Dickinson, 2012; Baird et al., 2013) reduce their approach velocity approximately linearly with distance to the surface. This suggests that these insects use a landing control strategy in which they aim to keep the relative rate of expansion constant throughout the landing in order to reduce their velocity automatically with distance. However, when analyzing individual landing maneuvers of bumblebees, Goyal et al. (2021) showed that individual bumblebees tended to regularly deviate from the average constant-expansion-rate approach dynamics. In fact, bumblebees reduce their approach velocity with distance in multiple bouts, during which they maintain a constant relative rate of expansion (referred to as a set-point) and between which they tend to increase this set-point. In between the bouts, the animals show various flight behaviors ranging from hovering to smoothly accelerating towards the new set-point of optical expansion. This modular landing strategy of decelerating at multiple distinct set-points results in faster landings than the simple strategy of flying at a single optical expansion set-point (Goyal et al., 2021).

What remains unclear is whether the above-described modular landing strategy is used exclusively by bumblebees, or whether other insects such as honeybees also use it but that it was previously not recognized due to the limitations of the analysis method. Here, we aim to answer this question by using the individual landing analysis approach developed by Goyal et al. (2021) to analyze the flight dynamics of honeybees landing on a vertical platform carrying various visual patterns. We find that honeybees do indeed use a modular landing strategy similar to what has been described for bumblebees, suggesting that this strategy is commonly used by a range of flying insects. Moreover, this modular landing strategy allows honeybees to land robustly for a large range of initial flight conditions and visual landing platform patterns. This honeybee landing control system can be used as bioinspiration for the development of robust landing controllers in flying robots.

5.2 Materials and Methods

Animals, experimental setup and procedure

The experiments were carried out in an indoor facility where the temperature was maintained at $24 \pm 5^\circ\text{C}$, and the light levels, measured at the center of the arena, were 636 ± 297 lx (mean \pm standard deviation). In the setup, a colony of honeybees (*Apis mellifera ligustica*) was trained to fly from their hive placed in the facility wall to a vertical landing



(Caption on the next page.)

Figure 5.1: Experimental setup, conditions, and the landing kinematics of a honeybee. (A,B) The experimental setup viewed from the side and front, respectively. The setup consisted of a flight arena with two cameras that recorded the flight maneuvers of honeybees as they landed on a landing platform. The circular disc behind the landing platform could be replaced with discs with the different graphical patterns indicated in panel (C) (Baird et al., 2013). (D) The landing kinematics of honeybees is described in a Cartesian coordinate system with an origin at the center of the landing platform, the y axis is oriented normal to the platform, and the z axis is pointing vertically up. For each landing maneuver, we calculate the approach velocity $V = -dy/dt$, approach acceleration $A = dV/dt$ and relative-rate-of-expansion $r = V/y$ that the honeybee experiences for its motion along the y -axis. (E) The temporal variation of the state variables (y, V, A, r) for a typical landing maneuver of a honeybee on a random Julesz pattern. (F) The variation of V and r with perpendicular distance to the landing platform y for the same example. (E,F) Black arrow shows the direction in which abscissa data varies as a honeybee approaches the landing platform.

platform connected to a food source (Figure 5.1A,B). The platform consisted of a 60 cm square Perspex transparent shield plate with a 60 cm diameter disc that could present a variety of visual patterns (Figure 5.1C). A 15 mm diameter hole in the center of the landing platform, allowed honeybees to reach a sugar water feeder behind the platform.

The 60 cm disc provided the bees with visual information required for landing; we used ten different visual patterns to study how this visual information affects landing control (Figure 5.1C). Each pattern was printed using black ink on white paper and then matt laminated. The different patterns were (Figure 5.1C): (1) a random Julesz pattern of 1 cm large gray squares with a mean luminance of 50% gray, and an overlaid Gaussian filter; (2) a ring pattern of 3.5 cm wide, concentric black-and-white rings; (3) a checkerboard pattern of 3.5 cm black-and-white squares; (4) a spoke pattern of 12 black-and-white, evenly spaced sectors; (5–7) 3-arm, 4-arm and 6-arm spiral patterns, respectively (for details, see Baird et al., 2013); (8, 9) 3.5 cm wide black-and-white vertical and horizontal stripe patterns, respectively; (10) a homogeneous 50% gray pattern. Note that the data recorded in the presence of ring, checkerboard, spoke, 3-arm spiral, 6-arm spiral and a part of it for 4-arm spiral has previously been published by analyzing the average of landing maneuvers belonging to a particular treatment (landing pattern) (Baird et al., 2013).

The landing platform was located at the back of a 1.5 m \times 1.5 m \times 1.5 m netted flight arena, with a 15 cm \times 15 cm entrance hole on the opposite side. A netting door in front of the entrance hole allowed us to introduce only a single honeybee into the setup each time. Honeybees were marked with paint for individual identification.

Each experimental day consisted of several sets of at least 1 h in which bees were allowed to land on a single type of landing platform. Before each experimental day, all honeybees were allowed to freely visit the food source for at least 48 h. During this training period, the landing platform had a checkerboard pattern disc mounted. During the experiments, only a single honeybee was allowed into the arena at one time, and several landings of that individual on the landing platform were recorded. Between experimental sets, the visual pattern on the landing platform was changed. This process took place in typically 15 min,

during which honeybees were prevented from approaching the setup. The landing platform patterns were changed in a randomized order over at least two different days and two different time-points during the day to control for the effect of external factors, such as temperature, humidity, and time of day. In addition to the set number, we also recorded the sequential flight number for each individual to account for its familiarity with the setup.

The flights of honeybees towards the landing platform were recorded using a stereoscopic videography system consisting of a pair of synchronized high-speed cameras (MotionPro 10k, Redlake Inc.). The cameras recorded the landing bees at 400 Hz. The position of the bee in the resulting image sequences was digitized and calibrated into 3D coordinates using the camera calibration toolbox in Matlab (Mathworks Inc.).

Estimation of state variables and set-points of relative rate of expansion

We expressed the recorded landing maneuvers of honeybees in a Cartesian coordinate system with its origin at the center of the landing platform, y -axis normal to the platform, and z -axis oriented upwards (Figure 5.1D). The landing kinematics of each maneuver was then defined in a space-time array of the coordinate system $\mathbf{X} = (x, y, z, t)$; here, time t equals zero at the end of the trajectory, i.e. when the honeybee reached the landing surface. The kinematics data was post-processed using the following steps. First, to allow the use of the custom analysis tools from Goyal et al. (2021) on the data, we reduced the temporal dynamics of the landing to 175 Hz using modified Akima cubic Hermite interpolation (`makima` in Matlab 2020a; see Section S5.3.1 for details). Secondly, to reduce the tracking noise from these maneuvers, we filtered the kinematics data using a low-pass second-order two-directional Butterworth filter (`filtfilt` in Matlab 2020a) with a cut-off frequency of 20 Hz. Finally, we determined the corresponding velocity vector $\mathbf{U} = (u, v, w)$ and acceleration vector $\mathbf{A} = (a_x, a_y, a_z)$ of each landing using numerical differentiation with a second-order central differencing scheme.

To determine how honeybees land, we used four state variables that describe the movement in the direction normal to the landing platform. These variables are: normal distance from the landing platform $y(t)$, flight velocity towards the platform $V = -v(t)$, acceleration towards the platform $A(t) = -a_y(t)$, and the relative rate of image expansion that a honeybee experiences during its landing approach $r(t) = V(t)/y(t)$. Here, we used the velocity perpendicular to the platform for the computation of relative rate of expansion as honeybees needed to progressively reduce this component as they advanced towards the landing platform; although similar results are obtained when the three-dimensional velocity is used to compute the relative rate of expansion.

To determine if honeybees use a modular landing strategy, similar to the one described for bumblebees, we used the analysis method developed by Goyal et al. (2021). Most importantly, we used the algorithm that identifies the landing approach segments in which

honeybees held the relative rate of expansion (r) approximately constant as they decelerated toward the landing platform. These track segments and constant values are referred to as constant- r segments and the corresponding set-points of relative rate of expansion (r^*), respectively. The set-point value (r^*) was estimated by computing the mean relative expansion rate in a constant- r segment (Figure 5.3A). Additionally, we computed for each constant- r segment the mean approach velocity (V^*), the mean distance of the honeybee from the landing platform (y^*), the distance travelled during the constant- r segment (Δy^*), and the time duration of the constant- r segment (Δt^*). Thus, the dynamics of each constant- r segment was identified using the parameter set (r^* , V^* , y^* , Δy^* , Δt^*). Finally, for landing approaches that contained two or more constant- r segments, we also identified the step-change in set-point that occurred between two consecutive constant- r segments (Δr^*) (Figure 5.4B).

To determine the constant- r segments in a landing trajectory, the set-point extraction algorithm uses three linear regressions between the relative rate of expansion r and distance to the platform y – one in the complete segment, and two others in its equal halves. It first involves the identification of the expected t -distributions of the six regression parameters (two from each linear regression) by analyzing manually-identified constant- r segments in a smaller dataset. It then automatically identifies constant- r segments in the complete dataset. During this automatic step, it selects an arbitrary track segment to be a constant- r segment if six regression parameters in that segment lie within a band around their expected mean values. This band is given by $f \times \sigma$ around the mean of a parameter. Here, σ is the scale-parameter of a t -distribution which is identified for each regression parameter and factor f denotes the number of scale-parameters (this band is similar to the number of standard deviations around the mean of a normally distributed variable) (Section S5.3.1). Increasing f leads to more constant- r segments, but it also increases the possibility of false positives. Here, we present the results for $f = 1.5$, but our results remain similar for a wide range of f ($0.5 \leq f \leq 2.5$). For exact details about the constant- r detection algorithm and the independence of results with factor f , see Supplementary Section S5.3.1 and Figure S5.1.

The algorithm used to find constant- r segments does not capture all the set-points at which honeybees fly during landing. This can either be due to the factor f limiting the variation in r for a segment to be identified as a constant- r segment, or a fundamental limitation of the algorithm itself. This limitation arises because the algorithm can identify a set-point only if the honeybee flies at it for long enough time-period. In many cases, though, a honeybee may not reach the set-point due to several reasons e.g., it can change the set-point before reaching its previous set-point, or it aborts the landing before reaching its set-point. This problem can mostly be overcome by increasing the sample size of the study (Goyal et al., 2021). Here, we analyzed hundreds of landing maneuvers of honeybees, which should be enough for the individual-based analysis approach developed by Goyal et al. (2021).

Statistical analysis

We used R 4.0.3 (The R Foundation, Austria) for all statistical analyses. Previous analyses have shown that inter-individual variation is similar to the intra-individual variation for landing approaches of honeybees (Baird et al., 2013). Therefore, we treated individual flights of honeybees as independent data points, even when we analyzed multiple landings from the same bee. In all models, we used the flight number and set number as random factors to account for learning and time of day, respectively. We used the `lmer` function in R to develop different linear mixed-effects models and to perform Bonferroni corrections to adjust the statistically significant values for comparison among means of different groups. p values < 0.05 were considered statistically significant. The details of all statistical models along with their results are provided in Supplementary Section S5.3.2 and Tables S5.1–S5.4.

5.3 Results

Using our experimental setup, we recorded 309 landing maneuvers of honeybees (Table S5.5), and examined the average and individual landing approaches to understand how honeybees land on a vertical platform with a variable visual pattern.

The average landing approach of honeybees on a vertical landing platform

We first analyzed how the average honeybee controlled its approach velocity as it advanced towards the landing surface. We did this for all recorded landing maneuvers combined (Figure 5.2A) and for the average landing per treatment (landing platform pattern) (Figure 5.2B,C). For all average flights, we found that honeybees reduced their mean approach velocity V approximately linearly with the perpendicular distance to the landing surface y . This average analysis suggested that the honeybees approached the landing surface by keeping the relative rate of expansion nearly constant at a set-point $r^* = 3.26 [0.16] \text{ s}^{-1}$, as estimated within the distance range of $0.15 \text{ m} \leq y \leq 0.35 \text{ m}$ (mean [standard error]).

To determine how the set-point r^* varied among different landing patterns, we used a linear mixed-effects model on the r^* data of all maneuvers (Section S5.3.2, Table S5.1). Honeybees exhibited the highest expansion rate set-point and thus, flew fastest towards the landing platform with horizontal stripes ($r^* = 3.52 [0.16] \text{ s}^{-1}$, mean [standard error]) and gray pattern ($r^* = 3.81 [0.16] \text{ s}^{-1}$). In contrast, they exhibited the lowest set-point and thus flew slowest towards the landing platforms with a random Julesz pattern ($r^* = 2.80 [0.16] \text{ s}^{-1}$), rings ($r^* = 3.05 [0.16] \text{ s}^{-1}$) and 4-arm spiral patterns ($r^* = 3.02 [0.16] \text{ s}^{-1}$). The set-point r^* when landing on the platforms with the other visual patterns lay between these two groups (Figure 5.2B,C).

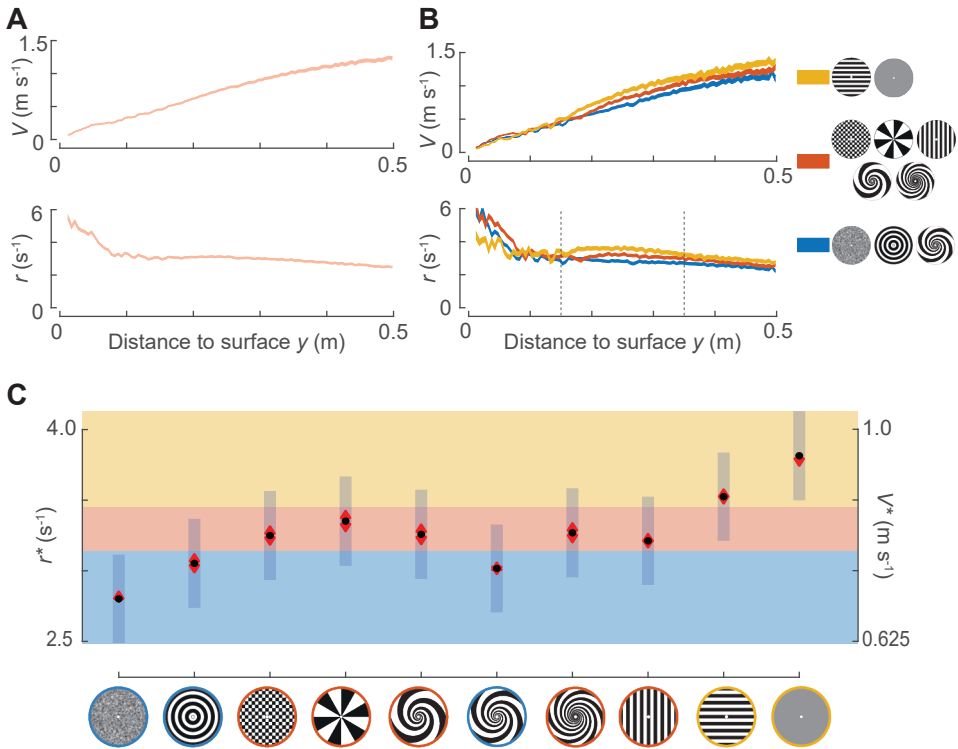


Figure 5.2: On average, honeybees decrease their approach velocity linearly with the perpendicular distance to the landing platform. (A,B) The variation of approach velocity V and relative-rate-of-expansion r with perpendicular distance to the landing platform y for (A) all recorded landing maneuvers, and (B) for the approaches averaged over three different group of patterns, as defined on the right of (B). The curves show the average approach dynamics, whereby the thickness of the curves represent the standard error of the means. (C) The average set-point of relative rate of expansion r^* for the different landing patterns as predicted by a linear mixed-effects model (Table S5.1). The right axis shows the corresponding average approach velocity V^* at distance $y = 0.25$ m from the landing platform. Black dots depict estimated means, vertical blue bars are 95% confidence intervals, and red arrows show whether r^* and V^* differ significantly among landing patterns (no overlap indicates statistically significant differences). The average set-points of relative rate of expansion r^* for each landing pattern was determined within the distance range of $0.15 \text{ m} \leq y \leq 0.35 \text{ m}$, indicated in (B). (B,C) The three landing platform groups are defined for the purpose of visualizing the results.

The landing approach kinematics of individual honeybees

In contrast to the continuous average landing behavior, we observed that for many individual landing maneuvers the variation of the relative rate of expansion is not constant around one set-point. Instead, often honeybees seemed to land by flying at multiple set-points (Figures 5.1F, 5.3A and 5.4B,C), although landings with a single set-point were also observed (Figure 5.4A).

To analyze these multi-setpoint landing dynamics in detail, we extracted all track segments in which honeybees kept the relative rate of expansion nearly constant using the de-

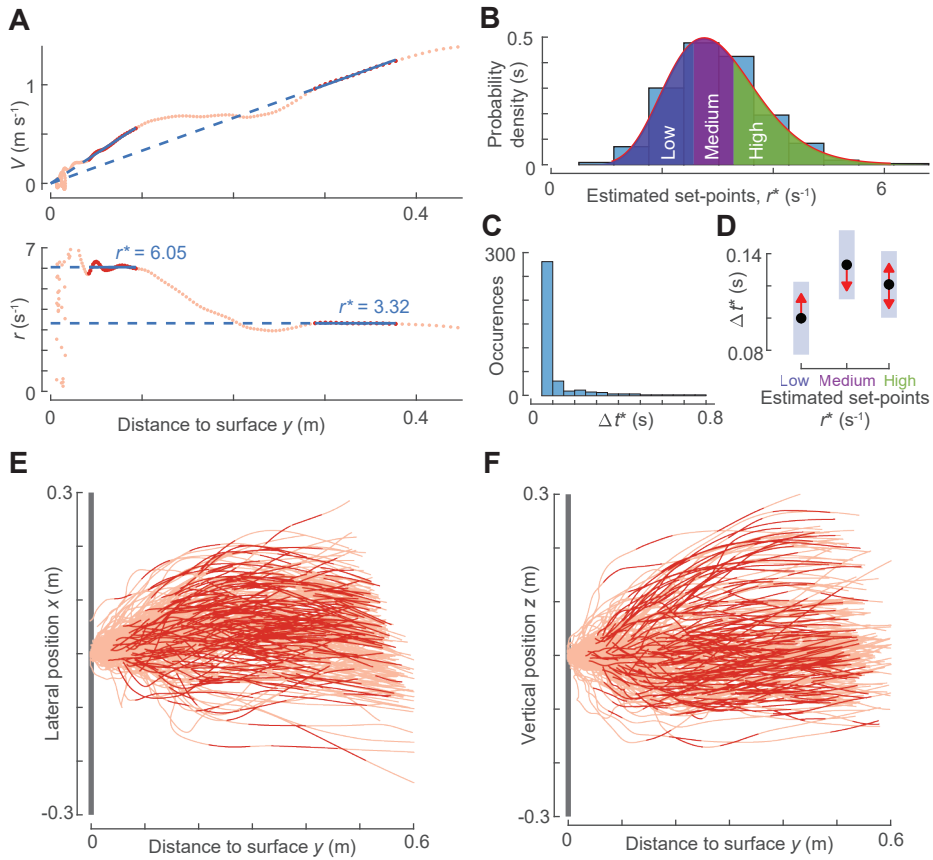


Figure 5.3: Honeybees exhibit a range of set-points during a single landing maneuver. (A) The variation of approach velocity V and relative rate of expansion r with perpendicular distance to the landing platform y for the example shown in Figure 5.1E,F. We use an automatic detection algorithm (Goyal et al., 2021) to identify the track segments in which honeybees held r approximately constant. The identified constant- r segments are highlighted in red, and corresponding values of the expansion-rate set-points r^* are shown in blue (as slopes and ordinate values in top and bottom panel, respectively). (B) Probability density of all identified set-points ($n = 359$) in all recorded landing maneuvers. The observed probability density is approximated using a gamma distribution (red curve) and divided into three groups: low expansion-rate set-points ($r^* \leq 2.58 \text{ s}^{-1}$), medium set-points ($2.58 \text{ s}^{-1} < r^* \leq 3.29 \text{ s}^{-1}$) and high set-points ($r^* > 3.29 \text{ s}^{-1}$). Each group has an equal $1/3^{\text{rd}}$ probability of occurrence. (C) Histogram of time travelled during a constant- r segment Δt^* for all 359 constant- r segments. (D) The variation in Δt^* with the low, medium and high r^* set-points groups defined in panel (B) (Table S5.2). Black dots depict estimated means, vertical blue bars are 95% confidence intervals, and red arrows show whether Δt^* differ significantly between groups (no overlap indicates statistically significant differences). (E,F) Top (E) and side (F) views of the trajectories of all 309 recorded landing maneuvers; the sections identified as constant- r segments are highlighted in red.

tection algorithm developed in Goyal et al. (2021) (Figure 5.3), and determined parameter set (r^* , V^* , y^* , Δy^* , Δt^*) for each segment. The following results were obtained:

(1) Honeybees exhibit a range of set-points and travel longer near the medium set-points as compared to the low set-points

For the detection threshold factor $f = 1.5$ in the set-point extraction algorithm, we identified 359 constant- r segments within 227 of the 309 recorded landing tracks (Figure 5.3E,F) (for the sensitivity for our results to a wide range of detection threshold factor f , see Figure S5.1). The identified set-points of relative rate of expansion r^* in these constant- r segments varied within a wide range (Figure 5.3B). The observed distribution of r^* can be approximated by a gamma distribution (median $r^* = 2.93 \text{ s}^{-1}$, $a = 12.80$ [11.14 – 14.87], $b = 0.23$ [0.20 – 0.27], mean [95% confidence intervals]) (Evans et al., 2000).

To identify if honeybees possessed an inclination to fly at certain set-points, we divided the observed distribution of set-points into three regions with equal probability: low ($r^* \leq 2.58 \text{ s}^{-1}$), medium ($2.58 \text{ s}^{-1} < r^* \leq 3.29 \text{ s}^{-1}$) and high ($r^* > 3.29 \text{ s}^{-1}$). We then used a linear mixed model to test whether the duration for which the bees flew near their set-point (Δt^*) differed between these three set-point groups (Figure 5.3C,D, Section S5.3.2, Table S5.2). We found that honeybees in the medium set-point group exhibited 33% longer travel time than the lowest set-point group (low r^* -group: $\Delta t^* = 0.10 \text{ s}$; medium r^* -group: $\Delta t^* = 0.13 \text{ s}$; Table S5.2, p -value = 0.037). Travel time in the highest set-point group did not differ significantly from the others, and landing patterns also did not significantly affect travel time (Section S5.3.2, Table S5.2).

We then tested whether this variation in Δt^* also caused a variation in distance travelled (Δy^*) between the three set-point groups (Section S5.3.2, Table S5.2). This linear mixed model shows that honeybees in the medium and high set-point groups travelled 31% and 33% longer distances during their constant- r segment compared to the low set-point group, respectively (low r^* -group: $\Delta y^* = 0.069$ [0.006] m; medium r^* -group: $\Delta y^* = 0.099$ [0.006] m; high r^* -group: $\Delta y^* = 0.102$ [0.006] m).

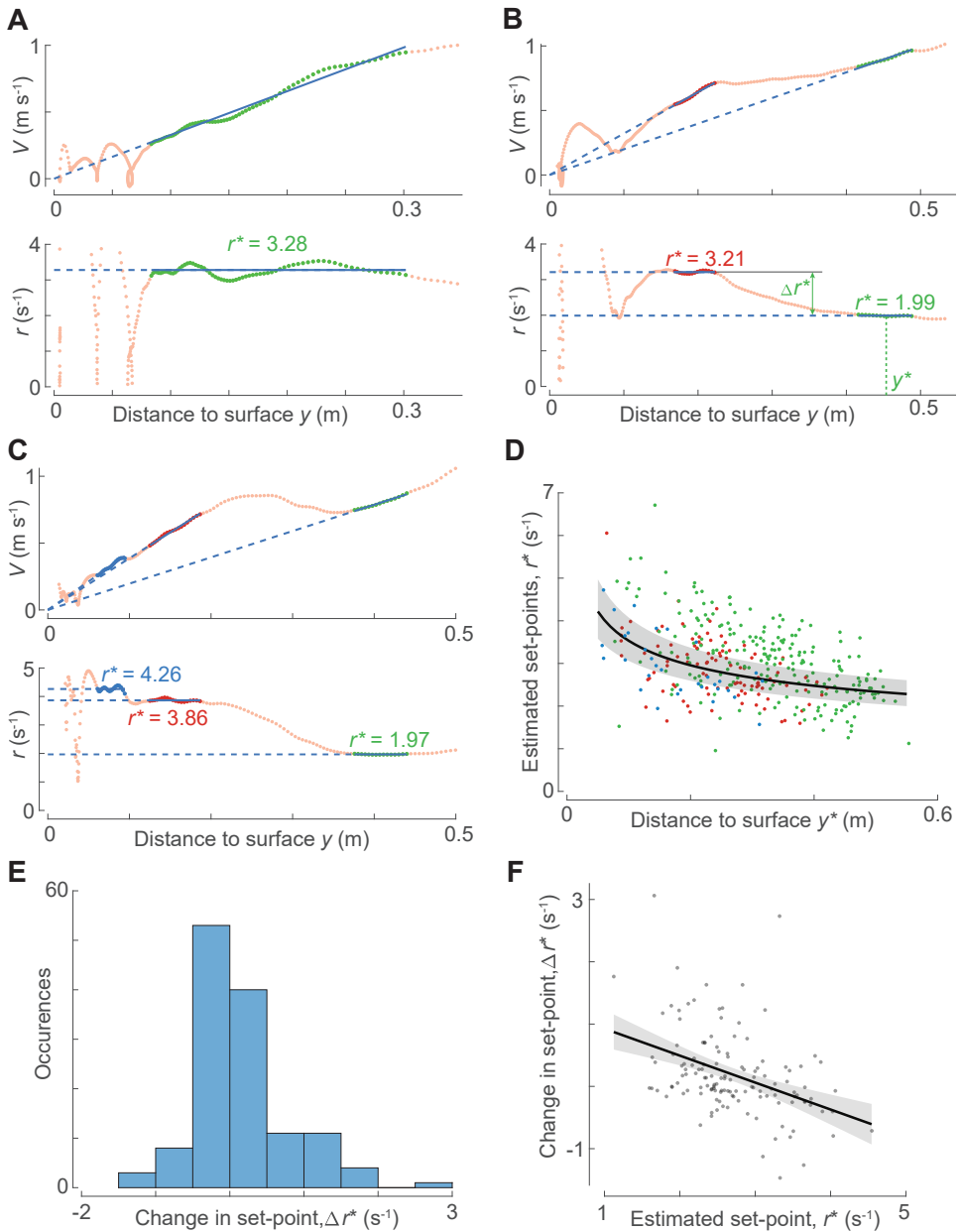
(2) Honeybees use their stepwise modulation of the relative rate of expansion set-point to converge towards a medium set-point

We consequently tested whether these switches towards a new set-point tended to be upwards or downwards. To do so, we determined the change in set-point between all two consecutive constant- r segments within a single landing trajectory (Δr^*) (Figure 5.4). Within the 227 landing maneuvers identified with the constant- r segments, 100 landings had more than one constant- r segment. Within these 100 landings, we identified 132 pairs of consecutive constant- r segments. Typical examples of these multi-constant- r segments are shown in Figure 5.3A and Figure 5.4B,C.

The change in set-point (Δr^*) between consecutive constant- r segments varied within a large range (Figure 5.4E), whereby honeybees transitioned 64 times to a lower set-point and 68 times to a higher set-point. During these transitions, they decreased their set-point with an average step size of $\Delta r^* = -0.28 \pm 0.32 \text{ s}^{-1}$ or increased it on average with a step

size of $\Delta r^* = 0.63 \pm 0.62 \text{ s}^{-1}$, respectively (mean \pm standard deviation).

We used a mixed-effects model to test how these changes in set-point varied with the magnitude of the first constant- r segment of each pair (Figure 5.4F, Section S5.3.2, Table S5.3).



(Caption on the next page.)

Figure 5.4: Throughout a landing maneuver, honeybees regularly adjust their set-point of optical expansion rate in a stepwise manner. (A–C) The variation of approach velocity V and relative rate of expansion r with perpendicular distance to the landing platform y for various landing maneuvers: (A) a landing in which the honeybee continues to fly at a single optical-expansion-rate set-point; (B) a landing in which the bee switches halfway the approach to a higher set-point; (C) a landing in which the bee flew at three distinct optical-expansion-rate set-points. (D) The variation of set-points of optical expansion rate r^* with the corresponding mean distance to the landing platform y^* , as defined in panel (B). The data points show results for all identified constant- r segments, whereby the first, second and third (or higher) constant- r segments identified in a landing maneuver are highlighted in green, red and blue, respectively ($n = 359$). The shaded curve shows the $(r^* - y^*)$ trend predicted by the linear mixed-effects model (black) with 95% confidence intervals (gray) (see Table S5.4 for statistical results) (A–D). (E) Histogram of change in the set-point Δr^* between two consecutive constant- r segments as defined in panel (B) ($n = 132$ set-point changes identified in 100 tracks with two or more set-points). (F) The variation of the change in the set-point Δr^* with the set-point magnitude r^* . The data points show results for all identified set-point changes, and the shaded curve shows the statistical model output (black) and 95% confidence intervals (gray) (see Table S5.3 for statistical results).

Independent of landing platform type and distance from the platform, the change in set-point varied linearly with the magnitude of the set-point, with a negative slope ($d\Delta r^*/dr^* = -0.433 [0.085]$, p -value < 0.001), and with a zero change in set-point ($\Delta r^* = 0 \text{ s}^{-1}$) at $r^* = 3.14 \text{ s}^{-1}$. Thus, honeybees tended to stepwise increase their set-point when flying at a set-point smaller than the $r_0^* = 3.14 \text{ s}^{-1}$, and switched to a lower set-point when operating at a set-point larger than r_0^* ; in addition, the shift magnitude varies linearly with the difference between the current expansion rate set-point and the so-called switch-reversal set-point (r_0^*). Because the slope $d\Delta r^*/dr^* = -0.433$ is less than -1 , a honeybee will on average convert 43% towards this switch-reversal set-point.

This shows that landing honeybees tend to fly at a constant relative optical expansion rate for a certain period of time. The duration of this period is dependent on the magnitude of the constant- r set-point, whereby the duration is longer at medium set-points as compared to the low set-points. When switching from one set-point to the next, they tend to converge on average 43% towards the set-point $r_0^* = 3.14 \text{ s}^{-1}$, which lies in the medium set-point group ($2.58 \text{ s}^{-1} < r^* \leq 3.29 \text{ s}^{-1}$).

(3) The variation of relative rate of expansion set-points with distance from the landing platform

In 227 landing maneuvers identified with the constant- r segments, we further tested how the set-point of relative rate of expansion varied with distance to the landing platform (Figure 5.4A–D). Similar to a bumblebee study (Goyal et al., 2021), we found a linear relationship between the logarithmic transformations of the set-points r^* and the mean distance to the surface y^* (Figures S5.2 and 5.4D, Section S5.3.2, Table S5.4). We used a linear mixed-effects model to find an estimate of the slope m of this linear variation. The model predicted that honeybees, on an average, increased their set-point with decreasing distance to the surface at a rate $m = -0.258 [0.029]$ (mean [standard error]) (this m is equal-

ent to a parameter time-to-contact-rate $\hat{\tau}$ used to describe the landing strategy of birds, Lee et al. 1991, 1993; Whitehead 2020). This average increase in set-point with reducing distance from the platform can be explained by the fact that the average stepwise increase between consecutive constant- r segments was 2.25 times larger than the average stepwise decrease (average stepwise increase: $\Delta r^* = 0.63 \pm 0.62 \text{ s}^{-1}$; average stepwise decrease: $\Delta r^* = -0.28 \pm 0.32 \text{ s}^{-1}$).

(4) Expansion cues influence the mean set-point at which honeybees fly during landing

The linear mixed-effects model between the set-points r^* and the mean distance to the surface y^* also allowed us to predict how the observed set-points varied among different landing patterns (Figure 5.5). Similar to the average approach analysis, we found that honeybees exhibited higher set-point and thus, flew faster towards the landing platform (during the constant- r segments) when presented with the horizontal stripes ($r^* = 3.16 [0.20] \text{ s}^{-1}$) and the gray pattern ($r^* = 3.47 [0.28] \text{ s}^{-1}$). Moreover, they exhibited lower set-points and thus, flew slower (during the constant- r segments) in the presence of random Julesz ($r^* = 2.66 [0.18] \text{ s}^{-1}$), ring ($r^* = 2.54 [0.19] \text{ s}^{-1}$) and 4-arm spiral pattern ($r^* = 2.75 [0.16] \text{ s}^{-1}$). The set-point r^* in the presence of other landing patterns lay between these two groups (Figure 5.5A,B, Table S5.4).

Among the tested landing platform patterns, honeybees exhibited 30%, 37% and 26% higher mean set-point r^* in the presence of gray pattern as compared to the random Julesz, ring and 4-arm spiral patterns, respectively. Additionally, honeybees exhibited 19% and 24% higher mean set-point r^* in the presence of horizontal stripes as compared to the random Julesz, and ring patterns, respectively (Figure 5.5A, Table S5.4). All comparisons among other landing patterns were statistically insignificant. Note that this increase in the mean set-point results in an equivalent increase in the mean approach velocity V^* at the average distance from the landing platform ($y^* = 0.287 \text{ m}$).

5.4 Discussion

Here we have examined how honeybees use optical expansion cues to control their landing on a vertical platform. For this purpose, we recorded 309 landings of honeybees on ten different landing platforms with variable levels of visual information, ranging from a uniform gray background with very little visual information to a rich Julesz optical pattern. The types of landings recorded and analyzed here are expected to be similar to the landings in nature when honeybees fly between the flower patches or when they land on their hive. Note that although we analyzed landings on vertical surfaces, such expansion cues are elicited during an approach from any direction, and towards a surface of any orientation including a large variety of objects (Baird et al., 2013).

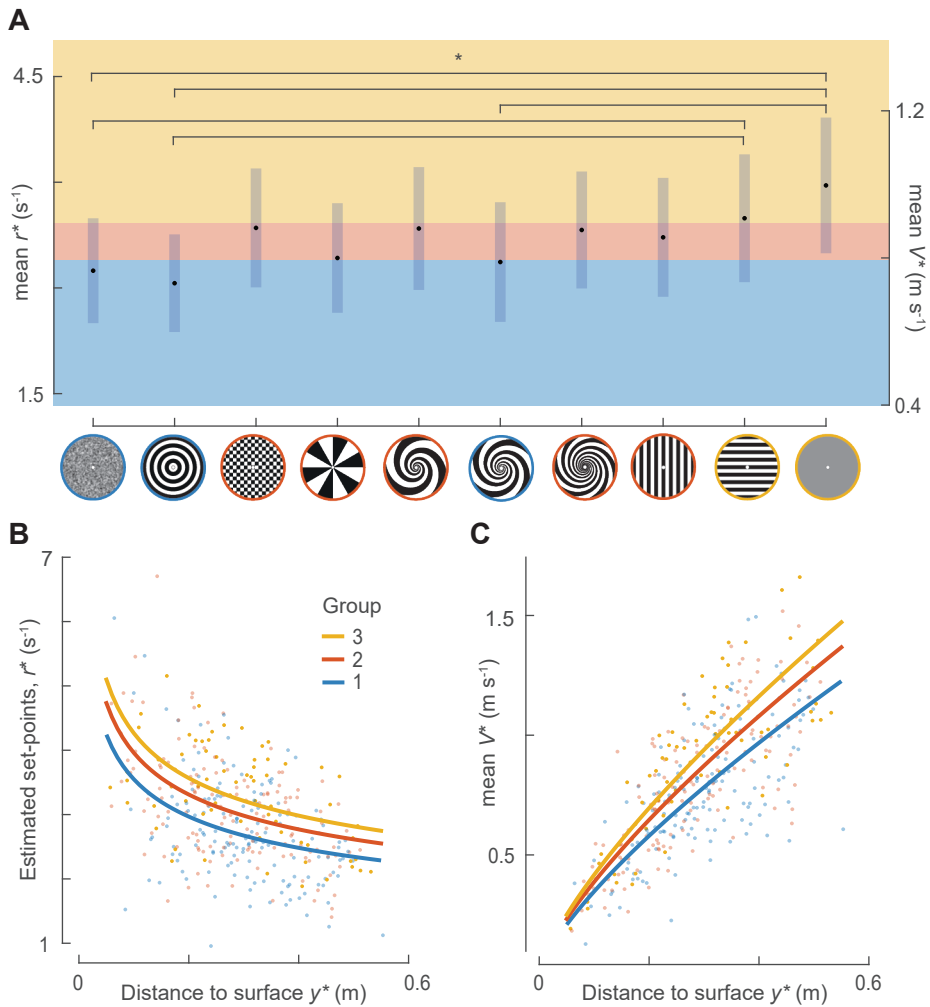


Figure 5.5: The mean set-points of relative rate of expansion at which honeybees land varies with the type of landing platform. (A) The mean set-points of relative rate of expansion r^* for honeybees landing on platforms with the 10 different visual patterns. The axis on the right shows the corresponding mean approach velocity V^* at the average distance from the landing platform ($y^* = 0.287$ m). Black dots and vertical bars indicate the estimated means and 95% confidence intervals, respectively. The significant differences between patterns are indicated on the top (Table S5.4). The patterns are grouped in the same three clusters as identified in average landing analysis (Figure 5.2). The groups are: (blue) the lowest r^* group consisting of random Julesz, rings and 4-arm spiral patterns; (yellow) the highest r^* group with horizontal stripes and gray pattern; (orange) the medium r^* group with the remaining patterns. (B,C) The variation of set-points of optical expansion rate r^* (B), and the mean approach velocity V^* (C) with mean distance to the landing platform y^* . The data points show results for all identified set-points of relative rate of expansion, and are color-coded according to the groups defined in panel (A).

The average landing approach of honeybees

To find out how honeybees land, we used two complementary methods to analyze the 309 recorded landing maneuvers. These include the analysis of the average landing trajectories per treatment as developed by Baird et al. (2013), and the analysis based on the individual landing trajectories as developed by Goyal et al. (2021).

The average landing trajectory analysis reveals that honeybees that approach a landing platform reduce their approach velocity linearly with distance to the surface, and thereby keep the relative optic expansion rate approximately constant throughout the approach. This suggests that, on average, honeybees approach a landing surface by flying at a single constant relative rate of optical expansion. These results are in concurrence with those of previous studies on the landing strategies of honeybees (*Apis mellifera ligustica*, Baird et al. 2013) and bumblebees (*Bombus impatiens*, Chang et al. 2016 and *Bombus terrestris*, Goyal et al. 2021).

The value of the mean set-point r^* predicted in this analysis ($r^* = 3.26 [0.16] \text{ s}^{-1}$) is similar to that reported previously in honeybees ($r^* = 3.11 \text{ s}^{-1}$, computed from Figure 2 in Baird et al. 2013). This is also true for the mean set-point r^* in the presence of the landing patterns for which the data is same in this and Baird et al. (2013) study (4.6%, 3.4% and 10.1% difference for ring, checkerboard and spoke patterns, respectively). The small differences between the values obtained in the two studies are due to the differences in the methods of estimating a set-point. In contrast to Baird et al. (2013), we force the intercept of linear variation of approach velocity with distance to be zero to estimate the set-point of relative rate of expansion (Goyal et al., 2021). This is done in order to be consistent with the definition of relative rate of expansion (Wagner, 1982; Sun and Frost, 1998; Baird et al., 2013). Note that we could not compare the differences in r^* for other common patterns between the two studies as the set-point r^* for those patterns is not reported in Baird et al. (2013); nevertheless a similar level of differences can be expected for them as well.

The landing strategy of honeybees

The average trajectory analysis of landing honeybees in this study provided a useful insight into how honeybees varied their mean approach velocity with distance to the landing surface, but it failed to capture the detailed variations in flight kinematics observed during individual landings (compare Figure 5.2A,B with Figure 5.4A–C). Specifically, it missed the multiple set-points of relative rate of expansion that honeybees exhibit during their approach and instead suggested that they flew at a single set-point throughout their approach.

To capture these multiple set-point dynamics, we applied the individual track-based analysis method developed by Goyal et al. (2021) to all individual recorded landings. Using this method, we identified 227 landing maneuvers with 359 track segments in which honeybees flew approximately at a constant relative rate of expansion. The distribution of set-points estimated in these segments includes the set-points computed using average tra-

jectory analysis in this and the previous study on the landing strategy of honeybees (Baird et al., 2013). Moreover, honeybees increased on average their set-point r^* with decreasing distance to the surface y^* . This variation was captured by a linear fit between their logarithmic transformations with negative slope m (-0.258 [0.029]). Thus, we conclude that honeybees land by using a modular strategy; they fly at a set-point of relative rate of expansion for a period of time, after which they rapidly switch to a new set-point, which was on average higher than the previous set-point.

The set-point switch behavior of honeybees

In addition to revealing their landing strategy, the analysis of individual maneuvers describes how honeybees switch between the set-points of relative rate of expansion. Our result shows that honeybees are more likely to increase their set-points when they fly at a set-point lower than the switch-reversal set-point ($r_0^* = 3.14 \text{ s}^{-1}$), and they tended to switch to a lower set-point when operating at a set-point value higher than r_0^* . Moreover, the set-point switching magnitude (Δr^*) depends on average linearly on the current optic expansion rate set-point (r^*) with a slope of $d\Delta r^*/dr^* = -0.433$ [0.085]. Thus, when switching to a new optic expansion rate set-points, honeybees tended to converge for on average 43% towards the switch-reversal set-point of $r_0^* = 3.14 \text{ s}^{-1}$. Because the majority of landing honeybees started their landing approach at r^* values lower than $r_0^* = 3.14 \text{ s}^{-1}$ (Figure 5.4F), this could lead to the increase in optic expansion rate set-point with reducing distance from the platform (Figure 5.4D). However, there is another possibility that could also contribute to this increase in set-point with reducing distance. Honeybees may intermittently obtain an estimate of distance to the surface and consequently use it to trigger a change in the set-point (de Croon, 2016; Goyal et al., 2021). This might not have been captured by our analysis of set-point switching behavior due to the existence of high variation of step-change (Δr^*) in the set-point around the mean step-change predicted by our model (Figure 5.4F).

Nevertheless, the dynamics of stepwise converging towards an average optic expansion rate set-point $r_0^* = 3.14 \text{ s}^{-1}$ allows honeybees that start their landing approach at a large range of flight speeds (Figure S5.3) to convert to a relatively narrow band of approach velocities closer to the platform (Figure 5.5). This might be important for making successful landings, and minimizing the chance of occurring damage when hitting the platform uncontrollably.

Honeybees adjust the set-point with distance depending upon the optic cues being used during landing

Honeybees use optical expansion cues to land on vertical surfaces (Baird et al., 2013). Here we have analyzed individual landing trajectories to reveal that often honeybees adjust their set-point as they approach the surface. But, when optical expansion cues are weak or ab-

sent, such as when landing on horizontal surfaces, individual track-based analysis shows that honeybees decrease their forward speed proportionately with distance (Srinivasan et al., 2000). During such grazing landings, their direction of motion is almost parallel to the surface, which produces primarily front-to-back translatory optic flow. In such a scenario, honeybees do not vary their set-point as they approach the surface. Thus, it can be concluded that honeybees adjust set-point with distance during landing when they use optical expansion cues, and not when they use primarily translatory optic flow. The flexibility of set-point adjustment might exist for expansion cues and not for translatory optic flow, as expansion cues are elicited during an approach towards a wide variety of surfaces (Baird et al., 2013). Moreover, this observation also suggests that the visual system of honeybees is likely to be organized into two types of movement-detecting systems: (a) visual sensors which monitor motion in the frontal field of view and uses image expansion cues with variable set-points, and (b) visual sensors which monitor the motion in the ventral field of view and uses image translation cues with a fixed set-point.

Stepwise regulation of set-point of optical expansion rate approximates the constant- $\dot{\tau}$ landing strategy of birds

The dependence of set-point of optical expansion rate with distance to the landing surface is captured by a linear relationship between their logarithmic transformations (Figure S5.2). The slope m of this linear relationship is referred to as a time-to-contact-rate $\dot{\tau}$ (Baird et al., 2013; Goyal et al., 2021) and is equivalent to the parameter $\dot{\tau}$ used in literature to describe the landings of birds (Lee et al., 1991, 1993; Whitehead, 2020). Pigeons (*Columba livia*), hummingbirds (*Colibri coruscans*) and mallard ducks (*Anas platyrhynchos*) are suggested to hold constant the time-to-contact-rate $\dot{\tau}$ during their landing approach (Lee et al., 1991, 1993; Whitehead, 2020). The landing strategies of bees identified in this study can be recognized as a discrete approximation of the landing strategy of birds (Goyal et al., 2021). This is because the visual guidance strategy of bees results in a stepwise increase of the optical expansion rate with reducing distance to the surface, whereas the visual guidance of birds results in a continuous increase in the optical expansion rate with reducing distance (Goyal et al., 2021).

Expansion cues affect the landing strategy of honeybees

We varied the expansion cues that honeybees use during landing by using different patterns. Among the tested patterns, both the average trajectory analysis per treatment and the analysis on individual tracks show that honeybees exhibited the highest set-points, and thus flew fastest, when landing on the gray platform and the horizontal stripe platform; they flew slowest when landing on the random Julesz, ring and 4-arm spiral platforms (Figures 5.2 and 5.5). Because the gray pattern offers weaker expansion cues than the latter three patterns, the observed behaviour is in agreement with the results from earlier investigations

which show that insects, including honeybees, fly faster when front-to-back translatory optic cues are reduced (Baird, 2005; Barron and Srinivasan, 2006; Baird et al., 2010, 2011; Linander et al., 2015; Baird et al., 2020, 2021). Moreover, honeybees exhibit similar approach velocities in the presence of horizontal stripes and the gray patterns. This suggests that honeybees do not parse the vertical expansion flow well, something that may be a limitation of their sensory system, as pure vertical expansion cues would be rarely encountered by them in the natural world.

Our results also show that honeybees use a similar landing approach in the case of the 3-, 4- and 6-arm spiral patterns. This suggests that honeybees can measure the relative rate of expansion largely independently of the spatial frequency content in the landing patterns. This finding is consistent with the other flight behaviours of honeybees which use angular velocity of the image and are insensitive to the spatial content in the image (Srinivasan et al., 1991; Srinivasan, 1992; Srinivasan et al., 1996; Si et al., 2003; Baird, 2005; Baird et al., 2013).

In contrast to the behaviour displayed by bumblebees (*Bombus terrestris*) (Goyal et al., 2021), the individual analysis of landing maneuvers in this study did not yield any differences among the checkerboard and spoke patterns. Bumblebees display a cautious landing approach by decelerating faster (higher slope of set-point with distance, m in the presence of weaker expansion information, as would prevail, for example, for the spoke pattern. Such a difference was not observed in the present study, potentially due to the limited number of flights recorded for each pattern – more landing tracks per pattern are required to conclusively quantify how expansion cues affect the slope of set-point with distance. Nevertheless, the recorded landing maneuvers are sufficient to identify the landing strategy of honeybees and to ascertain whether or not expansion cues affect their strategy.

Note that the modular landing strategy of honeybees described here is similar to the modular landing strategy found in bumblebees (Goyal et al., 2021). In addition to similarities, there are some differences between them as well. We compare the key aspects of this modular landing strategy among the two species and elucidate the likely causes of the observed differences in **Chapter 6**.

Conclusion

Honeybees use visual expansion cues to land and reach their food sources. Based on their average approach, it was previously proposed that they perform such landings by approximately holding constant the relative rate of expansion at a single value (referred to as set-point) throughout their landing approach. In this study, we perform an additional individual-track based analysis to show that honeybees actually use a range of set-points, and often land by stepwise adjusting their set-point with reducing distance to the landing surface. Moreover, we found a set-point switching mechanism that allowed honeybees to converge to stereotypic landing conditions near the surface, for a large range of initial flight speeds and visual landing platform patterns.

The presence of this modular landing strategy in bumblebees (Goyal et al., 2021) and now honeybees suggests that it is likely to be found in other flying insects which use visual cues to land. Furthermore, our results can help guide searches for the neural circuits that underlie landing control. They can also inspire similar control strategies on man-made flying systems.

Data and code availability

The landing maneuvers of honeybees gathered in this study will be publicly available as a data repository and the code used for the analysis is available at: https://github.com/kaku289/nimble-bbee-analysis/tree/landing_honeybees.

Acknowledgements

The behavioural experiments were supported in part by the ARC Centre of Excellence in Vision Science (CE0561903), ARC Discovery Grant DP0559306, and the US Asian Office of Aerospace R&D (FA4869-07-1-0010). This project is also supported by the Nederlandse Organisatie voor Wetenschappelijk Onderzoek - Toegepaste en Technische Wetenschappen (NWO-TTW grant number 15039). We thank Paul Helliwell for his assistance with beekeeping and Johan L. van Leeuwen for providing useful comments on the manuscript.

Author contributions

Conceptualization, P.G., E.B., F.T.M., M.V.S.; Methodology, P.G., E.B.; Software, P.G.; Validation, P.G.; Formal Analysis, P.G.; Investigation, E.B., M.V.S.; Resources, M.V.S., F.T.M.; Data Curation, P.G.; Writing - Original Draft, P.G.; Writing - Review & Editing, P.G., E.B., M.V.S., F.T.M.; Visualization, P.G.; Supervision, M.V.S., F.T.M.; Project Administration, P.G., M.V.S., F.T.M.; Funding Acquisition, M.V.S., F.T.M.;

Declaration of interests

The authors declare no competing interests.

References

- Baird, E. (2005). Visual control of flight speed in honeybees. *Journal of Experimental Biology* 208, 3895–3905.
- Baird, E., Boeddeker, N., Ibbotson, M. R. and Srinivasan, M. V. (2013). A universal strategy for visually guided landing. *Proceedings of the National Academy of Sciences of the United States of America* 110, 18686–18691.
- Baird, E., Boeddeker, N. and Srinivasan, M. V. (2021). The effect of optic flow cues on honeybee flight control in wind. *Proceedings of the Royal Society B: Biological Sciences* 288, 20203051.

- Baird, E., Kornfeldt, T. and Dacke, M. (2010). Minimum viewing angle for visually guided ground speed control in bumblebees. *Journal of Experimental Biology* **213**, 1625–1632.
- Baird, E., Kreiss, E., Wcislo, W., Warrant, E. and Dacke, M. (2011). Nocturnal insects use optic flow for flight control. *Biology Letters* **7**, 499–501.
- Baird, E., Tichit, P. and Guiraud, M. (2020). The neuroecology of bee flight behaviours. *Current Opinion in Insect Science* **42**, 8–13.
- Barron, A. and Srinivasan, M. V. (2006). Visual regulation of ground speed and headwind compensation in freely flying honey bees (*Apis mellifera* L.). *Journal of Experimental Biology* **209**, 978–984.
- Chang, J. J., Crall, J. D. and Combes, S. A. (2016). Wind alters landing dynamics in bumblebees. *The Journal of Experimental Biology* **219**, 2819–2822.
- de Croon, G. C. H. E. (2016). Monocular distance estimation with optical flow maneuvers and efference copies: a stability-based strategy. *Bioinspiration & Biomimetics* **11**, 016004.
- Edwards, M. and Ibbotson, M. R. (2007). Relative sensitivities to large-field optic-flow patterns varying in direction and speed. *Perception* **36**, 113–124.
- Evans, M., Hastings, N. and Peacock, B. (2000). *Statistical Distributions*. Wiley Series in Probability and Statistics. Wiley.
- Gibson, J. J. (1955). The optical expansion-pattern in aerial locomotion. *The American journal of psychology* **68**, 480–484.
- Goyal, P., Cribellier, A., de Croon, G. C. H. E., Lankheet, M. J., van Leeuwen, J. L., Pieters, R. P. M. and Muijres, F. T. (2021). Bumblebees land rapidly and robustly using a sophisticated modular flight control strategy. *iScience* **24**, 102407.
- Lee, D. N. (1976). A theory of visual control of braking based on information about time to collision. *Perception* **5**, 437–459.
- Lee, D. N., Davies, M. N. O., Green, P. R. and (Ruud). Van Der Weel, F. R. (1993). Visual control of velocity of approach by pigeons when landing. *Journal of Experimental Biology* **180**, 85–104.
- Lee, D. N., Reddish, P. E. and Rand, D. T. (1991). Aerial docking by hummingbirds. *Naturwissenschaften* **78**, 526–527.
- Linander, N., Dacke, M. and Baird, E. (2015). Bumblebees measure optic flow for position and speed control flexibly within the frontal visual field. *Journal of Experimental Biology* **218**, 1051–1059.
- Ribbands, C. R. (1949). The Foraging Method of Individual Honey-Bees. *The Journal of Animal Ecology* **18**, 47.
- Shackleton, K., Balfour, N. J., Toufailya, H. A., Alves, D. A., Bento, J. M. and Ratnieks, F. L. W. (2019). Unique nest entrance structure of *Partamona helleri* stingless bees leads

- to remarkable ‘crash-landing’ behaviour. *Insectes Sociaux* 2019 66:3 66, 471–477.
- Si, A., Srinivasan, M. V. and Zhang, S.** (2003). Honeybee navigation: properties of the visually driven ‘odometer’. *Journal of Experimental Biology* 206, 1265–1273.
- Srinivasan, M., Zhang, S., Lehrer, M. and Collett, T.** (1996). Honeybee navigation en route to the goal: visual flight control and odometry. *Journal of Experimental Biology* 199, 237–244.
- Srinivasan, M. V.** (1992). Distance Perception in Insects. *Current Directions in Psychological Science* 1, 22–26.
- Srinivasan, M. V., Lehrer, M., Kirchner, W. H. and Zhang, S. W.** (1991). Range perception through apparent image speed in freely flying honeybees. *Visual neuroscience* 6, 519–535.
- Srinivasan, M. V., Zhang, S. W., Chahl, J. S., Barth, E. and Venkatesh, S.** (2000). How honeybees make grazing landings on flat surfaces. *Biological Cybernetics* 83, 171–183.
- Sun, H. and Frost, B. J.** (1998). Computation of different optical variables of looming objects in pigeon nucleus rotundus neurons. *Nature Neuroscience* 1, 296–303.
- Tichit, P., Alves-dos Santos, I., Dacke, M. and Baird, E.** (2020a). Accelerated landing in a stingless bee and its unexpected benefits for traffic congestion. *Proceedings of the Royal Society B* 287, 20192720.
- Tichit, P., Alves-dos Santos, I., Dacke, M. and Baird, E.** (2020b). Accelerated landings in stingless bees are triggered by visual threshold cues. *Biology letters* 16, 20200437.
- Van Breugel, F. and Dickinson, M. H.** (2012). The visual control of landing and obstacle avoidance in the fruit fly *Drosophila melanogaster*. *Journal of Experimental Biology* 215, 1783–1798.
- Wagner, H.** (1982). Flow-field variables trigger landing in flies. *Nature* 297, 147–148.
- Whitehead, J. G.** (2020). *An examination of the kinematics and behavior of mallards (*Anas platyrhynchos*) during water landings*. Ph.D. thesis, Virginia Tech.

Supplemental information

Visual guidance of landing approaches in honeybees

Pulkit Goyal, Emily Baird, Mandyam V. Srinivasan, Florian T. Muijres

S5.1 Figures

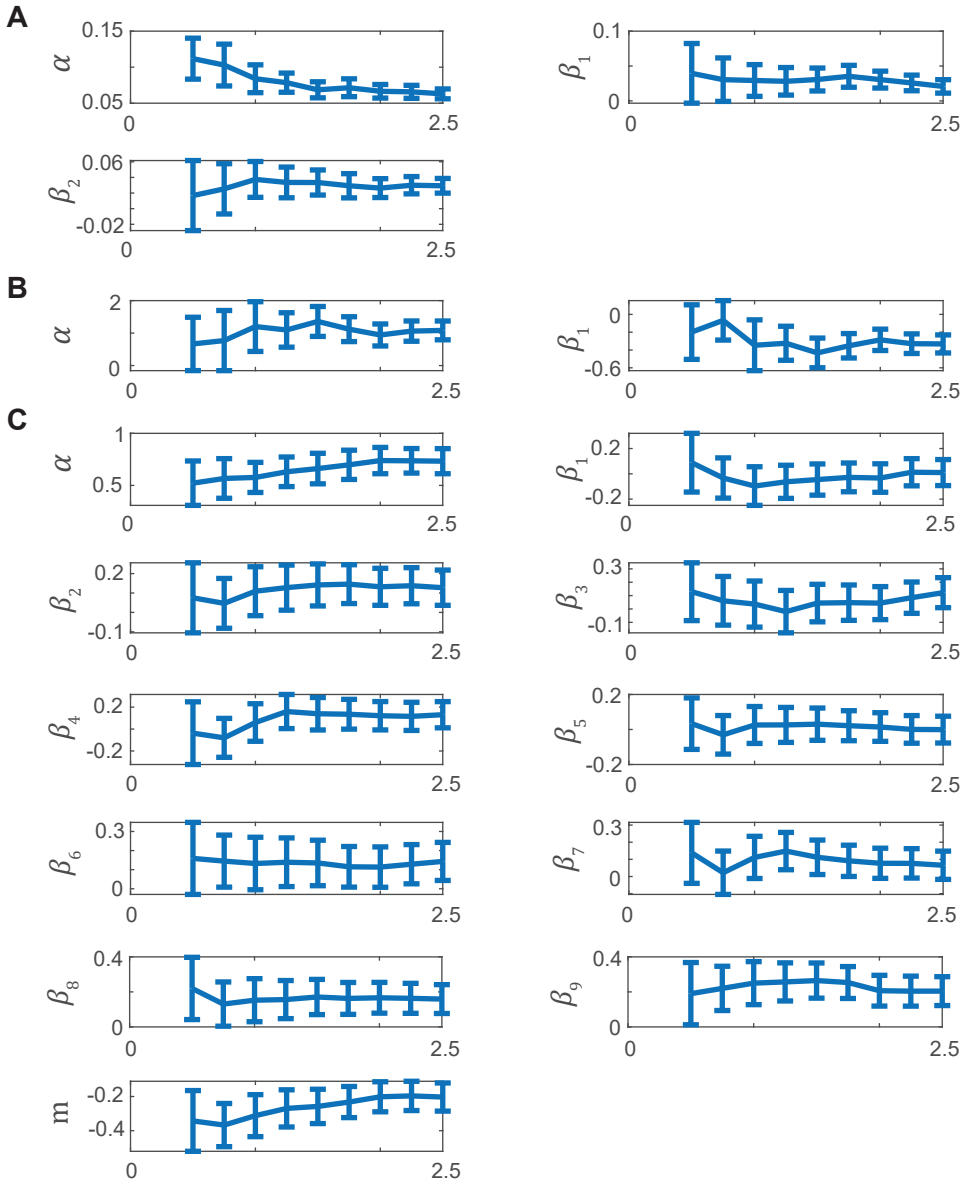


Figure S5.1: The effect of factor f on the results. (A) The variation of distance covered by honeybees Δy^* with three regions of optical expansion rate set-point r^* for different factors f (Equation S5.2: $\Delta y_{i,s,f}^* \sim N(\alpha + \alpha_s + \alpha_f + \beta_1 \text{MEDIUM}_{i,s,f} + \beta_2 \text{HIGH}_{i,s,f}, \sigma^2)$). The similar results are observed for the travel time Δt^* . (B) The variation of difference between the new and the current set-point Δr^* with the current set-point r^* for different factors f (Equation S5.3: $\Delta r_{i,s,f}^* \sim N(\alpha + \alpha_s + \alpha_f + \beta_1 r_{i,s,f}^*, \sigma^2)$). (C) The dependence of the set-point r^* on distance to the platform y^* along with the effect of different landing patterns for different factors f (Equation S5.4: $\log(r_{i,s,f}^*) \sim N(\alpha + \alpha_s + \alpha_f + \sum_{j=1}^9 \beta_j \text{PATTERN}_{j,i,s,f} + m \log(y_{i,s,f}^*), \sigma^2)$). (A–C) The vertical bars for each coefficient indicate 95% confidence intervals.

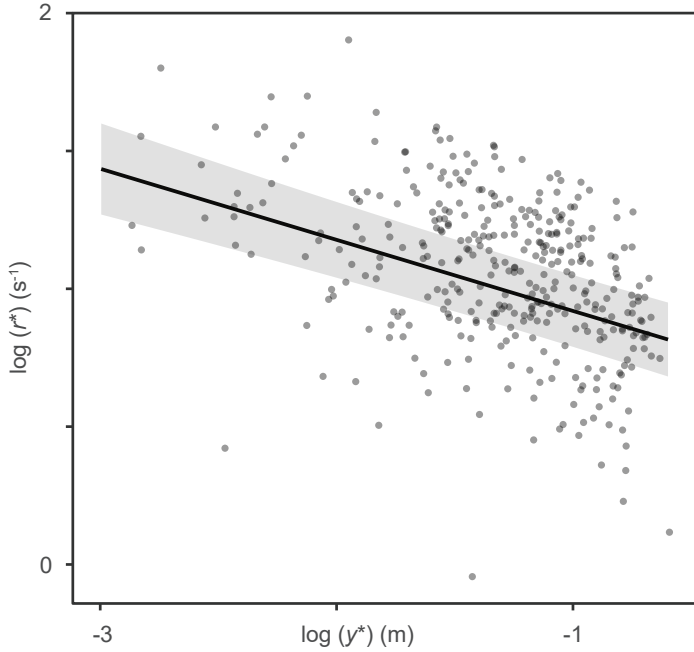


Figure S5.2: The variation of set-point of optical expansion rate r^* with distance to the surface y^* in the logarithmic domain as identified by the linear mixed-effects model in Equation S5.4 (Table S5.4).

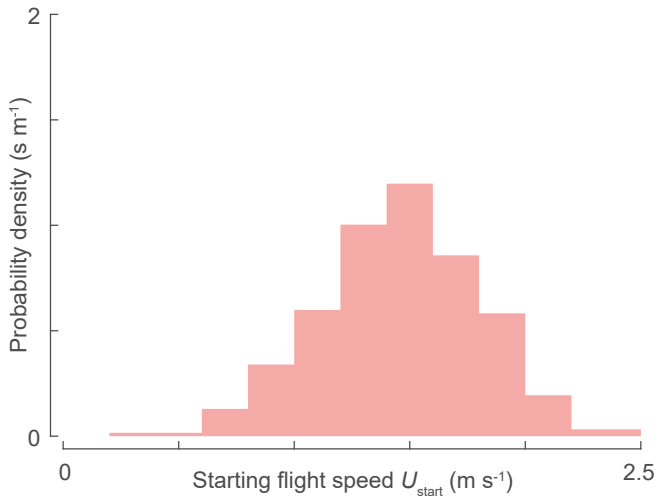


Figure S5.3: The probability density of the 3D flight speeds U_{start} of honeybees at the start of the landing maneuvers.

S5.2 Tables

Table S5.1: The analysis of mean relative rate of expansion in the presence of different landing patterns for average-per-treatment analysis method. The data comprises of 309 landing maneuvers between $0.15 \text{ m} \leq y \leq 0.35 \text{ m}$, where y is the distance to the platform. Post-hoc tests compare differences between mean relative rate of expansion (statistical model as given by Equation S5.1: $r_{i,s,f} \sim N(\alpha + \alpha_s + \alpha_f + \sum_{j=1}^9 \beta_j \text{PATTERN}_{j,i,s,f}, \sigma^2)$).

Fixed effect	Estimate	Std error	t value	Pr(> t)
α	2.80	0.16	17.52	0.00121
β_1	0.25	0.04	7.10	$1.34E - 12$
β_2	0.45	0.04	12.56	$5.66E - 36$
β_3	0.55	0.04	14.57	$8.89E - 48$
β_4	0.46	0.04	12.23	$3.06E - 34$
β_5	0.22	0.03	7.79	$7.21E - 15$
β_6	0.47	0.04	12.79	$2.76E - 37$
β_7	0.41	0.03	13.71	$1.61E - 42$
β_8	0.72	0.03	23.56	$1.4E - 120$
β_9	1.01	0.04	26.95	$3.2E - 156$
Post-hoc contrasts*	Estimate	Std error	z ratio	p value
R - S4	0.04	0.03	1.11	1
C - S	-0.10	0.04	-2.45	0.65
C - S3	-0.01	0.04	-0.20	1
C - S6	-0.02	0.04	-0.48	1
C - V	0.04	0.03	1.08	1
S - S3	0.09	0.04	2.17	1
S - S6	0.08	0.04	1.94	1
S3 - S6	-0.01	0.04	-0.26	1
S3 - V	0.05	0.04	1.26	1
S6 - V	0.06	0.04	1.60	1

*Random Julesz (J), Ring (R), Checkerboard (C), Spoke (S), 3-arm Spiral (S3), 4-arm Spiral (S4), 6-arm Spiral (S6), Vertical stripes (V), Horizontal stripes (H), Grey (G) landing patterns.

*Only non-significant comparisons are shown here. All other comparisons are statistically significant.

Table S5.2: The analysis of distance covered and travel time of honeybees at different set-points of relative rate of expansion. The data is extracted from 359 constant- r segments in 227 landing maneuvers of honeybees (factor $f = 1.5$). The post-hoc tests compare differences between the mean distance covered (Δy^*) or the mean travel time (Δt^*) in three set-point regions: low ($r^* \leq 2.58 \text{ s}^{-1}$), medium ($2.58 \text{ s}^{-1} < r^* \leq 3.29 \text{ s}^{-1}$) and high ($r^* > 3.29 \text{ s}^{-1}$) (statistical model as given by Equation S5.2: $\Delta y_{i,s,f}^*$ or $\Delta t_{i,s,f}^* \sim N(\alpha + \alpha_s + \alpha_f + \beta_1 \text{MEDIUM}_{i,s,f} + \beta_2 \text{HIGH}_{i,s,f}, \sigma^2)$).

Effect on Δy^*				
Fixed effect	Estimate	Std error	t value	Pr(> t)
α	0.069	0.006	12.053	$2.73E - 28$
β_1	0.031	0.008	3.659	0.000291
β_2	0.033	0.008	4.083	$5.49E - 05$
Post-hoc contrasts*	Estimate	Std error	z ratio	p value
Low - Medium	-0.031	0.01	-3.55	$1.32E - 03$
Low - High	-0.033	0.01	-4.03	$2.09E - 04$
Medium - High	-0.003	0.01	-0.32	1

Effect on Δt^*				
Fixed effect	Estimate	Std error	t value	Pr(> t)
α	0.100	0.009	11.294	$4.29E - 15$
β_1	0.033	0.013	2.589	0.010
β_2	0.021	0.013	1.675	0.095
Post-hoc contrasts*	Estimate	Std error	z ratio	p value
Low - Medium	-0.033	0.013	-2.51	0.037
Low - High	-0.021	0.013	-1.65	0.298
Medium - High	0.012	0.013	0.92	1

Table S5.3: The analysis of transition between the set-points of relative rate of expansion observed in honeybees during their approach towards a landing surface. The data is extracted from 132 transitions in 100 landing maneuvers of honeybees with more than one constant- r segments (factor $f = 1.5$). (statistical model as given by Equation S5.3: $\Delta r_{i,s,f}^* \sim N(\alpha + \alpha_s + \alpha_f + \beta_1 r_{i,s,f}^*, \sigma^2)$).

Fixed effect	Estimate	Std error	t value	Pr(> t)
α	1.36	0.24	5.78	$5.33E - 08$
β_1	-0.43	0.08	-5.09	$1.22E - 06$

Table S5.4: The analysis of how honeybees adjust their set-point of relative rate of expansion with distance to the landing platform and landing patterns. The data comprises of 359 constant- r segments identified in 227 landing maneuvers of honeybees (factor $f = 1.5$). Post-hoc tests compare differences in $\log(r^*)$ in the presence of different landing platforms (statistical model as given by Equation S5.4: $\log(r_{i,s,f}^*) \sim N(\alpha + \alpha_s + \alpha_f + \sum_{j=1}^9 \beta_j \text{PATTERN}_{j,i,s,f} + m \log(y_{i,s,f}^*), \sigma^2)$).

Fixed effect	Estimate	Std error	t value	Pr(> t)
α	0.662	0.075	8.85	$1.42E - 04$
β_1	-0.045	0.063	-0.72	0.47
β_2	0.142	0.055	2.56	0.01
β_3	0.044	0.072	0.62	0.54
β_4	0.140	0.075	1.85	0.07
β_5	0.030	0.047	0.65	0.52
β_6	0.135	0.061	2.22	0.03
β_7	0.112	0.051	2.19	0.03
β_8	0.171	0.051	3.34	$9.39E - 04$
β_9	0.265	0.070	3.80	$1.71E - 04$
m	-0.258	0.029	-8.89	$3.50E - 17$
Post-hoc contrasts* in $\log(r^*)$	Estimate	Std error	z ratio	p value
J - H	-0.171	0.052	-3.29	0.049
J - G	-0.265	0.070	-3.78	0.008
R - H	-0.216	0.062	-3.46	0.027
R - G	-0.310	0.078	-3.96	0.004
S4 - G	-0.234	0.066	-3.53	0.022

*Random Julesz (J), Ring (R), Checkerboard (C), Spoke (S), 3-arm Spiral (S3), 4-arm Spiral (S4), 6-arm Spiral (S6), Vertical stripes (V), Horizontal stripes (H), Grey (G) landing patterns.

*Only significant comparisons are shown here. All other comparisons are statistically non-significant.

Table S5.5: The number of landing manoeuvres recorded in each tested treatment and the number of landing manoeuvres that are identified with constant- r segments for different values of factor f .

Landing pattern	Number of landing manoeuvres	Factors f								
		0.5	0.75	1	1.25	1.5	1.75	2	2.25	2.5
Random Julesz	31	15	21	23	24	26	28	30	30	30
Ring	21	4	8	11	14	14	15	15	17	18
Checkerboard	22	8	15	18	19	20	20	21	22	22
Spoke	19	6	6	7	7	10	10	13	15	16
3-arm Spiral	19	3	7	10	11	11	13	15	15	16
4-arm Spiral	67	26	36	46	50	56	56	57	59	61
6-arm Spiral	21	7	11	13	16	16	18	18	18	19
Vertical stripes	43	11	18	23	28	30	31	32	36	38
Horizontal stripes	44	14	25	26	28	31	33	36	37	38
Grey	22	4	8	12	12	13	14	16	19	19
Total landings	309	98	155	189	209	227	238	253	268	277

S5.3 Supporting text

S5.3.1 Extraction of set-points of relative rate of expansion

We used an algorithm developed in Goyal et al. (2021) to extract the constant- r track segments in which honeybees decelerated at an approximately constant relative rate of expansion. For a constant- r segment, three linear regressions are computed - one in the full segment and other two in its equal halves. These linear regressions adjudge the constancy of r with distance to the surface y . The first step of set-point extraction algorithm involves the identification of expected t -distributions of six linear regression parameters (two from each regression). For this purpose, we manually selected 282 constant- r segments in 193 landing maneuvers of honeybees and computed the desired t -distributions. Similar to the bumblebee study, these t -distributions have location parameter μ close to zero and scale parameter σ , which dictates their spread around μ , defined in terms of two parameters: $\sigma_1 = 0.29$ and $\sigma_2 = 1.02$ (see Goyal et al. 2021 for details). In the second step of set-point extraction algorithm, we used these identified t -distributions to automatically select constant- r segments in the complete dataset. This step computes these six regression parameters in all possible track segments of different sizes (with 15 – 200 data points) in a landing maneuver and selects those track segments as probable constant- r segments in which these regression parameters lie within a number of scale parameters around their mean values (specified by a threshold factor f). Among these probable segments, a set of non-overlapping segments are identified as constant- r segments. This selection of non-overlapping segments is identified by the root mean square error of the estimated set-point from the observed variation in r . To make this selection similar to the bumblebee study, we reduced the sampling rate of the landing maneuvers of honeybees to 175 Hz.

S5.3.2 Statistical models

We developed linear mixed-effects models for both the average-per-treatment and per-track analyses.

The average-per-treatment model

To determine how the mean of relative rate of expansion varied with patterns on the landing disc, we used the following model:

$$r_{i,s,f} \sim N(\alpha + \alpha_s + \alpha_f + \sum_{j=1}^9 \beta_j \text{PATTERN}_{j,i,s,f}, \sigma^2) \quad (\text{S5.1})$$

where $r_{i,s,f}$ is the i -th measurement of relative rate of expansion from the f -th flight number in the s -th set, α is the regression intercept for random Julesz pattern (overall intercept), α_s is the set-specific intercept, α_f is the flight-number-specific intercept, PATTERN_j indicates j -th pattern in the set {Ring, Checkerboard, Spoke, 3-arm spiral, 4-arm spiral, 6-

arm spiral, vertical stripes, horizontal stripes, grey}, $\text{PATTERN}_{j,i,s,f}$ indicates if j -th landing pattern is present for the i -th measurement from the f -th flight number in the s -th set ($0 = \text{no}$, $1 = \text{yes}$), $\beta_j \forall j \in \{1, 2, \dots, 9\}$ represent the differences of fixed-effects from the overall intercept, and σ is the residual standard deviation. The statistical output and the results from post-hoc tests for 309 landing maneuvers of honeybees are given in Table S5.1.

The per-track models

We used three statistical models to report results from the analysis of individual landing maneuvers of honeybees.

1. To find if honeybees preferred to fly at certain set-points of relative rate of expansion, we tested how the distance covered (Δy^*) or travel time (Δt^*) during each set-point varied with the three set-point regions: low ($r^* \leq 2.58 \text{ s}^{-1}$), medium ($2.58 \text{ s}^{-1} < r^* \leq 3.29 \text{ s}^{-1}$) and high ($r^* > 3.29 \text{ s}^{-1}$) along with the landing patterns. The model dredging revealed that the landing patterns did not influence this relationship. Therefore, we used the following reduced model:

$$\Delta y_{i,s,f}^* \text{ or } \Delta t_{i,s,f}^* \sim N(\alpha + \alpha_s + \alpha_f + \beta_1 \text{MEDIUM}_{i,s,f} + \beta_2 \text{HIGH}_{i,s,f}, \sigma^2) \quad (\text{S5.2})$$

where $\Delta y_{i,s,f}^*$ or $\Delta t_{i,s,f}^*$ is the i -th measurement from the f -th flight number in the s -th set, α is the regression intercept for low set-point region (overall intercept), α_s is the set-specific intercept, α_f is the flight-number-specific intercept, $\text{MEDIUM}_{i,s,f}$ and $\text{HIGH}_{i,s,f}$ indicate if that measurement belongs to the medium and high set-point region, respectively ($0 = \text{no}$, $1 = \text{yes}$), $\beta_j \forall j \in \{1, 2\}$ represent the differences of fixed-effects from the overall intercept, and σ is the residual standard deviation. The statistical output and the results from post-hoc tests are given in Table S5.2.

2. To find how honeybees selected the new set-point of relative rate of expansion, we analyzed the transition between two consecutive set-points in landing maneuvers with more than one constant- r segments. Specifically, for each transition, we tested how difference between the new and the current set-point (Δr^*) varied with the current set-point (r^*), the distance at which the current set-point is observed (y^*), and the landing patterns. The model dredging revealed that y^* and landing patterns did not influence the relationship between Δr^* and r^* . Therefore, we used the following model:

$$\Delta r_{i,s,f}^* \sim N(\alpha + \alpha_s + \alpha_f + \beta_1 r_{i,s,f}^*, \sigma^2) \quad (\text{S5.3})$$

where $r_{i,s,f}^*$ and $\Delta r_{i,s,f}^*$ are the i -th set-point and the step-change in it, respectively, from the f -th flight number in the s -th set, α and β_1 are the regression intercept and slope, respectively, α_s is the set-specific intercept, α_f is the flight-number-specific

intercept, and σ is the residual standard deviation. The statistical output is given in Table S5.3.

3. To find how honeybees adjusted their set-point (r^*) with distance to the platform (y^*) and landing patterns, we used the following model:

$$\log(r_{i,s,f}^*) \sim N\left(\alpha + \alpha_s + \alpha_f + \sum_{j=1}^9 \beta_j \text{PATTERN}_{j,i,s,f} + m \log(y_{i,s,f}^*), \sigma^2\right) \quad (\text{S5.4})$$

where $r_{i,s,f}^*$ and $y_{i,s,f}^*$ are the i -th measurements of the set-point of relative rate of expansion and the mean distance, respectively, from the f -th flight number in the s -th set, α is the regression intercept for random Julesz pattern (overall intercept), α_s is the set-specific intercept, α_f is the flight-number-specific intercept, PATTERN_j indicates j -th pattern in the set {Ring, Checkerboard, Spoke, 3-arm spiral, 4-arm spiral, 6-arm spiral, vertical stripes, horizontal stripes, grey}, $\text{PATTERN}_{j,i,s,f}$ indicates if j -th landing pattern is present for the i -th measurement from the f -th flight number in the s -th set (0 = no, 1 = yes), $\beta_j \forall j \in \{1, 2, \dots, 9\}$ represent the differences of fixed-effects (landing patterns) from the overall intercept, m represents the regression slope for predictor $\log(y^*)$, and σ is the residual standard deviation. The statistical output and the results from post-hoc tests are given in Table S5.4.

References

- Goyal, P., Cribellier, A., de Croon, G. C. H. E., Lankheet, M. J., van Leeuwen, J. L., Pieters, R. P. M. and Muijres, F. T. (2021). Bumblebees land rapidly and robustly using a sophisticated modular flight control strategy. *iScience* **24**, 102407.



Chapter 6

General discussion

Landing is mandatory for all flying animals and is arguably one of the most difficult flight behaviors (Baird et al., 2020). A successful landing requires precise control of flight speed with distance to the surface — poor control can result in high-impact collisions. This is especially important for bees that frequently land on flowers to gather food (Michener, 2007; Goulson, 2010) and are prone to permanent wing damage due to repeated collisions (Foster and Cartar, 2011; Mountcastle and Combes, 2014; Rajabi et al., 2020). Bees perform 100 to 1000 landings on flowers in a single hour of foraging to collect nectar and pollen, which are essential for their survival and reproduction (Ribbands, 1949; Heinrich, 1979, 2004; Goodwin et al., 2011; Couvillon et al., 2015).

Depending upon their ecological niche, bees perform these landings in a wide range of environmental conditions. For example, most bees forage during the day, including the commonly known ones such as bumblebees (*Bombus terrestris*) and honeybees (*Apis mellifera ligustica*) (Michener, 2007; Goulson, 2010). In contrast, there are few nocturnal bees such as sweat bees (*Megalopta genalis*) in Panama and carpenter bees (*Xylocopa tranquebarica*) in India which forage during the night (Kelber et al., 2006; Warrant, 2007; Somanathan et al., 2020). Despite their time of activity, all bees use vision during foraging (Land, 2004; Warrant et al., 2004; Warrant, 2007, 2008). In this thesis, I aimed to find how two diurnal bee species — bumblebees (*Bombus terrestris*) and honeybees (*Apis mellifera ligustica*) — use visual cues to control their flight speed with distance to the landing surface.

Understanding the control mechanism that underlies this behavior can provide crucial insights into their sensorimotor integration required for landing (Taylor et al., 2008; Huston and Jayaraman, 2011; Cowan et al., 2014; Roth et al., 2014; Dickinson and Muijres, 2016). It will also allow us to better understand their ecology (Shackleton et al., 2019; Baird et al., 2020; Tichit et al., 2020a). Furthermore, the knowledge of flight control in bees can also be useful for bioinspired control mechanisms in man-made aerial vehicles (Franceschini et al., 2007; Srinivasan, 2011b; Serres and Ruffier, 2017; Karásek et al., 2018).

In this thesis, I used novel analyses methods to determine the visual guidance strategy and the sensorimotor control system of bees. In **Chapter 2** (cited as Goyal et al. 2021 in text), I described how bumblebees use optical expansion cues to regulate their flight speed with distance to the surface during two types of landing maneuvers — the ones that occur immediately after a take-off and the others that occur from a free-flight condition. These maneuvers correspond to the types of landings that bumblebees exhibit when visiting closely situated flowers within a flower patch, and when landing after travelling between the flowers in different patches or to their hive, respectively. In **Chapter 3**, I described how bumblebees use the sensorimotor control system to control their flight speed in a moment-to-moment fashion. For this purpose, I used the natural excitation of the sensorimotor control system that bumblebees offer during landing. This was done for both types of landing maneuvers. Additionally, in both **Chapters 2 and 3**, I explored how the environmental light intensity and the strength of visual cues available on the landing surface affected the visual guidance strategy and the sensorimotor control during landing in bumblebees.

In **Chapter 4**, I examined how wind — a ubiquitous characteristic of the natural environment — affects the flight control of bumblebees during landing. Finally, in **Chapter 5**, I used the custom-developed analysis methodology to revise the landing strategy of honeybees proposed in literature (Baird et al., 2013).

In this general discussion, I place the knowledge gained in this thesis on the visual guidance and flight control of landing bees in a broader context of flight control in bees specifically, and flying animals in general. Moreover, I depict how this knowledge can be used for bioinspiration in man-made aerial vehicles.

For this purpose, I first integrated the important findings of this research with the existing literature about the landing and flight control in bees (Section 6.1). I then reflected on how birds might control their flight during landing (Section 6.2). Afterwards, I gathered useful insights that were gained from this research and could be applied to man-made aerial vehicles (Section 6.3). Finally, I built a case for relying on the analysis of individual maneuvers that could be utilized by future studies aimed at understanding insect flight control, especially during landing (Section 6.4). I also depicted the limitations of this research and proposed a direction for future research in the area of landing control.

6.1 How do bees land?

Like many day-active flying animals, bumblebees (*Bombus terrestris*) and honeybees (*Apis mellifera ligustica*) are suggested to rely on optical expansion cues to control their approach speed during landing (Lee et al., 1991, 1993; Van Breugel and Dickinson, 2012; Baird et al., 2013; Chang et al., 2016; Balebail et al., 2019; Liu et al., 2019; Shackleton et al., 2019; Tichit et al., 2020b). Their self-motion during a landing approach causes various features (vertices, edges etc.) in the visual scene to appear to expand radially outward from a point that is being approached (Gibson, 1955; Edwards and Ibbotson, 2007). A bee can use these expansion cues to measure the relative rate of expansion (r), which is also referred to as optical expansion rate (Lee, 1976; Wagner, 1982; Baird et al., 2013). The optical expansion rate r equals the ratio of their approach velocity V and their distance from the landing surface y as $r = V/y$ (Wagner, 1982; Baird et al., 2013).

To understand how bees use the optical expansion rate during landing, a method of averaging multiple landing maneuvers is commonly used in literature (Baird et al., 2013; Chang et al., 2016; Shackleton et al., 2019; Tichit et al., 2020b). In this method, the variation of approach velocity V with distance to the surface y is averaged over multiple landing maneuvers for a specific treatment condition. These treatments can be, for example, a particular graphical pattern on the landing platform or a light condition. Using this method, honeybees (*Apis mellifera ligustica*) are suggested to reduce their velocity linearly with distance (Baird et al., 2013). Based on this observation, it has been proposed that honeybees advance towards the landing surface by keeping the optical expansion rate constant at one set-point r^* . This consequently suggests that honeybees do not require the measurements

of either distance to the surface or their speed to perform touchdown at low flight velocity (Baird et al., 2013). Based on the analysis of averaging multiple landing maneuvers, a similar landing strategy has also been suggested to be present in bumblebees (*Bombus impatiens*), stingless bees (*Melipona scutellaris*, *Scaptotrigona depilis* and *Partamona helleri*) and fruit flies (*Drosophila melanogaster*), at least up until certain distance from the surface (Van Breugel and Dickinson, 2012; Chang et al., 2016; Shackleton et al., 2019; Baird et al., 2020; Tichit et al., 2020a).

In this thesis, I developed a new method that focused on analyzing the individual landing maneuvers instead of the average maneuver of recorded landings. This analysis methodology revealed that the aforementioned average analysis failed to capture the detailed dynamics of landing honeybees (*A. ligustica*) and bumblebees (*B. terrestris*). The results depict that both bumblebees and honeybees do not hold their optical expansion rate at a fixed set-point r^* throughout their approach. They instead approach the landing surface by stepwise modulating this set-point. Here, I synthesize the salient results of this research, including a comparison between the modular landing strategies of the two studied species, bumblebees and honeybees. Furthermore, I elucidate the contribution of this research to the existing knowledge in literature.

6.1.1 The visual guidance strategies of landing honeybees and bumblebees along with their comparison

The analysis of individual landing maneuvers in this research showed that both honeybees (*A. ligustica*, **Chapter 5**) and bumblebees (*B. terrestris*, Goyal et al. 2021) exhibit a similar modular landing strategy, but with some key differences. First, both honeybees and bumblebees exhibit a range of set-points during landing with distributions that can be captured by gamma distributions (Evans et al., 2000). However, honeybees exhibited a narrower distribution and higher mean set-point than bumblebees (Figure 6.1A). Second, both species increased their set-point with reducing distance to the surface, but honeybees increased it at a higher rate. This rate is captured by a slope m of the linear relationship between the logarithmic transformations of the set-point of optical expansion rate and the distance at which it is observed. This slope m is referred to as a time-to-contact-rate $\dot{\tau}$ (Baird et al., 2013; Goyal et al., 2021) and is equivalent to the parameter $\dot{\tau}$ used in literature to describe the landings of birds (Lee et al., 1991, 1993; Baird et al., 2013; Whitehead, 2020). Honeybees exhibited a higher time-to-contact-rate ($m = -0.258 [0.029]$, **Chapter 5**) as compared to the bumblebees ($m = -0.73 [0.01]$, **Chapter 2**) (Figure 6.1E) (mean [standard error]).

Despite having different slopes, the dependence of set-point with distance in both species suggests that they use an estimate of distance to the surface to modulate their set-point r^* during landing. This observation is especially pertinent as visual expansion cues provide the animal with the ratio of velocity and distance, but not these quantities sep-

arately. Moreover, unlike vertebrates, bees cannot estimate distances using binocular stereopsis (at least at the observed distances) or focal adjustment (Srinivasan, 1992). There are different possibilities on how these bees may estimate the distance to the surface for set-point adjustment, but more research is required to find the underlying mechanism (Corke and Good, 1992; Van Breugel et al., 2014; de Croon, 2016; Ho et al., 2017; Baird et al., 2021; de Croon et al., 2021).

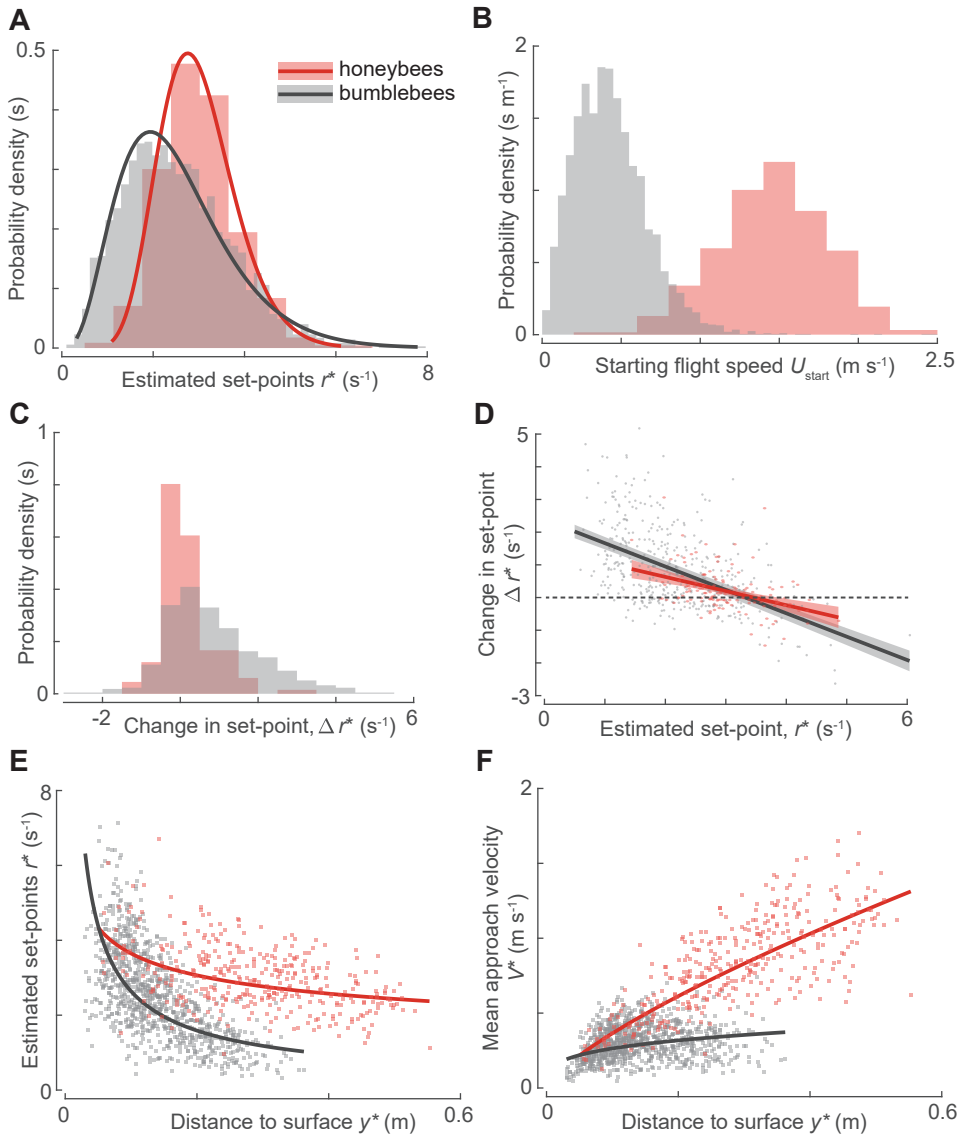
Another key aspect for comparison is the set-point switching behavior of honeybees and bumblebees. The results from **Chapter 5** depicted that the switch to a new set-point within a landing maneuver, on average, depended on the current set-point r^* at which honeybees were flying. They were more likely to decrease or increase their set-point if their current set-point was higher or lower than their switch-reversal set-point ($r_0^* = 3.14 \text{ s}^{-1}$). To make the comparison of this behavior between the two species, I first analyzed this behavior in bumblebees landing from a free-flight condition as this closely resembled the landings in honeybees. I found that the switch-reversal set-point in bumblebees is dependent on the environmental light intensity. It is 43% higher in the highest tested light intensity (144.9 lx, $r^* = 3 \text{ s}^{-1}$) than in the lowest tested light intensity (13.7 lx, $r^* = 2.1 \text{ s}^{-1}$) (Table 6.1). In comparison to honeybees, bumblebees exhibited a very similar switch-reversal set-point in the highest tested light condition (only a difference of 4.5%), but a 62.8% lower slope of change in the set-point (Δr^*) with the current set-point (r^*) (Figure 6.iD). In addition, bumblebees switched to a higher set-point more often (72.7%) as compared to honeybees (51.5%) and exhibited a wider Δr^* distribution (Figure 6.iC).

The aforementioned differences among the landing strategies of honeybees and bumblebees could arise from the differences between the two species or the differences in their speeds at the beginning of their landing maneuvers (Figure 6.iB). The latter factor likely contributed more strongly since honeybees were flying faster at the start of their landing tracks. In contrast, after following their landing strategy, they exhibited approach velocities similar to bumblebees near the landing surface (Figure 6.iD). Thus, the studied honeybees had to slow down more rapidly, explaining why they increased their set-point less often and adjusted their set-point with distance at a higher rate. This eventually can lead to honeybees producing more braking force as compared to bumblebees during their landing maneuver.

The differences in the initial speeds between the two tested species was probably a combined result of the differences in the light intensities during the experiments, and the maximum distance available in front of the landing platforms. To ascertain the exact cause of these differences, an additional study is needed wherein the landing maneuvers of different insects can be recorded with a systematic variation in the environmental conditions and the distance in front of the landing platform.

In conclusion, it can be said that the analysis of individual landing maneuvers of both bumblebees and honeybees revealed a visual guidance strategy that is more sophisticated than the simpler strategy suggested previously in the literature (Baird et al., 2013; Chang et al., 2016). Moreover, this discussion also indicates that honeybees and bumblebees in the

most similar conditions exhibit these sophisticated strategies in surprisingly similar ways. For example, both exhibit set-point modulation during landing and have only 4.5% difference in the switch-reversal set-point.



(Caption on the next page.)

Figure 6.1: Comparison of the landing strategies observed in honeybees (red; Chapter 5) and bumblebees (gray; Goyal et al. 2021). (A–C) The probability density of (A) the set-points of relative rate of expansion r^* , (B) the starting 3D flight speeds U_{start} , and (C) the change in set-point between two consecutive constant- r segments Δr^* for the landings of honeybees (red) and bumblebees (gray). (D) The variation of change in set-point Δr^* with the set-point magnitude r^* for honeybees (red, Table S5.3) and bumblebees (gray, Table 6.1). (E,F) The variation of (E) the set-points of relative rate of expansion r^* and (F) the mean approach velocity V^* with mean distance to the landing platform y^* , for honeybees (red) and bumblebees (gray) as they approached a landing surface. (D–F) The data points show the results of all identified constant- r segments, and the curves show the statistical model outputs (and 95% confidence intervals in panel (D)). The bumblebee results (gray data) are of bumblebees landing from free-flight on a vertical landing platform in sunrise light conditions (144.9 lx) (results are averaged over checkerboard and spokes patterns) (see Goyal et al. 2021 for details). Note that the solid lines in panels E and F also correspond to the theoretical curves that would result from following the constant time-to-contact-rate τ landing strategies suggested in birds (Lee et al., 1991, 1993; Whitehead, 2020).

Table 6.1: The analysis of transition between the set-points of relative rate of expansion observed in bumblebees during their approach towards a landing surface. The data is extracted from 1,122 transitions in 902 landing maneuvers of bumblebees. In these maneuvers, bumblebees landed from a free-flight condition and exhibited more than one constant- r segment. (statistical model: $\Delta r_{i,d,a,s}^* \sim N(\alpha + \alpha_d + \alpha_a + \alpha_s + \beta_1 r_{i,d,a,s}^* + \beta_2 \text{MEDIUMlight} + \beta_3 \text{HIGHlight}, \sigma^2)$), the description of variables in the model is similar to Equation S5.3).

Fixed effect	Estimate	Std error	t value	Pr(> t)
α	1.42	0.11	13.21	$9.57E - 05$
β_1	-0.71	0.03	-20.48	$2.56E - 79$
β_2	0.32	0.07	4.51	$7.24E - 06$
β_3	0.73	0.07	10.24	$1.48E - 23$

6.1.2 Landing after take-off versus landing from free-flight

The bumblebees in the experimental setups, described in **Chapter 2** (Goyal et al., 2021) and **Chapter 4**, landed on a surface either directly after a take-off or from a free-flight. These landings resemble the landings of bees in nature when they visit flowers within a flower patch, or when they fly between flower patches (Heinrich, 1979). The research in this thesis revealed how these landing maneuvers differ from each other (Goyal et al., 2021). The analysis based on the individual maneuvers suggested that bumblebees adjusted their variation of set-point with distance (time-to-contact-rate m) in order to land more rapidly after a take-off than from a free-flight. This was observed in all tested abiotic conditions (**Chapter 2**: visual cues and light intensity; **Chapter 4**: various wind speeds). This functional adjustment of varying set-point differently with distance depending upon the starting condition of landing may have been shaped by the ecology of bumblebees. They may have learned to perform these landings more precisely and routinely in order to rapidly explore flowers within a flower patch. However, for insects such as flies that do not seemingly have a bias towards performing landings from one starting condition, this vari-

ation among starting conditions in set-point adjustment might be negligible. To test this hypothesis, more research in identifying the behavior and ecology of different insects is warranted.

Note that this difference between the landings after a take-off or from free-flight can also be influenced by the movement of the bumblebees parallel to the landing disc. While advancing towards the surface, bumblebees need to adjust their position in a direction parallel to the surface to reach closer to the desired landing location on a vertical platform. The bumblebees landing from free-flight are expected to start their maneuver more laterally to the platform as compared to the bumblebees landing after a take-off from the opposite platform. The presence of lateral distance at the start of the maneuver results in a different retinal image of the visual landing pattern compared to when a bumblebee starts its maneuver directly in front of the platform. Thus, the lateral distance can potentially influence how expansion cues are used during landing. More research is needed to understand the effect of the presence of lateral distance on the variation between the two landing types.

It is also important to mention that bumblebees in our experimental setups performed fewer landings directly after a take-off than from a free-flight condition (Goyal et al. 2021, **Chapter 4**). This is in contrast to more landings expected in nature after a take-off as compared to the landings from free-flight. This probably happened because, after visiting the food source, bumblebees in our setup may have continued to another foraging flight instead of going back to the hive. This is similar to what they would do in nature where *ad libitum* access to the food is not expected to be present so close to the hive. Such foraging behavior would subsequently result in bumblebees landing from a free-flight condition on either of the two landing platforms available in our setup. Over time, this would aggregate in more landings from the free-flight condition than after a take-off.

6.1.3 A mechanism to both decelerate and accelerate during landing

The results in **Chapter 2** revealed that the bumblebees modulated their set-point within a landing approach in a stepwise manner. This revelation allowed me to circumvent the need of designing a new experimental setup for exciting their sensorimotor control dynamics. The excitation is needed to understand how an animal uses its different subsystems (controller, sensory system, motor system) together to exhibit a certain behavior (Taylor et al., 2008; Cowan et al., 2014; Roth et al., 2014; Dickinson and Muijres, 2016; Stöckl et al., 2017). It is usually achieved by exposing the system (here a landing bee) to well-defined known inputs such as a step or a sinusoidal input (Verhaegen and Verduyt, 2007). Here, such excitations occurred naturally every time a bee switched to a new set-point.

We used these natural stepwise excitations of the closed-loop control system offered by bumblebees to verify that they land by regulating the optical expansion rate in a moment-to-moment fashion. Our results indicated that the landing bumblebees produced control

forces (causing body accelerations due to change in wing and body kinematics) to reach their estimated set-points of optical expansion rate (**Chapter 3**).

This analysis also showed that bumblebees mostly used the transient response of their stepwise excitation to accelerate towards the surface and the steady-state phase to always decelerate. This result uncovered a functional mechanism by which an animal can decelerate as well as accelerate towards a landing surface.

A similar mechanism might have been used by *Partamona belleri* (Shackleton et al., 2019) and *Scaptotrigona depilis* (Tichit et al., 2020b) stingless bees, which are reported to accelerate towards the surface near the end of the landing maneuver (Baird et al., 2020). Note that the acceleration phases in these bees are observed using an analysis based on the average of landing maneuvers, and thus, there is a possibility that these phases could be present even at distances farther from the ones reported in the literature. This can be ascertained by using an analysis based on the individual landing maneuvers, similar to the one developed in this study.

Despite this caveat, acceleration phases during landing offer several advantages. In literature, the stingless bees are suggested to exhibit this acceleration phase as a possible adaptation for defending the nest entrance from the predators or to reduce the traffic congestion near it (Shackleton et al., 2019; Tichit et al., 2020a). Our results depicted that the stepwise adjustment of the set-point along with these acceleration phases allowed bumblebees to land quicker than when they would follow the constant set-point strategy suggested previously in literature (Goyal et al., 2021).

6.1.4 Effect of environmental conditions

In this research, we explored how the strength of expansion cues (**Chapters 2, 3**), light intensity (**Chapter 2, 3**) and wind (**Chapter 4**) influenced the landing strategy and the sensorimotor control system of bumblebees (*Bombus terrestris*). Here, I synthesize the results for each environmental condition successively.

Bumblebees land more cautiously in the presence of weak expansion cues

We tested how bumblebees adjusted their guidance strategy during landing in the presence of different strengths of expansion cues (**Chapters 2, 3**). For this purpose, we offered bumblebees two landing patterns, namely checkerboard and spoke patterns, that provided them relatively stronger and weaker expansion cues, respectively. We found that bumblebees modulated their set-point of optical expansion rate with distance differently for these two patterns (**Chapter 2**).

During cruising flight, which is based on the front-to-back translatory optic flow, diurnal bees are shown to exhibit faster speeds in the presence of weak optic cues (Baird, 2005;

Barron and Srinivasan, 2006; Baird et al., 2010, 2011; Linander et al., 2015; Baird et al., 2020, 2021). Based on these results, one can expect that landing bees would end up flying close to the surface at higher approach velocities, and hence, with higher momentum in the presence of reduced expansion cues. But we consistently observed the opposite in bumblebees (**Chapter 2**), suggesting that they adapt their landing behavior based on the type of landing platform. When optic expansion cues were weak, they adjusted their set-point with distance to perform more careful landings (**Chapter 2**). Additionally, our results in **Chapter 3** showed that bumblebees were able to exhibit similar sensorimotor control responses in the presence of both landing patterns. Combined together, these observations suggest that the visual system of bumblebees is capable of extracting the expansion cues from either of the landing platforms, but bumblebees still exhibit a more cautious approach in the presence of weaker expansion cues. They may have evolved this strategy as a precautionary measure to avoid high-impact collisions.

It is important to mention that no significant differences were observed between the landings on the checkerboard and spoke patterns in honeybees (**Chapter 5**). This was probably due to the low number of landings recorded for each landing pattern in the case of honeybees.

Landing bumblebees adjust both their set-point and sensorimotor control response in dim light conditions

Vision becomes less reliable in dim light (Reber et al., 2015). This happens partly due to an increase in shot noise relative to the visual signal along with the transducer and dark noises at low light levels (Barlow, 1956; Lillywhite, 1977, 1981; Lillywhite and Laughlin, 1979; Laughlin and Lillywhite, 1982; Warrant and McIntyre, 1993; Warrant, 2008; Reber et al., 2015, 2016). However, the bumblebees can forage early in the morning as well as late in the evening (Spaethe and Weidenmüller, 2002). Like other insects and nocturnal bees, they are able to do this because they possess adaptations to control their flight under low light conditions (Rose and Menzel, 1981; Greiner et al., 2004; Warrant et al., 2004; Spiewok and Schmolz, 2006; Frederiksen and Warrant, 2008; Reber et al., 2015, 2016; Sponberg et al., 2015; Reber et al., 2016). In this thesis, we analyzed how bumblebees control their landing approach in three light intensities ranging from twilight to sunrise (**Chapters 2, 3**).

During cruising flight, which is based on the translatory front-to-back optic cues, bumblebees fly at lower speeds and exhibit an increase in photoreceptor integration time with a decrease in light intensity (Baird et al., 2015; Reber et al., 2015). But, it is not known how this behavioral adaptation (reduced flight speeds) is mechanistically achieved or how this retinal adaptation (increased integration time) influences the sensorimotor control mechanism of bumblebees.

We found answers to these questions in landing bumblebees which could also be applicable to the cruising bumblebees. Our results showed that landing bumblebees exhibited

a behavioral adaptation similar to that observed in cruising bumblebees — they flew slower in dim light. They mechanistically achieved this adaptation by exhibiting a lower set-point of optical expansion rate in lower light intensity (Chapter 2). Moreover, our results also showed that bumblebees exhibited a slower sensorimotor control response in lower light intensity (Chapter 3). This could be a result of the potentially increased latency in the measurement of optical expansion rate owing to the increased integration time of photoreceptors in dim light or other adaptations such as lower controller gain in dim light.

Landing bumblebees adjust both their set-point and sensorimotor control response to compensate for the adverse effect of steady sidewinds

Insects regularly experience winds in the natural environment. These winds are often characterized as a combination of mean flow and the fluctuations around it (Stull, 1988; Garratt, 1994). The effect of these winds on the landing dynamics of insects (Chang et al., 2016) has received little attention in literature compared to their effect on free-flight (Barron and Srinivasan, 2006; Fuller et al., 2014; Ravi et al., 2015; Engels et al., 2016; Shepard et al., 2016; Crall et al., 2017; Baird et al., 2021; Laurent et al., 2021). In this research, we investigated the landing dynamics of bumblebees in the presence of different steady winds ranging from 0 to 3.41 m s^{-1} in a direction parallel to the landing surface (Chapter 4). Bumblebees regularly experience such crosswinds in nature (Riley et al., 1999; Peat and Goulson, 2005; Crall et al., 2017).

In the presence of steady sidewinds, we found that bumblebees exhibited a visual guidance strategy and sensorimotor control response similar to that in still air, but with some noteworthy differences (Chapter 4). Compared to still air, bumblebees more often exhibited low approach velocity phases ($V < 0.05 \text{ m s}^{-1}$) in higher winds. This phenomenon is detrimental to their foraging efficiency as it can lead to an increase in their travel time. But, bumblebees compensated for this potential increase in travel time by adjusting their set-point of optical expansion rate and the sensorimotor control response with wind speed. As a result, they exhibited faster transient response and higher set-points in higher winds, which enabled them to travel rapidly towards the landing surface. With these adaptations, bumblebees were able to fully compensate for the increase in travel time when they landed from a free-flight, but only partly when they landed shortly after a take-off.

Moreover, the steady wind inputs in our experimental setup ensured that bumblebees experienced the same wind speed throughout their landing approach (until 4 cm distance from the landing surface). As the change in wind speed leads to a change in the airspeed, I analyzed how the mean acceleration (mean control force per unit mass) during the transient response of the sensorimotor control system varied with different airspeeds. This was done to understand how landing bumblebees integrated information from an airspeed measuring mechanoreceptor, possibly antennae (Taylor and Krapp, 2007; Jakobi et al., 2018), with their visual feedback loop (proposed in Chapter 3).

I found a linear relationship between the mean acceleration and the airspeed, suggesting that the landing bumblebees have a positive feedback with a constant gain from their airspeed measuring mechanosensory modality to their vision based regulator (**Chapter 4**). Free-flying *Drosophila* are suggested to possess a similar multi-sensor control architecture (Fuller et al., 2014). This positive feedback from the fast antennal system provides active damping to the relatively slow vision-based regulator. Similar active damping has been observed in numerous other scenarios of insect flight (Cowan et al., 2006; Hedrick et al., 2009; Cheng and Deng, 2011; Hedrick, 2011; Elzinga et al., 2012; Dyhr et al., 2013; Taylor et al., 2013; Sun, 2014).

In **Chapter 4**, I also analyzed how the occurrence of low approach velocity phases varied with distance to the landing surface, the wind conditions and the landing types (landings starting from take-off or free-flight). The results from this analysis provided support to the hypothesis that the low approach velocity phases are the result of instabilities arising out of a closed-loop controller that uses optical expansion rate as a control variable (de Croon, 2016; Goyal et al., 2021). These results revealed an adverse effect of wind on the landing dynamics along with the compensation mechanism of bumblebees. Moreover, they provided insights into the multi-modal sensorimotor control architecture and the low approach velocity phases of landing bumblebees.

Despite these new interesting insights, more research is needed to completely understand how natural winds affect the landing dynamics in bumblebees and how they cope with these effects. This is because natural winds comprise of mean flow and the fluctuations around it. Moreover, winds can cause swaying of flowers (Kapustjansky et al., 2009; Hennessy et al., 2020), which may make it difficult for the bumblebees to reliably extract the visual expansion cues. The combination of the mean flow, fluctuations around it, and the swaying of flowers likely pose additional challenges for the sensorimotor control system of the landing bumblebees. How bumblebees mitigate this combination of wind effects still remains to be uncovered.

6.2 How do birds land?

Similar to the analysis of landing dynamics in insects, the method of averaging multiple landing maneuvers has been used in the literature to understand how birds land (Lee et al., 1991, 1993; Whitehead, 2020). This method revealed that, in contrast to bees, pigeons (*Columba livia*), hummingbirds (*Colibri coruscans*) and mallard ducks (*Anas platyrhynchos*) might hold the time-to-contact-rate $\dot{\tau}$ constant during their landing approach ($\dot{\tau}$ is represented above as a parameter m) (Lee et al., 1991, 1993; Whitehead, 2020). The landing strategies of bees identified in this research can be recognized as a discrete approximation of the landing strategy of birds (Goyal et al., 2021). This is because the visual guidance strategy of bees results in a stepwise increase of the optical expansion rate with reducing distance to the surface, whereas the visual guidance of birds results in a continuous increase in the optical expansion rate with reducing distance (Goyal et al., 2021).

How do birds execute their visual guidance strategy? To my knowledge, it is currently not known how birds use their sensorimotor control system in a moment-to-moment fashion to exhibit the constant time-to-contact-rate guidance strategy during landing. In contrast to bees, many birds can estimate the distance to the surface using stereopsis or head movements (Davies and Green, 2012). This distance estimate can allow birds to solve the spatiotemporal problem of decreasing their approach velocity with reducing distance to the surface in a manner similar to how humans solve the visually guided problem of braking. Humans perform this braking task for example, when grasping an object or when decelerating at the end of a lane changing maneuver during driving (Bardy and Warren, 1997; Chatziastros and Buelthoff, 2002; Hecht and Savelsbergh, 2004; Rock et al., 2006; DeLucia and Tharanathan, 2009; Anderson and Bingham, 2010, 2011). More experimental studies involving birds are required to understand the sensorimotor control that underlies their landing behavior.

6.3 Bioinspiration for man-made aerial vehicles

The optical expansion rate provides bumblebees and honeybees with the ratio of their speed and distance to the surface, but not these quantities separately. This situation is similar to the one in a drone where a single camera is used (e.g., due to weight limitations) for controlling the landing approach (de Croon, 2016; Ho et al., 2017). Hence, an understanding of how bees use these cues to control their speed during landing can inspire monocular vision-based methods of landing control in man-made systems (Srinivasan, 2011b; Serres and Ruffier, 2017).

In this research, both bumblebees and honeybees are shown to exhibit a guidance strategy of actively adjusting their set-point of optical expansion rate. This set-point adjustment offers several advantages. It allows them to (a) land rapidly (**Chapter 2**), (b) fly slowly and compensate for the increase in photoreceptor integration time in dim light conditions (**Chapters 2, 3**), (c) approach a surface with weaker expansion cues more carefully (**Chapter 2**), and (d) compensate for the adverse effect of steady sidewinds during landing. This mechanism of set-point adjustment can be employed in man-made aerial vehicles for fast landing or to adapt to the changes in the environmental conditions.

In addition, the adjustment of set-point of optical expansion rate during landing can be used as a method to make the distance to the surface observable with monocular vision (observability analysis similar to Van Breugel et al. 2014 and Ho et al. 2017 will hold for the landing trajectories involving the set-point adjustment). The estimates of distance can be obtained by using any of the following methods: (a) using the transient (Corke and Good, 1992) and steady-state phases (Van Breugel et al., 2014) of the step-response of optical expansion rate, (b) using known control inputs in an extended Kalman filter (Ho et al., 2017), (c) exploiting the dependency of onset of oscillations in optical expansion rate on the distance to the surface (de Croon, 2016).

Our results also suggest that bumblebees use an estimate of airspeed to control their flight in the presence of winds during landing. This suggests a need of an airspeed sensor to be present onboard drones for them to be as nimble as a bee while mitigating the effects of winds.

6.4 Perspectives on flight control in bees

6.4.1 Moving towards the analyses based on individual maneuvers

In this study, I used two methodologies to understand how bees land — one based on the average dynamics of multiple recorded landing maneuvers (also used in the literature) and the other based on the individual landing maneuvers (developed in this research).

The results in **Chapters 2, 4 and 5** show that the average landing maneuver failed to capture the actual visual guidance strategy of individual bees. This happened because the averaging of multiple landing maneuvers over a distance normal to the surface does not account for the phase in which the animal is at a particular distance and point in time. In landing bees, this phase can be: (1) an ‘entry’ transient phase when the animal is converging towards the desired set-point of optical expansion rate, (2) a ‘steady-state’ phase when the animal is flying near the set-point, or (3) an ‘exit’ transient phase when the animal starts to hover or flies away from the surface for a short period. As at different distances from the surface, the landing bees can be in any of these phases, averaging multiple maneuvers can lead to very different dynamics than that exhibited by individual bees.

For example, as environmental light intensity increased, the average landing maneuver suggested that bumblebees increased their optical expansion rate set-point — a behavior also observed by analyzing the individual maneuvers (**Chapter 2**). In contrast, with increase in wind speeds, the average landing maneuver suggested that bumblebees decreased or kept their set-point the same — a behavior opposite to the one depicted by the analysis of individual maneuvers (**Chapter 4**). Thus, it can be said that averaging multiple maneuvers can lead to the suppression of transients that are useful in accurately depicting the landing behavior of an animal.

In the analysis of individual maneuvers, this limitation was circumvented by first identifying the different phases of the sensorimotor control system in the landing maneuvers of bees, and then analyzing these phases separately to understand their landing dynamics (see **Chapters 2, 3 and 4** for details about the extraction and analysis of the steady-state, entry transient and exit transient phases, respectively). The analysis of the individual maneuvers revealed that the landing bees are capable of performing more sophisticated control with their small brain than previously suggested by the average analysis. The notable examples are the ability to step-wise modulate and track a set-point within a landing approach, possibly able to use an estimate of the distance to the surface during landing, and adjusting both the set-point and the sensorimotor control to deal with the challenging environmental conditions (low light intensity, weak expansion cues and fast winds) during

their landing approach.

It is important to mention that if an animal is likely to exhibit only a single phase during flight, the analysis of an average of the recorded landing maneuvers can be adequate to find out its characteristics e.g., when honeybees were flying near a set-point during grazing landings or cruise-flight (Srinivasan et al., 2000; Srinivasan, 2011a,b). It can then also be used to find how the desired set-point changes with the environmental conditions e.g., when honeybees were flying near a set-point in the presence of different headwinds and tailwinds (Baird et al., 2021). This method only fails when different phases of the sensorimotor control system occur at the same distance in multiple maneuvers such as during landing approaches of bees on the vertical surfaces (**Chapters 2 – 5**).

Though extremely useful, there are challenges involved in using the analysis methodology based on individual maneuvers for studying the landing dynamics of an animal. First, a large number of landing maneuvers have to be recorded. These can be difficult to gather if an animal is hard to train in a desired experimental setup or if the animal under investigation is not a relentless lander. This problem can be solved, in part, by performing the experiments for longer duration and using an experimental setup that can automatically gather data in real-time. Second, it may not be possible to extract the transient or the steady-state phases of a sensorimotor control response. This can happen when the sensory measurement being used for the landing control is not known, for example in birds (Section 6.2).

Despite these associated challenges, I propose that (if possible) the future studies aimed at understanding the flight control in animals, especially landing, should analyze the individual maneuvers rather than the average of multiple maneuvers.

6.4.2 A limitation of this research

In addition to the limitations of the methods that are explained in individual studies (**Chapters 2 – 5**), here, I present a limitation of the whole research.

In this research, we identified the role of optic expansion cues in the landing dynamics of bees. For this purpose, we only considered the motion of a bee towards the landing surface. However, a landing bee can also exhibit a substantial motion in the directions parallel to the landing surface (Figures 2.4, 4.4 and 5.3). This motion corresponds to a bee changing its lateral or vertical position to reach closer to the desired location on the landing surface. This self-motion of bees parallel to the landing surface can cause translational optic flow in their retina. Moreover, bumblebees are observed to have different body orientations during their landing approach e.g., when landing after a take-off (Figure 2.2) or when landing in the presence of winds (Figure 4.2). These body rotations can cause rotational optic flow in their retina. The role of this translational and rotational optic flow in the landing dynamics of bees is not addressed in this thesis and still remains to be uncovered.

6.4.3 Gaining more knowledge about the landing dynamics of bees

The modular landing strategy identified in this research is exhibited by both honeybees and bumblebees. It is therefore likely that other diurnal bee species also exhibit this modular landing strategy. Other bee species may have evolved a specialized version of this modular landing strategy to serve a particular ecological function e.g., stingless bees may have learned to increase their set-point closer to the hive in order to reduce traffic congestion near its entrance (Section 6.1).

In contrast to diurnal bees, there are few other bee species (*ca.* 250) that are nocturnal and belong to the families Andrenidae, Apidae, Colletidae and Halictidae (Wcislo and Tierney, 2009). These bees possess visual adaptations that render them more sensitive to light (Greiner et al., 2004), but the role of optic cues in their flight control (including landing) is not yet completely understood (Baird et al., 2020). Along with the diel activity, other factors such as variations within species (sex, caste, and size) or habitat differences influence the visual ecology of bees (Tichit, 2021) and thus, they may also shape their visual guidance strategy during landing. But we currently do not have enough data to understand these effects.

In addition to identifying the landing strategy, the research in this thesis also focused on understanding how different subsystems (sensory system, motor system and controller) of bumblebees work together to execute this visual guidance strategy. The next step in future research on landing control may focus on finding the neural basis of individual subsystems and the connections between them. This would shed light on the underlying physiological mechanisms that enable the execution of sequence of steps in the feedback loop. These steps correspond to obtaining the sensory measurement, setting a set-point (and stepwise changing it), comparing the set-point with the sensory measurement and producing motor actions to bring the sensory measurement closer to the set-point. There is some knowledge available about the underlying neural basis of optic-flow-based flight control in honeybees (Srinivasan, 2011a; Ibbotson et al., 2017) and flies (e.g. see Vogt and Desplan 2007; Silies et al. 2014; Suver et al. 2016). But the neural basis of estimating the relative rate of expansion from optic flow still remains elusive (Balebail et al., 2019). More neuroethological studies are required to identify the neurons that estimate the relative rate of expansion in insects and form the basis of the proposed control feedback loop.

References

- Anderson, J. and Bingham, G. P. (2010). A solution to the online guidance problem for targeted reaches: Proportional rate control using relative disparity τ . *Experimental Brain Research* 205, 291–306.
- Anderson, J. and Bingham, G. P. (2011). Locomoting-to-reach: Information variables and control strategies for nested actions. *Experimental Brain Research* 214, 631–644.

- Baird, E. (2005). Visual control of flight speed in honeybees. *Journal of Experimental Biology* 208, 3895–3905.
- Baird, E., Boeddeker, N., Ibbotson, M. R. and Srinivasan, M. V. (2013). A universal strategy for visually guided landing. *Proceedings of the National Academy of Sciences of the United States of America* 110, 18686–18691.
- Baird, E., Boeddeker, N. and Srinivasan, M. V. (2021). The effect of optic flow cues on honeybee flight control in wind. *Proceedings of the Royal Society B: Biological Sciences* 288, 20203051.
- Baird, E., Fernandez, D. C., Wcislo, W. T. and Warrant, E. J. (2015). Flight control and landing precision in the nocturnal bee *Megalopta* is robust to large changes in light intensity. *Frontiers in Physiology* 6, 1–7.
- Baird, E., Kornfeldt, T. and Dacke, M. (2010). Minimum viewing angle for visually guided ground speed control in bumblebees. *Journal of Experimental Biology* 213, 1625–1632.
- Baird, E., Kreiss, E., Wcislo, W., Warrant, E. and Dacke, M. (2011). Nocturnal insects use optic flow for flight control. *Biology Letters* 7, 499–501.
- Baird, E., Tichit, P. and Guiraud, M. (2020). The neuroecology of bee flight behaviours. *Current Opinion in Insect Science* 42, 8–13.
- Balebail, S., Raja, S. K. and Sane, S. P. (2019). Landing maneuvers of houseflies on vertical and inverted surfaces. *PLoS ONE* 14, 1–17.
- Bardy, B. G. and Warren, W. H. (1997). Visual control of braking in goal-directed action and sport. *Journal of Sports Sciences* 15, 607–620.
- Barlow, H. B. (1956). Retinal Noise and Absolute Threshold. *JOSA, Vol. 46, Issue 8, pp. 634-639* 46, 634–639.
- Barron, A. and Srinivasan, M. V. (2006). Visual regulation of ground speed and head-wind compensation in freely flying honey bees (*Apis mellifera* L.). *Journal of Experimental Biology* 209, 978–984.
- Chang, J. J., Crall, J. D. and Combes, S. A. (2016). Wind alters landing dynamics in bumblebees. *The Journal of Experimental Biology* 219, 2819–2822.
- Chatziastros, A. and Buelthoff, H. H. (2002). Prospective control of lane changing and tau-dot. *Journal of Vision* 2, 639–639.
- Cheng, B. and Deng, X. (2011). Translational and rotational damping of flapping flight and its dynamics and stability at hovering. *IEEE Trans Robot* 27, 849–864.
- Corke, P. I. and Good, M. C. (1992). Dynamic effects in high-performance visual servoing. *Proceedings - IEEE International Conference on Robotics and Automation* 2, 1838–1843.
- Couvillon, M. J., Walter, C. M., Blows, E. M., Czaczkes, T. J., Alton, K. L. and Ratnieks, F. L. (2015). Busy Bees: Variation in Insect Flower-Visiting Rates across Multiple

- Plant Species. *Psyche (London)* 2015.
- Cowan, N., Lee, J. and Full, R. (2006). Task-level control of rapid wall following in the American cockroach. *Journal of Experimental Biology* 209, 1617–1629.
- Cowan, N. J., Ankarali, M. M., Dyhr, J. P., Madhav, M. S., Roth, E., Sefati, S., Sponberg, S., Stamper, S. A., Fortune, E. S. and Daniel, T. L. (2014). Feedback control as a framework for understanding tradeoffs in biology. *Integrative and Comparative Biology* 54, 223–237.
- Crall, J. D., Chang, J. J., Oppenheimer, R. L. and Combes, S. A. (2017). Foraging in an unsteady world: Bumblebee flight performance in fieldrealistic turbulence. *Interface Focus* 7.
- Davies, M. N. O. and Green, P. R. (2012). *Perception and Motor Control in Birds: An Ecological Approach*. Springer Berlin Heidelberg.
- de Croon, G. C. H. E. (2016). Monocular distance estimation with optical flow maneuvers and efference copies: a stability-based strategy. *Bioinspiration & Biomimetics* 11, 016004.
- de Croon, G. C. H. E., De Wagter, C. and Seidl, T. (2021). Enhancing optical-flow-based control by learning visual appearance cues for flying robots. *Nature Machine Intelligence* 3, 33–41.
- DeLucia, P. R. and Tharanathan, A. (2009). Responses to Deceleration During Car Following: Roles of Optic Flow, Warnings, Expectations, and Interruptions. *Journal of Experimental Psychology: Applied* 15, 334–350.
- Dickinson, M. H. and Mujires, F. T. (2016). The aerodynamics and control of free flight manoeuvres in *Drosophila*. *Philosophical Transactions of the Royal Society B: Biological Sciences* 371, 20150388.
- Dyhr, J. P., Morgansen, K. A., Daniel, T. L. and Cowan, N. J. (2013). Flexible strategies for flight control: an active role for the abdomen. *Journal of Experimental Biology* 216, 1523–1536.
- Edwards, M. and Ibbotson, M. R. (2007). Relative sensitivities to large-field optic-flow patterns varying in direction and speed. *Perception* 36, 113–124.
- Elzinga, M., Dickson, W. and Dickinson, M. (2012). The influence of sensory delay on the yaw dynamics of a flapping insect. *J R Soc Interface* 9, 1685–1696.
- Engels, T., Kolomenskiy, D., Schneider, K., Lehmann, F. O. and Sesterhenn, J. (2016). Bumblebee Flight in Heavy Turbulence. *Physical Review Letters* 116, 1–5.
- Evans, M., Hastings, N. and Peacock, B. (2000). *Statistical Distributions*. Wiley Series in Probability and Statistics. Wiley.
- Foster, D. J. and Cartar, R. V. (2011). What causes wing wear in foraging bumble bees? *Journal of Experimental Biology* 214, 1896–1901.
- Franceschini, N., Ruffier, F. and Serres, J. (2007). A Bio-Inspired Flying Robot Sheds

Light on Insect Piloting Abilities. *Current Biology* 17, 329–335.

- Frederiksen, R. and Warrant, E. J.** (2008). Visual sensitivity in the crepuscular owl butterfly *Caligo memnon* and the diurnal blue morpho *Morpho peleides*: a clue to explain the evolution of nocturnal apposition eyes? *Journal of Experimental Biology* 211, 844–851.
- Fuller, S. B., Straw, A. D., Peek, M. Y., Murray, R. M. and Dickinson, M. H.** (2014). Flying *Drosophila* stabilize their vision-based velocity controller by sensing wind with their antennae. *Proceedings of the National Academy of Sciences* 111, E1182—E1191.
- Garratt, J. R.** (1994). The atmospheric boundary layer. *Earth-Science Reviews* 37, 89–134.
- Gibson, J. J.** (1955). The optical expansion-pattern in aerial locomotion. *The American journal of psychology* 68, 480–484.
- Goodwin, R., Cox, H., Taylor, M., Evans, L. and McBrydie, H.** (2011). Number of honey bee visits required to fully pollinate white clover (*Trifolium repens*) seed crops in Canterbury, New Zealand. *New Zealand Journal of Crop and Horticultural Science* 39, 7–19.
- Goulson, D.** (2010). *Bumblebees: Behaviour, Ecology, and Conservation*. Oxford biology. OUP Oxford.
- Goyal, P., Cribellier, A., de Croon, G. C. H. E., Lankheet, M. J., van Leeuwen, J. L., Pieters, R. P. M. and Muijres, F. T.** (2021). Bumblebees land rapidly and robustly using a sophisticated modular flight control strategy. *iScience* 24, 102407.
- Greiner, B., Ribí, W. A. and Warrant, E. J.** (2004). Retinal and optical adaptations for nocturnal vision in the halictid bee *Megalopta genalis*. *Cell and Tissue Research* 2004 316:3 316, 377–390.
- Hecht, H. and Savelsbergh, G. J. P.** (2004). *Time-to-contact*. Elsevier, 509 pp.
- Hedrick, T.** (2011). Damping in flapping flight and its implications for manoeuvring, scaling and evolution. *Journal of Experimental Biology* 214, 4073–4081.
- Hedrick, T., Cheng, B. and Deng, X.** (2009). Wingbeat Time and the Scaling of Passive Rotational Damping in Flapping Flight. *Science* 324, 252–255.
- Heinrich, B.** (1979). Resource heterogeneity and patterns of movement in foraging bumblebees. *Oecologia* 40, 235–245.
- Heinrich, B.** (2004). *Bumblebee economics*. Harvard University Press, 245 pp.
- Hennessy, G., Harris, C., Eaton, C., Wright, P., Jackson, E., Goulson, D. and Rattnieks, F. F.** (2020). Gone with the wind: effects of wind on honey bee visit rate and foraging behaviour. *Animal Behaviour* 161, 23–31.
- Ho, H. W., de Croon, G. C. and Chu, Q.** (2017). Distance and velocity estimation using optical flow from a monocular camera. *International Journal of Micro Air Vehicles* 9, 198–208.

- Huston, S. J. and Jayaraman, V. (2011). Studying sensorimotor integration in insects. *Current Opinion in Neurobiology* 21, 527–534.
- Ibbotson, M. R., Hung, Y. S., Meffin, H., Boeddeker, N. and Srinivasan, M. V. (2017). Neural basis of forward flight control and landing in honeybees. *Scientific Reports* 7, 1–15.
- Jakobi, T., Kolomenskiy, D., Ikeda, T., Watkins, S., Fisher, A., Liu, H. and Ravi, S. (2018). Bees with attitude: the effects of directed gusts on flight trajectories. *Biology Open* 7.
- Kapustjansky, A., Chittka, L. and Spaethe, J. (2009). Bees use three-dimensional information to improve target detection. *Naturwissenschaften* 2009 97:2 97, 229–233.
- Karásek, M., Muijres, F. T., Wagter, C. D., Remes, B. D. W. and de Croon, G. C. H. E. (2018). A tailless aerial robotic flapper reveals that flies use torque coupling in rapid banked turns. *Science* 361, 1089–1094.
- Kelber, A., Warrant, E. J., Pfaff, M., Wallén, R., Theobald, J. C., Wcislo, W. T. and Raguso, R. A. (2006). Light intensity limits foraging activity in nocturnal and crepuscular bees. *Behavioral Ecology* 17, 63–72.
- Land, M. F. (2004). Nocturnal vision: Bees in the dark. *Current Biology* 14, R615–R616.
- Laughlin, S. B. and Lillywhite, P. G. (1982). Intrinsic noise in locust photoreceptors. *The Journal of Physiology* 332, 25–45.
- Laurent, K. M., Fogg, B., Ginsburg, T., Halverson, C., Lanzone, M. J., Miller, T. A., Winkler, D. W. and Bewley, G. P. (2021). Turbulence explains the accelerations of an eagle in natural flight. *Proceedings of the National Academy of Sciences of the United States of America* 118.
- Lee, D. N. (1976). A theory of visual control of braking based on information about time to collision. *Perception* 5, 437–459.
- Lee, D. N., Davies, M. N. O., Green, P. R. and (Ruud). Van Der Weel, F. R. (1993). Visual control of velocity of approach by pigeons when landing. *Journal of Experimental Biology* 180, 85–104.
- Lee, D. N., Reddish, P. E. and Rand, D. T. (1991). Aerial docking by hummingbirds. *Naturwissenschaften* 78, 526–527.
- Lillywhite, P. G. (1977). Single photon signals and transduction in an insect eye. *Journal of comparative physiology* 1977 122:2 122, 189–200.
- Lillywhite, P. G. (1981). Multiplicative intrinsic noise and the limits to visual performance. *Vision Research* 21, 291–296.
- Lillywhite, P. G. and Laughlin, S. B. (1979). Transducer noise in a photoreceptor. *Nature* 1979 277:5697 277, 569–572.
- Linander, N., Dacke, M. and Baird, E. (2015). Bumblebees measure optic flow for pos-

- ition and speed control flexibly within the frontal visual field. *Journal of Experimental Biology* **218**, 1051–1059.
- Liu, P., Sane, S. P., Mongeau, J. M., Zhao, J. and Cheng, B. (2019). Flies land upside down on a ceiling using rapid visually mediated rotational maneuvers. *Science Advances* **5**.
- Michener, C. D. (2007). *The Bees of the World*. Johns Hopkins University Press.
- Mountcastle, A. M. and Combes, S. A. (2014). Biomechanical strategies for mitigating collision damage in insect wings: Structural design versus embedded elastic materials. *Journal of Experimental Biology* **217**, 1108–1115.
- Peat, J. and Goulson, D. (2005). Effects of Experience and Weather on Foraging Rate and Pollen versus Nectar Collection in the Bumblebee, *Bombus terrestris*. *Behavioral Ecology and Sociobiology* **58**, 152–156.
- Rajabi, H., Dirks, J. H. and Gorb, S. N. (2020). Insect wing damage: Causes, consequences and compensatory mechanisms. *Journal of Experimental Biology* **223**.
- Ravi, S., Crall, J. D., McNeilly, L., Gagliardi, S. F., Biewener, A. A. and Combes, S. A. (2015). Hummingbird flight stability and control in freestream turbulent winds. *Journal of Experimental Biology* **218**, 1444–1452.
- Reber, T., Dacke, M., Warrant, E. and Baird, E. (2016). Bumblebees perform well-controlled landings in dim light. *Frontiers in Behavioral Neuroscience* **10**, 1–10.
- Reber, T., Vähäkainu, A., Baird, E., Weckström, M., Warrant, E. and Dacke, M. (2015). Effect of light intensity on flight control and temporal properties of photoreceptors in bumblebees. *Journal of Experimental Biology* **218**, 1339–1346.
- Ribbands, C. R. (1949). The Foraging Method of Individual Honey-Bees. *The Journal of Animal Ecology* **18**, 47.
- Riley, J. R., Reynolds, D. R., Smith, A. D., Edwards, A. S., Osborne, J. L., Williams, I. H. and McCartney, H. A. (1999). Compensation for wind drift by bumble-bees. *Nature* **400**:6740 **400**, 126–126.
- Rock, P. B., Harris, M. G. and Yates, T. (2006). A test of the tau-dot hypothesis of braking control in the real world. *Journal of Experimental Psychology: Human Perception and Performance* **32**, 1479–1484.
- Rose, R. and Menzel, R. (1981). Luminance dependence of pigment color discrimination in bees. *Journal of comparative physiology* **141**, 379–388.
- Roth, E., Sponberg, S. and Cowan, N. J. (2014). A comparative approach to closed-loop computation. *Current Opinion in Neurobiology* **25**, 54–62.
- Serres, J. R. and Ruffier, F. (2017). Optic flow-based collision-free strategies: From insects to robots. *Arthropod Structure & Development* **46**, 703–717.
- Shackleton, K., Balfour, N. J., Toufalia, H. A., Alves, D. A., Bento, J. M. and Ratnieks,

- F. L. W. (2019). Unique nest entrance structure of *Partamona helleri* stingless bees leads to remarkable ‘crash-landing’ behaviour. *Insectes Sociaux* 2019 66:3 66, 471–477.
- Shepard, E. L. C., Ross, A. N. and Portugal, S. J. (2016). Moving in a moving medium: new perspectives on flight. *Philosophical Transactions of the Royal Society B: Biological Sciences* 371.
- Silies, M., Gohl, D. M. and Clandinin, T. R. (2014). Motion-Detecting Circuits in Flies: Coming into View. *Annual review of neuroscience* 37, 307–327.
- Somanathan, H., Krishna, S., Jos, E. M., Gowda, V., Kelber, A. and Borges, R. M. (2020). Nocturnal Bees Feed on Diurnal Leftovers and Pay the Price of Day “ Night Lifestyle Transition. *Frontiers in Ecology and Evolution* 0, 288.
- Spaethe, J. and Weidenmüller, A. (2002). Size variation and foraging rate in bumblebees (*Bombus terrestris*). *Insectes Sociaux* 2002 49:2 49, 142–146.
- Spiewok, S. and Schmolz, E. (2006). Changes in temperature and light alter the flight speed of hornets (*Vespa crabro* L.). *Physiological and biochemical zoology: PBZ* 79, 188–193.
- Sponberg, S., Dyrh, J. P., Hall, R. W. and Daniel, T. L. (2015). Luminance-dependent visual processing enables moth flight in low light. *Science (New York, N.Y.)* 348, 1245–1248.
- Srinivasan, M. V. (1992). Distance Perception in Insects. *Current Directions in Psychological Science* 1, 22–26.
- Srinivasan, M. V. (2011a). Honeybees as a Model for the Study of Visually Guided Flight, Navigation, and Biologically Inspired Robotics. *Physiological Reviews* 91, 413–460.
- Srinivasan, M. V. (2011b). Visual control of navigation in insects and its relevance for robotics. *Current Opinion in Neurobiology* 21, 535–543.
- Srinivasan, M. V., Zhang, S. W., Chahl, J. S., Barth, E. and Venkatesh, S. (2000). How honeybees make grazing landings on flat surfaces. *Biological Cybernetics* 83, 171–183.
- Stöckl, A. L., Kihlström, K., Chandler, S. and Sponberg, S. (2017). Comparative system identification of flower tracking performance in three hawkmoth species reveals adaptations for dim light vision. *Philosophical Transactions of the Royal Society B: Biological Sciences* 372.
- Stull, R. B. (1988). *An introduction to boundary layer meteorology*, volume 13. Springer Science & Business Media.
- Sun, M. (2014). Insect flight dynamics: Stability and control. *Reviews of Modern Physics* 86, 615–646.
- Suver, M. P., Huda, A., Iwasaki, N., Safarik, S. and Dickinson, M. H. (2016). An Array of Descending Visual Interneurons Encoding Self-Motion in *Drosophila*. *Journal of Neuroscience* 36, 11768–11780.

- Taylor, G. J., Luu, T., Ball, D. and Srinivasan, M. V. (2013). Vision and air flow combine to streamline flying honeybees - Supplement material. *Scientific Reports* 3, 1–37.
- Taylor, G. K., Bacic, M., Bomphrey, R. J., Carruthers, A. C., Gillies, J., Walker, S. M. and Thomas, A. L. R. (2008). New experimental approaches to the biology of flight control systems. *Journal of Experimental Biology* 211, 258–266.
- Taylor, G. K. and Krapp, H. G. (2007). Sensory Systems and Flight Stability: What do Insects Measure and Why? In *Insect Mechanics and Control*, volume 34, pp. 231–316. Academic Press.
- Tichit, P. (2021). *The visual ecology of bees - Tales of diverse eyes and behaviours*. Ph.D. thesis, Lund University.
- Tichit, P., Alves-dos Santos, I., Dacke, M. and Baird, E. (2020a). Accelerated landing in a stingless bee and its unexpected benefits for traffic congestion. *Proceedings of the Royal Society B* 287, 20192720.
- Tichit, P., Alves-dos Santos, I., Dacke, M. and Baird, E. (2020b). Accelerated landings in stingless bees are triggered by visual threshold cues. *Biology letters* 16, 20200437.
- Van Breugel, F. and Dickinson, M. H. (2012). The visual control of landing and obstacle avoidance in the fruit fly *Drosophila melanogaster*. *Journal of Experimental Biology* 215, 1783–1798.
- Van Breugel, F., Morgansen, K. and Dickinson, M. H. (2014). Monocular distance estimation from optic flow during active landing maneuvers. *Bioinspiration and Biomimetics* 9, 025002.
- Verhaegen, M. and Verdult, V. (2007). Filtering and System Identification: A Least Squares Approach. *Filtering and System Identification A Least Squares Approach* 9780521875, 1–405.
- Vogt, N. and Desplan, C. (2007). The First Steps in *Drosophila* Motion Detection. *Neuron* 56, 5.
- Wagner, H. (1982). Flow-field variables trigger landing in flies. *Nature* 297, 147–148.
- Warrant, E. J. (2007). Nocturnal bees. *Current Biology* 17, R991–R992.
- Warrant, E. J. (2008). Seeing in the dark: vision and visual behaviour in nocturnal bees and wasps. *Journal of Experimental Biology* 211, 1737–1746.
- Warrant, E. J., Kelber, A., Gislén, A., Greiner, B., Ribi, W. and Wcislo, W. T. (2004). Nocturnal Vision and Landmark Orientation in a Tropical Halictid Bee. *Current Biology* 14, 1309–1318.
- Warrant, E. J. and McIntyre, P. D. (1993). Arthropod eye design and the physical limits to spatial resolving power. *Progress in Neurobiology* 40, 413–461.
- Wcislo, W. T. and Tierney, S. M. (2009). Behavioural environments and niche construction: The evolution of dim-light foraging in bees. *Biological Reviews* 84, 19–37.

Whitehead, J. G. (2020). *An examination of the kinematics and behavior of mallards (*Anas platyrhynchos*) during water landings*. Ph.D. thesis, Virginia Tech.

Summary

Landing is arguably one of the most important behaviors that flying animals regularly perform. It involves a precise control of approach speed as an animal draws closer to the landing surface. A poor control can result in high-impact collisions with the surface which can be harmful for animals. Despite its importance in flight, how animals approach a surface for landing is not yet fully understood. In this research, I contribute to answering this question by examining the landing approaches of bumblebees and honeybees. Bees, including bumblebees and honeybees, perform 100 to 1000 landings in an hour of foraging. They perform these landings relentlessly to gather the nectar and pollen, essential for their survival and reproduction. In this research, I used novel analyses methods to investigate how do bees land.

Many flying animals use visual cues during landing. In **Chapter 2**, we present how bumblebees use visual expansion cues to advance towards the landing surface. For this purpose, we first designed an indoor experimental apparatus to automatically record the landing maneuvers of foraging bumblebees. We then analyzed 4, 672 landing maneuvers using a novel method. This method analyses the individual maneuvers and is more comprehensive than the method of averaging multiple maneuvers used in literature. Using this novel method, we found the visual guidance strategy of landing bumblebees. Our results show that the landing bumblebees exhibit a series of deceleration bouts during which they keep the relative rate of optical expansion approximately constant. This constant is referred to as set-point and from one bout to the next, bumblebees tend to shift to a higher set-point. This newly-found guidance strategy results in an approach dynamics that is strikingly similar to that of pigeons and hummingbirds. In addition, we also found how bumblebees adjust this visual guidance strategy to travel faster when landing directly after a take-off than from a free-flight condition. Moreover, we also elucidated how bumblebees adjust this guidance strategy for different strengths of optic expansion cues available from the landing surface (checkerboard versus spoke patterns) and different light intensities, ranging from twilight to sunrise. This guidance strategy helps to explain how these important pollinators rapidly visit flowers and forage in challenging environmental conditions.

In addition to the deceleration phases, we found that landing bumblebees occasionally exhibit low approach velocity phases ($V < 0.05 \text{ m s}^{-1}$) while transitioning from one set-point to another. These low approach velocity phases are similar to the hovering phases identified in the literature; they result in bumblebees hovering or sometimes even flying away from the surface for a short while. In **Chapter 2**, we also proposed that these low approach velocity phases are likely the instabilities arising out of a control system that uses optical expansion rate as a control variable.

For achieving a goal such as evading a threat or reaching a set-point, animals use their sensorimotor control system to continuously parse the sensory information and change the wingbeat and body kinematics to produce the required forces and torques. In **Chapter 3**, we focus on the sensorimotor control system that the landing bumblebees use to execute their visual guidance strategy. We used the natural stepwise excitation offered by landing bumblebees to analyze how their different subsystems (sensory system, controller and motor system) function together to reach the set-points of optical expansion rate. Our results showed that their closed-loop sensorimotor control system regulates the relative rate of expansion during landing. The track segments before and during a set-point are the transient and steady-state responses of such a control system. Bumblebees use the transient response to mostly accelerate and the steady-state response to always decelerate during their landing approach. We also identified how the transient response varied amongst different environmental conditions (light intensity and the strength of optic expansion cues) and starting conditions (landings from a free-flight or after take-off). Based on these results, we propose a sensorimotor control system of landing bumblebees that facilitates a rapid and robust execution of their visual guidance strategy.

Bumblebees regularly experience winds during foraging. The winds in nature can be characterized as mean winds and fluctuations around them. In **Chapter 4**, we investigated how the mean winds affect the visual guidance strategy, the sensorimotor control system, and the landing performance of foraging bumblebees. In particular, we used six steady sidewinds ranging from $0 - 3.41 \text{ m s}^{-1}$ that foraging bumblebees often encounter. We found that the visual guidance strategy and the sensorimotor control response of bumblebees in these wind conditions is similar to that in the still-air, but bumblebees exhibit some important adaptations in these conditions. Compared to the still-air situation, bumblebees more often exhibit low approach velocity phases in higher wind speeds. This can lead to an increase in the travel time and hence, can adversely affect their foraging efficiency. But, bumblebees exhibit faster transient responses and higher set-points with increasing wind speed which enable them to travel faster. This in turn allows bumblebees to compensate for the increase in travel time that would otherwise occur due to more low approach-velocity phases in faster winds. In addition to revealing the adverse effects of winds and the compensation mechanism of bumblebees during landing, we used the natural excitation of their sensorimotor control system to propose how they integrate information from their airspeed measuring mechanoreceptors with their visual feedback loop.

In **Chapter 5**, we revise the previously proposed visual guidance strategy of landing honeybees. In literature, honeybees are shown to linearly decrease their approach velocity with the reducing distance by analyzing the average of multiple landing maneuvers. Based on this result, it has been suggested that they land by holding the relative rate of optical expansion constant throughout their approach. We use the novel analysis technique, developed in **Chapter 2**, to show that the individual honeybees do not follow such a strategy. They instead stepwise modulate their set-point of optical expansion rate during landing.

Moreover, we extend the analysis to find the mechanism that allows honeybees to converge to a stereotypic landing maneuver closer to the landing surface, for a large range of initial flight speeds and visual landing platform patterns.

Finally, in **Chapter 6**, I synthesize the results of this research and place them in a broader context of flight control in bees specifically, and other flying animals in general. For this, I first compare the landing strategies of bumblebees and honeybees found in this thesis and elucidate the likely causes of the differences between their strategies. Then, I discuss how birds might perform control during landing. Additionally, I also discuss how the knowledge obtained through this research can be used for bioinspired applications. Finally, I present an outlook on the future research in the area of landing dynamics of insects and birds.

Considering all results together, in this thesis, we developed a novel analysis method and used it to reveal that bumblebees and honeybees have evolved a sophisticated flight control strategy to execute rapid landings. Moreover, we have shown that they have developed ways to adjust this modular guidance strategy to deal with the challenges offered by the environment.

ਸੰਖੇਪ

ਸਤਹ 'ਤੇ ਉਤਰਨ ਨੂੰ ਸਭ ਤੋਂ ਮਹੱਤਵਪੂਰਨ ਵਿਵਹਾਰਾਂ ਵਿੱਚੋਂ ਇੱਕ ਮੰਨਿਆ ਜਾ ਸਕਦਾ ਹੈ ਜੋ ਉੱਡਦੇ ਜਾਨਵਰ ਨਿਯਮਿਤ ਤੌਰ 'ਤੇ ਕਰਦੇ ਹਨ। ਜਦੋਂ ਕੋਈ ਜਾਨਵਰ ਸਤਹ 'ਤੇ ਪਹੁੰਚ ਰਿਹਾ ਹੁੰਦਾ ਹੈ, ਤਾਂ ਸਫਲਤਾਪੂਰਵਕ ਉਤਰਨ ਲਈ ਇਸਨੂੰ ਆਪਣੀ ਪਹੁੰਚਣ ਦੀ ਗਤੀ ਨੂੰ ਨਿਯੰਤਰਿਤ ਕਰਨਾ ਪੈਂਦਾ ਹੈ। ਇੱਕ ਮਾੜੇ ਨਿਯੰਤਰਣ ਦੇ ਨਤੀਜੇ ਵਜੋਂ ਸਤਹ ਨਾਲ ਉੱਚ-ਪ੍ਰਭਾਵੀ ਟੱਕਰ ਹੋ ਸਕਦੀ ਹੈ ਜੋ ਜਾਨਵਰਾਂ ਲਈ ਨੁਕਸਾਨਦੇਹ ਹੋ ਸਕਦੀ ਹੈ। ਉਡਾਣ ਵਿੱਚ ਇਸਦੀ ਮਹੱਤਤਾ ਦੇ ਬਾਵਜੂਦ, ਜਾਨਵਰ ਇੱਕ ਸਤਹ ਤੱਕ ਕਿਵੇਂ ਪਹੁੰਚਦੇ ਹਨ, ਅਜੇ ਤੱਕ ਪੂਰੀ ਤਰ੍ਹਾਂ ਸਮਝਿਆ ਨਹੀਂ ਗਿਆ ਹੈ। ਇਸ ਖੋਜ ਵਿੱਚ, ਮੈਂ ਭੰਵਰੇ ਅਤੇ ਮਧੂ-ਮੱਖੀਆਂ ਦੇ ਸਤਹ 'ਤੇ ਉਤਰਨ ਦੇ ਤਰੀਕੇ ਦੀ ਜਾਂਚ ਕਰਕੇ ਇਸ ਸਵਾਲ ਦਾ ਜਵਾਬ ਦਿੰਨਾ ਹਾਂ। ਭੰਵਰੇ ਅਤੇ ਮਧੂ-ਮੱਖੀਆਂ ਚਾਰੇ ਦੇ ਇੱਕ ਘੰਟੇ ਵਿੱਚ ਹੀ 100 ਤੋਂ 1000 ਵਾਰ ਸਤਹ 'ਤੇ ਉੱਤਰਦੇ ਹਨ। ਉਹ ਇਹ ਫੁੱਲਾਂ ਤੋਂ ਰਸ ਅਤੇ ਪਰਾਗ ਨੂੰ ਇਕੱਠਾ ਕਰਨ ਲਈ ਕਰਦੇ ਹਨ। ਇਹ ਰਸ ਅਤੇ ਪਰਾਗ ਉਨ੍ਹਾਂ ਦੀ ਉੱਤਰਜੀਵਤਾ ਅਤੇ ਪ੍ਰਜਨਨ ਲਈ ਜ਼ਰੂਰੀ ਹੁੰਦਾ ਹੈ। ਮੈਂ ਇਸ ਖੋਜ ਵਿੱਚ, ਇਹ ਜਾਂਚ ਕਰਨ ਲਈ ਕਿ ਭੰਵਰੇ ਅਤੇ ਮਧੂ-ਮੱਖੀਆਂ ਇੱਕ ਸਤਹ 'ਤੇ ਕਿਵੇਂ ਉੱਤਰਦੇ ਹਨ, ਨਵੇਂ ਵਿਸ਼ਲੇਸ਼ਣ ਦੇ ਤਰੀਕਿਆਂ ਦੀ ਵਰਤੋਂ ਕਰਦਾ ਹਾਂ।

ਬਹੁਤ ਸਾਰੇ ਉੱਡਣ ਵਾਲੇ ਜਾਨਵਰ ਸਤਹ 'ਤੇ ਉਤਰਨ ਦੌਰਾਨ ਦ੍ਰਿਸ਼ ਸੰਕੇਤਾਂ ਦੀ ਵਰਤੋਂ ਕਰਦੇ ਹਨ। **ਅਧਿਆਇ 2** ਵਿੱਚ, ਅਸੀਂ ਪੇਸ਼ ਕਰਦੇ ਹਾਂ ਕਿ ਕਿਵੇਂ ਭੰਵਰੇ ਸਤਹ ਵੱਲ ਅੱਗੇ ਵਧਣ ਲਈ ਦ੍ਰਿਸ਼ ਵਿਸਤਾਰ ਸੰਕੇਤਾਂ ਦੀ ਵਰਤੋਂ ਕਰਦੇ ਹਨ। ਇਸ ਮਕਸਦ ਲਈ, ਅਸੀਂ ਸਭ ਤੋਂ ਪਹਿਲਾਂ ਇੱਕ ਅੰਦਰੂਨੀ ਪ੍ਰਯੋਗਾਤਮਕ ਉਪਕਰਣ ਤਿਆਰ ਕੀਤਾ ਹੈ ਤਾਂ ਜੋ ਭੰਵਰਿਆਂ ਦੇ ਲੈਂਡਿੰਗ ਅਭਿਆਸਾਂ ਨੂੰ ਆਪਣੇ ਆਪ ਉੱਲੇਖ ਕੀਤਾ ਜਾ ਸਕੇ। ਅਸੀਂ ਫਿਰ ਇੱਕ ਨਵੀਂ ਵਿਧੀ ਦੀ ਵਰਤੋਂ ਕਰਦੇ ਹੋਏ 4,672 ਸਤਹ 'ਤੇ ਉਤਰਨ ਦੇ ਅਭਿਆਸਾਂ ਦਾ ਵਿਸ਼ਲੇਸ਼ਣ ਕੀਤਾ। ਇਹ ਵਿਧੀ ਹਰ ਅਭਿਆਸ ਦਾ ਵਿਸ਼ਲੇਸ਼ਣ ਕਰਦੀ ਹੈ ਅਤੇ ਸਾਹਿਤ ਵਿੱਚ ਵਰਤੇ ਗਏ ਕਈ ਅਭਿਆਸਾਂ ਦੀ ਔਸਤ ਦੇ ਵਿਸ਼ਲੇਸ਼ਣ ਵਿਧੀ ਨਾਲੋਂ ਵਧੇਰੇ ਵਿਆਪਕ ਹੈ। ਇਸ ਨਵੀਨਤਮ ਵਿਧੀ ਦੀ ਵਰਤੋਂ ਕਰਦੇ ਹੋਏ, ਸਾਨੂੰ ਭੰਵਰਿਆਂ ਦੀ ਦ੍ਰਿਸ਼ ਮਾਰਗਦਰਸ਼ਨ ਰਣਨੀਤੀ ਮਿਲੀ। ਸਾਡੇ ਨਤੀਜੇ ਦਿਖਾਉਂਦੇ ਹਨ ਕਿ ਸਤਹ 'ਤੇ ਉੱਤਰਦੇ ਹੋਏ ਭੰਵਰੇ ਗਤੀ ਦੀ ਗਿਰਾਵਟ ਦੇ ਕਈ ਪੜਾਅ ਪ੍ਰਦਰਸ਼ਿਤ ਕਰਦੇ ਹਨ। ਹਰ ਪੜਾਅ ਦੌਰਾਨ ਉਹ ਦ੍ਰਿਸ਼ ਵਿਸਤਾਰ ਦੀ ਅਨੁਸਾਰੀ ਦਰ ਨੂੰ ਲਗਭਗ ਸਥਿਰ ਰੱਖਦੇ ਹਨ। ਇਸ ਸਥਿਰਤਾ ਨੂੰ ਇੱਕ ਸਥਿਤ-ਬਿੰਦੂ ਵਜੋਂ ਜਾਣਿਆ ਜਾਂਦਾ ਹੈ ਅਤੇ ਇੱਕ ਪੜਾਅ ਤੋਂ ਦੂਜੇ ਤੱਕ, ਭੰਵਰੇ ਇੱਕ ਉੱਚੇ ਸਥਿਤ-ਬਿੰਦੂ 'ਤੇ ਪਹੁੰਚ ਜਾਂਦੇ ਹਨ। ਇਹ ਨਵੀਂ ਲੱਭੀ ਗਈ ਮਾਰਗਦਰਸ਼ਨ ਰਣਨੀਤੀ ਦੇ ਨਤੀਜੇ ਵਜੋਂ ਭੰਵਰਿਆਂ ਦੀ ਪਹੁੰਚ ਦੀ ਗਤੀਸ਼ੀਲਤਾ ਕਬੂਤਰਾਂ ਅਤੇ ਹਮਿੰਗਬਰਡਾਂ ਦੇ ਸਮਾਨ ਹੈ। ਇਸ ਤੋਂ ਇਲਾਵਾ, ਅਸੀਂ ਇਹ ਵੀ ਪਾਇਆ ਕਿ ਭੰਵਰੇ ਇਸ ਦ੍ਰਿਸ਼ ਮਾਰਗਦਰਸ਼ਨ ਰਣਨੀਤੀ ਨੂੰ ਇੱਕ ਫ੍ਰੀ-ਫਲਾਈਟ ਸਥਿਤੀ ਦੀ ਬਜਾਏ ਟੇਕ-ਆਫ ਤੋਂ ਬਾਅਦ ਸਿੱਧੇ ਉਤਰਨ ਵੇਲੇ ਤੇਜ਼ੀ ਨਾਲ ਯਾਤਰਾ ਕਰਨ ਲਈ ਕਿਵੇਂ ਬਦਲਦੇ ਹਨ। ਇਸ ਤੋਂ ਇਲਾਵਾ, ਅਸੀਂ ਇਹ ਵੀ ਲੱਭਿਆ ਹੈ ਕਿ ਕਿਵੇਂ ਭੰਵਰੇ ਲੈਂਡਿੰਗ ਸਤਹ (ਚੈਕਰਬੋਰਡ ਬਨਾਮ ਸਪੇਕ ਪੈਟਰਨ) ਤੋਂ ਉਪਲਬਧ ਦ੍ਰਿਸ਼ ਵਿਸਤਾਰ ਸੰਕੇਤਾਂ ਦੀ ਵੱਖ-ਵੱਖ ਤਾਕਤ ਦੀ ਮੌਜੂਦਗੀ ਵਿੱਚ ਅਤੇ ਸੰਧਿਆ ਤੋਂ ਸੂਰਜ ਚੜ੍ਹਨ ਤੱਕ ਦੀਆਂ ਵੱਖ-ਵੱਖ ਰੋਸ਼ਨੀ ਦੀ ਤੀਬਰਤਾ ਵਿੱਚ ਇਸ ਮਾਰਗਦਰਸ਼ਨ ਰਣਨੀਤੀ ਨੂੰ ਕਿਵੇਂ ਬਦਲਦੇ ਹਨ। ਇਹ ਮਾਰਗਦਰਸ਼ਨ ਰਣਨੀਤੀ ਇਹ ਦੱਸਣ ਵਿੱਚ ਮਦਦ ਕਰਦੀ ਹੈ ਕਿ ਕਿਵੇਂ ਇਹ ਪਰਾਗਿਤ ਕਰਨ ਵਾਲੇ ਮਹੱਤਵਪੂਰਨ ਜਾਨਵਰ ਵਾਤਾਵਰਣ ਦੀਆਂ ਚੁਣੌਤੀਪੂਰਨ ਸਥਿਤੀਆਂ ਵਿੱਚ ਤੇਜ਼ੀ ਨਾਲ ਫੁੱਲਾਂ 'ਤੇ ਉੱਤਰਦੇ ਹਨ।

ਗਤੀ ਦੀ ਗਿਰਾਵਟ ਦੇ ਪੜਾਵਾਂ ਤੋਂ ਇਲਾਵਾ, ਅਸੀਂ ਦੇਖਿਆ ਕਿ ਭੰਵਰੇ ਸਤਹ 'ਤੇ ਉਤਰਨ ਦੌਰਾਨ ਕਦੇ-ਕਦਾਈਂ ਇੱਕ ਸਥਿਤ-ਬਿੰਦੂ ਤੋਂ ਦੂਜੇ ਸਥਿਤ-ਬਿੰਦੂ ਵਿੱਚ ਤਬਦੀਲੀ ਕਰਦੇ ਸਮੇਂ ਘੱਟ ਵੇਗ ਵਾਲੇ ਪੜਾਅ ਵੀ ($V < 0.05 \text{ m s}^{-1}$) ਪ੍ਰਦਰਸ਼ਿਤ ਕਰਦੇ ਹਨ। ਇਹ ਘੱਟ ਵੇਗ ਦੇ ਪੜਾਅ ਸਾਹਿਤ ਵਿੱਚ ਪਛਾਣੇ ਗਏ ਹੋਵਰਿੰਗ ਪੜਾਵਾਂ ਦੇ ਸਮਾਨ ਹਨ। ਇਹਨਾਂ ਪੜਾਵਾਂ ਦੌਰਾਨ ਭੰਵਰੇ ਇੱਕ ਥਾਂ ਤੇ ਮੰਡਰਾਂਦੇ ਜਾਂ ਕਈ ਵਾਰ ਥੋੜ੍ਹੇ ਸਮੇਂ ਲਈ ਸਤਹ ਤੋਂ ਦੂਰ ਉੱਡ ਜਾਂਦੇ ਹਨ। **ਅਧਿਆਇ 2** ਵਿੱਚ, ਅਸੀਂ ਇਹ ਵੀ ਪ੍ਰਸਤਾਵਿਤ ਕੀਤਾ ਹੈ ਕਿ ਇਹ ਘੱਟ ਵੇਗ ਦੇ ਪੜਾਅ ਇੱਕ ਨਿਯੰਤਰਣ ਪ੍ਰਣਾਲੀ ਤੋਂ ਪੈਦਾ ਹੋਣ ਵਾਲੀਆਂ ਅਸਥਿਰਤਾਵਾਂ ਹਨ ਜੋ ਇੱਕ ਨਿਯੰਤਰਣ ਪਰਿਵਰਤੀ ਵਜੋਂ ਦ੍ਰਿਸ਼ ਵਿਸਤਾਰ ਦਰ ਦੀ ਵਰਤੋਂ ਕਰਦਾ ਹੈ।

ਕਿਸੇ ਟੀਚੇ ਨੂੰ ਪ੍ਰਾਪਤ ਕਰਨ ਲਈ ਜਿਵੇਂ ਕਿ ਕਿਸੇ ਖਤਰੇ ਤੋਂ ਬਚਣਾ ਜਾਂ ਇੱਕ ਸਥਿਤ-ਬਿੰਦੂ 'ਤੇ ਪਹੁੰਚਣਾ, ਜਾਨਵਰ ਆਪਣੇ ਸੈਂਸਰੀਮੇਟਰ ਨਿਯੰਤਰਣ ਪ੍ਰਣਾਲੀ ਦੀ ਵਰਤੋਂ ਕਰਦਾ ਹੈ ਅਤੇ ਲੋੜੀਂਦੇ ਬਲ ਅਤੇ ਟਾਰਕ ਪੈਦਾ ਕਰਨ ਲਈ ਵਿੰਗਬੀਟ ਅਤੇ ਸਰੀਰਕ ਗਤਿਕੀ ਨੂੰ ਬਦਲਦਾ ਹੈ। **ਅਧਿਆਇ 3** ਵਿੱਚ, ਅਸੀਂ ਸੈਂਸਰੀਮੇਟਰ ਨਿਯੰਤਰਣ ਪ੍ਰਣਾਲੀ 'ਤੇ ਧਿਆਨ ਕੇਂਦਰਿਤ ਕੀਤਾ ਹੈ ਜਿਸਦੀ ਵਰਤੋਂ ਭੰਵਰੇ ਸਤਹ 'ਤੇ ਉਤਰਨ ਦੌਰਾਨ ਆਪਣੀ ਦ੍ਰਿਸ਼ ਮਾਰਗਦਰਸ਼ਨ ਰਣਨੀਤੀ ਵਿੱਚ ਕਰਦੇ ਹਨ। ਇਹ ਜਾਣਨ ਲਈ ਕਿ ਭੰਵਰੇ ਕਿਵੇਂ ਦ੍ਰਿਸ਼ ਵਿਸਤਾਰ ਦਰ ਦੇ ਸਥਿਤ-ਬਿੰਦੂ 'ਤੇ ਪਹੁੰਚਣ ਲਈ ਆਪਣੀ ਵੱਖੋ-ਵੱਖ ਉਪ-ਪ੍ਰਣਾਲੀਆਂ (ਸੰਵੇਦੀ ਪ੍ਰਣਾਲੀ, ਨਿਯੰਤਰਕ ਅਤੇ ਮੋਟਰ ਪ੍ਰਣਾਲੀ) ਨੂੰ ਇੱਕਠੇ ਕਿਵੇਂ ਕੰਮ ਵਿੱਚ ਲਿਆਉਂਦੇ ਹੁਣ, ਅਸੀਂ ਕੁਦਰਤੀ ਪੜਾਅਵਾਰ ਉਤੇਜਨਾ ਦੀ ਵਰਤੋਂ ਕੀਤੀ ਹੈ। ਸਾਡੇ ਨਤੀਜਿਆਂ ਨੇ ਦਿਖਾਇਆ ਕਿ ਉਹਨਾਂ ਦੀ ਬੰਦ-ਲੂਪ ਸੈਂਸਰੀਮੇਟਰ ਨਿਯੰਤਰਣ ਪ੍ਰਣਾਲੀ ਉਤਰਨ ਦੌਰਾਨ ਵਿਸਤਾਰ ਦੀ ਅਨੁਸਾਰੀ ਦਰ ਨੂੰ ਨਿਯੰਤਰਿਤ ਕਰਦੀ ਹੈ। ਇੱਕ ਸਥਿਤ-ਬਿੰਦੂ ਤੋਂ ਪਹਿਲਾਂ ਅਤੇ ਉਹਦੇ ਦੌਰਾਨ ਆਗਮਨ ਦੇ ਹਿੱਸੇ ਅਜਿਹੇ ਨਿਯੰਤਰਣ ਪ੍ਰਣਾਲੀ ਦੇ ਅਸਥਾਈ ਅਤੇ ਸਥਿਰ-ਹਾਲਤ ਦੀਆਂ ਪ੍ਰਤੀਕਿਰਿਆਵਾਂ ਹਨ। ਭੰਵਰੇ ਉਤਰਨ ਦੌਰਾਨ ਆਪਣੀ ਗਤੀ ਨੂੰ ਵਦਾਨ ਲਈ ਜਿਆਦਾਤਰ ਅਸਥਾਈ ਪ੍ਰਤੀਕਿਰਿਆ ਦੀ ਵਰਤੋਂ ਕਰਦੇ ਹਨ ਅਤੇ ਗਤੀ ਨੂੰ ਘੱਟ ਕਰਨ ਲਈ ਹਮੇਸ਼ਾ ਸਥਿਰ-ਹਾਲਤ ਵਾਲੀ ਪ੍ਰਤੀਕਿਰਿਆ ਦੀ ਵਰਤੋਂ ਕਰਦੇ ਹਨ। ਅਸੀਂ ਇਹ ਵੀ ਲੱਭਿਆ ਹੈ ਕਿ ਅਸਥਾਈ ਪ੍ਰਤੀਕਿਰਿਆ ਕਿਵੇਂ ਵਾਤਾਵਰਣਕ ਸਥਿਤੀਆਂ (ਰੌਸ਼ਨੀ ਦੀ ਤੀਬਰਤਾ ਅਤੇ ਆਪਟਿਕ ਵਿਸਤਾਰ ਸੰਕੇਤਾਂ ਦੀ ਤਾਕਤ) ਅਤੇ ਸ਼ੁਰੂਆਤੀ ਸਥਿਤੀਆਂ (ਫ੍ਰੀ-ਫਲਾਈਟ ਤੋਂ ਉਤਰਨਾ ਜਾਂ ਟੇਕ-ਆਫ ਤੋਂ ਬਾਅਦ ਉਤਰਨਾ) ਨਾਲ ਬਦਲਦੀ ਹੈ। ਇਹਨਾਂ ਨਤੀਜਿਆਂ ਦੇ ਆਧਾਰ 'ਤੇ, ਅਸੀਂ ਭੰਵਰੇ ਦੀ ਇੱਕ ਸੈਂਸਰੀਮੇਟਰ ਨਿਯੰਤਰਣ ਪ੍ਰਣਾਲੀ ਦਾ ਪ੍ਰਸਤਾਵ ਕਰਦੇ ਹਾਂ ਜਿਹਦੀ ਵਰਤੋਂ ਉਹ ਆਪਣੀ ਦ੍ਰਿਸ਼ ਮਾਰਗਦਰਸ਼ਨ ਰਣਨੀਤੀ ਨੂੰ ਚਲਾਉਣ ਵਾਸਤੇ ਕਰਦੇ ਹਨ।

ਚਾਰੇ ਦੇ ਦੌਰਾਨ ਭੰਵਰੇ ਨਿਯਮਿਤ ਤੌਰ 'ਤੇ ਹਵਾਵਾਂ ਦਾ ਅਨੁਭਵ ਕਰਦੇ ਹਨ। ਕੁਦਰਤ ਵਿੱਚ ਹਵਾਵਾਂ ਨੂੰ ਮੱਧਮ ਹਵਾਵਾਂ ਅਤੇ ਉਹਨਾਂ ਦੇ ਆਲੇ ਦੁਆਲੇ ਉਤਰਾਅ-ਚੜ੍ਹਾਅ ਵਜੋਂ ਦਰਸਾਇਆ ਜਾ ਸਕਦਾ ਹੈ। **ਅਧਿਆਇ 4** ਵਿੱਚ, ਅਸੀਂ ਜਾਂਚ ਕੀਤੀ ਕਿ ਮੱਧਮ ਹਵਾਵਾਂ ਦ੍ਰਿਸ਼ ਮਾਰਗਦਰਸ਼ਨ ਰਣਨੀਤੀ, ਸੈਂਸਰੀਮੇਟਰ ਨਿਯੰਤਰਣ ਪ੍ਰਣਾਲੀ ਅਤੇ ਭੰਵਰਿਆਂ ਦੀ ਉਤਰਨ ਦੀ ਯੋਗਤਾ ਨੂੰ ਕਿਵੇਂ ਪ੍ਰਭਾਵਿਤ ਕਰਦੀਆਂ ਹਨ। ਇਸ ਮਕਸਦ ਲਈ, ਅਸੀਂ 0 ਤੋਂ ਲੈ ਕੇ 3.41 m s^{-1} ਤਕ ਛੇ ਸਥਿਰ ਪਾਸੇ ਵੱਲ ਦੀਆਂ ਹਵਾਵਾਂ ਦੀ ਵਰਤੋਂ ਕੀਤੀ ਹੈ ਜਿਹਨਾਂ ਦੇ ਨਾਲ ਭੰਵਰਿਆਂ ਦਾ ਅਕਸਰ ਸਾਹਮਣਾ ਹੁੰਦਾ ਹੈ। ਅਸੀਂ ਦੇਖਿਆ ਹੈ ਕਿ ਇਹਨਾਂ ਹਵਾਵਾਂ ਦੀ ਮੌਜੂਦਗੀ ਵਿੱਚ ਭੰਵਰੇ ਦੀ ਦ੍ਰਿਸ਼ ਮਾਰਗਦਰਸ਼ਨ ਰਣਨੀਤੀ ਅਤੇ ਸੈਂਸਰੀਮੇਟਰ ਨਿਯੰਤਰਣ ਪ੍ਰਣਾਲੀ ਹਵਾਵਾਂ ਦੀ ਗੈਰਹਾਜ਼ਰੀ ਦੇ ਸਮਾਨ ਹੈ, ਪਰ ਇਹ ਹਵਾਵਾਂ ਵਿੱਚ ਕੁਝ ਮਹੱਤਵਪੂਰਨ ਅਨੁਕੂਲਨ ਪ੍ਰਦਰਸ਼ਿਤ ਕਰਦੀਆਂ ਹਨ। ਹਵਾ ਦੀ ਗੈਰਹਾਜ਼ਰੀ ਦੀ ਸਥਿਤੀ ਦੇ ਮੁਕਾਬਲੇ, ਭੰਵਰੇ ਉੱਚ ਹਵਾ ਦੀ ਗਤੀ ਵਿੱਚ ਵਧੇਰੇ ਵਾਰ ਘੱਟ ਵੇਗ ਦੇ ਪੜਾਵਾਂ ਨੂੰ ਪ੍ਰਦਰਸ਼ਿਤ ਕਰਦੇ ਹਨ। ਇਸ ਨਾਲ ਯਾਤਰਾ ਦੇ ਸਮੇਂ ਵਿੱਚ ਵਾਧਾ ਹੋ ਸਕਦਾ ਹੈ ਅਤੇ ਇਸਲਈ, ਉਹਨਾਂ ਦੀ ਚਾਰੇ ਦੀ ਕੁਸ਼ਲਤਾ 'ਤੇ ਬੁਰਾ ਪ੍ਰਭਾਵ ਪੈ ਸਕਦਾ ਹੈ। ਪਰ, ਭੰਵਰੇ ਵਧਦੀ ਹਵਾ ਦੀ ਗਤੀ ਦੇ ਨਾਲ ਤੇਜ਼ ਅਸਥਾਈ ਪ੍ਰਤੀਕਿਰਿਆਵਾਂ ਅਤੇ ਉੱਚ ਸਥਿਤ-ਬਿੰਦੂ ਵੀ ਪ੍ਰਦਰਸ਼ਿਤ ਕਰਦੇ ਹਨ ਜੋ ਉਹਨਾਂ ਨੂੰ ਤੇਜ਼ੀ ਨਾਲ ਯਾਤਰਾ ਕਰਨ ਦੇ ਯੋਗ ਬਣਾਉਂਦਾ ਹੈ। ਇਹ ਉਹਨਾਂ ਦੀ ਯਾਤਰਾ ਦੇ ਸਮੇਂ ਵਿੱਚ ਹੋਣ ਵਾਲੇ ਵਾਧੇ ਨੂੰ ਰੋਕਦਾ ਹੈ। ਸਤਹ 'ਤੇ ਉਤਰਨ ਦੌਰਾਨ ਹਵਾਵਾਂ ਦੇ ਮਾੜੇ ਪ੍ਰਭਾਵਾਂ ਅਤੇ ਭੰਵਰਿਆਂ ਦੀ ਯਾਤਰਾ ਦੇ ਸਮੇਂ ਵਿੱਚ ਹੋਣ ਵਾਲੇ ਵਾਧੇ ਨੂੰ ਰੋਕਣ ਦੀ ਵਿਧੀ ਨੂੰ ਲੱਭਣ ਤੋਂ ਇਲਾਵਾ, ਅਸੀਂ ਇਹ ਵੀ ਪ੍ਰਸਤਾਵਿਤ ਕਰਦੇ ਹਾਂ ਕਿ ਉਹ ਆਪਣੀ ਸੈਂਸਰੀਮੇਟਰ ਨਿਯੰਤਰਣ ਪ੍ਰਣਾਲੀ ਦੇ ਨਾਲ ਹਵਾ ਦੀ ਗਤੀ ਦੀ ਵਰਤੋਂ ਕਿਵੇਂ ਕਰਦੇ ਹਨ। ਇਸ ਮਕਸਦ ਲਈ ਅਸੀਂ ਕੁਦਰਤੀ ਪੜਾਅਵਾਰ ਉਤੇਜਨਾ ਦੀ ਵਰਤੋਂ ਕੀਤੀ ਹੈ।

ਅਧਿਆਇ 5 ਵਿੱਚ, ਅਸੀਂ ਸਾਹਿਤ ਵਿੱਚ ਪਹਿਲਾਂ ਪ੍ਰਸਤਾਵਿਤ ਮਧੁ-ਮੱਖੀਆਂ ਦੀ ਸਤਹ 'ਤੇ ਉਤਰਨ ਦੀ ਦ੍ਰਿਸ਼ ਮਾਰਗਦਰਸ਼ਨ ਰਣਨੀਤੀ ਨੂੰ ਸੰਸ਼ੋਧਿਤ ਕਰਦੇ ਹਾਂ। ਸਾਹਿਤ ਵਿੱਚ, ਮਧੁ-ਮੱਖੀਆਂ ਦੇ ਕਈ ਸਤਹ 'ਤੇ ਉਤਰਨ ਦੇ ਅਭਿਆਸਾਂ ਦੀ ਔਸਤ ਦਾ ਵਿਸ਼ਲੇਸ਼ਣ ਕਰਕੇ ਇਹ ਦੱਸਿਆ ਗਿਆ ਹੈ ਕਿ ਉਹ ਆਪਣਾ ਵੇਗ ਸਤਹ ਤੋਂ ਦੂਰੀ ਦੇ ਨਾਲ ਰੈਖਿਖ ਤੌਰ 'ਤੇ ਘਟਾਉਂਦੇ ਹਨ। ਇਸ ਨਤੀਜੇ ਦੇ ਆਧਾਰ 'ਤੇ, ਇਹ ਸੁਝਾਅ ਦਿੱਤਾ ਗਿਆ ਹੈ ਕਿ ਉਹ ਆਪਣੀ ਪਹੁੰਚ ਦੌਰਾਨ ਦ੍ਰਿਸ਼ ਵਿਸਤਾਰ ਦੀ ਅਨੁਸਾਰੀ ਦਰ ਨੂੰ ਸਥਿਰ ਰੱਖਦੇ ਹੋਏ ਉਤਰਦੇ ਹਨ। ਅਸੀਂ **ਅਧਿਆਇ 2** ਵਿੱਚ ਵਿਕਸਤ ਨਵੀਂ ਵਿਸ਼ਲੇਸ਼ਣ ਤਕਨੀਕ ਦੀ ਵਰਤੋਂ ਇਹ ਦਿਖਾਉਣ ਲਈ ਕਰਦੇ ਹਾਂ ਕਿ ਮਧੁ-ਮੱਖੀਆਂ ਅਜਿਹੀ ਰਣਨੀਤੀ ਦਾ ਪਾਲਣ ਨਹੀਂ ਕਰਦੀਆਂ ਹਨ। ਉਹ ਇਸ ਦੀ ਬਜਾਏ ਸਤਹ 'ਤੇ ਉਤਰਨ ਦੌਰਾਨ ਦ੍ਰਿਸ਼ ਵਿਸਤਾਰ ਦਰ ਦੇ ਸਥਿਤ-ਬਿੰਦੂਆਂ ਨੂੰ ਪੜਾਅਵਾਰ ਤਰੀਕੇ ਨਾਲ ਬਦਲਦੀਆਂ ਹਨ। ਇਸ ਤੋਂ ਇਲਾਵਾ, ਅਸੀਂ ਉਸ ਵਿਧੀ ਦਾ

ਵਿਸ਼ਲੇਸ਼ਣ ਵੀ ਕਰਦੇ ਹਾਂ ਜਿਸਦੀ ਮਦਦ ਨਾਲ ਮਧੂ-ਮੱਖੀਆਂ ਵੱਖੋ-ਵੱਖ ਸ਼ੁਰੂਆਤੀ ਉਡਾਣ ਦੀ ਗਤੀਆਂ ਅਤੇ ਦ੍ਰਿਸ਼ ਪਲੇਟਫਾਰਮ ਪੈਟਰਨਾਂ ਦੀ ਮੌਜੂਦਗੀ ਵਿੱਚ ਸਫਲਤਾਪੂਰਵਕ ਸਤਹ 'ਤੇ ਉਤਰਦੀਆਂ ਹਨ।

ਅੰਤ ਵਿੱਚ, **ਅਧਿਆਇ 6** ਵਿੱਚ, ਮੈਂ ਇਸ ਖੋਜ ਦੇ ਨਤੀਜਿਆਂ ਦਾ ਸੰਸ਼ਲੇਸ਼ਣ ਕਰਦਾ ਹਾਂ ਅਤੇ ਉਹਨਾਂ ਨੂੰ ਭੰਵਰੇ, ਮਧੂ-ਮੱਖੀਆਂ ਅਤੇ ਹੋਰ ਉੱਡਣ ਵਾਲੇ ਜਾਨਵਰਾਂ ਵਿੱਚ ਉਡਾਣ ਨਿਯੰਤਰਣ ਦੇ ਇੱਕ ਵਿਆਪਕ ਸੰਦਰਭ ਵਿੱਚ ਰੱਖਦਾ ਹਾਂ। ਇਸ ਦੇ ਲਈ, ਮੈਂ ਪਹਿਲਾਂ ਭੰਵਰੇ ਅਤੇ ਮਧੂ-ਮੱਖੀਆਂ ਦੇ ਸਤਹ 'ਤੇ ਉਤਰਨ ਦੀਆਂ ਰਣਨੀਤੀਆਂ ਦੀ ਤੁਲਨਾ ਕਰਦਾ ਹਾਂ ਅਤੇ ਉਹਨਾਂ ਦੀਆਂ ਰਣਨੀਤੀਆਂ ਵਿੱਚ ਅੰਤਰ ਦੇ ਸੰਭਾਵਿਤ ਕਾਰਨਾਂ ਨੂੰ ਸਪੱਸ਼ਟ ਕਰਦਾ ਹਾਂ। ਫਿਰ, ਮੈਂ ਚਰਚਾ ਕਰਦਾ ਹਾਂ ਕਿ ਸਤਹ 'ਤੇ ਉਤਰਨ ਦੌਰਾਨ ਪੰਛੀ ਆਪਣੀ ਉਡਾਣ ਕਿਵੇਂ ਨਿਯੰਤਰਣ ਕਰ ਸਕਦੇ ਹਨ। ਇਸ ਤੋਂ ਇਲਾਵਾ, ਮੈਂ ਇਹ ਵੀ ਚਰਚਾ ਕਰਦਾ ਹਾਂ ਕਿ ਇਸ ਖੋਜ ਵਿੱਚ ਪ੍ਰਾਪਤ ਕੀਤੇ ਗਿਆਨ ਨੂੰ ਜੀਵ-ਪ੍ਰੇਰਿਤ ਅਨੁਪ੍ਰਯੋਗਾਂ ਲਈ ਕਿਵੇਂ ਵਰਤਿਆ ਜਾ ਸਕਦਾ ਹੈ। ਅੰਤ ਵਿੱਚ, ਮੈਂ ਕੀੜੇ-ਮਕੌੜਿਆਂ ਅਤੇ ਪੰਛੀਆਂ ਦੇ ਸਤਹ 'ਤੇ ਉਤਰਨ ਦੀ ਗਤੀਸ਼ੀਲਤਾ ਦੇ ਖੇਤਰ ਵਿੱਚ ਭਵਿੱਖੀ ਖੋਜ ਬਾਰੇ ਇੱਕ ਨਜ਼ਰੀਆ ਪੇਸ਼ ਕਰਦਾ ਹਾਂ।

ਸਾਰੇ ਨਤੀਜਿਆਂ ਨੂੰ ਇਕੱਠੇ ਵਿਚਾਰਦੇ ਹੋਏ, ਇਸ ਖੋਜ ਵਿੱਚ, ਅਸੀਂ ਇੱਕ ਨਵੀਂ ਵਿਸ਼ਲੇਸ਼ਣ ਤਕਨੀਕ ਵਿਕਸਿਤ ਕੀਤਾ ਹੈ। ਇਸ ਨਵੀਂ ਵਿਸ਼ਲੇਸ਼ਣ ਤਕਨੀਕ ਦੀ ਵਰਤੋਂ ਕਰਕੇ ਅਸੀਂ ਇਹ ਲੱਭਿਆ ਹੈ ਕਿ ਭੰਵਰੇ ਅਤੇ ਮਧੂ-ਮੱਖੀਆਂ ਨੇ ਸਤਹ 'ਤੇ ਤੇਜ਼ੀ ਨਾਲ ਉਤਰਨ ਲਈ ਇੱਕ ਖਾਸ ਦ੍ਰਿਸ਼ ਮਾਰਗਦਰਸ਼ਨ ਰਣਨੀਤੀ ਵਿਕਸਿਤ ਕੀਤੀ ਹੈ। ਇਸ ਤੋਂ ਇਲਾਵਾ, ਅਸੀਂ ਦਿਖਾਇਆ ਹੈ ਕਿ ਉਨ੍ਹਾਂ ਨੇ ਵਾਤਾਵਰਣ ਦੁਆਰਾ ਪੇਸ਼ ਕੀਤੀਆਂ ਚੁਣੌਤੀਆਂ ਨਾਲ ਨਜਿੱਠਣ ਲਈ ਇਸ ਮਾਰਗਦਰਸ਼ਨ ਰਣਨੀਤੀ ਨੂੰ ਅਨੁਕੂਲ ਕਰਨ ਦੇ ਤਰੀਕੇ ਵਿਕਸਿਤ ਕੀਤੇ ਹਨ।

सारांश

अवतरण यकीनन सबसे महत्वपूर्ण व्यवहारों में से एक है जो उड़ने वाले जानवर नियमित रूप से करते हैं। जब एक जानवर अवतरण सतह के करीब आ रहा होता है, उसे सफल अवतरण करने के लिए अपनी आगमन गति का सटीक नियंत्रण करना पड़ता है। एक खराब नियंत्रण के परिणामस्वरूप सतह के साथ उच्च प्रभाव वाली टक्कर हो सकती है। यह टक्कर जानवरों के लिए हानिकारक हो सकती है। उड़ान में इसके महत्व के बावजूद, अवतरण के लिए जानवर सतह पर कैसे पहुंचते हैं, यह हम पूरी तरह से नहीं समझते हैं। मैं इस शोध-प्रबंध में भौरों और मधुमक्खियों के अवतरणों की जांच करके इस प्रश्न का उत्तर देने में योगदान देता हूँ। भौरों और मधुमक्खियाँ चारे की तलाश के एक ही घंटे के दौरान 100 से 1000 अवतरण करती हैं। वे फूलों से रस और पराग इकट्ठा करने के लिए इन अवतरणों को अथक रूप से करती हैं। यह रस और पराग उनकी उत्तरजीविता और प्रजनन के लिए आवश्यक हैं। ये मधुमक्खियाँ कैसे एक सतह पर उतरती हैं, यह जांचने के लिए मैंने इस शोध-प्रबंध में नवीन विश्लेषण विधियों का उपयोग किया है।

कई उड़ने वाले जानवर अवतरण के दौरान दृश्य संकेतों का उपयोग करते हैं। **अध्याय 2** में, हम यह प्रस्तुत करते हैं कि कैसे भौरों दृश्य विस्तार संकेतों का उपयोग अवतरण सतह की ओर बढ़ने के लिए करते हैं। इस उद्देश्य के लिए, हमने सबसे पहले एक आभ्यंतरिक प्रायोगिक उपकरण तैयार किया है जो स्वचालित रूप से भौरों के अवतरणों को अभिलेखित करता है। फिर हमने एक नई पद्धति का उपयोग करते हुए 4,672 अवतरणों का विश्लेषण किया। यह विधि हर अवतरण का विश्लेषण करती है और साहित्य में उपयोग किए जाने वाले विविध अवतरणों की औसत के विश्लेषण पद्धति से अधिक व्यापक है। इस नवीन पद्धति का उपयोग करके हमने भौरों के अवतरणों की दृश्य मार्गदर्शन रणनीति ढूंढी है। हमारे परिणाम बताते हैं कि सतह की ओर बढ़ते हुए भौरों कई चरणों में अवतरण करते हैं। हर अवतरण चरण के दौरान वे दृश्य विस्तार की सापेक्ष दर को लगभग स्थिर रखते हैं। इस स्थिरांक को एक स्थिर-बिंदु के रूप में संदर्भित किया जाता है और एक अवतरण चरण से अगले तक, भौरों ऊंचे स्थिर-बिंदु पर स्थानांतरित हो जाते हैं। इस नवीन मार्गदर्शन रणनीति के परिणामस्वरूप भौरों की अवतरण गतिकी कबूतरों और गुंजन पक्षियों के समान हो जाती है। हमने यह भी पाया कि भौरा एक फ्री-फ्लाइट स्थिति की तुलना में टेक-ऑफ के बाद जब सीधे उतरता है तो कैसे इस दृश्य मार्गदर्शन रणनीति को तेजी से यात्रा करने के लिए समायोजित करता है। हमने यह भी स्पष्ट किया कि कैसे भौरा अवतरण सतह (चेकरबोर्ड बनाम स्पोक प्रारूप) से उपलब्ध विभिन्न दृश्य विस्तार संकेतों की उपस्थिति में और सांझ से सूर्योदय तक की विभिन्न प्रकाश तीव्रता की उपस्थिति में इस मार्गदर्शन रणनीति को समायोजित करता है। यह मार्गदर्शन रणनीति समझने में मदद करती है कि कैसे ये महत्वपूर्ण परागणकर्ता चुनौतीपूर्ण पर्यावरणीय परिस्थितियों में तीव्रता से फूलों की ओर अवतरण करते हैं।

अवतरण चरणों के अलावा हमने पाया कि अवतरित भौरों कभी-कभी एक स्थिर-बिंदु से दूसरे में परिवर्तित करते समय कम वेग चरणों ($V < 0.05 \text{ m s}^{-1}$) का प्रदर्शन भी करते हैं। ये निम्न वेग चरण साहित्य में पहचाने गए होवरिंग चरणों के समान हैं। इन होवरिंग चरणों के परिणामस्वरूप भौरों एक जगह पर मँडराते हैं या कभी-कभी थोड़ी देर के लिए सतह से दूर उड़ते हैं। **अध्याय 2** में,

हमने यह भी प्रस्तावित किया कि ये निम्न वेग चरण एक नियंत्रण प्रणाली से उत्पन्न होने वाली अस्थिरताएं हैं जो एक नियंत्रण परिवर्ती के रूप में दृश्य विस्तार दर का उपयोग करती हैं।

एक लक्ष्य को प्राप्त करने के लिए जैसे कि किसी खतरे से बचने या एक स्थिर-बिंदु तक पहुंचने के लिए, जानवर अपनी संवेदयांत्रिक नियंत्रण प्रणाली का उपयोग करते हैं और आवश्यक बलों और आघूर्ण-बलों का उत्पादन करने के लिए विंगबीट और शारीरिक गतिकी को बदलते हैं। हमने **अध्याय 3** में संवेदयांत्रिक नियंत्रण प्रणाली पर ध्यान केंद्रित किया है जिसका उपयोग भोरें अपनी दृश्य मार्गदर्शन रणनीति का निष्पादन करने के लिए करते हैं। यह जानने के लिए की भोरें कैसे दृश्य विस्तार दर के स्थिर-बिंदु तक पहुंचने के लिए अपनी विभिन्न उप-प्रणालियों (संवेदी प्रणाली, नियंत्रक और यांत्रिक प्रणाली) को एक साथ प्रयोग में लाते हैं, हमने प्राकृतिक चरणबद्ध उत्तेजना का उपयोग किया है। हमारे परिणामों से पता चला है कि उनकी बंद-परिपथ संवेदयांत्रिक नियंत्रण प्रणाली अवतरण के दौरान सापेक्ष दृश्य विस्तार की दर को नियंत्रित करती है। एक स्थिर-बिंदु से पहले और उसके दौरान आगमन के खंड ऐसे नियंत्रण प्रणाली की अस्थायी और स्थिर-स्थिति प्रतिक्रियाएं हैं। भोरें अपने अवतरण के दौरान अधिकतम गति से बढ़ने के लिए अस्थायी प्रतिक्रिया का उपयोग करते हैं और धीमे होने के लिए हमेशा स्थिर-स्थिति प्रतिक्रिया का उपयोग करते हैं। हमने यह भी प्रदर्शित किया है कि परीक्षण की गई पर्यावरणीय परिस्थितियों (प्रकाश की तीव्रता और दृश्य विस्तार संकेत) और शुरुआती स्थितियों (फ्री-फ्लाइट से या टेक-ऑफ के बाद अवतरण) के बीच अस्थायी प्रतिक्रिया कैसे भिन्न होती है। इन परिणामों के आधार पर हम भोरों के अवतरण के लिए एक संवेदयांत्रिक नियंत्रण प्रणाली प्रस्तुत करते हैं जो उनकी दृश्य मार्गदर्शन रणनीति का ठोस निष्पादन करती है।

भोरें नियमित रूप से चारे की तलाश के दौरान हवाओं का अनुभव करते हैं। प्रकृति में हवाओं को उनकी औसत गतियों और उनके आसपास उतार-चढ़ाव के रूप में वर्णित किया जा सकता है। **अध्याय 4** में हमने जांच की कि कैसे औसत हवाएं दृश्य मार्गदर्शन रणनीति, संवेदयांत्रिक नियंत्रण प्रणाली और भोरों की अवतरण क्षमता को प्रभावित करती हैं। इस उद्देश्य के लिए हमने 0 से लेकर 3.41m s^{-1} तक छह औसत पार्श्विक हवाओं का उपयोग किया है जिनका भोरें प्रकृति में सामान्यतः सामना करते हैं। हमने पाया कि हवा की उपस्थिति में दृश्य मार्गदर्शन रणनीति और भोरों की संवेदयांत्रिक नियंत्रण प्रतिक्रिया हवा की अनुपस्थिति के समान है, लेकिन भोरें हवाओं की उपस्थिति में कुछ महत्वपूर्ण अनुकूलन प्रदर्शित करते हैं। स्थिर हवा की स्थिति की तुलना में, भोरें अधिक बार उच्च हवा की गति में निम्न वेग चरणों का प्रदर्शन करते हैं। इससे यात्रा के समय में वृद्धि हो सकती है और इसलिए उनकी चारा क्षमता पर प्रतिकूल प्रभाव पड़ सकता है। लेकिन भोरें हवा की गति बढ़ने के साथ तीव्र अस्थायी प्रतिक्रियाएं और उच्च स्थिर-बिंदु प्रदर्शित करते हैं जो उन्हें तेजी से यात्रा करने में सक्षम बनाता है। यह भोरों के यात्रा समय में वृद्धि को रोकता है जो अन्यथा उच्च हवाओं में अधिक निम्न वेग चरणों के कारण होता। अवतरण के दौरान हवाओं के प्रतिकूल प्रभावों और भोरों की क्षतिपूर्ति क्रियाविधि को प्रकाशित करने के अलावा, हम यह भी प्रस्तावित करते हैं कि वे अपने दृश्य प्रतिपुष्टि परिपथ के साथ वायुगति मापने वाली ज्ञानेन्द्रियों से जानकारी को कैसे संघटित करते हैं। इस उद्देश्य के लिए हमने उनकी संवेदयांत्रिक नियंत्रण प्रणाली की प्राकृतिक उत्तेजना का उपयोग किया है।

अध्याय 5 में, हम पहले से साहित्य में प्रस्तावित मधुमक्खियों के अवतरणों की दृश्य मार्गदर्शन रणनीति को संशोधित करते हैं। साहित्य में मधुमक्खियों के कई अवतरणों के औसत का विश्लेषण करके यह दिखाया गया है कि वे अपना आगमन वेग सतह से दूरी के साथ रैखिक रूप से कम करते

हैं। इस परिणाम के आधार पर यह सुझाव दिया गया है कि वे अपने पूरे आगमन में दृश्य विस्तार की सापेक्ष दर को स्थिर रखते हुए अवतरण करते हैं। हम **अध्याय 2** में विकसित नवीन विश्लेषण तकनीक का उपयोग करके यह दिखाते हैं कि मधुमक्खियां ऐसी रणनीति का पालन नहीं करती हैं। इसके बजाय वे अवतरण के दौरान दृश्य विस्तार दर के स्थिर-बिंदु को चरणबद्ध तरीके से संशोधित करते हैं। हम उस क्रियाविधि का भी विस्तार करते हैं जो मधुमक्खियों को विभिन्न प्रारंभिक उड़ान गति और अवतरण मंच प्रारूप की उपस्थिति में ठोस रूप से सफलतापूर्वक अवतरण करने में इस्तेमाल करती हैं।

अंततः मैं **अध्याय 6** में इस शोध-प्रबंध के परिणामों को संश्लेषित करता हूं और उन्हें भोरों, मधुमक्खियों और अन्य उड़ने वाले जानवरों में उड़ान नियंत्रण के व्यापक संदर्भ में प्रस्तुत करता हूं। मैं इसके लिए सबसे पहले इस शोध-प्रबंध में पाए जाने वाले भोरों और मधुमक्खियों की अवतरण रणनीतियों की तुलना करता हूं और उनकी रणनीतियों के बीच अंतर के संभावित कारणों को स्पष्ट करता हूं। मैं फिर चर्चा करता हूं कि अवतरण के दौरान पक्षी कैसे नियंत्रण कर सकते हैं। इसके अतिरिक्त मैं यह भी चर्चा करता हूं कि इस प्रबंध में प्राप्त ज्ञान का उपयोग जैव प्रेरित अनुप्रयोगों के लिए कैसे किया जा सकता है। अंततः मैं कीड़ों और पक्षियों की अवतरण गतिकी के क्षेत्र में भविष्य के अनुसंधान पर एक दृष्टिकोण प्रस्तुत करता हूं।

सभी परिणामों को एक साथ ध्यान में रखते हुए, हमने इस शोध-प्रबंध में एक नवीन विश्लेषण विकसित किया है। इस नवीन विश्लेषण का उपयोग करके हमने यह प्रदर्शित किया कि भोरों और मधुमक्खियों ने तेजी से अवतरण निष्पादित करने के लिए एक परिष्कृत उड़ान नियंत्रण रणनीति विकसित की है। इसके अलावा हमने दिखाया है कि उन्होंने पर्यावरण द्वारा प्रस्तुत की जाने वाली चुनौतियों से निपटने के लिए इस प्रतिरूपक मार्गदर्शन रणनीति को समायोजित करने के तरीके विकसित किए हैं।

Acknowledgements

A lot of people have helped me to finish this thesis and survive the past four years. Here, I would like to devote this space to thank them.

First and foremost, I want to express my sincere thanks to my promotors. **Florian**, thank you for giving me the opportunity to perform this research and having a confidence in me as I transitioned from rockets to bees. You always made time for a meeting and were open for discussing problems and new ideas. Thank you for providing the support, independence and useful feedback during research. This has helped me to critically review and develop my own ideas. I would also like to thank you for helping me to settle in when I arrived in the Netherlands. You have also then lent me a bike, which was extremely useful to me. I would also like to extend my sincere gratitude to **Johan**. The experienced advice from you during our meetings has pushed me for clearer explanations and helped me greatly in my personal growth. Thanks to both of you for your cooperation and understanding when I worked from India for five months.

Thank you **Guido** for sharing your research on monocular distance estimation and for all the interesting discussions and feedback. Thanks to **Emily**, **Prof. Srinivasan** and **Florian** for a joint collaboration that widens the scope of the results of this PhD thesis. **Martin**, thank you for all the interesting discussions. I enjoyed them very much. I have learnt a lot from your ability to ‘zoom out’ during our group meetings.

Many thanks to the technicians of EZO who are always willing to help the PhD candidates. **Remco**, you provided the technical help in building the wind tunnel experimental setup along with the solutions to many problems I encountered during trials. **Henk**, you were quick in arranging any hardware I needed and helped me numerous times to resolve IT related issues. **Karen**, you helped me with the rearing of blowflies. It is unfortunate that, due to lack of time, we could not perform experiments with them. **Annemarie**, you helped me with all the administrative tasks. Thank you for your patience and support all along. Also, I enjoyed our morning catch-ups very much.

I also got help to perform some experiments that unfortunately did not form a part of this thesis. **Emma**, **Florian**, **Lana**, **Martin** and **Leo** – thank you for helping me out so that I could take my planned holidays.

During this research, I had the pleasure of supervising (or working alongside) a few students. **Laura**, thank you for letting me ‘tag along’ in your experiments. It helped me when I performed experiments with the bumblebees. **Emma**, I really enjoyed working with you. With you in the lab, I had someone else to talk to in the dark and not just the bees! You were always enthusiastic and offered good advice during trials. **Cas**, thank you for taking

up the project that I wanted to do from the very beginning of my PhD. Although, we have hit a wall a couple of times, you have been resilient. I wish you all the best for finishing your thesis, and for your future career in teaching.

The atmosphere in E-wing has made working during the PhD a lot of fun. This is possible due to the great people of the Experimental Zoology and Cell Biology & Immunology groups. Thanks to **Adria, Andres, Annelieke, Antoine, Arifa, Camille, Carmen, Cees, Esther, Gauthier, Henri, Jules, Julia, Julian, Lana, Mark, Marloes, Mike, Mirelle, Mojtaba, Myrthe, Noraly, Olaf, Paulina, Pim, Sem, Tiffany, Uroš** and **Wouter** for all the fun activities, PhD weekends, evening drinks, PhD movies, barbecues and Labuitje. You have given me very pleasant memories and I will cherish them for a long time. Thanks to you and to **Annemarie, Ellen, Florian, Guillermo, Heleen, Henk, Henri, Intesaaf, Johan, Karen, Leo, Lisa (fish), Lisa (frog), Martin, Remco, Sander G, Sander K** and **Steffen** for all the interesting (and useful?) discussions during lunch and coffee breaks, and Thank you dinners. During my PhD, I shared office with the ‘engineering boys’ — **Antoine, Cees** and **Wouter**. Thank you for all the discussions, music and nice moments in the office. Finally, special thanks to my paranymphs **Antoine** and **Noraly**. It means a lot to me to share the stage with you on this occasion!

Besides PhD, I also did some fun activities with my friends that helped in relieving stress and bringing balance to my mental health. Thanks to **Antoine, Florian, Cees, Mike** and **Uroš** for introducing me to bouldering. For about three years, I worked with **Annelieke, Antoine, Lisa (fish), Noraly, Cas** and **Lisa (frog)** to combat weeds in our vegetable garden and (seldomly) get some vegetables. I also had the joy of going on fantastic adventures, solving creative mazes, betting on a snail race, slaying dragons and acting all stupid: thanks to the team of dungeons and dragons — **Noraly, Lana, Antoine, Tiffany** and **Henri**.

I also had the pleasure of sharing uncountable joyful moments with **Arifa, Farya, Masooma** and **Altaf**. Thanks to all of you and to **Nasira** aunty, **Suzy** aunty and **Mubarik** uncle for all the conversations, parties, impromptu singing and dancing sessions, finger-licking delicious food, movie nights, barbecues, vacations to Switserzland and Mallorca, and other fun activities. You have been my anchor of spontaneity in this ‘world’ of planning. Furthermore, thanks for all the love and care!! It was vital for me especially during the tough times.

I would also like to thank **Dr. Kamesh Subbarao, Mr. Vinod Kumar, Guido, Ewoud, Simon Schopferer, Dr. Marilena Pavel, Dr. R. V. Ramanan** and **Dr. Rajesh G**. Your support and guidance at different stages of my career has helped me to eventually reach at this point. Thanks to my dear friend **Kuldeep** for all the fun and unwavering support in the last 14 years. Also, thanks to **Shiva, Bharat** and **Vishal** for all the cheerful moments.

I am immensely thankful **Sunita maaasi** for your love and care. I wish you were here to see this moment. Also, a huge thanks to my **mother, father** and **sister** for their unwavering support and belief in me. Your love and encouragement has always been vital for me.

Kiyaansh — although you cannot read this yet, thanks for your smiles and laughter. They have been very important to me especially during the last year of my PhD.

About the author

Pulkit Goyal was born in 1989 in Punjab, India. He grew up in a city called Bathinda and has spent his youth there assimilating culture, and learning – among other things – mathematics. Due to his fascination in flying objects, he decided to do his bachelors in Aerospace Engineering. For this, he moved to southern India and joined Indian Institute of Space Science and Technology (IIST) in Thiruvananthapuram, Kerala. There, he learned the basics of aerodynamics, flight dynamics, structural dynamics, manufacturing and propulsion technology. In addition, he did a minor in robotics.



Near the end of his bachelors, he got an opportunity to do his thesis in Aerospace Systems Laboratory (ASL) at the University of Texas at Arlington, USA. There, Dr. Kamesh Subbarao introduced him to Kalman theory and its several applications in control systems. His bachelor thesis involved one of those applications – it dealt with the estimation of size of space debris using astrometric and photometric measurements. This experience of 3.5 months got him hooked to dynamics and control systems, and inspired his pursuit of professional activities in the next decade.

After bachelors, he joined Indian Space Research Organisation (ISRO) as a scientist in the domain of aerodynamic design and analysis. His responsibilities there included (a) characterization of loads acting on the rockets and crew module for human spaceflight as they travel through Earth's atmosphere, and (b) designing and testing of concepts for future missions. For both purposes, he used computational fluid dynamics, wind tunnel tests, and custom-designed analytical tools to take into account various effects such as Reynolds number and multiple jet interactions.

In between his career at the Indian space agency, he moved to the Netherlands to pursue an MSc programme Control and Simulation on scholarship at the Faculty of Aerospace Engineering in Delft University of Technology. There, he enjoyed learning about the design, simulation, and testing of control systems for different aerospace and mechanical systems. During his internship at German Aerospace Center (DLR) in Braunschweig, Germany, he developed and implemented a sensor-based approach for two sensor configurations to estimate wind velocity and airspeed for a fixed-wing unmanned aircraft. During his thesis at Micro Aerial Vehicle lab at TU delft, he developed and implemented a real-time mission planning strategy for deployment of a sensor network using a fleet of drones. To continue his journey in the area of control systems, he later joined Experimental Zoology group at

Wageningen University to find how bees land. The result of this quest lies before you.

Next to his work, he has interest in cultural art. He is good in Bhangra (a traditional folk dance of Punjab) and horrific at singing. But both are likely to be a part of his life in foreseeable future.

List of symbols

A	Approach acceleration towards the landing platform (m s^{-2})
a	A Parameter of a gamma distribution
\bar{A}_e	Average approach acceleration A during an entry segment (m s^{-2})
A^*	Mean value of approach acceleration A in a constant- r segment (m s^{-2})
b	A Parameter of a gamma distribution
D	Distance from the surface in a free-flight condition (m)
Δr_e	Step-change of optical expansion rate required in an entry segment (s^{-1})
Δr^*	Change in the set-point of optical expansion rate between two consecutive constant- r segments in a landing approach (s^{-1})
Δt	Time duration of an entry segment (s)
ΔV	Change in the approach velocity during an entry segment (m s^{-1})
Δy_1	Displacement normal to the landing surface during a constant- r segment, same as Δy^* (m)
Δy_2	Displacement normal to the landing surface for a set of consecutive constant- r segments in a landing approach (m)
Δy^*	Displacement normal to the landing surface during a constant- r segment, same as Δy_1 (m)
F	Fit percentage
f	Threshold factor used in the set-point extraction algorithm
m	Slope of linear relationship between the logarithmic transformations of the set-points of optical expansion rate r^* and the mean distance to the surface y^* ; a parameter similar to the time-to-contact-rate $\dot{\tau}$
$P_{\text{low } V}$	Probability of a bumblebee exhibiting a low approach velocity phase
r	Relative rate of expansion or optical expansion rate (s^{-1})
r_0	Optical expansion rate at the start of the entry segment (s^{-1})
R^2	Coefficient of determination
$r_c(t)$	Temporal variation of relative rate of expansion in a combined pair of constant- r and entry segments (s^{-1})
\dot{r}	Optical expansion acceleration; calculated as the time derivative of optical expansion rate (s^{-2})
\dot{r}_e	Estimate of optical expansion acceleration in an entry segment (s^{-2})
$r_f(t)$	Low-pass filtered temporal variation of relative rate of expansion in a combined pair of constant- r and entry segments (s^{-1})
r^*	Set-point of relative rate of expansion or optical expansion rate; mean value of optical expansion rate in a constant- r segment (s^{-1})

$r_s(t)$	Temporal variation of relative rate of expansion in a combined pair of constant- r and entry segments obtained after simulating a transfer function (s^{-1})
r_0^*	Switch-reversal set-point of optical expansion rate (s^{-1})
t	Time-to-touchdown (s)
τ	Time-to-contact parameter, inverse of optical expansion rate r (s)
$\dot{\tau}$	Time-to-contact-rate, time derivative of time-to-contact τ
T_{OF}	Front-to-back translatory optic flow in a free-flight (s^{-1})
T_{OF}^*	Set-point of front-to-back translatory optic flow in a free-flight (s^{-1})
Δt^*	Time duration during a constant- r segment (s)
\bar{U}_{Ae}	Average airspeed U_A during an entry segment ($m s^{-1}$)
U_H	Average flight speed between two consecutive constant- r segments for a hybrid landing strategy ($m s^{-1}$)
U_r	Average flight speed between two consecutive constant- r segments for a constant- r landing strategy ($m s^{-1}$)
U_{start}	Three-dimensional speed at the start of the landing maneuver ($m s^{-1}$)
$U_{\dot{\tau}}$	Average flight speed between two consecutive constant- r segments for a constant- $\dot{\tau}$ landing strategy ($m s^{-1}$)
V	Approach velocity towards the landing platform ($m s^{-1}$)
\mathbf{A}	Acceleration vector (a_x, a_y, a_z) ($m s^{-2}$)
\mathbf{U}	Ground-velocity vector (u, v, w) or (u_G, v_G, w_G) in a landing platform coordinate system, same as \mathbf{U}_G ($m s^{-1}$)
\mathbf{U}_A	Air-velocity vector (u_A, v_A, w_A) in a landing platform coordinate system ($m s^{-1}$)
\mathbf{U}_G	Ground-velocity vector (u, v, w) or (u_G, v_G, w_G) in a landing platform coordinate system, same as \mathbf{U} ($m s^{-1}$)
\mathbf{U}_W	Wind-velocity vector ($u_W, 0, 0$) in a landing platform coordinate system ($m s^{-1}$)
\mathbf{X}	Space-time array (x, y, z, t)
V_F	Flight speed in a free-flight condition ($m s^{-1}$)
V^*	Mean value of approach velocity V in a constant- r segment ($m s^{-1}$)
x	An axis of a landing platform coordinate system; defined in a plane parallel to the ground (m)
y	An axis of a landing platform coordinate system; defined in a direction normal to the landing platform (m)
y_0	Initial distance from the landing platform at which the entry segment starts (m)
y^*	Mean value of distance to the surface in a constant- r segment (m)
z	An axis of a landing platform coordinate system; defined in a vertically up direction (m)

Educational and training activities

The basic package	2 ECTS
WIAS Introduction course	2017
Scientific Integrity & Ethics in Animal Sciences	2018
Disciplinary competences	14 ECTS
Literature review	2018
Robust and Multivariable Control Design course	2019
Statistics for the Life Sciences	2018
Advanced Statistics course - Design of Experiments	2018
Professional competences	7 ECTS
WIAS course High-Impact Writing in Science	2019
Scientific Writing course	2019
Dutch Language courses	2020–21
Searching & Organising Literature course	2021
Project & Time Management course	2021
The Essentials of Scientific Writing & Presenting course	2021
WIAS course The Final Touch	2021
Presentation skills	4 ECTS
WIAS Science Day, Oral Presentation	2019
Learning & Memory in Animal Kingdom Conference, Poster Presentation	2019
SICB Online Conference, Oral Presentation	2020
SEB Online Conference, Oral Presentation	2021
Teaching competences	6 ECTS
Supervising MSc thesis (Emma Rietveld)	2019
Supervising MSc thesis (Cas van den Munckhof)	2020–21
Teaching assistant for Functional Zoology course	2018
Teaching assistant for Functional Zoology course	2019
Teaching assistant for Functional Zoology course	2020
Education and training activities in total	33 ECTS

Completion of the training activities is in fulfilment of the requirements for the education certificate of the Graduate School Wageningen Institute of Animal Sciences (WIAS). One ECTS equals a study load of 28 hours.

The research described in this thesis was financially supported by the Netherlands Organisation for Scientific Research (Nederlandse Organisatie voor Wetenschappelijk Onderzoek - Toegepaste en Technische Wetenschappen), grant number NWO-TTW 15039.

Financial support from the Experimental Zoology Group of Wageningen University for printing this thesis is gratefully acknowledged.

Layout and cover design by Pulkit Goyal (cover image by Perez Vöcking from Pixabay)

Thesis template by Cees J. Voesenek

Printed by ProefschriftMaken

